MICHIGAN STATE UNIVERSITY LIBRARIES
3 1293 01394 7423

This is to certify that the

dissertation entitled

A SYNOPTIC CLIMATOLOGY OF WARM-SEASON
LOW LEVEL WIND MAXIMA IN THE GREAT PLAINS
AND THEIR RELATIONSHIP TO CONVECTION

presented by

Claudia K. Walters

has been accepted towards fulfillment
of the requirements for

Ph.D. degree in Geography

Major professor

Date July 11, 1997

MSU is an Affirmative Action/Equal Opportunity Institution

0-12771

LIBRARY
Michigan State
University

PLACE IN RETURN BOX to remove this checkout from your record.
TO AVOID FINES return on or before date due.

DATE DUE	DATE DUE	DATE DUE
JAN 1 6 2005		

MSU Is An Affirmative Action/Equal Opportunity Institution
c:\circ\datedue.pm3-p.1

A SYN
IN

A SYNOPTIC CLIMATOLOGY OF WARM-SEASON LOW LEVEL WIND MAXIMA IN THE GREAT PLAINS AND THEIR RELATIONSHIP TO CONVECTION

VOLUME I

By

Claudia K. Walters

A DISSERTATION

Submitted to
Michigan State University
in partial fulfillment of the requirements
for the degree of

DOCTOR OF PHILOSOPHY

Department of Geography

1997

Copyright by
CLAUDIA K. WALTERS
1997

A SYNOPTIC CL
IN THE GRE

In the United S
Plains and are thoug
thunderstorms. The
kilometers wide and
to both boundary-lay
upper-level jet streak

This study has
characteristics of low-
relationship between
and 3) to distinguish,

Vertical profiles
rawinsonde stations a
of 1522 jet cases (wind
located below 900 mb
mechanisms. These jet
frequent at the height
speed and direction. Je
diurnal signature and a
and 600 mb appears to

The horizontal wi
identified jet cases. The
airflow configuration. F

ABSTRACT

A SYNOPTIC CLIMATOLOGY OF WARM-SEASON LOW LEVEL WIND MAXIMA IN THE GREAT PLAINS AND THEIR RELATIONSHIP TO CONVECTION

By

Claudia K. Walters

In the United States, low-level wind maxima occur most frequently in the Great Plains and are thought to play a major role in the initiation and intensification of thunderstorms. These lower tropospheric wind maxima are generally several hundred kilometers wide and up to several thousand kilometers long. They have been attributed to both boundary-layer forcing mechanisms and to synoptic-scale mechanisms (e.g. upper-level jet streaks, frontal boundaries).

This study has three goals: 1) to identify the temporal and spatial variations in the characteristics of low-level wind maxima in the Great Plains, 2) to clarify the relationship between low-level wind maxima and the spatial distribution of convection, and 3) to distinguish, if possible, between boundary-layer and synoptically-driven jets.

Vertical profiles of wind speed and wind direction were plotted at eight rawinsonde stations across the Great Plains. The spatial and temporal characteristics of 1522 jet cases (wind speed maxima in the vertical profiles) show that wind maxima located below 900 mb appear to be most strongly influenced by boundary-layer mechanisms. These jet cases have a distinct preference for the morning hours, are most frequent at the height of the warm season, and display a large diurnal shift in wind speed and direction. Jet cases that occur above 800 mb, on the other hand, lack a diurnal signature and appear to be primarily synoptically forced. The layer between 900 and 800 mb appears to act as a transition zone.

The horizontal wind field was then analyzed at the level of maximum wind for the identified jet cases. The resulting jet events were manually classified based on their airflow configuration. For each of the twelve identified airflow configuration types,

composite analys

convection, and e

several important

much more variec

different elevation

lightning activity

4- the majority of

and synoptic-scale

composite analyses were prepared of the low-level airflow, the spatial distribution of convection, and environmental parameters. The analysis of the jet events resulted in several important findings: 1) the spatial configuration of low-level wind maxima is much more varied than previously portrayed, 2) the existence of multiple airstreams at different elevations is common, 3) most of the spatial variation of cloud-to-ground lightning activity can be related to the convergence fields of the multiple airstreams, and 4) the majority of the different jet types appear to be influenced by both boundary-layer and synoptic-scale forcing mechanisms.

to my parents

I wish to exp

enthusiasm with c

ior the many hours

low-level wind ma

members of my Ph

Richard E. Groop,

help. For their hel

and Jim Brown.

A project such

First and foremost I

dark spots in the tu

Alan Haddow and

roommates in the ea

Mary Mapes, Kathy

geography graduate

breaks from program

motivation to compl

with proofreading, c

ACKNOWLEDGMENTS

I wish to express my sincere gratitude to my Ph.D. advisor, Julie A. Winkler, whose ıthusiasm with climatology sparked my interest in the field. I am particularly grateful r the many hours she spent with me laboring over hundreds and hundreds of maps of w-level wind maxima trying to make sense of it all. I also wish to thank the other ıembers of my Ph.D. advisory committee, Drs. Jeffrey A. Andresen, Daniel G. Brown, ichard E. Groop, and Jay R. Harman, for their always open doors and willingness to elp. For their help with all computer-related problems, I am grateful to Mike Lipsey ıd Jim Brown.

A project such as this one cannot be completed without strong mental support. rst and foremost I want to thank my husband Douglas who helped me throught the ırk spots in the tunnel. For their help to see the light at the other end, I am grateful to an Haddow and Alejandro Diaz. I am going to miss those workout breakfasts. My ɔmmates in the early stages of this project knew the boat we were all in. Thanks, ıry Mapes, Kathy Mapes and Sherry Wynn! I would also like to thank my fellow ɔgraphy graduate students, Cathy DeLain, Ken Duda and Galia Gaidarova. The ːaks from programming, plotting, writing, etc. always provided a little extra ıtivation to complete the project. And, finally, a big thanks to my father for his help h proofreading, cutting and pasting.

LIST OF TABLES

LIST OF FIGURES

CHAPTER 1
INTRODUCTION
Overview and
Review of Liter
Climatology
Case Studie
Troposp
Seasona
Diurnal
Turb
E
E
Noct
Surfa
Latit
Role
Impa
Advectiv
Low-Level Je
Low-Lev
Devel
Intera
The L
Temp
Bound
Frontal Bo
Convection A
Great Plai
Boundary-
Warm Adv
Vertical M
Mesoscale
Squall Line
Summary .....
Specific Objective

CHAPTER 2
DATA AND METHO
Data .....

TABLE OF CONTENTS

T OF TABLES xii

T OF FIGURES xiv

APTER 1
RODUCTION AND REVIEW OF LITERATURE 1
Overview and General Objectives 1
Review of Literature 4
Climatologies of North American Low-Level Wind Maxima 5
Case Studies and Modeling Studies of Boundary-Layer Jets 9
Tropospheric Oscillations 10
Seasonal and Diurnal Variations in the BLJ Characteristics 12
Diurnal Variations in Boundary Layer Conditions 14
Turbulent Energy Transfer and Eddy Viscosity 14
Energy transfer 15
Eddy viscosity 16
Nocturnal Inversion 17
Surface Pressure Features 19
Latitude Dependence 20
Role of Topography 20
Impact of Soil Moisture 21
Advective and Kinematic Properties of the BLJ 22
Low-Level Jet Studies 23
Low-Level Jets Associated with Mid-latitude Cyclones 24
Development of LLJs in Cyclones 24
Interaction between Upper-Level Jet and Low-Level Jet 27
The LLJ as Part of the Warm Conveyor Belt 31
Temporal Variations 32
Boundary-Layer Structure 33
Frontal Boundary Situations 34
Convection Associated with Boundary-Layer Jets and Low-Level Jets 39
Great Plains Convection 39
Boundary-Layer Convergence 41
Warm Advection 42
Vertical Motion and Latent Heat Release 43
Mesoscale Convective Systems and Mesoscale Convective Complexes 43
Squall Lines 46
Summary 46
pecific Objectives of Study 48

PTER 2
A AND METHODOLOGY 53
ata 53

Rawinson
Cloud-to-
Study Area a
Methods .....
Identificat
Characte
Rawin
Definit
Pre
Cu
Sho
Charac
Analysis o
Mappi
Identify
Classify
Compo
Analysis of
Analysis of
Analysis of
Surface
Geostro
500-mb
200-mb
Summary ...

CHAPTER 3
FREQUENCY OF S
Temporal Variat
Maxima .....
Monthly Var
Diurnal Vari
Spatial Variation
Spatial Variation
Speed and Direc
Summary .....

CHAPTER 4
AIRFLOW CONFIG
CONVECTION.....
Introduction a
AC_EW Jets (Ant
East-West) .....
Airflow Confi
Temperature a
Convection ....
AC_SWNE Jets (A
zone oriented S
Airflow Confi
Temperature a
Convection ....

Rawinsonde Observations 54
Cloud-to-Ground Lightning Observations 56
Study Area and Study Period 57
Methods 58
Identification of Low-Level Wind Maxima and Analysis of Characteristis of Low-Level Wind Maxima 58
Rawinsonde Sites 58
Definition of a Low-Level Wind Maximum 60
Previous Jet Criteria 60
Current Jet Criteria 62
Short-hand Description 63
Characteristics of Low-Level Wind Maxima 65
Analysis of Airflow Configurations 69
Mapping the Wind Fields 69
Identifying Jet Events and Multiple Jet Levels 71
Classifying the Airflow Configurations 73
Compositing the Wind Field 76
Analysis of the Temperature and Moisture Fields 78
Analysis of Convection 79
Analysis of Lower-, Mid- and Upper Tropospheric Environment 80
Surface Pressure and Surface Pressure Tendency 81
Geostrophic andAgeostrophic Wind Components 81
500-mb Geopotential Height 82
200-mb Wind Field and 200-mb Convergence 83
Summary 83

APTER 3
QUENCY OF SOUTHERLY LOW-LEVEL WIND MAXIMA 85
Temporal Variations in the Frequency of Southerly Low-Level Wind Maxima 85
Monthly Variations 85
Diurnal Variations 87
patial Variations in the Frequency of Low-Level Wind Maxima 89
patial Variations in the Height of Low-Level Wind Maxima 91
peed and Direction of Low-Level Wind Maxima 94
ummary 94

PTER 4
LOW CONFIGURATION TYPES AND THEIR RELATIONSHIP TO VECTION 96
Introduction and Overview 94
C_EW Jets (Anticyclonically curved jet with Confluence oriented East-West) 97
Airflow Configuration and Convergence 97
Temperature and Moisture 102
Convection 104
C_SWNE Jets (Anticyclonically curved wind maximum with Confluence zone oriented SouthWest-NorthEast) 106
Airflow Configuration and Convergence 106
Temperature and Moisture 110
Convection 113

KC_SWNE Je
SouthWest
Airflow C
Temperat
Convectio
SD_SWNE Jet
Deformatio
Airflow C
Convectio
SD_NWSE Jet
Deformatio
Airflow Co
Temperatu
Convectio
CC Jets (Cyclo
Airflow Co
Temperatu
Convection
LAC_SWNE Je
and Confluen
Airflow Co
Temperatu
Convection
L2A Jets ((Long
Airflow Co
Temperatur
Convection
LSKC_SWNE Je
in SouthWeste
Airflow Con
Temperature
Convection ..
LSPLIT Jets (Lo
Airflow Con
Temperature
Convection ..
LKC_SWNE Jets
Airflow Conf
Temperature
Convection ...
LCC Jets (Long w
Airflow Confi
Temperature
Convection ...
Summary .....

CHAPTER 5
LOWER, MID- AND
LEVEL WIND MAXI
AC_EW Jets .....
Surface Pressu
Geostrophic a
Mid-troposph

KC_SWNE Jets (wind maxima with "Kurl" and Confluence oriented SouthWest-NorthEast) 117
Airflow Configuration and Convergence 117
Temperature and Moisture 120
Convection 123
SD_SWNE Jets (low-level wind maximum with "Split" airflow and Deformation zone oriented SouthWest-NorthEast 123
Airflow Configuration and Convergence 129
Convection 129
SD_NWSE Jets (low-level wind axima with "Split" flow and Deformation zone oriented NorthWest-SouthEast) 132
Airflow Configuration and Convergence 132
Temperature and Moisture 135
Convection 138
CC Jets (Cyclonically-curved wind maxima with Confluence zone) 138
Airflow Configuration and Convergence 138
Temperature and Moisture 145
Convection 145
LAC_SWNE Jets (Long wind maximum with Anticyclonic curvature and Confluence oriented SouthWest-NorthEast) 148
Airflow Configuration and Convergence 148
Temperature and Moisture 151
Convection 153
L2A Jets ((Long wind maximum with 2 Anticyclonic circulation centers 153
Airflow Configuration and Convergence 153
Temperature and Moisture 160
Convection 160
LSKC_SWNE Jet (Long with Split and Kurl and Confluence zone oriented in SouthWesterly-NorthEasterly direction) 164
Airflow Configuration and Convergence 164
Temperature and Moisture 167
Convection 170
LSPLIT Jets (Long with 'Split') 172
Airflow Configuration and Convergence 172
Temperature and Moisture 175
Convection 175
LKC_SWNE Jets (Long with Kurl and Confluence in SW-NE direction) 179
Airflow Configuration and Convergence 179
Temperature and Moisture 182
Convection 185
LCC Jets (Long with Cyclonic Flow and Confluence) 185
Airflow Configuration and Convergence 185
Temperature and Moisture 189
Convection 192
ummary 195

PTER 5
ER, MID- AND UPPER TROPOSPHERIC ENVIRONMENT OF LOW-L WIND MAXIMA 202
C_EW Jets 203
Surface Pressure and Surface Pressure Tendency 203
Geostrophic and Ageostrophic Wind 205
Mid-tropospheric Heights and Upper-tropospheric Wind Field 208

AC_SWNE Je
Surface Pr
Geostroph
Mid-tropo
KC_SWNE Je
Surface Pr
Geostroph
Mid-tropo
SD_SWNE Jet
Surface Pr
Geostroph
Mid-tropo
SD_NWSE Jet
Surface Pre
Geostrophi
Mid-tropos
CC Jets.....
Surface Pre
Geostrophi
Mid-tropos
LAC_SWNE Je
Surface Pres
Geostrophic
Mid-troposp
L2A Jets.....
Surface Pres
Geostrophic
Mid-troposp
LSKC_SWNE Je
Surface Press
Geostrophic
Mid-troposp
LSPLIT Jets.....
Surface Press
Geostrophic a
Mid-troposph
LKC_SWNE Jets
Surface Pressu
Geostrophic a
Mid-troposph
LCC Jets.....
Surface Pressu
Geostrophic a
Mid-troposph
Summary .....

CHAPTER 6
DISCUSSION AND C
The Climatology
Great Plains.....
Boundary-Layer
Airflow Configur
to Convection.....

AC_SWNE Jets 210
Surface Pressure and Surface Pressure Tendency 210
Geostrophic and Ageostrophic Wind 212
Mid-tropospheric Heights and Upper-tropospheric Wind Field 214
KC_SWNE Jets 216
Surface Pressure and Surface Pressure Tendency 216
Geostrophic and Ageostrophic Wind 218
Mid-tropospheric Heights and Upper-tropospheric Wind Field 220
3D_SWNE Jets 223
Surface Pressure and Surface Pressure Tendency 223
Geostrophic and Ageostrophic Wind 223
Mid-tropospheric Heights and Upper-tropospheric Wind Field 226
3D_NWSE Jets 228
Surface Pressure and Surface Pressure Tendency 228
Geostrophic and Ageostrophic Wind 230
Mid-tropospheric Heights and Upper-tropospheric Wind Field 230
CC Jets 233
Surface Pressure and Surface Pressure Tendency 233
Geostrophic and Ageostrophic Wind 235
Mid-tropospheric Heights and Upper-tropospheric Wind Field 237
LAC_SWNE Jets 239
Surface Pressure and Surface Pressure Tendency 239
Geostrophic and Ageostrophic Wind 241
Mid-tropospheric Heights and Upper-tropospheric Wind Field 241
L2A Jets 243
Surface Pressure and Surface Pressure Tendency 243
Geostrophic and Ageostrophic Wind 245
Mid-tropospheric Heights and Upper-tropospheric Wind Field 245
LSKC_SWNE Jet 248
Surface Pressure and Surface Pressure Tendency 248
Geostrophic and Ageostrophic Wind 250
Mid-tropospheric Heights and Upper-tropospheric Wind Field 252
LSPLIT Jets 255
Surface Pressure and Surface Pressure Tendency 255
Geostrophic and Ageostrophic Wind 257
Mid-tropospheric Heights and Upper-tropospheric Wind Field 257
KC_SWNE Jets 260
Surface Pressure and Surface Pressure Tendency 260
Geostrophic and Ageostrophic Wind 262
Mid-tropospheric Heights and Upper-tropospheric Wind Field 262
CC Jets 264
Surface Pressure and Surface Pressure Tendency 264
Geostrophic and Ageostrophic Wind 267
Mid-tropospheric Heights and Upper-tropospheric Wind Field 267
ummary 269

PTER 6
USSION AND CONCLUSIONS 273
he Climatology of Low-Level Wind Maxima and Convection in the
Great Plains 273
oundary-Layer Forced Versus Synoptically-Driven Wind Maxima 278
irflow Configurations of Low-Level Wind Maxima and the Relationship
o Convection 283

The Large-S
Maxima Oc
Low-Leve
Low-Leve
The Role
Temperat
Addressing
CHAPTER 7
FUTURE RESEA
APPENDIX A: GI
APPENDIX B: SO
APPENDIX C: AI
CITED LITERATU

The Large-Scale Environment in which Central Plains Low-Level Wind Maxima Occur....286
Low-Level Wind Maxima Under Weak Midtropospheric Circulation....286
Low-Level Wind Maxima Under Strong Midtropospheric Circulation....288
The Role of Upper-Level Jet Streaks....292
Temperature and Moisture Patterns....293
Addressing the Research Questions....294

APTER 7
TURE RESEARCH....297

'ENDIX A: GEMPAK INTERPOLATION SCHEME....300

'ENDIX B: SOUTHERLY LOW-LEVEL WIND MAXIMA....302

'ENDIX C: AIRFLOW CONFIGURATION TYPES....332

ED LITERATURE....339

Tables

2.1 Elevati

2.2 Classifi

2.3 Frequen

3.1 Percenta

3.2 Height o

3.3 Mean W

3.4 Median

4.1 Number

4.2 Character

4.3 Character

4.4 Number o

4.5 Character

4.6 Number o

4.7 Characteri

4.8 Number o

4.9 Characteris

4.10 Number of

4.11 Characteris

4.12 Number of

4.13 Number of

4.14 Characteris

LIST OF TABLES

les

1 Elevation of Rawinsonde Stations (in m MSL) 59

2 Classification Criteria of Speed Profile Categories 65

3 Frequency of Events and Non-Events..... 73

1 Percentage of Morning (1200 UTC) Jets..... 88

2 Height of Wind Maxima..... 91

3 Mean Wind Speed (in ms^{-1}) by Category 94

4 Median Wind Direction by Category..... 94

1 Number of Events by Speed Profile Category -- *AC_EW* Jets 99

2 Characteristics of *AC_EW* Jets..... 99

3 Characteristics of *AC_SWNE* Jets.....108

4 Number of Events by Speed Profile Category -- *AC_SWNE* Jets 108

5 Characteristics of *KC_SWNE* Jets 119

Number of Events by Speed Profile Category -- *KC_SWNE* Jets.....119

Characteristics of *SD_SWNE* Jets.....126

Number of Events by Speed Profile Category -- *SD_SWNE* Jets 127

Characteristics of *SD_NWSE* Jets.....132

0 Number of Events by Speed Profile Category -- *SD_NWSE* Jets 134

1 Characteristics of *CC* Jets.....141

2 Number of Events by Speed Profile Category -- *CC* Jets 142

3 Number of Events by Speed Profile Category -- *LAC_SWNE* Jets 150

4 Characteristics of *LAC_SWNE* Jets.....150

4.15 Chara
4.16 Numb
4.17 Numb
4.18 Charac
4.19 Numbe
4.20 Charac
4.21 Numbe
4.22 Charact
4.23 Number
4.24 Charact
4.25 Tempora
Characte

15 Characteristics of *L2A* Jets.....157

16 Number of Events by Speed Profile Category -- *L2A* Jets.....158

17 Number of Events by Speed Profile Category -- *LSKC_SWNE* Jets.....166

18 Characteristics of *LSKC_SWNE* Jets.....166

19 Number of Events by Speed Profile Category -- *LSPLIT* Jets.....172

20 Characteristics of *LSPLIT* Jets.....174

21 Number of Events by Speed Profile Category -- *LKC_SWNE* Jets.....179

22 Characteristics of *LKC_SWNE* Jets.....181

23 Number of Events by Speed Profile Category -- *LCC* Jets.....188

24 Characteristics of *LCC* Jets.....188

25 Temporal, Geographical, Height, Speed Profile and Convergence Pattern Characteristics of Airflow Configuration Types.....199

Figures

2.1 Central

2.2 Topogr
above M

2.3 Schema

2.4 Example

2.5 Example

2.6 Example

2.7 Example

2.8 Example

2.9 Example

2.10 Example

2.11 Example

2.12 Example

2.13 Large Stu

2.14 Grid Spaci

2.15 Example o

3.1 Monthly Fr

3.2 Monthly Fr

3.3 Monthly Fr
of Day.....

3.4 Transects o

3.5 Frequency

LIST OF FIGURES

gures

2.1 Central Plains Region with Location of Rawinsonde Stations 57

2.2 Topography of the Central United States. Elevation is in Kilometers above Mean Sea Level (MSL) 59

2.3 Schematic of Vertical Speed Profile 63

2.4 Example of Category a1 Wind Maximum 66

2.5 Example of Category a2 Wind Maximum 66

2.6 Example of Category a3 Wind Maximum 66

2.7 Example of Category a4 Wind Maximum 67

2.8 Example of Category b1 Wind Maximum 67

2.9 Example of Category b2 Wind Maximum 67

2.10 Example of Category b3 Wind Maximum 68

2.11 Example of Category b4 Wind Maximum 68

2.12 Example of Category C Wind Maximum 68

2.13 Large Study Area with Location of Rawinsonde Stations 70

.14 Grid Spacing in Analysis Grids 77

.15 Example of Data Coverage 78

.1 Monthly Frequency of Southerly Low-Level Wind Maxima 86

.2 Monthly Frequency of Southerly Low-Level Wind Maxima by Height 86

.3 Monthly Frequency of Southerly Low-Level Wind Maxima by Time of Day 88

4 Transects of Rawinsonde Stations 89

5 Frequency of Low-Level Wind Maxima by Rawinsonde Station 90

3.6 Diurn
3.7 Pressu
3.8 Mean
3.9 Low-L
3.10 Low-L
4.1 Compo
black li
4.2 Compo
streaml
diverge
4.3 Geograp
4.4 Compos
Figure 4.
4.5 Compos
4.6 Composi
Ratio (g
Airflow
composit
4.7 Composi
on Level
Figure 4.6
4.8 Percentag
plotted or
4.9 Percentag
Composit
4.10 Composite
Figure 4.1
4.11 Composite
4.12 Geographi
4.13 Composite
Figure 4.1
4.14 Composite
4.15 Composite
Figure 4.1

.6 Diurnal Variation of Low-Level Wind Maxima by Rawinsonde Station..... 90

.7 Pressure Levels of Wind Maxima 92

.8 Mean Height of Wind Maxima (MSL) 92

.9 Low-Level Wind Maxima by Station by Category, 1200 UTC 93

.10 Low-Level Wind Maxima by Station by Category, 0000 UTC 93

.1 Composite Isotachs and Streamlines, Level 1 -- *AC_EW* Jets. Solid black lines are streamlines, dotted gray lines are isotachs..... 98

.2 Composite Divergence, Level 1 -- *AC_EW* Jets. Light dashed lines are streamlines, light solid lines are isotachs, heavy lines represent divergence field..... 98

.3 Geographical Centers of Isotach Maxima -- *AC_EW* Jets.....100

.4 Composite Isotachs and Streamlines, Level 2 -- *AC_EW* Jets. As in Figure 4.1 101

.5 Composite Divergence, Level 2 -- *AC_EW* Jets. As in Figure 4.2 101

.6 Composite 900-mb Temperature (°C; heavy solid lines) and Mixing Ratio (g kg^{-1}; heavy dashed lines) plotted on Level 1 Composite Airflow Configuration -- *AC_EW* Jets. The light dashed lines are the composite streamlines, the light solid lines are composite isotachs.....103

.7 Composite 850-mb Temperature (°C) and Mixing Ratio (g kg^{-1}) plotted on Level 2 Composite Airflow Configuration -- *AC_EW* Jets. As in Figure 4.6 103

.8 Percentage of Jet Events with Lightning Activity in Individual Grid Cells plotted on Level 1 Composite Airflow Configuration -- *AC_EW* Jets.....105

.9 Percentage of Jet Events with Lightning Activity plotted on Level 2 Composite Airflow Configuration -- *AC_EW* Jets 105

.10 Composite Isotachs and Streamlines, Level 1 -- *AC_SWNE* Jets. As in Figure 4.1 107

.11 Composite Divergence, Level 1 -- *AC_SWNE* Jets. As in Figure 4.2 107

.12 Geographical Centers of Isotach Maxima -- *AC_SWNE* Jets.....109

.13 Composite Isotachs and Streamlines, Level 2 -- *AC_SWNE* Jets. As in Figure 4.1 111

.14 Composite Divergence, Level 2 -- *AC_SWNE* Jets. As in Figure 4.2 111

.15 Composite Isotachs and Streamlines, Level 3 -- *AC_SWNE* Jets. As in Figure 4.1 112

4.16 Comp

4.17 Comp
on Lev
Figure

4.18 Compo
on Lev
Figure

4.19 Percent
Compo

4.20 Percent
Compo

4.21 Percenta
Compos

4.22 Compos
Figure 4

4.23 Compos

4.24 Geograp

4.25 Composi
Figure 4.

4.26 Composi

4.27 Composit
on Level
Figure 4.6

4.28 Composit
on Level 2
Figure 4.6

4.29 Percentage
Composite

4.30 Percentage
Composite

4.31 Composite
Figure 4.1

4.32 Composite

4.33 Geographic

4.34 Composite
Figure 4.1

4.16 Composite Divergence, Level 3 -- *AC_SWNE* Jets. As in Figure 4.2 112

4.17 Composite 900-mb Temperature (°C) and Mixing Ratio (g kg^{-1}) plotted on Level 1 Composite Airflow Configuration -- *AC_ SWNE* Jets. As in Figure 4.6 114

4.18 Composite 850-mb Temperature (°C) and Mixing Ratio (g kg^{-1}) plotted on Level 2 Composite Airflow Configuration -- *AC_ SWNE* Jets. As in Figure 4.6 114

4.19 Percentage of Jet Events with Lightning Activity plotted on Level 1 Composite Airflow Configuration -- *AC_ SWNE* Jets 115

4.20 Percentage of Jet Events with Lightning Activity plotted on Level 2 Composite Airflow Configuration -- *AC_ SWNE* Jets 116

4.21 Percentage of Jet Events with Lightning Activity plotted on Level 3 Composite Airflow Configuration -- *AC_SWNE* Jets 116

4.22 Composite Isotachs and Streamlines, Level 1 -- *KC_SWNE* Jets. As in Figure 4.1 118

4.23 Composite Divergence, Level 1 -- *KC_SWNE* Jets. As in Figure 4.2 118

4.24 Geographical Centers of Isotach Maxima -- *KC_SWNE* Jets 119

4.25 Composite Isotachs and Streamlines, Level 2 -- *KC_SWNE* Jets. As in Figure 4.1 121

4.26 Composite Divergence, Level 2 -- *KC_SWNE* Jets. As in Figure 4.2 121

4.27 Composite 900-mb Temperature (°C) and Mixing Ratio (g kg^{-1}) plotted on Level 1 Composite Airflow Configuration -- *KC_EW* Jets. As in Figure 4.6 122

4.28 Composite 850-mb Temperature (°C) and Mixing Ratio (g kg^{-1}) plotted on Level 2 Composite Airflow Configuration -- *KC_EW* Jets. As in Figure 4.6 122

4.29 Percentage of Jet Events with Lightning Activity plotted on Level 1 Composite Airflow Configuration -- *KC_SWNE* Jets 124

4.30 Percentage of Jet Events with Lightning Activity plotted on Level 2 Composite Airflow Configuration -- *KC_SWNE* Jets 124

4.31 Composite Isotachs and Streamlines, Level 1 -- *SD_SWNE* Jets. As in Figure 4.1 125

4.32 Composite Divergence, Level 1 -- *SD_SWNE* Jets. As in Figure 4.2 125

4.33 Geographical Centers of Isotach Maxima -- *SD_SWNE* Jets 126

4.34 Composite Isotachs and Streamlines, Level 2 -- *SD_SWNE* Jets. As in Figure 4.1 128

4.35 Comp

4.36 Compo
on Lev
Figure

4.37 Compo
on Lev
Figure

4.38 Percent
Compo

4.39 Percenta
Compos

4.40 Compos
Figure 4.

4.41 Compos

4.42 Geograp

4.43 Composi
Figure 4.1

4.44 Composi

4.45 Composit
on Level
Figure 4.6

4.46 Composit
on Level 2
Figure 4.6

4.47 Percentage
Composite

4.48 Percentage
Composite

4.49 Composite

4.50 Composite

4.51 Geographic

4.52 Composite

4.53 Composite

4.54 Composite

4.35 Composite Divergence, Level 2 -- *SD_SWNE* Jets. As in Figure 4.2 128

4.36 Composite 900-mb Temperature (°C) and Mixing Ratio (g kg^{-1}) plotted on Level 1 Composite Airflow Configuration -- *SD_SWNE* Jets. As in Figure 4.6 130

4.37 Composite 850-mb Temperature (°C) and Mixing Ratio (g kg^{-1}) plotted on Level 2 Composite Airflow Configuration -- *SD_SWNE* Jets. As in Figure 4.6 130

4.38 Percentage of Jet Events with Lightning Activity plotted on Level 1 Composite Airflow Configuration -- *SD_SWNE* Jets 131

4.39 Percentage of Jet Events with Lightning Activity plotted on Level 2 Composite Airflow Configuration -- *SD_SWNE* Jets 131

4.40 Composite Isotachs and Streamlines, Level 1 -- *SD_NWSE* Jets. As in Figure 4.1 133

4.41 Composite Divergence, Level 1 -- *SD_NWSE* Jets. As in Figure 4.2 133

4.42 Geographical Centers of Isotach Maxima -- *SD_NWSE* Jets.....134

4.43 Composite Isotachs and Streamlines, Level 2 -- *SD_NWSE* Jets. As in Figure 4.1 136

4.44 Composite Divergence, Level 2 -- *SD_NWSE* Jets. As in Figure 4.2 136

4.45 Composite 900-mb Temperature (°C) and Mixing Ratio (g kg^{-1}) plotted on Level 1 Composite Airflow Configuration -- *SD_NWSE* Jets. As in Figure 4.6 137

4.46 Composite 850-mb Temperature (°C) and Mixing Ratio (g kg^{-1}) plotted on Level 2 Composite Airflow Configuration -- *SD_NWSE* Jets. As in Figure 4.6 137

4.47 Percentage of Jet Events with Lightning Activity plotted on Level 1 Composite Airflow Configuration -- *SD_NWSE* Jets 139

4.48 Percentage of Jet Events with Lightning Activity plotted on Level 2 Composite Airflow Configuration -- *SD_NWSE* Jets 139

4.49 Composite Isotachs and Streamlines, Level 1 -- *CC* Jets. As in Figure 4.1 ...140

4.50 Composite Divergence, Level 1 -- *CC* Jets. As in Figure 4.2 140

4.51 Geographical Centers of Isotach Maxima -- *CC* Jets.....141

4.52 Composite Isotachs and Streamlines, Level 2 -- *CC* Jets. As in Figure 4.1 ...143

4.53 Composite Divergence, Level 2 -- *CC* Jets. As in Figure 4.2 143

4.54 Composite Isotachs and Streamlines, Level 3 -- *CC* Jets. As in Figure 4.1 ...144

4.55 Compo

4.56 Compo
on Lev

4.57 Compo
on Lev

4.58 Percent
Compo

4.59 Percent
Compo

4.60 Percenta
Compos

4.61 Compos
Figure 4.

4.62 Compos

4.63 Geograp

4.64 Composi
Figure 4.1

4.65 Composi

4.66 Composit
on Level
Figure 4.6

4.67 Composit
on Level 2
Figure 4.6

4.68 Percentag
Composite

4.69 Percentage
Composite

4.70 Composite
Figure 4.1 ...

4.71 Composite

4.72 Geographic

4.73 Composite
Figure 4.1 ...

4.74 Composite

4.55 Composite Divergence, Level 3 -- *CC* Jets. As in Figure 4.2 144

4.56 Composite 900-mb Temperature (°C) and Mixing Ratio (g kg^{-1}) plotted on Level 1 Composite Airflow Configuration -- *CC* Jets. As in Figure 4.6 ...146

4.57 Composite 850-mb Temperature (°C) and Mixing Ratio (g kg^{-1}) plotted on Level 2 Composite Airflow Configuration -- *CC* Jets. As in Figure 4.6 ...146

4.58 Percentage of Jet Events with Lightning Activity plotted on Level 1 Composite Airflow Configuration -- *CC* Jets 147

4.59 Percentage of Jet Events with Lightning Activity plotted on Level 2 Composite Airflow Configuration -- *CC* Jets 147

4.60 Percentage of Jet Events with Lightning Activity plotted on Level 3 Composite Airflow Configuration -- *CC* Jets 148

4.61 Composite Isotachs and Streamlines, Level 1 -- *LAC_SWNE* Jets. As in Figure 4.1 149

4.62 Composite Divergence, Level 1 -- *LAC_SWNE* Jets. As in Figure 4.2 149

4.63 Geographical Centers of Isotach Maxima -- *LAC_SWNE* Jets.....151

4.64 Composite Isotachs and Streamlines, Level 2 -- *LAC_SWNE* Jets. As in Figure 4.1 152

4.65 Composite Divergence, Level 2 -- *LAC_SWNE* Jets. As in Figure 4.2 152

4.66 Composite 900-mb Temperature (°C) and Mixing Ratio (g kg^{-1}) plotted on Level 1 Composite Airflow Configuration -- *LAC_SWNE* Jets. As in Figure 4.6 154

4.67 Composite 850-mb Temperature (°C) and Mixing Ratio (g kg^{-1}) plotted on Level 2 Composite Airflow Configuration -- *LAC_SWNE* Jets. As in Figure 4.6 154

4.68 Percentage of Jet Events with Lightning Activity plotted on Level 1 Composite Airflow Configuration -- *LAC_SWNE* Jets 155

4.69 Percentage of Jet Events with Lightning Activity plotted on Level 2 Composite Airflow Configuration -- *LAC_SWNE* Jets 155

4.70 Composite Isotachs and Streamlines, Level 1 -- *L2A* Jets. As in Figure 4.1 156

4.71 Composite Divergence, Level 1 -- *L2A* Jets. As in Figure 4.2 156

4.72 Geographical Centers of Isotach Maxima -- *L2A* Jets.....158

4.73 Composite Isotachs and Streamlines, Level 2 -- *L2A* Jets. As in Figure 4.1 159

4.74 Composite Divergence, Level 2 -- *L2A* Jets. As in Figure 4.2.....159

4.75 Comp
Figure
4.76 Comp
4.77 Compo
on Lev
Figure
4.78 Compo
on Lev
Figure
4.79 Percent
Compo
4.80 Percenta
Compos
4.81 Percenta
Compos
4.82 Compos
Figure 4.
4.83 Composi
4.84 Geograph
4.85 Composi
Figure 4.1
4.86 Composit
4.87 Composit
on Level 1
Figure 4.6
4.88 Composit
on Level 2
Figure 4.6
4.89 Percentage
Composite
4.90 Percentage
Composite
4.91 Composite
Figure 4.1
4.92 Composite
4.93 Geographic

4.75 Composite Isotachs and Streamlines, Level 3 - *L2A* Jets. As in Figure 4.1 161

4.76 Composite Divergence, Level 3 -- L2A Jets. As in Figure 4.2 161

4.77 Composite 900-mb Temperature (°C) and Mixing Ratio (g kg^{-1}) plotted on Level 1 Composite Airflow Configuration -- L2A Jets. As in Figure 4.6 162

4.78 Composite 850-mb Temperature (°C) and Mixing Ratio (g kg^{-1}) plotted on Level 2 Composite Airflow Configuration -- L2A Jets. As in Figure 4.6 162

4.79 Percentage of Jet Events with Lightning Activity plotted on Level 1 Composite Airflow Configuration -- *L2A* Jets 163

4.80 Percentage of Jet Events with Lightning Activity plotted on Level 2 Composite Airflow Configuration -- *L2A* Jets 163

4.81 Percentage of Jet Events with Lightning Activity plotted on Level 3 Composite Airflow Configuration -- *L2A* Jets 164

4.82 Composite Isotachs and Streamlines, Level 1 -- *LSKC_SWNE* Jets. As in Figure 4.1 165

4.83 Composite Divergence, Level 1 -- *LSKC_SWNE* Jets. As in Figure 4.2 165

4.84 Geographical Centers of Isotach Maxima -- *LSKC_SWNE* Jets 167

4.85 Composite Isotachs and Streamlines, Level 2 -- *LSKC_SWNE* Jets. As in Figure 4.1 168

4.86 Composite Divergence, Level 2 -- *LSKC_SWNE* Jets. As in Figure 4.2 168

4.87 Composite 900-mb Temperature (°C) and Mixing Ratio (g kg^{-1}) plotted on Level 1 Composite Airflow Configuration -- *LSKC_SWNE* Jets. As in Figure 4.6 169

4.88 Composite 850-mb Temperature (°C) and Mixing Ratio (g kg^{-1}) plotted on Level 2 Composite Airflow Configuration -- *LSKC_SWNE* Jets. As in Figure 4.6 169

4.89 Percentage of Jet Events with Lightning Activity plotted on Level 1 Composite Airflow Configuration -- *LSKC_SWNE* Jets 171

4.90 Percentage of Jet Events with Lightning Activity plotted on Level 2 Composite Airflow Configuration -- *LSKC_SWNE* Jets 171

4.91 Composite Isotachs and Streamlines, Level 1 -- *LSPLIT* Jets. As in Figure 4.1 173

4.92 Composite Divergence, Level 1 -- *LSPLIT* Jets. As in Figure 4.2 173

4.93 Geographical Centers of Isotach Maxima -- *LSPLIT* Jets 174

4.94 Composite Isotachs and St
Figure 4.1 .....

4.95 Composite Divergence, Le

4.96 Composite 900-mb Temper
on Level 1 Composite Airfl
Figure 4.6 .....

4.97 Composite 850-mb Temper
on Level 2 Composite Airfl
Figure 4.6 .....

4.98 Percentage of Jet Events wit
Composite Airflow Configu

4.99 Percentage of Jet Events wit
Composite Airflow Configu

4.100 Composite Isotachs and Str
Figure 4.1 .....

4.101 Composite Divergence, Leve

4.102 Geographical Centers of Isot

4.103 Composite Isotachs and Stre
Figure 4.1 .....

4.104 Composite Divergence, Leve

4.105 Composite 900-mb Temperat
on Level 1 Composite Airflow
Figure 4.6 .....

4.106 Composite 850-mb Temperat
on Level 2 Composite Airflow
Figure 4.6 .....

4.107 Percentage of Jet Events with
Composite Airflow Configura

4.108 Percentage of Jet Events with
Composite Airflow Configura

4.109 Composite Isotachs and Strea
Figure 4.1 .....

4.110 Composite Divergence, Level

4.111 Geographical Centers of Isotac

4.94 Composite Isotachs and Streamlines, Level 2 -- *LSPLIT* Jets. As in Figure 4.1 176

4.95 Composite Divergence, Level 2 -- *LSPLIT* Jets. As in Figure 4.2 176

4.96 Composite 900-mb Temperature (°C) and Mixing Ratio (g kg^{-1}) plotted on Level 1 Composite Airflow Configuration -- *LSPLIT* Jets. As in Figure 4.6 177

4.97 Composite 850-mb Temperature (°C) and Mixing Ratio (g kg^{-1}) plotted on Level 2 Composite Airflow Configuration -- *LSPLIT* Jets. As in Figure 4.6 177

4.98 Percentage of Jet Events with Lightning Activity plotted on Level 1 Composite Airflow Configuration -- *LSPLIT* Jets 178

4.99 Percentage of Jet Events with Lightning Activity plotted on Level 2 Composite Airflow Configuration -- *LSPLIT* Jets 178

4.100 Composite Isotachs and Streamlines, Level 1 -- *LKC_SWNE* Jets. As in Figure 4.1 180

4.101 Composite Divergence, Level 1 -- *LKC_SWNE* Jets. As in Figure 4.2 180

4.102 Geographical Centers of Isotach Maxima -- *LKC_SWNE* Jets 181

4.103 Composite Isotachs and Streamlines, Level 2 -- *LKC_SWNE* Jets. As in Figure 4.1 183

4.104 Composite Divergence, Level 2 -- *LKC_SWNE* Jets. As in Figure 4.2 183

4.105 Composite 900-mb Temperature (°C) and Mixing Ratio (g kg^{-1}) plotted on Level 1 Composite Airflow Configuration -- *LKC_SWNE* Jets. As in Figure 4.6 184

4.106 Composite 850-mb Temperature (°C) and Mixing Ratio (g kg^{-1}) plotted on Level 2 Composite Airflow Configuration -- *LKC_SWNE* Jets. As in Figure 4.6 184

4.107 Percentage of Jet Events with Lightning Activity plotted on Level 1 Composite Airflow Configuration -- *LKC_SWNE* Jets 186

4.108 Percentage of Jet Events with Lightning Activity plotted on Level 2 Composite Airflow Configuration -- *LKC_SWNE* Jets 186

4.109 Composite Isotachs and Streamlines, Level 1 -- *LCC* Jets. As in Figure 4.1 187

4.110 Composite Divergence, Level 1 -- *LCC* Jets. As in Figure 4.2 187

4.111 Geographical Centers of Isotach Maxima -- *LCC* Jets 189

4.112 Composite Isotachs and St
Figure 4.1 .....

4.113 Composite Divergence, Le

4.114 Composite Isotachs and St
Figure 4.1 .....

4.115 Composite Divergence, Le

4.116 Composite 900-mb Temper
on Level 1 Composite Airfl
Figure 4.6 .....

4.117 Composite 850-mb Temper
on Level 2 Composite Airfl
Figure 4.6 .....

4.118 Percentage of Jet Events wit
Composite Airflow Configu

4.119 Percentage of Jet Events wit
Composite Airflow Configu

4.120 Percentage of Jet Events wit
Composite Airflow Configu

4.121 Airflow Configuration Types

5.1 Composite Surface Pressure
Configuration -- *AC_EW* Jets
dashed lines are streamlines,

5.2 Composite 12-h Surface Pres
Composite Airflow Configur
equal 12-h pressure change (i
light solid lines are isotachs ...

5.3 Composite Geostrophic Wind
scale arrow is 10 ms^{-1} .....

5.4 Composite Ageostrophic Win

5.5 Composite 500-mb Geopotent
Airflow Configuration -- *AC_*
geopotential height (in meters)
solid lines are isotachs .....

5.6 Composite 200-mb Isotachs ar
Composite Airflow Configura
200-mb isotachs (in ms^{-1}); dark
light dashed lines are low-level
isotachs.....

4.112 Composite Isotachs and Streamlines, Level 2 -- *LCC* Jets. As in Figure 4.1 190

4.113 Composite Divergence, Level 2 -- *LCC* Jets. As in Figure 4.2 190

4.114 Composite Isotachs and Streamlines, Level 3 -- *LCC* Jets. As in Figure 4.1 191

4.115 Composite Divergence, Level 3 -- *LCC* Jets. As in Figure 4.2 191

4.116 Composite 900-mb Temperature (°C) and Mixing Ratio (g kg^{-1}) plotted on Level 1 Composite Airflow Configuration -- *LCC* Jets. As in Figure 4.6 193

4.117 Composite 850-mb Temperature (°C) and Mixing Ratio (g kg^{-1}) plotted on Level 2 Composite Airflow Configuration -- *LCC* Jets. As in Figure 4.6 193

4.118 Percentage of Jet Events with Lightning Activity plotted on Level 1 Composite Airflow Configuration -- *LCC* Jets 194

4.119 Percentage of Jet Events with Lightning Activity plotted on Level 2 Composite Airflow Configuration -- *LCC* Jets 194

4.120 Percentage of Jet Events with Lightning Activity plotted on Level 3 Composite Airflow Configuration -- *LCC* Jets 195

4.121 Airflow Configuration Types 197

5.1 Composite Surface Pressure plotted on Level 1 Composite Airflow Configuration -- *AC_EW* Jets. Dark solid lines are isobars (in mb), light dashed lines are streamlines, light solid lines are isotachs 204

5.2 Composite 12-h Surface Pressure Tendency plotted on Level 1 Composite Airflow Configuration -- *AC_EW* Jets. Dark lines are lines of equal 12-h pressure change (in mb). Light dashed lines are streamlines, light solid lines are isotachs 204

5.3 Composite Geostrophic Wind, Level 1 -- *AC_EW* Jets. The length of the scale arrow is 10 ms^{-1} 206

5.4 Composite Ageostrophic Wind, Level 1 -- *AC_EW* Jets. As in Figure 5.3 206

5.5 Composite 500-mb Geopotential Heights plotted on Level 1 Composite Airflow Configuration -- *AC_EW* Jets. Dark solid lines represent geopotential height (in meters), light dashed lines are streamlines, light solid lines are isotachs 208

5.6 Composite 200-mb Isotachs and Streamlines plotted on Level 1 Composite Airflow Configuration -- *AC_EW* Jets. Dark solid lines are 200-mb isotachs (in ms^{-1}); dark dashed lines are 200-mb streamlines; light dashed lines are low-level streamlines; light solid lines are low-level isotachs 209

5.7 Composite 200-mb Diverg
Configuration -- *AC_EW* Je
divergence (in 10^{-5} s^{-1}); light
solid lines are low-level iso

5.8 Composite Surface Pressur
Configuration -- *AC_ SWN*

5.9 Composite 12-h Surface Pr
Composite Airflow Config

5.10 Composite Geostrophic Wi
Figure 5.3 .....

5.11 Composite Ageostrophic W
Figure 5.3 .....

5.12 Composite 500-mb Geopote
Airflow Configuration -- *AC*

5.13 Composite 200-mb Isotachs
Composite Airflow Configu

5.14 Composite 200-mb Divergen
Configuration -- *AC_ SWNE*

5.15 Composite Surface Pressure
Configuration -- *KC_SWNE J*

5.16 Composite 12-h Surface Pres
Composite Airflow Configur

5.17 Composite Geostrophic Win
Figure 5.3 .....

5.18 Composite Ageostrophic Wi
Figure 5.3 .....

5.19 Composite 500-mb Geopoten
Airflow Configuration -- *KC_*

5.20 Composite 200-mb Isotachs a
Composite Airflow Configura

5.21 Composite 200-mb Divergenc
Configuration -- *KC_SWNE* Je

5.22 Composite Surface Pressure p
Configuration -- *SD_SWNE* Je

5.23 Composite 12-h Surface Pressu
Airflow Configuration -- *SD_S*

5.7 Composite 200-mb Divergence plotted on Level 1 Composite Airflow Configuration -- *AC_EW* Jets. Dark solid lines represent 200-mb divergence (in 10^{-5} s^{-1}); light dashed lines are low-level streamlines; light solid lines are low-level isotachs....210

5.8 Composite Surface Pressure plotted on Level 1 Composite Airflow Configuration -- *AC_ SWNE* Jets. As in Figure 5.1 211

5.9 Composite 12-h Surface Pressure Tendency plotted on Level 1 Composite Airflow Configuration -- *AC_ SWNE* Jets. As in Figure 5.2....211

5.10 Composite Geostrophic Wind, Level 1 -- *AC_SWNE* Jets. As in Figure 5.3 213

5.11 Composite Ageostrophic Wind, Level 1 -- *AC_ SWNE* Jets. As in Figure 5.3 213

5.12 Composite 500-mb Geopotential Height plotted on Level 1 Composite Airflow Configuration -- *AC_SWNE* Jets. As in Figure 5.5....214

5.13 Composite 200-mb Isotachs and Streamlines plotted on Level 1 Composite Airflow Configuration -- *AC_ SWNE* Jets. As in Figure 5.6....215

5.14 Composite 200-mb Divergence plotted on Level 1 Composite Airflow Configuration -- *AC_ SWNE* Jets. As in Figure 5.7 216

5.15 Composite Surface Pressure plotted on Level 1 Composite Airflow Configuration -- *KC_SWNE* Jets. As in Figure 5.1....217

5.16 Composite 12-h Surface Pressure Tendency plotted on Level 1 Composite Airflow Configuration -- *KC_SWNE* Jets. As in Figure 5.2 217

5.17 Composite Geostrophic Wind, Level 1 -- *KC_SWNE* Jets. As in Figure 5.3 219

5.18 Composite Ageostrophic Wind, Level 1 -- *KC_SWNE* Jets. As in Figure 5.3 219

5.19 Composite 500-mb Geopotential Height plotted on Level 1 Composite Airflow Configuration -- *KC_SWNE* Jets. As in Figure 5.5....221

5.20 Composite 200-mb Isotachs and Streamlines plotted on Level 1 Composite Airflow Configuration -- *KC_SWNE* Jets. As in Figure 5.6 221

5.21 Composite 200-mb Divergence plotted on Level 1 Composite Airflow Configuration -- *KC_SWNE* Jets. As in Figure 5.7....222

5.22 Composite Surface Pressure plotted on Level 1 Composite Airflow Configuration -- *SD_SWNE* Jets. As in Figure 5.1 224

5.23 Composite 12-h Surface Pressure Tendency plotted on Level 1 Composite Airflow Configuration -- *SD_SWNE* Jets. As in Figure 5.2....224

5.24 Composite Geostrophic W
Figure 5.3 .....

5.25 Composite Ageostrophic W
Figure 5.3 .....

5.26 Composite 500-mb Geopot
Airflow Configuration -- SI

5.27 Composite 200-mb Isotachs
Composite Airflow Configu

5.28 Composite 200-mb Diverge
Configuration -- SD_SWNE

5.29 Composite Surface Pressure
Configuration -- SD_NWSE

5.30 Composite 12-h Surface Pres
Composite Airflow Configu

5.31 Composite Geostrophic Wir
Figure 5.3 .....

5.32 Composite Ageostrophic Wi
Figure 5.3 .....

5.33 Composite 500-mb Geopoter
Airflow Configuration -- SD_

5.34 Composite 200-mb Isotachs a
Composite Airflow Configur

5.35 Composite 200-mb Divergenc
Configuration -- SD_NWSE Je

5.36 Composite Surface Pressure p
Configuration -- CC Jets. As i

5.37 Composite 12-h Surface Press
Airflow Configuration -- CC Je

5.38 Composite Geostrophic Wind

5.39 Composite Ageostrophic Win

5.40 Composite 500-mb Geopotent
Airflow Configuration -- CC Je

5.41 Composite 200-mb Isotachs ar
Composite Airflow Configurat

5.42 Composite 200-mb Divergence
Configuration -- CC Jets. As in

5.24 Composite Geostrophic Wind, Level 1 -- *SD_SWNE* Jets. As in Figure 5.3 225

5.25 Composite Ageostrophic Wind, Level 1 -- *SD_SWNE* Jets. As in Figure 5.3 225

5.26 Composite 500-mb Geopotential Height plotted on Level 1 Composite Airflow Configuration -- *SD_SWNE* Jets. As in Figure 5.5 226

5.27 Composite 200-mb Isotachs and Streamlines plotted on Level 1 Composite Airflow Configuration -- *SD_SWNE* Jets. As in Figure 5.6 227

5.28 Composite 200-mb Divergence plotted on Level 1 Composite Airflow Configuration -- *SD_SWNE* Jets. As in Figure 5.7 228

5.29 Composite Surface Pressure plotted on Level 1 Composite Airflow Configuration -- *SD_NWSE* Jets. As in Figure 5.1 229

5.30 Composite 12-h Surface Pressure Tendency plotted on Level 1 Composite Airflow Configuration -- *SD_NWSE* Jets. As in Figure 5.2 229

5.31 Composite Geostrophic Wind, Level 1 -- *SD_NWSE* Jets. As in Figure 5.3 231

5.32 Composite Ageostrophic Wind, Level 1 -- *SD_NWSE* Jets. As in Figure 5.3 231

5.33 Composite 500-mb Geopotential Height plotted on Level 1 Composite Airflow Configuration -- *SD_NWSE* Jets. As in Figure 5.5 232

5.34 Composite 200-mb Isotachs and Streamlines plotted on Level 1 Composite Airflow Configuration -- *SD_NWSE* Jets. As in Figure 5.6 232

5.35 Composite 200-mb Divergence plotted on Level 1 Composite Airflow Configuration -- *SD_NWSE* Jets. As in Figure 5.7 233

5.36 Composite Surface Pressure plotted on Level 1 Composite Airflow Configuration -- *CC* Jets. As in Figure 5.1 234

5.37 Composite 12-h Surface Pressure Tendency plotted on Level 1 Composite Airflow Configuration -- *CC* Jets. As in Figure 5.2 234

5.38 Composite Geostrophic Wind, Level 1 -- *CC* Jets. As in Figure 5.3 236

5.39 Composite Ageostrophic Wind, Level 1 -- *CC* Jets. As in Figure 5.3 236

5.40 Composite 500-mb Geopotential Height plotted on Level 1 Composite Airflow Configuration -- *CC* Jets. As in Figure 5.5 237

5.41 Composite 200-mb Isotachs and Streamlines plotted on Level 1 Composite Airflow Configuration -- *CC* Jets. As in Figure 5.6 238

5.42 Composite 200-mb Divergence plotted on Level 1 Composite Airflow Configuration -- *CC* Jets. As in Figure 5.7 238

5.43 Composite Surface Pressur
Configuration -- LAC_SWN

5.44 Composite 12-h Surface Pr
Composite Airflow Config

5.45 Composite Geostrophic Wi
Figure 5.3 .....

5.46 Composite Ageostrophic W
Figure 5.3 .....

5.47 Composite 500-mb Geopote
Airflow Configuration -- LA

5.48 Composite 200-mb Isotachs
Composite Airflow Configu

5.49 Composite 200-mb Diverge
Configuration -- LAC_SWN

5.50 Composite Surface Pressure
Configuration -- L2A Jets. A

5.51 Composite 12-h Surface Pre
Composite Airflow Configu

5.52 Composite Geostrophic Wir

5.53 Composite Ageostrophic Wi

5.54 Composite 500-mb Geopoten
Airflow Configuration -- L2A

5.55 Composite 200-mb Isotachs
Composite Airflow Configur

5.56 Composite 200-mb Divergen
Configuration -- L2A Jets. As

5.57 Composite Surface Pressure
Configuration -- LSKC_SWN

5.58 Composite 12-h Surface Pres
Composite Airflow Configur

5.59 Composite Geostrophic Wind
Figure 5.3 .....

5.60 Composite Ageostrophic Wir
Figure 5.3 .....

5.61 Composite 500-mb Geopoten
Airflow Configuration -- LSK

5.43 Composite Surface Pressure plotted on Level 1 Composite Airflow Configuration -- *LAC_SWNE* Jets. As in Figure 5.1 240

5.44 Composite 12-h Surface Pressure Tendency plotted on Level 1 Composite Airflow Configuration -- *LAC_SWNE* Jets. As in Figure 5.2 240

5.45 Composite Geostrophic Wind, Level 1 -- *LAC_SWNE* Jets. As in Figure 5.3 242

5.46 Composite Ageostrophic Wind, Level 1 -- *LAC_SWNE* Jets. As in Figure 5.3 242

5.47 Composite 500-mb Geopotential Height plotted on Level 1 Composite Airflow Configuration -- *LAC_SWNE* Jets. As in Figure 5.5 243

5.48 Composite 200-mb Isotachs and Streamlines plotted on Level 1 Composite Airflow Configuration -- *LAC_SWNE* Jets. As in Figure 5.6 244

5.49 Composite 200-mb Divergence plotted on Level 1 Composite Airflow Configuration -- *LAC_SWNE* Jets. As in Figure 5.7 244

5.50 Composite Surface Pressure plotted on Level 1 Composite Airflow Configuration -- *L2A* Jets. As in Figure 5.1 246

5.51 Composite 12-h Surface Pressure Tendency plotted on Level 1 Composite Airflow Configuration -- *L2A* Jets. As in Figure 5.2 246

5.52 Composite Geostrophic Wind, Level 1 -- *L2A* Jets. As in Figure 5.3 247

5.53 Composite Ageostrophic Wind, Level 1 -- *L2A* Jets. As in Figure 5.3 247

5.54 Composite 500-mb Geopotential Height plotted on Level 1 Composite Airflow Configuration -- *L2A* Jets. As in Figure 5.5 248

5.55 Composite 200-mb Isotachs and Streamlines plotted on Level 1 Composite Airflow Configuration -- *L2A* Jets. As in Figure 5.6 249

5.56 Composite 200-mb Divergence plotted on Level 1 Composite Airflow Configuration -- *L2A* Jets. As in Figure 5.7 249

5.57 Composite Surface Pressure plotted on Level 1 Composite Airflow Configuration -- *LSKC_SWNE* Jets. As in Figure 5.1 251

5.58 Composite 12-h Surface Pressure Tendency plotted on Level 1 Composite Airflow Configuration -- *LSKC_SWNE* Jets. As in Figure 5.2 251

5.59 Composite Geostrophic Wind, Level 1 -- *LSKC_SWNE* Jets. As in Figure 5.3 253

5.60 Composite Ageostrophic Wind, Level 1 -- *LSKC_SWNE* Jets. As in Figure 5.3 253

5.61 Composite 500-mb Geopotential Height plotted on Level 1 Composite Airflow Configuration -- *LSKC_SWNE* Jets. As in Figure 5.5 254

5.62 Composite 200-mb Isotachs
Composite Airflow Configu

5.63 Composite 200-mb Divergen
Configuration -- *LSKC_SW*

5.64 Composite Surface Pressure
Configuration -- *LSPLIT* jets

5.65 Composite 12-h Surface Pres
Composite Airflow Configu

5.66 Composite Geostrophic Win

5.67 Composite Ageostrophic Wi

5.68 Composite 500-mb Geopoten
Airflow Configuration -- *LSI*

5.69 Composite 200-mb Isotachs
Composite Airflow Configur

5.70 Composite 200-mb Divergen
Configuration -- *LSPLIT* Jets.

5.71 Composite Surface Pressure
Configuration -- *LKC_SWNE*

5.72 Composite 12-h Surface Pres
Composite Airflow Configura

5.73 Composite Geostrophic Wind
Figure 5.3 .....

5.74 Composite Ageostrophic Wir
Figure 5.3 .....

5.75 Composite 500-mb Geopotent
Airflow Configuration -- *LKC*

5.76 Composite 200-mb Isotachs a
Composite Airflow Configura

5.77 Composite 200-mb Divergenc
Configuration -- *LKC_SWNE* J

5.78 Composite Surface Pressure p
Configuration -- *LCC* Jets. As

5.79 Composite 12-h Surface Pressu

5.80 Composite Airflow Configura
Composite Geostrophic Wind,

5.62 Composite 200-mb Isotachs and Streamlines plotted on Level 1 Composite Airflow Configuration -- *LSKC_SWNE* Jets. As in Figure 5.6 254

5.63 Composite 200-mb Divergence plotted on Level 1 Composite Airflow Configuration -- *LSKC_SWNE* Jets. As in Figure 5.7.....255

5.64 Composite Surface Pressure plotted on Level 1 Composite Airflow Configuration -- *LSPLIT* Jets. As in Figure 5.1.....256

5.65 Composite 12-h Surface Pressure Tendency plotted on Level 1 Composite Airflow Configuration -- *LSPLIT* Jets. As in Figure 5.2.....256

5.66 Composite Geostrophic Wind, Level 1 -- *LSPLIT* Jets. As in Figure 5.3 258

5.67 Composite Ageostrophic Wind, Level 1 -- *LSPLIT* Jets. As in Figure 5.3 258

5.68 Composite 500-mb Geopotential Height plotted on Level 1 Composite Airflow Configuration -- *LSPLIT* Jets. As in Figure 5.5 259

5.69 Composite 200-mb Isotachs and Streamlines plotted on Level 1 Composite Airflow Configuration -- *LSPLIT* Jets. As in Figure 5.6.....259

5.70 Composite 200-mb Divergence plotted on Level 1 Composite Airflow Configuration -- *LSPLIT* Jets. As in Figure 5.7.....260

5.71 Composite Surface Pressure plotted on Level 1 Composite Airflow Configuration -- *LKC_SWNE* Jets. As in Figure 5.1.....261

5.72 Composite 12-h Surface Pressure Tendency plotted on Level 1 Composite Airflow Configuration -- *LKC_SWNE* Jets. As in Figure 5.2 261

5.73 Composite Geostrophic Wind, Level 1 -- *LKC_SWNE* Jets. As in Figure 5.3 263

5.74 Composite Ageostrophic Wind, Level 1 -- *LKC_SWNE* Jets. As in Figure 5.3 263

5.75 Composite 500-mb Geopotential Height plotted on Level 1 Composite Airflow Configuration -- *LKC_SWNE* Jets. As in Figure 5.5.....264

5.76 Composite 200-mb Isotachs and Streamlines plotted on Level 1 Composite Airflow Configuration -- *LKC_SWNE* Jets. As in Figure 5.6 265

5.77 Composite 200-mb Divergence plotted on Level 1 Composite Airflow Configuration -- *LKC_SWNE* Jets. As in Figure 5.7.....265

5.78 Composite Surface Pressure plotted on Level 1 Composite Airflow Configuration -- *LCC* Jets. As in Figure 5.1 266

5.79 Composite 12-h Surface Pressure Tendency plotted on Level 1 Composite Airflow Configuration -- *LCC* Jets. As in Figure 5.2.....266

5.80 Composite Geostrophic Wind, Level 1 -- *LCC* Jets. As in Figure 5.3.....268

5.81 Composite Ageostrophic W

5.82 Composite 500-mb Geopote
Airflow Configuration -- LC

5.83 Composite 200-mb Isotachs
Composite Airflow Configu

5.84 Composite 200-mb Diverge
Configuration -- LCC Jets. A

5.81 Composite Ageostrophic Wind, Level 1 -- *LCC* Jets. As in Figure 5.3.....268

5.82 Composite 500-mb Geopotential Height plotted on Level 1 Composite Airflow Configuration -- *LCC* Jets. As in Figure 5.5.....269

5.83 Composite 200-mb Isotachs and Streamlines plotted on Level 1 Composite Airflow Configuration -- *LCC* Jets. As in Figure 5.6.....270

5.84 Composite 200-mb Divergence plotted on Level 1 Composite Airflow Configuration -- *LCC* Jets. As in Figure 5.7.....270

INTRODUCTION A

1.0verview and General Objectives

Lower tropospheric wind maxim

requently in many parts of the world.

region for low-level wind maxima is th

within the North American continent w

although less frequently, include Calif

the Carolina coastal plain (Sjostedt et a

and the Canadian Maritimes (Kreitzber

Occurrences of low-level wind maxima

1981, 1982), Africa (Findlater 1969; Ar

and Spencer-Smith 1988; Jury and Tos

Keenan et al. 1989), Asia (Findlater 196

and Ogura 1991; Chen and Chen 1995),

1994), and Antarctica (Chiba and Koba

Low-level jets have been attributed

of thunderstorms (Means 1952; Pitchfo

others) and mesoscale convective syste

Convective activity, particularly at night

differential advection of heat and moist

convergence downstream of the jet max

Chapter 1

INTRODUCTION AND REVIEW OF LITERATURE

1. Overview and General Objectives

Lower tropospheric wind maxima, or jets, are mesoscale phenomena that occur frequently in many parts of the world. In the United States, the geographically preferred region for low-level wind maxima is the central Plains (Bonner 1968). Other areas within the North American continent where low-level wind maxima have been reported, although less frequently, include California (Douglas 1995; Burk and Thompson 1996), the Carolina coastal plain (Sjostedt et al. 1990; Doyle and Warner 1991), New England and the Canadian Maritimes (Kreitzberg 1968; Dickison and Neumann 1982). Occurrences of low-level wind maxima have also been noted in south America (Virji 1981, 1982), Africa (Findlater 1969; Ardanuy 1979; Anderson 1984; Kelbe 1988; Jury and Spencer-Smith 1988; Jury and Tosen 1989), Australia (Wilson 1975; Brook 1985; Keenan et al. 1989), Asia (Findlater 1969; Tao and Chen 1987; Chou et al. 1990; Nagata and Ogura 1991; Chen and Chen 1995), Europe (Thorpe and Guymer 1977; Beyrich 1994), and Antarctica (Chiba and Kobayashi 1986).

Low-level jets have been attributed a major role in the initiation and intensification of thunderstorms (Means 1952; Pitchford and London 1962; Bonner 1966, 1968; and others) and mesoscale convective systems (Maddox and Doswell 1982; Maddox 1983). Convective activity, particularly at night, is thought to be initiated or enhanced through differential advection of heat and moisture by low-level jets (Uccellini 1980) and convergence downstream of the jet maxima (Bonner et al. 1968).

An understanding of the role of l

owever, complicated by the fact that

t low-level wind maxima in a variety

used to describe a boundary-layer win

oscillations in height, speed and direct

within an extended area of surface hig

disturbances such as frontal boundarie

pronounced in the early morning hours

of approximately 700 m above ground

land, is also applied to synoptically-d

boundary layer, often up to heights of

lack the pronounced diurnal oscillation

maximum. Recently, a number of inve

nomenclature between the two broad t

Chen et al. 1994).

This study has three main goals.

understanding of lower tropospheric je

variations in the characteristics of low-

United States. Second, the relationship

pattern of convection is examined. Thi

region, it is possible to distinguish betw

driven low-level wind maxima. In the

the temporal, and particularly the spat

maxima are much more complex and v

distribution of convection is clearly rel

maxima, and, finally, that it is not poss

forced and synoptically-driven wind m

An understanding of the role of low-level wind maxima in convective activity is, however, complicated by the fact that the term low-level jet is applied indiscriminately to low-level wind maxima in a variety of settings. On the one hand, 'low-level jet' is used to describe a boundary-layer wind maximum which exhibits strong diurnal oscillations in height, speed and direction. This wind maximum is generally observed within an extended area of surface high pressure in the absence of synoptic-scale disturbances such as frontal boundaries or transitory low pressure systems. It is most pronounced in the early morning hours when maximum speeds are observed at a height of approximately 700 m above ground level (AGL). The term 'low-level jet', on the other hand, is also applied to synoptically-driven wind maxima that extend beyond the boundary layer, often up to heights of 3 km AGL or more. These wind maxima often lack the pronounced diurnal oscillation which is so typical of the boundary-layer wind maximum. Recently, a number of investigators have called for a differentiation in nomenclature between the two broad types of low-level wind maxima (Uccellini 1990; Chen et al. 1994).

This study has three main goals. First, it aims to contribute to a better understanding of lower tropospheric jets by identifying the temporal and spatial variations in the characteristics of low-level wind maxima in the Central Plains of the United States. Second, the relationship between low-level wind maxima and the spatial pattern of convection is examined. Thirdly, it attempts to determine whether, for this region, it is possible to distinguish between boundary-layer forced and synoptically-driven low-level wind maxima. In the following chapters, it will be demonstrated that the temporal, and particularly the spatial characteristics of lower tropospheric wind maxima are much more complex and varied than previously thought, that the distribution of convection is clearly related to the spatial configuration of the wind maxima, and, finally, that it is not possible to easily distinguish between boundary-layer forced and synoptically-driven wind maxima. It appears, instead, that a combination

of large-scale setting and favorable bou

rmation of strong low-level wind ma

The study is organized into seve

comprehensive overview of the literatu

pecific objectives of this study. The li

wind maxima as their primary focus as

play a secondary role in the large-scale

ntroduces the data and methods utiliz

f this study, a number of individual a

describes the data sets and the study p

steps. The results for the first part of th

characteristics of all southerly low-level

warm-seasons in the Great Plains regio

described with respect to their tempora

characteristics. A subset of jet events is

the focus lies on the spatial configuratio

examines the wind field, the thermodyn

for twelve types of low-level wind maxi

Chapter 5, the typical large-scale enviro

low-level wind maxima are observed is

nature of lower-, mid- and upper-tropo

results of this empirical study are reviev

of lower tropospheric wind maxima. Cl

the findings and suggestions for further

of large-scale setting and favorable boundary-layer conditions are necessary for the formation of strong low-level wind maxima.

The study is organized into seven chapters. In the remainder of this chapter, a comprehensive overview of the literature is presented followed by a description of the specific objectives of this study. The literature review details studies that have low-level wind maxima as their primary focus as well as studies where low-level wind maxima play a secondary role in the large-scale environment of other phenomena. Chapter 2 introduces the data and methods utilized in the study. To meet the multiple objectives of this study, a number of individual analysis steps were required. Chapter 2 first describes the data sets and the study period, and then details the individual analysis steps. The results for the first part of the analysis are provided in Chapter 3, where the characteristics of all southerly low-level wind maxima that were observed during two warm-seasons in the Great Plains region are summarized. The wind maxima are described with respect to their temporal, spatial, speed, height, and directional characteristics. A subset of jet events is further investigated in Chapters 4 and 5 where the focus lies on the spatial configuration of the different analysis variables. Chapter 4 examines the wind field, the thermodynamic environment and the resulting convection for twelve types of low-level wind maxima with distinct spatial configuration. In Chapter 5, the typical large-scale environment within which the twelve different types of low-level wind maxima are observed is investigated. The environment is depicted by means of lower-, mid- and upper-tropospheric large-scale patterns. In Chapter 6, the results of this empirical study are reviewed and put into the context of previous studies of lower tropospheric wind maxima. Chapter 7 concludes this study with a summary of the findings and suggestions for further research.

2 Review of Literature

Low-level wind maxima have be

decades. These studies fall into two b

level wind maximum as their primary

maximum is analyzed as part of larger

the literature, the terminology recomm

a distinction is made between a) those

thought to be forced by boundary-laye

wind maxima that appear to be synopt

maxima within the planetary boundary

strong diurnal variation be referred to

maxima between the 900-mb and 600-m

kilometer above sea level) that are asso

referred to as "low-level jets" (LLJ). He

"low-level wind maxima" and "jets" w

and synoptically-driven wind maxima,

two types of wind maxima.

While only a few climatological a

studies of low-level wind maxima are n

the secondary focus are equally numero

discussed first, followed by the case stu

been categorized into either boundary-l

interpretation of the type of low-level w

study. Case studies of boundary-layer

studies of low-level jets. Within each ca

by subject area.

2. Review of Literature

Low-level wind maxima have been studied rather extensively for the last few decades. These studies fall into two broad categories: (a) studies which have the low-level wind maximum as their primary focus and (b) studies in which the low-level wind maximum is analyzed as part of larger circulation systems. In the following review of the literature, the terminology recommended by Chen et al. (1994) is adhered to, in that a distinction is made between a) those studies primarily concerned with wind maxima thought to be forced by boundary-layer mechanisms and b) those studies concerned with wind maxima that appear to be synoptically driven. Chen recommended that wind maxima within the planetary boundary layer with very strong vertical wind shear and strong diurnal variation be referred to as "boundary-layer jets" (BLJ) whereas wind maxima between the 900-mb and 600-mb levels (approximately 1 kilometer to 4 kilometer above sea level) that are associated with synoptic-scale weather systems be referred to as "low-level jets" (LLJ). However, in the following chapters, the terms "low-level wind maxima" and "jets" will be used to refer to both boundary-layer forced and synoptically-driven wind maxima, as no a priori distinction is made between the two types of wind maxima.

While only a few climatological analyses of low-level wind maxima exist, case studies of low-level wind maxima are numerous. Studies in which low-level winds are the secondary focus are equally numerous. Below, the few climatological studies are discussed first, followed by the case studies. As indicated above, case studies have been categorized into either boundary-layer jet cases or low-level jet cases based on my interpretation of the type of low-level wind maximum that is the main focus of the study. Case studies of boundary-layer jets are reviewed first, followed by the case studies of low-level jets. Within each category, the review of case studies is organized by subject area.

As mentioned previously, very f

treatment of low-level wind maxima.

Bonner's (1968) classic study of low-le

Employing two years of observations

rawinsonde stations, Bonner first exam

variations in the frequency of low leve

as a 'significant, low level maximum i

part of his study he did not take into a

of the observed jets. Therefore, statisti

distinction between boundary-layer jet

study. To incorporate the strength of w

categorization with criterion-0 jets bein

defined. Regardless of the selection cri

frequency is elongated in a north-south

Oklahoma-Kansas border. A much we

along the East Coast.

Bonner found that in the Great Pl

observations occur during the warm sea

time, southerly wind maxima predomin

are recorded more frequently in the mo

pronounced in the summer months than

morning jets is dependent upon latitude

jets evident at about 35° N during both

In the second part of his study, Bo

stations in the central United States. H

synoptic or subsynoptic influences were

a. Climatologies of North American Low-level Wind Maxima

As mentioned previously, very few authors have attempted a climatological treatment of low-level wind maxima. The earliest and most frequently-cited work is Bonner's (1968) classic study of low-level wind maxima in the United States. Employing two years of observations from the standard network of radiosonde/ rawinsonde stations, Bonner first examined the geographical, seasonal and diurnal variations in the frequency of low level wind maxima. Bonner defined a jet observation as a "significant, low level maximum in vertical profiles of the wind speed." In the first part of his study he did not take into account the synoptic or subsynoptic environment of the observed jets. Therefore, statistical summaries in this part do not make the distinction between boundary-layer jets and low-level jets that is proposed in this study. To incorporate the strength of wind maxima, Bonner employed a four-tier categorization with criterion-0 jets being the weakest and criterion-3 jets being the best defined. Regardless of the selection criterion, Bonner found that the maximum in jet frequency is elongated in a north-south direction and peaks at 95° to 100° W on the Oklahoma-Kansas border. A much weaker, secondary frequency maximum is evident along the East Coast.

Bonner found that in the Great Plains roughly 55 to 60 percent of all jet observations occur during the warm season (April through September). During that time, southerly wind maxima predominate. While low level wind maxima as a whole are recorded more frequently in the morning (1200 UTC), the diurnal variation is more pronounced in the summer months than during the cold season. The predominance of morning jets is dependent upon latitude, as well, with the highest percentage of morning jets evident at about 35° N during both summer and winter.

In the second part of his study, Bonner focused on southerly observations at 22 stations in the central United States. He explicitly excluded observations where synoptic or subsynoptic influences were present. Thus, this part of his analysis focused

on wind maxima which presumably w

southerly jets displayed a frequency m

While they were much more frequentl

exclusively a nocturnal phenomenon.

time of day, mean altitudes and mean

and 0600 CST at each station. As exp

were lower at 0600 CST than at 1800

755 m AGL with a standard deviation

found at 755 m points to a serious lim

height lies above the height of instrum

pressure level which is most commonl

height. Bonner noted, jet speeds varie

impossible to draw any isotach patter

intensity of the low level jet. At indivi

at night, as expected. Jet velocity did s

early morning jets being particularly fr

To describe the structure of the so

calculated composites of wind speed, t

in a coordinate system centered on the

drawn for 0.5 km and 1.0 km AGL. Th

0.5 km or 1.0 km level, was selected for

temperature and moisture patterns we

appeared to have a natural limit of app

subsequent decrease in wind speed alo

convergence downstream of the jet max

km of the jet maximum. The composit

approximately 600-700 km wide. Furth

on wind maxima which presumably would classify as 'boundary-layer jets.' These southerly jets displayed a frequency maximum in the months of August and September. While they were much more frequently observed in the early morning, they were not exclusively a nocturnal phenomenon. To compare the height and strength of the jets by time of day, mean altitudes and mean speeds were computed separately for 1800 CST and 0600 CST at each station. As expected, the mean altitudes at almost all stations were lower at 0600 CST than at 1800 CST. At 0600 CST, the overall mean height was 785 m AGL with a standard deviation of 127 m. The fact that the mean height was found at 785 m points to a serious limitation of many boundary-layer jet studies. This height lies above the height of instrument towers and below the 850-mb standard pressure level which is most commonly used for low-level wind studies. Unlike jet height, Bonner noted, jet speeds varied considerably from station to station and it was impossible to draw any isotach patterns which could indicate the mean speed and intensity of the low level jet. At individual stations, jet speeds were not always stronger at night, as expected. Jet velocity did show some annual variation, however, with strong early morning jets being particularly frequent in spring and late summer.

To describe the structure of the southerly low-level wind maxima, Bonner calculated composites of wind speed, temperature and mixing ratio for 28 morning jets in a coordinate system centered on the isotach maximum. Isotachs and streamlines were drawn for 0.5 km and 1.0 km AGL. The level closest to the isotach maximum, either the 0.5 km or 1.0 km level, was selected for subsequent analysis. In addition, the average temperature and moisture patterns were plotted for the 850 mb level. Wind speeds appeared to have a natural limit of approximately 55-50 kts. The increase and subsequent decrease in wind speed along the main axis of the jet resulted in mean convergence downstream of the jet maximum and mean divergence upstream within 150 km of the jet maximum. The composites also indicated that the average jet was approximately 600-700 km wide. Furthermore, the average temperature and moisture

patterns showed a gradient across the

and lowest in the northeast quadrant.

Since Bonner's classic study, onl

climatologically analyze the Great Plai

1995) employed two years of profiler

examine the frequency of warm season

maxima. They contrasted stronger wi

criteria used by Bonner (1968) with we

wind events (SWE). Mitchell et al.'s ar

maxima typically is largest in an elong

northern edge of their study area (i.e. s

finding, they showed a peak in total je

specifically in September. The one-hou

narrow the time of maximum jet occur

to the frequency maximum between 06

agreement with previous studies, Mitc

speed and direction of warm-season lo

became more pronounced as the wind

In the second part of their study,

scheme based on dynamical features a

weather elements (Pielke et al. 1991) to

frequency of wind maxima for differen

low-level wind maxima were most com

extratropical cyclone, under a polar hig

subtropical ridge. Low-level wind max

warm front or behind a cold front, whic

occurrence of frontal passages and thei

patterns showed a gradient across the jet with highest values in the southwest quadrant and lowest in the northeast quadrant.

Since Bonner's classic study, only one additional attempt has been made to climatologically analyze the Great Plains low-level wind maximum. Mitchell et al. (1995) employed two years of profiler data averaged over one-hourly intervals to examine the frequency of warm season (April - September) southerly low-level wind maxima. They contrasted stronger wind maxima which generally met the selection criteria used by Bonner (1968) with weaker wind maxima which they termed southerly wind events (SWE). Mitchell et al.'s analysis suggested that the speed of southerly wind maxima typically is largest in an elongated band from southeastern Oklahoma to the northern edge of their study area (i.e. southern Nebraska). Consistent with Bonner's finding, they showed a peak in total jet frequency at the end of the warm season, specifically in September. The one-hourly resolution of the profiler data allowed them to narrow the time of maximum jet occurrence to between 0600 and 0900 UTC, compared to the frequency maximum between 0600 and 1200 UTC identified by Bonner. In agreement with previous studies, Mitchell et al. detected a diurnal oscillation in the speed and direction of warm-season low-level wind maxima. The diurnal oscillation became more pronounced as the wind speed increased.

In the second part of their study, Mitchell et al. used a predetermined classification scheme based on dynamical features and airmass characteristics rather than on surface weather elements (Pielke et al. 1991) to evaluate, for one year (1992), the relative frequency of wind maxima for different synoptic environments. The authors found that low-level wind maxima were most commonly located within the warm sector of an extratropical cyclone, under a polar high, and in the vicinity or to the west of a subtropical ridge. Low-level wind maxima were observed less frequently ahead of a warm front or behind a cold front, which they attributed to both the infrequent occurrence of frontal passages and their transient nature. Mitchell et al. then normalized

the number of hours a wind maximum

ts synoptic class, which they interpret

arge-scale setting was to jet occurrenc

extratropical cyclone was particularly

passages were seen as neither prohibiti

gries some of the earlier findings whe

component to the formation of low-lev

vicinity or to the west of a subtropical

location under a polar high was found

synoptic environment was more impor

r the weaker jets.

In the final part of their study, M

SWJ that met some but not all of the

showed less diurnal variability than th

for SWJs were generally similar to thos

frequently associated with warm front

The Carolina low-level wind max

Sisolaeti et al. (1990). Like Bonner (19

without explicitly taking the synoptic e

common features between the Carolina

ets and employing different jet criteria

maximum also was observed in the earl

600-700 m AGL. Like the Great Plains

maximum in September. However, unli

southerly direction, the Carolina jet wa

low except during spring and summer

southwesterly jets was observed.

the number of hours a wind maximum was observed by the frequency of occurrence of its synoptic class, which they interpreted as a measure for how conducive an individual large-scale setting was to jet occurrence. They found that the warm sector of an extratropical cyclone was particularly conducive to jet occurrence, whereas frontal passages were seen as neither prohibiting nor promoting jet formation. Surprisingly, given some of the earlier findings where the subtropical high was seen as an essential component to the formation of low-level southerly wind maxima, the location in the vicinity or to the west of a subtropical ridge was thought to be least conducive. The location under a polar high was found to be equally unconducive. In general, the synoptic environment was more important for the stronger wind maxima as compared to the weaker jets.

In the final part of their study, Mitchell et al. evaluated southerly wind events (SWE) that met some but not all of the wind speed criteria by Bonner (1968). SWEs showed less diurnal variability than the stronger jets. Also, while synoptic environments for SWEs were generally similar to those for the stronger wind maxima, SWEs were more frequently associated with warm fronts.

The Carolina low-level wind maximum was the focus of a climatological study by Sjostedt et al. (1990). Like Bonner (1968), Sjostedt et al. focused on wind maxima without explicitly taking the synoptic environment into consideration. They found some common features between the Carolina and Great Plains jets despite using different data sets and employing different jet criteria than Bonner. The Carolina low-level wind maximum also was observed in the early morning hours and had typical altitudes of 600-700 m AGL. Like the Great Plains jet, the Carolina jet had a slight frequency maximum in September. However, unlike the former which was predominantly from a southerly direction, the Carolina jet was most frequently associated with northeasterly flow except during spring and summer when a higher percentage of southerly or southwesterly jets was observed.

A secondary goal of Sjostedt et a

between low-level wind maxima and

strong low-level wind maxima which

examined the synoptic conditions by

850 mb and 300 mb constant pressure

maps, 850 mb and 300 mb constant pr

a description of the relative positions

that most frequently an upper-troposp

observation time preceding the low-lev

subsequently formed on the anticyclon

upper-level jet's exit region. The autho

troposphere was observed in connecti

vorticity by the upper- tropospheric je

tropospheric air in the form of a low-le

toward a downstream region of maxim

Case Studies and Modeling Studies of

With respect to boundary-layer j

theoretical studies that focused mainly

studies that attempted to include othe

transfer can be observed. The earliest

from instrument towers, which only pe

planetary boundary layer. Wind maxi

analyzed. While rawinsonde and prof

maxima at higher levels, the analysis o

Compared to the other wind maxima, th

850-mb winds below a certain threshold a

A secondary goal of Sjostedt et al.'s study was to examine the relationship between low-level wind maxima and upper-level jets. The authors singled out fifty strong low-level wind maxima which met more stringent selection criteria[1] and examined the synoptic conditions by subjectively interpreting the surface chart and the 850 mb and 300 mb constant pressure charts. Since Sjostedt et al. relied on surface maps, 850 mb and 300 mb constant pressure charts only, their discussion was limited to a description of the relative positions of low-level and upper-level features. They found that most frequently an upper-tropospheric jet streak was evident at the 0000 UTC observation time preceding the low-level wind maximum. The wind maximum subsequently formed on the anticyclonic shear side of the 300-mb jet and within the upper-level jet's exit region. The authors hypothesized that sinking motion in the middle troposphere was observed in connection with the advection of anticyclonic shear vorticity by the upper- tropospheric jet streak. Beneath this sinking motion, lower tropospheric air in the form of a low-level wind maximum accelerated horizontally toward a downstream region of maximum sea-level pressure falls.

b. Case Studies and Modeling Studies of Boundary-Layer Jets

With respect to boundary-layer jet studies, a historical trend from descriptive and theoretical studies that focused mainly on the kinetic properties of the jet to modeling studies that attempted to include other parameters such as soil moisture and latent heat transfer can be observed. The earliest studies of boundary-layer jets were conducted from instrument towers, which only permitted the detection of wind maxima within the planetary boundary layer. Wind maxima above the height of the tower could not be analyzed. While rawinsonde and profiler observations enabled the detection of wind maxima at higher levels, the analysis of the wind maxima was frequently limited by the

[1] Compared to the other wind maxima, the stronger wind maxima had to display surface and 850-mb winds below a certain threshold and a stronger difference in wind speed between the

choice of standard pressure surfaces a
pressure surface, the 850-mb level, has
layer wind jet.

This section of the literature revi
jet by discussing the tropospheric osci
variations of the boundary-layer jet its
variations of the jet will be related to b
behavior of the jet. Finally, the advect
reviewed.

1) TROPOSPHERIC OSCILLATIONS

The boundary-layer wind maxim
tropospheric wind oscillation that exte
(Hering and Borden 1962; Darkow and
extends over a broad region from the
Texas coast northward to 45° N. In or
Hering and Borden (1962) calculated th
individual observation times (0000, 06
calculated over all observation times.
three vertical layers with distinct varia
layers were separated by levels of non
lowest oscillation (surface to 2 km) had
departure vector was observed betwee
the east during the early morning hour
afternoon. The average wind speed in
was twice the daytime speed. In a late

surface and the wind maximum in additio

choice of standard pressure surfaces as analysis surfaces. The lowest mandatory pressure surface, the 850-mb level, has been shown to generally lie above the boundary-layer wind jet.

This section of the literature review will first set the stage for the boundary-layer jet by discussing the tropospheric oscillation of which it is part. Next, the temporal variations of the boundary-layer jet itself will be presented. Thirdly, the temporal variations of the jet will be related to boundary-layer processes that influence the behavior of the jet. Finally, the advective and kinematic properties of the jet will be reviewed.

1) TROPOSPHERIC OSCILLATIONS

The boundary-layer wind maximum is part of a complex but well-defined diurnal tropospheric wind oscillation that extends from the surface up to approximately 30 km (Hering and Borden 1962; Darkow and Thompson 1968). This prominent oscillation extends over a broad region from the Rocky Mountains eastward to 85° W and from the Texas coast northward to 45° N. In one of the first studies to document this oscillation, Hering and Borden (1962) calculated the departure of the monthly mean wind vector for individual observation times (0000, 0600, 1200, 1800 CST) from a mean vector calculated over all observation times. The resulting departure vectors suggested that three vertical layers with distinct variations in wind speed and direction existed. These layers were separated by levels of non-oscillation at about 2 km and 8 km AGL. The lowest oscillation (surface to 2 km) had a diurnal amplitude of 3.5 ms^{-1}. The maximum departure vector was observed between 0.5 and 1 km AGL, and was directed toward the east during the early morning hours and toward the Rocky Mountains in the afternoon. The average wind speed in the boundary layer during the early morning hours was twice the daytime speed. In a later study, Bonner and Paegle (1970) confirmed

---

surface and the wind maximum in addition to the other criteria.

1.5-1.0 km as the height of the maximu

ndicated a slightly weaker diurnal am

detected a middle-layer oscillation (2 k

had its maximum diurnal variation at

scillation was found with a departure

departure vectors at the different levels

departure occurred 3 - 4 h later than th

ayer, which in turn followed the maxir

about the same time interval.

Darkow and Thompson (1968), e

examined the effect of an oscillating bo

hypothesized that the two oscillations

above the boundary layer were ageostr

oscillations within the boundary layer

ageostrophic wind is defined as the "ve

wind and the geostrophic wind" (Husc

Borden attempted to duplicate the gros

They assumed that the geostrophic win

ageostrophic components were perturb

their model they represented the atmos

homogeneous, incompressible fluid. Th

introduced into that upper fluid by requ

bottom of the upper fluid be identical t

boundary layer. The model results indi

horizontal wind vector in the boundary

occurred during the day, was sub-geost

ked. If the geostrophic departures were

0.5 - 1.0 km as the height of the maximum low-level oscillation, but their results indicated a slightly weaker diurnal amplitude of 2-3 ms^{-1}. Hering and Borden also detected a middle-layer oscillation (2 km to 8 km) with an amplitude of 2-2.5 ms^{-1} that had its maximum diurnal variation at approximately 4.5 km. Also, an upper-level oscillation was found with a departure amplitude of 2 ms^{-1} at 12 km. The maximum departure vectors at the different levels were observed at different times. The low-level departure occurred 3 - 4 h later than the maximum flow of opposite sign in the middle-layer, which in turn followed the maximum flow of opposite sign in the upper-layer by about the same time interval.

Darkow and Thompson (1968), expanding on Hering and Borden's (1962) work, examined the effect of an oscillating boundary layer on the atmosphere above it. They hypothesized that the two oscillations observed by Hering and Borden in the wind field above the boundary layer were ageostrophic oscillations propagated upward from oscillations within the boundary layer associated with low-level jet development. The ageostrophic wind is defined as the "vector difference between the real (or observed) wind and the geostrophic wind" (Huschke 1989). In a modeling study, Hering and Borden attempted to duplicate the gross features of the entire tropospheric oscillation. They assumed that the geostrophic wind was uniform in time and space and that the ageostrophic components were perturbations superimposed on the geostrophic wind. In their model they represented the atmosphere above the boundary layer as a homogeneous, incompressible fluid. The effects of the boundary-layer wind were introduced into that upper fluid by requiring that the vertical motion field along the bottom of the upper fluid be identical to the vertical motion field along the top of the boundary layer. The model results indicated that in the early evening the total horizontal wind vector in the boundary layer, where strong frictional retardation had occurred during the day, was sub-geostrophic with a cross-isobaric component to the left. If the geostrophic departures were distributed such that low-level convergence

existed within the boundary layer at t

maximum at a level where no departu

assumed the stratosphere as an upper

above the boundary layer and corresp

departures aloft (Darkow and Thomp

2) Seasonal and Diurnal Var

The boundary-layer wind maxim

oscillation, has received considerable

boundary-layer jet is most frequently

Darkow and Thompson 1968). Geogr

97° W and 100° W from South Texas

seasonal and geographic preferences o

pressure features. Several earlier stud

layer jet is frequently embedded in a s

an east-to-west sea-level pressure grad

western Gulf Coast/southern Texas ar

1954; Wexler 1961; Hoecker 1963; Dju

This large-scale setting is most frequen

mentioned above, a more recent study

level wind maxima were frequently ob

particular large-scale setting was found

development.

Several studies have suggested th

cloudless nights without intruding fro

frontal boundaries have been observed

1961; Izumi 1964). While the boundary

existed within the boundary layer at this time, vertical motion would reach a local maximum at a level where no departures due to friction were observed. If one also assumed the stratosphere as an upper boundary, there had to be vertical convergence above the boundary layer and corresponding divergence above that creating geostrophic departures aloft (Darkow and Thompson 1968).

2) SEASONAL AND DIURNAL VARIATIONS IN THE BLJ CHARACTERISTICS

The boundary-layer wind maximum, embedded in the lowest tropospheric oscillation, has received considerable attention. Numerous studies have shown that the boundary-layer jet is most frequently observed during spring and summer (Holton 1967; Darkow and Thompson 1968). Geographically, it is most prevalent in a strip between 95° W and 100° W from South Texas to Nebraska (Wexler 1961; Bonner 1968). These seasonal and geographic preferences often have been attributed to large-scale surface pressure features. Several earlier studies have suggested that the Great Plains boundary-layer jet is frequently embedded in a steady southerly or southwesterly flow induced by an east-to-west sea-level pressure gradient between a high pressure cell along the western Gulf Coast/southern Texas and a warm low-pressure area to the west (Means 1954; Wexler 1961; Hoecker 1963; Djuric and Damiani 1980; Djuric and Ladwig 1983). This large-scale setting is most frequently observed in the warm season. However, as mentioned above, a more recent study by Mitchell et al. (1995) showed that while low-level wind maxima were frequently observed in the vicinity of a subtropical ridge, this particular large-scale setting was found to be not very conducive to low-level jet development.

Several studies have suggested that the jet is particularly pronounced during cloudless nights without intruding fronts (Hoecker 1963; 1965). However, stationary frontal boundaries have been observed during some jet occurrences (Means 1954; Wexler 1961; Izumi 1964). While the boundary-layer jet is mainly a nocturnal phenomenon, it

has been shown to persist during the
nsolation enough to suppress the tur
1963).

A number of investigators have
below 1,500 m (e.g. Blackadar 1957; B
has been observed at approximately
Bonner and Paegle 1970), although w
(Kaimal and Izumi 1965).

Boundary-layer jets are not only
developed, in terms of their extent and
tours when wind speeds are most fre
1966; Mitchell et al. 1995). The jet vel
1900 to 1800 (LST) and super-geostro
(Wexler 1961). Mitchell et al. found t
wind speed of warm season low-level
Great Plains exceeded 16 ms^{-1}. Jet spe
(Hoxit 1975) or 0300 LST (Wexler 196
Gerhardt 1962) or 0800 LST (Hoecker
previously, early morning wind speed
afternoon maximum speeds (Wexler 1
frequently observed with speeds reach

The diurnal oscillation in height
clockwise rotation with time of the tip
Borden 1962; Hoecker 1965; Hoxit 197
gradient in his model, Blackadar (195
time to the right but remained constan
observed this rotation of wind vectors

has been shown to persist during the daytime hours when overcast cloudiness reduces insolation enough to suppress the turbulent stress needed to dissipate the jet (Hoecker 1963).

A number of investigators have agreed that boundary-layer jets are always found below 1,500 m (e.g. Blackadar 1957; Bonner 1968). Most frequently, the BLJ maximum has been observed at approximately 600 - 700 m AGL (Wexler 1961; Hoecker 1965; Bonner and Paegle 1970), although wind maxima have been reported as low as 300 m (Kaimal and Izumi 1965).

Boundary-layer jets are not only most frequent at night but are also the best developed, in terms of their extent and strength, during the nighttime and early morning hours when wind speeds are most frequently supergeostrophic (Blackadar 1957; Bonner 1968; Mitchell et al. 1995). The jet velocity is sub-geostrophic during the day from about 0900 to 1800 (LST) and super-geostrophic at night from about 1800 to 0900 LST (Wexler 1961). Mitchell et al. found that, between 0000 and 0600 LST, the average wind speed of warm season low-level wind maxima at most stations in the southern Great Plains exceeded 16 ms^{-1}. Jet speeds were largest at approximately 0200 LST (Hoxit 1975) or 0300 LST (Wexler 1961), although speed maxima as late as 0700 LST (Gerhardt 1962) or 0800 LST (Hoecker 1965) have been recorded. As mentioned previously, early morning wind speeds are often twice or more the magnitude of the afternoon maximum speeds (Wexler 1961). Nighttime velocities of 27 ms^{-1} have been frequently observed with speeds reaching 30 ms^{-1}, occasionally (Bonner 1968).

The diurnal oscillation in height and speed of the BLJ is accompanied by a clockwise rotation with time of the tips of the wind vectors (Blackadar 1957; Hering and Borden 1962; Hoecker 1965; Hoxit 1975). Assuming a constant horizontal pressure gradient in his model, Blackadar (1957) found that the ageostrophic wind rotated with time to the right but remained constant in magnitude. Hering and Borden (1962) observed this rotation of wind vectors to be uniform across neighboring stations in the

southern Great Plains. A uniform rota

ieal. Wexler (1961) and Hoecker (19

clockwise oscillation that consisted of

200/2200 CST and a predominantly

he elliptical path of the wind vectors

warmer part of the day. Parish et al (

general consisted of two components t

and isallobaric components. The inert

mposed on the actual wind at the tim

Wexler 1961; Blackadar 1957). The isa

east/west pressure gradient and subse

and was secondary in importance to th

3) DIURNAL VARIATIONS IN BOUN

The diurnal variations in bounda

controlled by diurnal changes in boun

energy transfer, eddy viscosity and th

to influence the Great Plains boundary

environment, latitude, the location eas

(i) *Turbulent Energy Transfer and*

Frictional decoupling is thought t

directional variations of the boundary

Blunt 1975). This decoupling results f

---

inertial period (the reciprocal of inertial
Brunkke 1959, p. 304). One pendulum da
suspended pendulum to complete an app
p. 416).

southern Great Plains. A uniform rotation with time was also evident at each vertical level. Wexler (1961) and Hoecker (1965), on the other hand, reported a modified clockwise oscillation that consisted of a linear acceleration from early afternoon until 2000/2200 CST and a predominantly clockwise turning after that. Wexler attributed the elliptical path of the wind vectors tips to the presence of frictional forces during the warmer part of the day. Parish et al (1988) showed that the ageostrophic wind in general consisted of two components that were largest in the early evening, the inertial and isallobaric components. The inertial component of period[2] 12 pendulum hours was imposed on the actual wind at the time of release of surface friction (Hoecker 1963; Wexler 1961; Blackadar 1957). The isallobaric flow was induced by a relaxing east/west pressure gradient and subsequently decreasing southerly geostrophic wind, and was secondary in importance to the frictional-decoupling inertial component.

3) DIURNAL VARIATIONS IN BOUNDARY LAYER CONDITIONS

The diurnal variations in boundary-layer jet height, speed and direction are controlled by diurnal changes in boundary-layer conditions, particularly of turbulent energy transfer, eddy viscosity and thermal stratification. Factors that have been shown to influence the Great Plains boundary-layer conditions are the large-scale synoptic environment, latitude, the location east of high topography, and soil moisture.

(i) Turbulent Energy Transfer and Eddy Viscosity

Frictional decoupling is thought to be directly responsible for the diurnal speed and directional variations of the boundary-layer wind (Hoecker 1965; Parish et al. 1988; Hoxit 1975). This decoupling results from the change from an adiabatic lapse rate in the

[2] Inertial period (the reciprocal of inertial frequency) is defined as a one-half pendulum day (Huschke 1959, p. 304). One pendulum day, in turn, is the time required for the plane of a freely suspended pendulum to complete an apparent rotation about the local vertical." (Huschke 1959, p. 416).

afternoon hours to a temperature inver

variations in the jet evolution are descr

ad eddy viscosity[3] throughout the cou

a. Energy transfer. In the middle

surface heating and subsequent heat tr

Momentum Boundary Layer (MBL) wi

The MBL is adjacent to the surface and

mixing due to surface friction becomes

ed kinetic energy dissipation are large

After sunset, the nocturnal bound

stable regime (Zeman 1979). Therefore

equilibrium when the surface heat flux

Izouit (1975) described the developmer

night in more detail. Shortly after suns

mechanical and buoyant mixing and le

MBL. Consequently, the total dissipati

decreases significantly and is largely co

wind direction and speed profiles in th

mixing processes, on the order of minu

located above the developing, ground-l

and frictional forces become insignifica

more pronounced than the variations r

increases to that for large-scale motion.

significant for several hours. Since diss

speeds increase rapidly to a maximum

[3] Eddy viscosity is defined as the "turbule
internal fluid friction." (Huschke 1959, p

afternoon hours to a temperature inversion at night (Hoxit 1975). Below, the diurnal variations in the jet evolution are described as they relate to changes in energy transfer and eddy viscosity[3] throughout the course of the day.

a. Energy transfer. In the middle of the afternoon, according to Hoxit (1975), surface heating and subsequent heat transfer into the lower troposphere result in a Momentum Boundary Layer (MBL) with adiabatic conditions that extends up to 2 km. The MBL is adjacent to the surface and its upper bound is the level at which turbulent mixing due to surface friction becomes negligible. At this time of day both kinetic energy and kinetic energy dissipation are large and in approximate balance.

After sunset, the nocturnal boundary layer changes rapidly from a convective to a stable regime (Zeman 1979). Therefore, the boundary layer in general is far from equilibrium when the surface heat flux ceases and is continually changing until sunrise. Hoxit (1975) described the development of the boundary layer during the course of the night in more detail. Shortly after sunset, cooling in the lower levels suppresses mechanical and buoyant mixing and leads to the formation of a new and much thinner MBL. Consequently, the total dissipation of kinetic energy by turbulent processes decreases significantly and is largely confined to the lowest few hundred meters. The wind direction and speed profiles in this thinner MBL adjust with the time scale of mixing processes, on the order of minutes. In the Inertial Boundary Layer (IBL), which is located above the developing, ground-based MBL, turbulent mixing decreases rapidly and frictional forces become insignificant. The kinetic energy variations in this layer are more pronounced than the variations near the surface. The adjustment time for motion increases to that for large-scale motion. Therefore, kinetic energy generation remains significant for several hours. Since dissipation mechanisms are largely eliminated, wind speeds increase rapidly to a maximum 1-3 hrs after midnight (Hoxit 1975). The

[3] Eddy viscosity is defined as the "turbulent transfer of momentum by eddies giving rise to an internal fluid friction." (Huschke 1959, p. 191).

conditions most conducive to jet devel

cooling rates and optimal geostrophic

By sunrise, the low-level stable la

near 300 m. In the IBL, the supergeost

component towards higher pressure (

toward higher pressure is observed in

during summer and fall. This upgradie

ultimately results in a decrease of the

After sunrise, according to Hoxit

based stable layer. Mixing in the MBL

speed change with height is reduced.

adiabatic lapse rate is created in the m

1970). As mixing reaches higher and hi

this time the winds at the top of the M

conclusion, Hoxit (1975) noted that the

combination of ageostrophic flow towa

processes. The rapid decay of the noct

(1979) as a prerequisite for generating t

made possible a large nocturnal jet the

b. Eddy viscosity. Blackadar (19

Paegle (1970), and Paegle and Rasch (1

shown that the ageostrophic winds aris

are inertial oscillations resulting from t

of sunset. In a theoretical study, Buaj

distribution of eddy viscosity in time a

wind variations. They noted that there

conditions most conducive to jet development, according to Zeman (1979), are large cooling rates and optimal geostrophic wind shear.

By sunrise, the low-level stable layer (MBL) is well developed with a height of less than 300 m. In the IBL, the supergeostrophic wind speeds lead to an ageostrophic component towards higher pressure (Hoecker 1965; Hoxit 1975). This tendency for flow toward higher pressure is observed in the 1-2 km layer for the period of 0300-0900 LST during summer and fall. This upgradient flow produces negative kinetic energy, which ultimately results in a decrease of the wind speed (Hoxit 1975).

After sunrise, according to Hoxit (1975), surface heating destroys the ground-based stable layer. Mixing in the MBL is enhanced and the rate of wind direction and speed change with height is reduced. Subsequently, a deep MBL with essentially adiabatic lapse rate is created in the morning and early afternoon hours (0900-1500 LST). As mixing reaches higher and higher, the IBL is destroyed by mid-afternoon. At this time the winds at the top of the MBL are back in gradient or geostrophic balance. In conclusion, Hoxit (1975) noted that the nocturnal wind maximum is destroyed by a combination of ageostrophic flow toward higher pressure and dissipation by turbulent processes. The rapid decay of the nocturnal boundary layer, in turn, was seen by Zeman (1979) as a prerequisite for generating the large geostrophic departures which ultimately made possible a large nocturnal jet the following day.

b. Eddy viscosity. Blackadar (1957), Buajitti and Blackadar (1957), Bonner and Paegle (1970), and Paegle and Rasch (1973), through the use of theoretical models, have shown that the ageostrophic winds arising in the nighttime hours in the 200-1500 m layer are inertial oscillations resulting from the rapid change in eddy viscosity around the time of sunset. In a theoretical study, Buajitti and Blackadar (1957) attempted to find the distribution of eddy viscosity in time and height that best accounted for the observed wind variations. They noted that there was an apparent inverse relationship between

the magnitude of the wind and eddy v

the observed variation of the winds we

and the amplitude of eddy viscosity de

distribution of eddy viscosity with heig

structure of the air mass. Eddy viscosi

considerably larger than ten times the r

values, on the other hand, was thought

Haqitti and Blackadar 1957). At the t

observed that supergeostrophic wind s

hodograph profile. He additionally noted

of the wind increased with increasing v

(iii) *Nocturnal Inversion*

As mentioned above, the bounda

nocturnal inversion that forms shortly

the night (Blackadar 1957; Izumi 1964)

especially pronounced and found at a

inversion situations. Gerhardt (1962),

and Izumi (1965) described how chang

development of the nocturnal wind ma

noted that, between 1700 CST and 030

level was accompanied by an increase

with the top of the inversion. They att

and wind speed to the fact that cold ai

upward in an organized fashion by mi

This organized upward moveme

throughout the nighttime hours. Izum

the magnitude of the wind and eddy viscosity. The amplitude, orientation and phase of the observed variation of the winds were best accounted for when both the mean value and the amplitude of eddy viscosity decreased with height. They speculated that the distribution of eddy viscosity with height might be a function of the temperature structure of the air mass. Eddy viscosity during the day reached a value which was considerably larger than ten times the nighttime value. The smallness of the nighttime values, on the other hand, was thought to account for the large supergeostrophic winds (Buajitti and Blackadar 1957). At the time of minimum eddy viscosity, Haltiner (1959) observed that supergeostrophic wind speeds as well as strong shear were evident in the jet-type profile. He additionally noted that the height of the maximum diurnal variation of the wind increased with increasing values of eddy viscosity.

(ii) Nocturnal Inversion

As mentioned above, the boundary-layer jet is frequently observed at the top of a nocturnal inversion that forms shortly before sunset and propagates upward throughout the night (Blackadar 1957; Izumi 1964). In an inversion situation, the jet nose is especially pronounced and found at a lower elevation (Hoecker 1965) compared to non-inversion situations. Gerhardt (1962), Izumi and Barad (1963), Izumi (1964) and Kaimal and Izumi (1965) described how changes in the temperature profile are related to the development of the nocturnal wind maximum. In a case study, Izumi and Barad (1963) noted that, between 1700 CST and 0300 CST, an abrupt decrease in wind speed at one level was accompanied by an increase of wind speed at the level above that coincides with the top of the inversion. They attributed the systematic behavior of temperature and wind speed to the fact that cold air and lower momentum were transported upward in an organized fashion by mixing during the formation of the jet.

This organized upward movement of the inversion was observed to continue throughout the nighttime hours. Izumi (1964), for example, noted that immediately after

sunrise warming in the lowest layers, c

upper layers, likely due to subsidence,

the lower portion of the inversion beco

above the inversion becomes more stal

Turbulent energy is transported vertica

stable layer due to the presence of a str

This mixing results in a systematically

conditions (Izumi 1964). The upward

accompanied by a stepwise upward tr

962). In a descriptive study of a low-

was still growing in intensity while ad

lower levels.

In a later study, Kaimal and Izum

nversion and dissipation of the jet in t

the breakdown of the surface inversion

et. Rather, as the inversion began to b

pward and a new inversion formed a

momentum loss through intense vertic

the jet continued to grow because of m

After sunrise, as the base of the inversi

growing convective layer, the jet grad

by 0840 CST (Kaimal and Izumi 1965

The interrelationship of a wind m

nversion was theoretically treated by

lowest meter, the observed rate of noc

radiational or conduction fluxes. Ther

the primary control of the rate of upw

sunrise warming in the lowest layers, cooling in the middle layers and warming in the upper layers, likely due to subsidence, lead to a sharp elevated inversion. Consequently, the lower portion of the inversion becomes less stable while at the same time the layer above the inversion becomes more stable and the wind shear within that layer increases. Turbulent energy is transported vertically and turbulent mixing increases within the stable layer due to the presence of a strong wind maximum in spite of the inversion. This mixing results in a systematically upward moving change from inversion to lapse conditions (Izumi 1964). The upward movement of the inversion, in turn, is accompanied by a stepwise upward trend in the level of maximum speeds (Gerhardt 1962). In a descriptive study of a low-level wind maximum, Gerhardt noted that the jet was still growing in intensity while adiabatic conditions were being reestablished at lower levels.

In a later study, Kaimal and Izumi (1965) described the breakdown of the inversion and dissipation of the jet in the morning in more detail. They pointed out that the breakdown of the surface inversion did not necessarily cause the destruction of the jet. Rather, as the inversion began to break down, the level of maximum wind jumped upward and a new inversion formed at the level of the wind maximum. Despite the momentum loss through intense vertical mixing at all levels below the wind maximum, the jet continued to grow because of momentum input from inertial and pressure forces. After sunrise, as the base of the inversion was continually pushed higher and higher by a growing convective layer, the jet gradually diminished until it was completely destroyed by 0840 CST (Kaimal and Izumi 1965).

The interrelationship of a wind maximum and the development of a nocturnal inversion was theoretically treated by Blackadar (1957). He found that above the lowest meter, the observed rate of nocturnal cooling was too large to be explained by radiational or conduction fluxes. Therefore, turbulent transfer was hypothesized to be the primary control of the rate of upward propagation of the inversion surface. The

wind profile was thought to be the mos

growth of the inversion was gradual ar

ckward maximum on top of the invers

nversion was kept under control. The

generate some turbulence within the inv

downward where it was lost by radiati

pward growth of the inversion during

ayers. In the same way, momentum w

nversion and transported down to the

Therefore, the profiles of temperature a

Blackadar 1957).

Other boundary-layer-jet cases ha

temperature stratification in the bound

nocturnal jet that occurred in a zone wi

was still decreasing with height (i.e. no

boundary-layer jet for which neither th

southerly and westerly components) no

to have any spatial relationship with t

(iii) *Surface Pressure Features*

According to Hoecker (1965), the

layer jet development are (1) steady so

pressure area to the west; (4) east-to-w

afternoon insolation; and (6) no intrud

account for most of these conditions ar

and a warm low pressure system to th

large-scale anticyclonic flow regime is

wind profile was thought to be the most important factor in determining whether the growth of the inversion was gradual and orderly. When a jet-like profile existed with the wind maximum on top of the inversion, the generation of turbulence within the inversion was kept under control. The wind shear, however, was likely sufficient to generate some turbulence within the inversion through which heat was transferred downward where it was lost by radiation. This heat loss resulted in the continuous upward growth of the inversion during the night since it was not compensated in upper layers. In the same way, momentum was removed from the upper portion of the inversion and transported down to the surface where it was dissipated more effectively. Therefore, the profiles of temperature and wind speed were expected to be similar (Blackadar 1957).

Other boundary-layer-jet cases have been reported, however, with different temperature stratification in the boundary layer. Bonner (1966), for instance, observed a nocturnal jet that occurred in a zone where the air was stable but where the temperature was still decreasing with height (i.e. no inversion existed). Hoecker (1965) described a boundary-layer jet for which neither the height of the total wind vector (both the southerly and westerly components) nor the height of the southerly component seemed to have any spatial relationship with the thermal stratification.

(iii) Surface Pressure Features

According to Hoecker (1965), the optimal meteorological conditions for boundary-layer jet development are (1) steady southerly flow; (2) cloudless night; (3) warm low-pressure area to the west; (4) east-to-west sea-level pressure gradient; (5) strong afternoon insolation; and (6) no intruding fronts. The two primary surface features that account for most of these conditions are a large-scale high pressure system to the east and a warm low pressure system to the west or northwest of the Central Plains. A large-scale anticyclonic flow regime is particularly conducive to boundary-layer jet

development due to the fact that turb
boundary Layer to the ground is muc
during the night (Paegle and Rasch 19
the day has been shown to cause stro

The presence of a shallow warm
Hoecker (1965), implies that the geos
studies, Hoecker noted a decrease of
and 1800 CST. The existence of a sha
sharper nose of the jet (Blackadar 19

(iv) *Latitude Dependence*

The diurnal wind variations, du
dependent. Buajitti and Blackadar (1
of the diurnal wind variations with in
oscillations equals the period of the fo
diurnal wind variation is expected at
component is also latitude dependen
simulation, hypothesized that the tim
occur earlier in the evening for progre
and Rasch (1973) indicated that while
the time of minimum eddy viscosity a
geostrophic velocity at 40° N.

(v) *Role of Topography*

Besides surface pressure feature
terrain of the Rocky Mountains has be
speed and direction (Bonner and Pae

development due to the fact that turbulent transfer of momentum through the Planetary Boundary Layer to the ground is much greater during the afternoon of a sunny day than during the night (Paegle and Rasch 1973). The resulting retardation of the flow during the day has been shown to cause strong winds at night (Blackadar 1957).

The presence of a shallow warm low pressure system in the area, according to Hoecker (1965), implies that the geostrophic wind decreases with height. In two case studies, Hoecker noted a decrease of the geostrophic wind speed with height at 0600 and 1800 CST. The existence of a sharp speed decrease, in turn, was responsible for a sharper nose of the jet (Blackadar 1957; Hoecker 1965).

(iv) Latitude Dependence

The diurnal wind variations, due to their inertial components, are latitude dependent. Buajitti and Blackadar (1957) proposed an increasingly smaller amplitude of the diurnal wind variations with increasing latitude. At 30° N the period of inertial oscillations equals the period of the forcing function (24 h); therefore, the maximum diurnal wind variation is expected at 30° N. The clockwise rotation of the ageostrophic component is also latitude dependent. Fast and McCorcle (1990), based on a simulation, hypothesized that the time of the maximum supergeostrophic wind should occur earlier in the evening for progressively higher latitudes. Model results by Paegle and Rasch (1973) indicated that while the wind was almost 50% supergeostrophic at the time of minimum eddy viscosity at 30° N, it only reached a speed of 30% above the geostrophic velocity at 40° N.

(v) Role of Topography

Besides surface pressure features and latitude, differential heating over the sloping terrain of the Rocky Mountains has been shown to enhance the diurnal changes in wind speed and direction (Bonner and Paegle 1970; Fast and McCorcle 1990). Bonner and

Paegle (1970), in a modeling study, fo
he west cools much more than the ai
sults in a southerly component to th
geostrophic wind at the surface is less
heating over the mountains, in turn, re
component of the thermal wind that p
component of the surface geostrophic
s larger than the geostrophic wind at
the oscillation in the surface geostroph
due to the daily heating cycle over slo
McCorcle (1990) also found the winds
simulation.

(v) *Impact of Soil Moisture*

Another factor that influences b
properties of soils (Paegle and McLaw
been shown to be a function of its alb
conductivity. Atmospheres above soi
given heat input (Paegle and McLawh
conjunction with topography, was th
His model suggests that as soil moistu
diurnal wind modulation decreases d
McCorcle (1990) came to the same co
evaporation. They found that evapor
much stronger vertical gradient of the
lower height. However, McCorcle (19
more complicated in an area of elevat

Paegle (1970), in a modeling study, found that at night, the air above the higher terrain in the west cools much more than the air farther east at the same pressure level. This results in a southerly component to the thermal wind (surface to 2 km), implying that the geostrophic wind at the surface is less than the geostrophic wind at 2 km. The daytime heating over the mountains, in turn, results in a pronounced increase in the northerly component of the thermal wind that produces an afternoon maximum in the southerly component of the surface geostrophic wind. At this time, the surface geostrophic wind is larger than the geostrophic wind at 2 km. Bonner and Paegle (1970) concluded that the oscillation in the surface geostrophic wind is driven by an alternating thermal wind due to the daily heating cycle over sloping terrain. In their simulations, Fast and McCorcle (1990) also found the winds over a slope to be stronger than in their flat simulation.

(vi) Impact of Soil Moisture

Another factor that influences boundary layer variations are the physical properties of soils (Paegle and McLawhorn 1983). The absorption of heat by soil has been shown to be a function of its albedo, moisture, density, heat capacity and conductivity. Atmospheres above soils with small conductivity respond strongly to a given heat input (Paegle and McLawhorn 1983). Soil moisture, particularly in conjunction with topography, was the focus of a recent analysis by McCorcle (1988). His model suggests that as soil moisture increases, the amplitude of the predicted diurnal wind modulation decreases due to decreased low-level buoyancy. Fast and McCorcle (1990) came to the same conclusion when they examined the effects of evaporation. They found that evaporation results in a reduction of the wind speed, a much stronger vertical gradient of the wind speed above the jet, and a jet maximum at lower height. However, McCorcle (1988) also found that the effect of soil moisture is more complicated in an area of elevated terrain. Saturated lower elevations lead to a

ssentially-direct circulation at the mo

component. Inertial turning of these c

wind speeds and enhanced boundary

higher elevations, on the other hand, t

buoyancy-driven oscillation and resu

4) ADVECTIVE AND KINEMATIC F

The boundary-layer jet is an imp

Great Plains due to its kinematic and

and reduce airmass stability by lifting

significantly increase low-level tempe

Blackadar 1957; Modahl 1979).

The boundary layer oscillation s

south-central (north-central) United S

reverse large-scale flow-pattern is evi

Borden 1962). The boundary-layer je

pattern consequently passes through

downstream (upstream) of the wind m

reverse is true for the afternoon hour

In addition to the region downstream

observed along the left flank of the je

shear of $0.44 \times 10^{-4} s^{-1}$ on the cyclonic

the jets. Paegle and Rasch (1973), in

into their model, also obtained a shar

to the right. In a study by Bonner (19

by time of day. While the daytime av

sharper left flank was evident in the

thermally-direct circulation at the moisture boundary that increases the ageostrophic component. Inertial turning of these combined circulations results in greater nocturnal wind speeds and enhanced boundary-layer convergence. When soils are saturated at higher elevations, on the other hand, the thermally direct circulation counteracts the buoyancy-driven oscillation and results in reduced jet speeds.

4) ADVECTIVE AND KINEMATIC PROPERTIES OF THE BLJ

The boundary-layer jet is an important contributor to the convective activity of the Great Plains due to its kinematic and advective properties. BLJs enhance baroclinicity and reduce airmass stability by lifting through convergent flow patterns. Also, BLJs significantly increase low-level temperature advection and moisture advection (Blackadar 1957; Modahl 1979).

The boundary layer oscillation sets up a large-scale convergence (divergence) in the south-central (north-central) United States during the afternoon hours. At night, the reverse large-scale flow-pattern is evident (Curtis and Panofsky 1958; Hering and Borden 1962). The boundary-layer jet that is embedded in this large-scale bipolar pattern consequently passes through an area of ascending (descending) motion downstream (upstream) of the wind maximum during the early morning hours. The reverse is true for the afternoon hours (Pitchford and London 1962; Bonner et al. 1968). In addition to the region downstream of the jet maximum, ascending motion is also observed along the left flank of the jet (Bonner 1966). Bonner (1968) reported lateral shear of $0.44 \times 10^{-4} s^{-1}$ on the cyclonic side and $-0.37 \times 10^{-4} s^{-1}$ on the anticyclonic side of the jets. Paegle and Rasch (1973), incorporating the effects of Great Plains topography into their model, also obtained a sharper drop in jet velocities to the left of the jet than to the right. In a study by Bonner (1966), the amount of lateral shear was seen to vary by time of day. While the daytime average winds showed a sharper right flank, a sharper left flank was evident in the nighttime average speeds (Bonner 1966).

Due to the anticyclonic inertial tu

ght, mixing ratio and mean temperat

e core (Means 1954; Bonner 1966).

: *Low-Level Jet Studies*

To distinguish wind maxima tha

wind maxima that are primarily the re

maxima in this section will be referre

have likely been included in the existi

due to the applied definitions of wind

subject of a comprehensive climatolog

means of case studies, composite stud

most frequently been conducted in pa

warm sector of mid-latitude cyclones,

streaks, or along frontal boundaries.

As integral parts of larger-scale

as the forcing mechanisms they are as

temporal preference for this type of lo

stronger dynamic forcing is present.

boundary-layer conditions in enhanci

maxima and southerly wind events to

favorable synoptic and boundary-lay

Low-level jets that are associate

often extend to greater elevations and

oscillation that is so typical of the bo

reported a period of strong southerly

Due to the anticyclonic inertial turning of the wind vectors during the course of the night, mixing ratio and mean temperature values at night are highest to the west of the jet core (Means 1954; Bonner 1966).

c. Low-Level Jet Studies

To distinguish wind maxima that are synoptically or subsynoptically driven from wind maxima that are primarily the result of boundary-layer forcing, low-level wind maxima in this section will be referred to as low-level jets. While some synoptic LLJs have likely been included in the existing climatological studies of low-level wind maxima due to the applied definitions of wind maxima, synoptic LLJs per se have not been the subject of a comprehensive climatological study. LLJs have rather been investigated by means of case studies, composite studies, or modeling studies. Also, LLJ studies have most frequently been conducted in particular large-scale environments, such as in the warm sector of mid-latitude cyclones, at the intersection with upper-tropospheric jet streaks, or along frontal boundaries.

As integral parts of larger-scale systems, LLJs show the same seasonal variations as the forcing mechanisms they are associated with. Therefore, one can expect a temporal preference for this type of low-level wind maximum for the cold season when stronger dynamic forcing is present. Mitchell et al. (1995) also pointed out the role of boundary-layer conditions in enhancing LLJs. He found warm-season low-level wind maxima and southerly wind events to be most frequent in September when both favorable synoptic and boundary-layer conditions existed.

Low-level jets that are associated with synoptic or subsynoptic-scale systems often extend to greater elevations and they do not show the pronounced diurnal oscillation that is so typical of the boundary-layer jet. Astling et al. (1985), for instance, reported a period of strong southerly wind that initially showed a marked diurnal

oscillation. When a weak trough ove

nd evolved into a large cyclone, the

Similar to the previous section, t

nterpretation of the driving influence

with cyclones will be discussed first, t

situations. While a number of studies

ystems have been conducted in the s

explicitly examining the role of LLJs i

States, except for Mitchell et al.'s (199

based on synoptic typing. Low-level

detail in other regions, however. Ther

will incorporate other geographical ar

1) LOW-LEVEL JETS ASSOCIATED

This section will first examine th

between upper-level jets (ULJs) and lo

"Warm Conveyor Belt". Next the jet st

reviewed. The last part will then discu

and its influence on the development

(i) *Development of LLJs in Cyclones*

The formation of LLJs during the

the focus of a number of studies. The

during cyclogenesis has been most freq

1967; Browning and Pardoe 1973; Ucc

1990; Chen and Kpaeyeh 1993). LLJ d

cyclogenesis along the East Coast (Ucc

oscillation. When a weak trough over the western United States increased in amplitude and evolved into a large cyclone, the diurnal oscillations became much less pronounced.

Similar to the previous section, this section has been organized based on my interpretation of the driving influence in individual studies. Low level jets associated with cyclones will be discussed first, followed by low-level jets in frontal boundary situations. While a number of studies examining the role of LLJs in low-pressure systems have been conducted in the southern Great Plains, I am not aware of studies explicitly examining the role of LLJs in frontal situations in the south-central United States, except for Mitchell et al.'s (1995) frequency analysis of LLJs in frontal situations based on synoptic typing. Low-level jets in frontal situations have been studied in detail in other regions, however. Therefore, this review of literature on the low-level jet will incorporate other geographical areas as well.

1) LOW-LEVEL JETS ASSOCIATED WITH MID-LATITUDE CYCLONES

This section will first examine the development of LLJs in cyclones, the interaction between upper-level jets (ULJs) and low-level jets and the role of the LLJ as part of the "Warm Conveyor Belt". Next the jet structure and temporal variation of the jet will be reviewed. The last part will then discuss the lower-tropospheric temperature structure and its influence on the development of the LLJ.

(i) Development of LLJs in Cyclones

The formation of LLJs during the development of a short baroclinic wave has been the focus of a number of studies. The LLJ development in the warm sector of cyclones during cyclogenesis has been most frequently studied in Colorado cyclones (Newton 1967; Browning and Pardoe 1973; Uccellini and Johnson 1979; Djuric and Damiani 1980; Chen and Kpaeyeh 1993). LLJ development has also been studied during cyclogenesis along the East Coast (Uccellini et al. 1987).

Based on eight, respectively 20

ad Ladwig (1983) described a mode

LLJ formation within cold season cyc

Damiani (1980) noted that, during th

of the LLJ occurs below a northerly or

associated with a previous cold outbr

warming, a surface low develops in th

with a fairly strong isallobaric compo

observed over eastern Colorado and

level trough and front move into the a

By this time the low-level jet is well es

upper-level trough, unlike the lee trou

s of synoptic scale and associated wi

yclone is situated underneath the exi

region when the next polar front appr

1990; Djuric and Ladwig 1983). Djuri

simultaneous development of the LLJ

theory that the pressure fall is the imm

(1981) found additional evidence for

wind near a region of pressure fall an

maximum. He was able to show that

sufficient to predict the origination of

Djuric and Damiani (1980) also

yclone developed along the polar fro

southerly wind was first observed in

Gulf of Mexico in approximately 20 h.

humid air entered the LLJ. While the

Based on eight, respectively 20 case studies, Djuric and Damiani (1980) and Djuric and Ladwig (1983) described a model of several individual developmental stages for LLJ formation within cold season cyclones in the southwestern Great Plains. Djuric and Damiani (1980) noted that, during the winter half year (October - March), the initiation of the LLJ occurs below a northerly or northwesterly 700 mb-level flow west of a trough associated with a previous cold outbreak over the Great Plains. Due to adiabatic warming, a surface low develops in the lee of the Rocky Mountains and southerly wind with a fairly strong isallobaric component toward the center of the pressure fall is observed over eastern Colorado and adjacent areas. One day later, a second upper-level trough and front move into the area from the west and a frontal cyclone develops. By this time the low-level jet is well established over the southern Plains. This second upper-level trough, unlike the lee trough at the time of origination of the southerly wind, is of synoptic scale and associated with a polar front. At this stage of development, the cyclone is situated underneath the exit region of a polar jet streak. The LLJ exits the region when the next polar front approaches from the northwest (Djuric and Damiani 1980; Djuric and Ladwig 1983). Djuric and Ladwig (1983) concluded that the simultaneous development of the LLJ and the surface low pressure system support the theory that the pressure fall is the immediate cause of a LLJ. In a modeling study, Djuric (1981) found additional evidence for the hypothesis that the LLJ starts as an isallobaric wind near a region of pressure fall and that the pressure fall is a direct cause of the wind maximum. He was able to show that a one-layer one-dimensional barotropic model was sufficient to predict the origination of an LLJ within a cyclone, its expansion and retreat.

Djuric and Damiani (1980) also observed that a LLJ was present whenever a cyclone developed along the polar front in the southwestern United States. The southerly wind was first observed in northwestern Texas. From there it spread to the Gulf of Mexico in approximately 20 h. After the entrance of the jet reached the Gulf, humid air entered the LLJ. While the southerly flow spread rapidly, the core of the LLJ

itself did not move very fast. During

and a secondary maximum along the

field.

The relative location of low-leve

an LLJ associated with cyclogenesis w

1967) for a severe weather outbreak.

short wave trough and a ULJ appear

the LLJ southeast of the surface low.

the Gulf of Mexico along the LLJ axis

horizontal divergence downstream of

tropospheric convergence.

Chen and Kpaeyeh (1993) furthe

circulation and the water vapor transp

Great Plains. They constructed comp

synoptime LLJs in the mature stage, d

being situated over the Gulf of Mexico

streamfunction fields at 200 and 850 m

level divergent center and a low-level c

The upper-level short-wave trough wa

a favorable environment for LLJ forma

itself is accelerated by the isallobaric w

exit region of the ULJ. The amount of

strength of the lower-tropospheric circ

thought to be instrumental in maintain

Kpaeyeh 1993).

LLJs have also been reported in t

the East Coast (Uccellini et al. 1986; 19

itself did not move very fast. During this time two maxima, one over eastern Oklahoma and a secondary maximum along the Texas coast, were frequently apparent in the wind field.

The relative location of low-level and upper-level features during the formation of an LLJ associated with cyclogenesis was incorporated in a composite figure by Newton (1967) for a severe weather outbreak. The cyclone and LLJ development occurs as a short wave trough and a ULJ appear east of the Rocky Mountains. The LLJ intersects the ULJ southeast of the surface low. Warm moist air is advected into the region from the Gulf of Mexico along the LLJ axis to the northern end of the jet. Upper-tropospheric horizontal divergence downstream of the short-wave trough is superimposed on lower-tropospheric convergence.

Chen and Kpaeyeh (1993) further examined the upper- and lower tropospheric circulation and the water vapor transport during LLJ occurrence within cyclones over the Great Plains. They constructed composite upper- and lower tropospheric charts for 64 springtime LLJs in the mature stage, defined by the location of the entrance to the jet being situated over the Gulf of Mexico. The geographically-fixed composite streamfunction fields at 200 and 850 mb for 11 springs revealed a coupling of an upper-level divergent center and a low-level convergent center ahead of the upper-level trough. The upper-level short-wave trough was seen as an indispensable component in creating a favorable environment for LLJ formation in the lee of the Rocky Mountains. The LLJ itself is accelerated by the isallobaric wind toward the 850-mb low pressure center in the exit region of the ULJ. The amount of water vapor transport was determined by the strength of the lower-tropospheric circulation. The lower tropospheric convergence was thought to be instrumental in maintaining the precipitation in this scenario (Chen and Kpaeyeh 1993).

LLJs have also been reported in the 850 mb wind field in secondary cyclones along the East Coast (Uccellini et al. 1986; 1987). The initial development of the Presidents'

Dry cyclone, for instance, was chara

inverted trough. Simultaneously, an

fact that the LLJ, the coastal front an

interpreted by Uccellini et al. (1986)

these features. Furthermore, simulat

streak circulation patterns and diaba

low-level winds and the initial devel

(b) *Interaction between Upper-Le*

The superposition of a ULJ on a

divergence and low-level convergence

early in the literature (e.g. Fawbush a

recently, the role of the ULJ in forcing

a transverse circulation has received c

Uccellini 1980; Uccellini et al. 1986).

Uccellini (1980) found evidence

southern Great Plains was influenced

and upper-tropospheric jet streaks. In

studies, Uccellini (1980) isolated two

associated with the reported low-level

were associated with troughing over th

jet streak propagating toward the Grea

cyclone or trough. These cases would

the classic diurnal oscillation in that th

persisted throughout the day. They, n

The remaining few cases in Uccellini's s

front range of the Rockies and weak up

Day cyclone, for instance, was characterized by the formation of a coastal front and an inverted trough. Simultaneously, an intense and highly ageostrophic LLJ formed. The fact that the LLJ, the coastal front and the cyclone formed simultaneously was interpreted by Uccellini et al. (1986) as indicative of a synergistic interaction between these features. Furthermore, simulations of this particular storm showed that both jet streak circulation patterns and diabatic processes contributed to the enhancement of the low-level winds and the initial development of the coastal cyclone (Uccellini et al. 1986).

(ii) Interaction between Upper-Level Jet and Low-Level Jet

The superposition of a ULJ on a LLJ and the resultant coupling of upper-level divergence and low-level convergence in severe storm scenarios was pointed out fairly early in the literature (e.g. Fawbush and Miller 1954; Beebe and Bates 1955). More recently, the role of the ULJ in forcing and/or enhancing the low-level wind field through a transverse circulation has received considerable attention (Uccellini and Johnson 1979; Uccellini 1980; Uccellini et al. 1986).

Uccellini (1980) found evidence that the behavior of low level wind maxima in the southern Great Plains was influenced by the combined effects of lee side cyclogenesis and upper-tropospheric jet streaks. In an examination of previously published case studies, Uccellini (1980) isolated two primary 300-mb flow patterns that were associated with the reported low-level wind maxima. Most low-level wind maxima were associated with troughing over the western United States, an upper-tropospheric jet streak propagating toward the Great Plains and the development of a lee side cyclone or trough. These cases would classify as LLJs in this study. They did not show the classic diurnal oscillation in that they did not disappear in the morning, but rather persisted throughout the day. They, nevertheless, showed the strongest speeds at night. The remaining few cases in Uccellini's study were found under a strong ridge over the front range of the Rockies and weak upper tropospheric flow over the southern Plains.

Not surprisingly, the low-level wind

upper-level pattern displayed a clear

this study, these cases would be cons

Achtor and Horn (1986) also re

the strength of the upper-troposph

composite wind fields for the 850-mb

which persisted for at least 72 hours

wind maximum than did cyclones th

wind field also showed stronger low-

that in the cases where 300 mb-jet str

to be proportional to the magnitude o

toward the left-front quadrant of the

Uccellini and Johnson (1979) an

convective storm over the Midwest.

pressure surface, the 300-K isentropic

suggested a direct interaction with th

embedded within the return branch of

an upper-tropospheric jet streak. It w

the 850-mb level to the 750-mb level)

(Uccellini and Johnson 1979).

In a later study, Uccellini et al.

tropospheric wind field interaction fo

and 200-mb wind fields underwent sig

The subtropical 200-mb jet stream amp

increased. As the divergence increase

indirect circulation perpendicular to th

isentropic surfaces from about 900 mb

Not surprisingly, the low-level wind maxima which were associated with the latter upper-level pattern displayed a clear diurnal oscillation with a nocturnal maximum. In this study, these cases would be considered boundary-layer jets.

Achtor and Horn (1986) also related the strength of the LLJ in developing cyclones to the strength of the upper-tropospheric wind field. By examining geographically-fixed composite wind fields for the 850-mb and the 300-mb levels, they found that cyclones which persisted for at least 72 hours developed under a more pronounced upper-level wind maximum than did cyclones that filled before that time. The composite 850-mb wind field also showed stronger low-level wind maxima. A statistical analysis revealed that in the cases where 300 mb-jet streaks were present, the strength of the LLJ tended to be proportional to the magnitude of the upper-level wind. The LLJ was oriented toward the left-front quadrant of the upper-level wind maximum.

Uccellini and Johnson (1979) analyzed the jet stream configurations for a severe convective storm over the Midwest. While the LLJ was clearly evident on the 850-mb pressure surface, the 300-K isentropic surface better depicted the extent of the LLJ and suggested a direct interaction with the upper-tropospheric jet streak. The LLJ was embedded within the return branch of the indirect circulation beneath the exit region of an upper-tropospheric jet streak. It was directed up sloped isentropic surfaces (from the 950-mb level to the 750-mb level) toward the cyclonic side of the upper-level jet (Uccellini and Johnson 1979).

In a later study, Uccellini et al. (1986) found evidence of upper- and lower-tropospheric wind field interaction for East Coast secondary cyclogenesis. The 850-mb and 200-mb wind fields underwent significant changes prior to the cyclone development. The subtropical 200-mb jet stream amplified, and divergence along the jet axis increased. As the divergence increased, a LLJ developed in the lower branch of an indirect circulation perpendicular to the ULJ axis. The LLJ again was directed up sloped isentropic surfaces from about 900 mb toward the 700 mb level (Uccellini et al. 1986).

Uccellini and Johnson (1979), w

irculation within the exit region of t

irculation within the exit region of a

irected toward the anticyclonic side

irected toward the cyclonic side. Th

yclonic side of the jet and sinking m

ndirect circulation is frontogenetic be

esults in additional cooling by lifting

esults in additional warming due to

bservational study, Sechrist and Wh

at the 300-mb level was indeed match

iscrepancy in the magnitude of the c

to curvature and other effects.

The magnitude of the horizonta

notion pattern is determined by the a

he absolute magnitude of the wind m

omponent dominates the ageostroph

level ageostrophic components have b

ndirect (and direct) circulation. The l

referred to as "isallobaric[5]" since they a

consequently, net mass adjustment. Th

ndirect circulation is mainly the result

1990). This isallobaric component resu

---

[4] The inertial-advective component of th
geostrophic wind that is due to advectio
entrance region of jet streaks ... and when
[5] The isallohypsic wind which is defined
he gradient of the isallohypsic field [fie
wind, even though pressure does not appe

Uccellini and Johnson (1979), with a numerical model, examined the indirect circulation within the exit region of the ULJ in more detail. They noted that the indirect circulation within the exit region of a ULJ consists of an upper-tropospheric branch directed toward the anticyclonic side of the jet and a lower-tropospheric return branch directed toward the cyclonic side. This configuration results in rising motion on the cyclonic side of the jet and sinking motion on the anticyclonic side of the jet. This indirect circulation is frontogenetic because rising motion on the cool side of the jet results in additional cooling by lifting and sinking motion on the warm side of the jet results in additional warming due to subsidence (Sechrist and Whittaker 1979). In an observational study, Sechrist and Whittaker (1979) verified that the convergence center at the 300-mb level was indeed matched by a divergence center at 850 mb. The discrepancy in the magnitude of the divergence values at the two levels was attributed to curvature and other effects.

The magnitude of the horizontal ageostrophic components and associated vertical motion pattern is determined by the along-stream variation of wind speed rather than the absolute magnitude of the wind maximum (Uccellini 1990). The inertial-advective[4] component dominates the ageostrophic wind at the upper-level. Therefore, the upper-level ageostrophic components have been termed "inertial-advective" components of the indirect (and direct) circulation. The lower-tropospheric ageostrophic components are referred to as "isallobaric[5]" since they are dominated by pressure gradient change and, consequently, net mass adjustment. The LLJ embedded in the lower branch of the indirect circulation is mainly the result of an increasing pressure gradient force (Uccellini, 1990). This isallobaric component resulted in a LLJ that was at a significant angle to the

---

[4] The inertial-advective component of the ageostrophic wind is defined as "that part of the ageostrophic wind that is due to advection of the wind by itself... [i]t is large in the exit and entrance region of jet streaks ... and when the flow is sharply curved." (Bluestein 1992, p. 175).

[5] The isallohypsic wind which is defined as "that part of the ageostrophic wind that is due to the gradient of the isallohypsic field [field of height change] ... is also called the isallobaric wind, even though pressure does not appear". (Bluestein 1992, p. 173-74).

LLJ (Uccellini and Johnson 1979). E
1980) proposed that the developme
eastward shift, is linked to the LLJ's
adjustment between the LLJ and the

The interaction between the up
destabilize the atmosphere through t
fields, differential heat and moisture
ascends along isentropic surfaces. A
tropospheric isentropic surface, the e
convergence (divergence) on the anti
1990). This mass divergence distribu
Together, these divergence distributio
surface below the jet streak. This incr
of the isallobaric wind component to
in an isentropic framework, in turn, is
framework. The vertical distribution
to convective destabilization (Uccelli
furthermore, showed that the LLJ sign
and heat transports into the inception
differential sensible heat and moistur
lowering of the level of free convection
thus effectively creating favorable con
storms.

Diabatic processes, in addition,
significantly increase the magnitude o
an important role in strengthening jet
developing convective complexes and

ULJ (Uccellini and Johnson 1979). Examining the movement of a LLJ in detail, Uccellini (1980) proposed that the development of the low level wind maximum, especially its eastward shift, is linked to the ULJ's propagation through a mutual mass-momentum adjustment between the ULJ and the LLJ (Uccellini 1980).

The interaction between the upper-level and low-level jets acts to convectively destabilize the atmosphere through the superposition of upper- and low-level divergence fields, differential heat and moisture transport and the release of latent heat as air ascends along isentropic surfaces. As mentioned previously, above a given mid-tropospheric isentropic surface, the exit region of the upper-level jet is marked by mass convergence (divergence) on the anticyclonic (cyclonic) side of the jet axis (Uccellini 1990). This mass divergence distribution is reversed below that particular surface. Together, these divergence distributions combine to increase the slope of the isentropic surface below the jet streak. This increased slope, in turn, contributes to a strengthening of the isallobaric wind component toward the cyclonic side of the jet. The upslope flow in an isentropic framework, in turn, is equivalent to warm advection in an isobaric framework. The vertical distribution of ageostrophic winds can therefore lead directly to convective destabilization (Uccellini 1990). Uccellini and Johnson (1979), furthermore, showed that the LLJ significantly increased the lower-tropospheric moisture and heat transports into the inception area of a severe convective storm. The differential sensible heat and moisture transports by the LLJ and ULJ resulted in a lowering of the level of free convection and in a height increase of the equilibrium level, thus effectively creating favorable conditions for the formation of deep convective storms.

Diabatic processes, in addition, modify the transverse circulation patterns and significantly increase the magnitude of vertical motions. Latent heat is thought to play an important role in strengthening jet streaks, particularly to the north and east of developing convective complexes and extratropical cyclones (Uccellini 1990). In a

simulation of an East Coast cyclone

reproduce the cyclone development

boundary layer and latent heat relea

out that the dynamic and diabatic p

difficult to separate the relative impo

mechanisms.

(iii) *The LLJ as Part of the Warm*

In recent years, relative-flow an

comma-shaped cloud pattern in mid-

airstreams: a warm conveyor belt, a

(Carr and Millard 1985). The airstrea

belt (WCB), the primary cloud produ

southwesterly flow along the cold fro

comma tail and body of the cloud pa

the surface low in the warm sector wi

disturbance to flow approximately pa

isentropic surfaces. The WCB turns a

upper-level westerly flow northeast o

(Carlson 1980).

A composite relative-wind analy

that a jet stream is located within the

the left-hand cloud edge (Cahir et al.

that the WCB corresponds to a belt of

maximum relative to the axis of the W

wind maximum in the upper troposph

WCB, the strongest winds at mid-leve

simulation of an East Coast cyclone, Uccellini et al. (1986) were able to most accurately reproduce the cyclone development when sensible and latent heat flux in the planetary boundary layer and latent heat release were included in the model. They also pointed out that the dynamic and diabatic processes act in a synergistic manner, and that it is difficult to separate the relative importance of upper- and lower-tropospheric forcing mechanisms.

(iii) The LLJ as Part of the Warm Conveyor Belt

In recent years, relative-flow analysis on isentropic surfaces has suggested that the comma-shaped cloud pattern in mid-latitude wave cyclones is the result of three airstreams: a warm conveyor belt, a cold conveyor belt and a dry stream (Carlson 1980; Carr and Millard 1985). The airstream of interest for this study is the 'warm conveyor belt' (WCB), the primary cloud producing flow (Carlson 1980). The WCB consists of a southwesterly flow along the cold front and north of the warm front that forms the comma tail and body of the cloud pattern. Warm, moist air, that originates far south of the surface low in the warm sector within an easterly flow, turns northward ahead of the disturbance to flow approximately parallel with the cold front, ascending along isentropic surfaces. The WCB turns anticyclonically above the warm front and joins the upper-level westerly flow northeast of the surface low near the upper-level ridge (Carlson 1980).

A composite relative-wind analysis of a number of warm conveyor belts revealed that a jet stream is located within the warm conveyor belt air stream, closely parallel to the left-hand cloud edge (Cahir et al. 1985). Hemler (1987) found additional evidence that the WCB corresponds to a belt of relatively strong winds. The location of the wind maximum relative to the axis of the WCB depends on the altitude, however. While the wind maximum in the upper troposphere is located close to the left-hand edge of the WCB, the strongest winds at mid-levels are found closer to the axis of the WCB some

distance from the left-hand cloud e

also showed with the help of a com

along the comma pattern. Brownin

ahead of the surface cold front in th

conveyor belt was still in contact w

50 mb on the order of 25-30 ms^{-1}, s

Browning (1990) found the wa

deep layer in which large quantities

transported poleward and upward.

highest amounts of moisture (Brown

more quickly and through greater ve

1960). Significant amounts of precip

especially where it ascended rapidly

particularly rapid after the WCB enc

(Browning 1990).

(iv) Temporal Variations

As part of mid-latitude pressur

would be expected to display the sam

they are associated with. Of particul

since cyclogenesis in the southern Pla

For the warm season (April-Septemb

frequency maximum in April and Ma

decline in frequency to a minimum in

a gradual increase. Hovanec and Hor

cyclogenesis in the Colorado area in s

distance from the left-hand cloud edge aloft (Hemler 1987). Carr and Millard (1987) also showed with the help of a composite analysis that the 850-mb winds were aligned along the comma pattern. Browning and Pardoe (1973) detected a LLJ immediately ahead of the surface cold front in the southern part of the warm conveyor belt where the conveyor belt was still in contact with the surface. They identified jet velocities at 900-850 mb on the order of 25-30 ms^{-1}, some reaching 40 ms^{-1}.

Browning (1990) found the warm conveyor belt to correspond to a 200-300 mb deep layer in which large quantities of heat, moisture and westerly momentum were transported poleward and upward. Air on the left edge of the WCB contained the highest amounts of moisture (Browning 1990). The air in the western section also rose more quickly and through greater vertical distance than air further to the east (Carlson 1980). Significant amounts of precipitation were generated in the warm conveyor belt, especially where it ascended rapidly in the low-to-middle troposphere. The ascent was particularly rapid after the WCB encountered a pronounced warm frontal zone (Browning 1990).

(iv) Temporal Variations

As part of mid-latitude pressure systems, LLJs in the warm sector of cyclones would be expected to display the same seasonal variation as the large-scale environment they are associated with. Of particular interest for this study are Colorado cyclones since cyclogenesis in the southern Plains has been shown to be linked to LLJ formation. For the warm season (April-September), Whittaker and Horn (1981) showed a relative frequency maximum in April and May for Colorado cyclones, followed by a rapid decline in frequency to a minimum in July. Following July, the cyclone frequency showed a gradual increase. Hovanec and Horn (1975) attributed the higher frequency of cyclogenesis in the Colorado area in spring to weaker static stability at that time and

also to the more frequent occurrenc
level jet streaks.

As noted above, LLJs in warm
observed frequency and wind speed
1983). Djuric and Ladwig (1983) do
morning (1200 UTC) for LLJs in cycl
with a sharper decrease of wind spe
more pronounced diurnal variation
significant decrease of wind speed i
al. (1995) verified the larger diurnal
low-level wind maxima in the South
interpreted the increased diurnal pha
importance of boundary-layer proces

Achtor and Horn (1986) also fo
the LLJ. In their analysis of composi
composite ageostrophic vectors over
easterly component at 0000 UTC, like
By 1200 UTC, the ageostrophic 850-n
These composite ageostrophic vectors
diurnal variation.

(b) Boundary-Layer Structure

The presence of an inversion is r
extratropical cyclones (Djuric and Da
Djuric and Damiani (1980), for instanc
cyclogenesis in the winter half-year ap
subsidence inversion. These inversion

also to the more frequent occurrence of short waves and associated propagating upper-level jet streaks.

As noted above, LLJs in warm sectors of cyclones have a weak diurnal variation in observed frequency and wind speed (Uccellini and Johnson 1979; Djuric and Ladwig 1983). Djuric and Ladwig (1983) documented a modest temporal preference for the morning (1200 UTC) for LLJs in cyclones in eastern Texas. The more prominent LLJs with a sharper decrease of wind speed above the level of maximum wind showed a more pronounced diurnal variation compared to those wind maxima that had a less significant decrease of wind speed in the vertical (Djuric and Ladwig 1983). Mitchell et al. (1995) verified the larger diurnal variation for more pronounced jets in a study of low-level wind maxima in the Southern Great Plains. The authors of both studies interpreted the increased diurnal phasing for stronger jets to be reflective of the importance of boundary-layer processes in modifying the LLJ.

Achtor and Horn (1986) also found an indication for diurnal influences modifying the LLJ. In their analysis of composite maps of 850-mb flow they noted that the composite ageostrophic vectors over the southern Plains displayed a predominantly easterly component at 0000 UTC, likely due to the influence of late-afternoon friction. By 1200 UTC, the ageostrophic 850-mb vectors at 1200 UTC were from the south. These composite ageostrophic vectors suggested that the direction of the LLJ has some diurnal variation.

(v) Boundary-Layer Structure

The presence of an inversion is repeatedly mentioned in LLJ case studies in extratropical cyclones (Djuric and Damiani 1980; Shen and Djuric 1981; Djuric 1981). Djuric and Damiani (1980), for instance, noted that low-level wind maxima during cyclogenesis in the winter half-year appeared almost always at the bottom of a subsidence inversion. These inversions seemed to be remnants of polar frontal

versions from preceding cold out

(981) noted that when pressure fal

set in motion. In the case of no inve

the atmosphere but it will not expa

preference for a jet to form in any la

flow is concentrated in the space un

Djuric 1981). In a modeling study,

presence of an inversion was essenti

2) FRONTAL BOUNDARY SITUA

While LLJs along frontal bound

and Pardoe 1973; Sortais et al. 1993

and the west coast of the United St

studies explicitly examining the role

central United States. Consequently

frontal situations outside the central

have been described by Browning a

Other studies of LLJs in connection

coast of France (Sortais et al. 1993;

States (Hobbs et al. 1980) and in Ta

Low-level wind maxima associ

lules during the winter half-year hav

parallel to the front. One or more LL

cold front (Browning and Harrold 1

cold fronts, the LLJs took on the form

wet-bulb potential temperature in th

Browning and Pardoe summarized th

inversions from preceding cold outbreaks (Djuric and Damiani 1980). Shen and Djuric (1981) noted that when pressure falls in one area of the atmosphere, air in the vicinity is set in motion. In the case of no inversion, the flow may expand through deep layers of the atmosphere but it will not expand far horizontally. In this case, there is no preference for a jet to form in any layer. In an inversion situation, on the other hand, the flow is concentrated in the space under and within the inversion, forming a jet (Shen and Djuric 1981). In a modeling study, Djuric (1981) was furthermore able to show that the presence of an inversion was essential during the formation of a LLJ during cyclogenesis.

2) FRONTAL BOUNDARY SITUATIONS

While LLJs along frontal boundaries have been reported in Europe (e.g. Browning and Pardoe 1973; Sortais et al. 1993; Kotroni et al. 1994), Asia (e.g. Chen and Yu 1988), and the west coast of the United States (Hobbs et al. 1980), I am not aware of any studies explicitly examining the role of wind maxima along frontal boundaries in the central United States. Consequently, the literature reviewed below focuses on LLJs in frontal situations outside the central U.S. LLJs ahead of cold fronts over the British Isles have been described by Browning and Harrold (1970) and Browning and Pardoe (1973). Other studies of LLJs in connection with cold fronts have been conducted on the west coast of France (Sortais et al. 1993; Kotroni et al. 1994), on the west coast of the United States (Hobbs et al. 1980) and in Taiwan (Chen and Yu 1988).

Low-level wind maxima associated with cold frontal passages over the British Isles during the winter half-year have been shown to consist of strong geostrophic flow parallel to the front. One or more LLJs were observed immediately ahead of the surface cold front (Browning and Harrold 1970; Browning and Pardoe 1973). Ahead of most cold fronts, the LLJs took on the form of a conveyor belt of almost saturated air of high wet-bulb potential temperature in the lowest 2-3 km (Browning and Monk 1982). Browning and Pardoe summarized the following characteristics based on a number of

case studies. The LLJs were eviden

nobile fronts. The average jet veloc

level, and the mean velocity half-wi

et each approximately 200 km acro

LLJs were embedded within the con

maximum velocity at 900 to 850 mb

at the top of the CBL which was ust

occurred just ahead of the surface co

addition, noted that the warm mois

subsidence inversion associated with

Browning and Pardoe (1973) a

relate the LLJ to patterns of convecti

requently observed at the sharp, cy

the surface cold front, air from the lo

rtically resulted in strong convecti

occasional thunder. This line convec

strong ascent was evident on the left

the right flank occurred over a band

The airflow toward the cold front in

had been advected parallel to the fro

Sortais et al. (1993) described a

Atlantic coast that had similar chara

and Harrold (1970) and Browning ar

observed in the warm sector 150 km

---

[4] Browning and Pardoe (1973) define th
[planetary boundary layer] but also exte
essentially been, influenced by thermally-d
characterized by the wet-bulb potential

case studies. The LLJs were evident during both day and night for stationary as well as mobile fronts. The average jet velocity was 27.5 ms^{-1}, the average height was the 880-mb level, and the mean velocity half-width was 600 km. At times there was more than one jet, each approximately 200 km across and often thousands of kilometers long. The LLJs were embedded within the convective boundary layer (CBL)[6]. They reached their maximum velocity at 900 to 850 mb and subsequently decreased in speed to a minimum at the top of the CBL which was usually capped by a stable layer. The most intense jets occurred just ahead of the surface cold front. Browning and Harrold (1970), in addition, noted that the warm moist air ahead of the cold front was located beneath a subsidence inversion associated with an anticyclone over Europe.

Browning and Pardoe (1973) and Browning and Harrold (1970) were also able to relate the LLJ to patterns of convection. They noted that vigorous line convection was frequently observed at the sharp, cyclonically sheared boundary of pre-frontal jets. At the surface cold front, air from the lowest km of the warm front ascending almost vertically resulted in strong convection accompanied by brief periods of hail and occasional thunder. This line convection was generally limited to 3 km depth. While strong ascent was evident on the left flank of the LLJ over a narrow band, the descent on the right flank occurred over a band which was broader by two orders of magnitude. The airflow toward the cold front in the lowest kilometer was fed by subsiding air which had been advected parallel to the front.

Sortais et al. (1993) described a LLJ ahead of a cold front along the French Atlantic coast that had similar characteristics to the jet cases described by Browning and Harrold (1970) and Browning and Pardoe (1973) over the British Isles. The jet was observed in the warm sector 150 km ahead of a cold front. It was located parallel to the

---

[6] Browning and Pardoe (1973) define the CBL as the boundary layer which "includes the PBL [planetary boundary layer] but also extends over the deeper layer which is being, or has recently been, influenced by thermally-driven convection from the surface." The CBL is characterized by the wet-bulb potential temperature being almost constant with height.

cold front in the first 2 km of the tr

rontal rain band developed along

the rain band moved eastward in u

simulations, Sortais et al. showed th

the LLJ and developing the frontal

In their study of a cold-fronta

pointed out the importance of LLJs

to their interaction between differen

strong (maximum speeds in excess

at a height of about 1100 m. Like th

and Browning and Pardoe (1973), th

both potential temperature was at a

The LLJ was also shown to be asymm

on its cold side than its warm side.

observed along the left flank of the

on the order of 5-10 ms^{-1} associated

km were found to be the result of fo

by strong convergence as the cold fr

(Koltroni et al. 1994).

Koltroni et al. (1994) attributed

transverse horizontal temperature gr

horizontal gradient resulted from a c

the warmest air from the south to im

temperature gradient was further int

investigators detected a pronounced

secondary clockwise circulation arou

around the frontal surface consisted

cold front in the first 2 km of the troposphere and had speeds in excess of 30 ms^{-1}. A frontal rain band developed along the west side of the LLJ and subsequently the LLJ and the rain band moved eastward in unison with the entire frontal system. In model simulations, Sortais et al. showed that diabatic processes were essential in intensifying the LLJ and developing the frontal band ahead of the cold front.

In their study of a cold-frontal LLJ over Brittany (France), Kotroni et al. (1994) pointed out the importance of LLJs in the dynamics of mid-latitude frontal systems due to their interaction between different scales of atmospheric motions. They observed a strong (maximum speeds in excess of 30 ms^{-1}), narrow (approximately 150 km wide) LLJ at a height of about 1100 m. Like the LLJs described by Browning and Harrold (1970) and Browning and Pardoe (1973), this LLJ was embedded in a region where the wet-bulb potential temperature was at a maximum in the horizontal (Kotroni et al. 1994). The LLJ was also shown to be asymmetric in nature with a stronger gradient of velocity on its cold side than its warm side. A narrow region (5-10 km) of heavy rain was observed along the left flank of the LLJ just ahead of the surface cold front. Updrafts on the order of 5-10 ms^{-1} associated with that line convection with typical heights of 1-2 km were found to be the result of forced rather than free convection. They were initiated by strong convergence as the cold front advanced on the moist warm air beneath the LLJ (Kotroni et al. 1994).

Kotroni et al. (1994) attributed the formation of the LLJ to a locally strong transverse horizontal temperature gradient within the warm conveyor belt. This horizontal gradient resulted from a cyclonic synoptic-scale circulation which transported the warmest air from the south to immediately ahead of the surface cold front. The temperature gradient was further intensified by ageostrophic circulations. The investigators detected a pronounced thermally direct cross-frontal circulation and a secondary clockwise circulation around the LLJ axis. The ageostrophic circulation around the frontal surface consisted of a strong flow of warm moist air toward the front

n the lowest layers that subsequen

return flow toward warm air behin

tion of a narrow region of strong ir

below the frontal surface. In the cl

(1984), like Browning and Pardoe (

on the left flank of the jet (maximu

weaker subsidence on its right flank

the left flank than on the right. Als

When inertial acceleration played a

produced but rather was advected

resulting in a linear mesoscale regio

mesoscale convergence appeared to

motions. Thus the prefrontal LLJ w

seemed to be a crucial factor in the

convection due to its promotion of a

Like Sortais et al. (1993), Kotr

associated with the vertical motion

intensification of the LLJ. First, it in

direct circulation and secondly, heat

potential-temperature gradient and

beneficial to LLJ development was a

conditional symmetric instability[7] in

diminished gravitational resistance t

ascending branch of the ageostrophi

cyclonic relative vertical vorticity.

[7] In the parcel theory of symmetric flo
vertically (Bluestein 1993, p. 340).

in the lowest layers that subsequently rose sharply at the leading edge of the front and a return flow toward warm air behind the front. In the cold air this circulation took on the form of a narrow region of strong increase in the frontward flow, descending along and below the frontal surface. In the clockwise circulation around the jet axis, Kotroni et al. (1994), like Browning and Pardoe (1973), found evidence for stronger ascending motion on the left flank of the jet (maximum of 30-60 cm s^{-1}) ahead of the frontal surface and weaker subsidence on its right flank. Consequently, the boundary layer was thicker on the left flank than on the right. Also, frictional dissipation was larger on the left flank. When inertial acceleration played a role, kinetic energy was not dissipated where it was produced but rather was advected from the warm side of the LLJ to the cold side resulting in a linear mesoscale region of convergence. In the presence of humidity, this mesoscale convergence appeared to be strong enough to trigger convective-scale vertical motions. Thus the prefrontal LLJ with its horizontal and vertical wind shear patterns seemed to be a crucial factor in the maintenance and intensification of the line convection due to its promotion of ageostrophic convergence in the boundary layer.

Like Sortais et al. (1993), Kotroni et al. (1994) noted that latent heat release associated with the vertical motion played an important role in the development and intensification of the LLJ. First, it increased the magnitude of the upward branch of the direct circulation and secondly, heating on the left flank of the LLJ increased the potential-temperature gradient and thus strengthened the LLJ. Another factor that was beneficial to LLJ development was an atmosphere that was neutral or slightly stable to conditional symmetric instability[7] in the lowest prefrontal layers. The resulting diminished gravitational resistance to sloping ascent was thought to enhance the ascending branch of the ageostrophic circulation and thus increase the production of cyclonic relative vertical vorticity.

---

[7] In the parcel theory of symmetric flow, a parcel is displaced along a tilted plane rather than vertically (Bluestein 1993, p. 340).

Hobbs et al. (1980) observed
front that crossed the Pacific Ocea
with speeds of over 25 ms⁻¹ was ev
ist cases described above for Euro
front. Also, a narrow cold-frontal
) was observed immediately ahea
updraft also originated in a region
the surface cold front (Hobbs et al

LLJs are frequently observed
front, in east Asia in late spring an
and extremely heavy rainfall event
observational studies. Chen and Y
heavy rainfall events in northern Ta
average per season were caused by
frontal cloud band. LLJs were not
convective systems (MCSs), but the
circulations by the MCSs over the s
LLJs were more frequently found o
850-mb surfaces, at a higher altitud
rainfall events were very closely rel
authors noted that the average win
extremely heavy precipitation. It su
rainfall. In composite vertical profil
for the period of 12 h prior to the in
frequency of LLJs decreased dramat
speed and frequency to vertical mixi

Hobbs et al. (1980) observed strong low-level winds within 70 km ahead of a cold front that crossed the Pacific Ocean and moved into Washington. The jet maximum with speeds of over 25 ms^{-1} was evident at an altitude of 0.8 km. Similar to cold-frontal jet cases described above for Europe, relative humidity peaked in the vicinity of the cold front. Also, a narrow cold-frontal rain band (5 km wide) with a strong updraft (1.2 ms^{-1}) was observed immediately ahead of the cold front. As for European cases, the updraft also originated in a region of strong convergence within the lowest kilometer at the surface cold front (Hobbs et al. 1980).

LLJs are frequently observed to the south of a lower-tropospheric front, the Mei-Yu front, in east Asia in late spring and early summer. A close relationship between LLJs and extremely heavy rainfall events in this frontal system has been noted in observational studies. Chen and Yu (1988), for instance, analyzed 20 years of extremely heavy rainfall events in northern Taiwan. They found that 1.8 extreme rain events on average per season were caused by mesoscale convective systems within the Mei-Yu frontal cloud band. LLJs were not only frequently associated with these mesoscale convective systems (MCSs), but they were also thought to be the result of enhanced circulations by the MCSs over the southern China coast. Chen and Yu noted that while LLJs were more frequently found on 700-mb constant pressure surfaces compared to 850-mb surfaces, at a higher altitude than in other frontal-jet studies, extremely heavy rainfall events were very closely related to LLJs at both the 850- and 700-mb levels. The authors noted that the average wind maximum was 19.8 ms^{-1} 12 h prior to the start of extremely heavy precipitation. It subsequently decreased during the period of the heavy rainfall. In composite vertical profiles, a secondary maximum near 960 m was evident for the period of 12 h prior to the initiation of rainfall. After a rainfall event, the frequency of LLJs decreased dramatically. Chen and Yu attributed this decrease in jet speed and frequency to vertical mixing by cumulus convection.

1 Convection Associated with Bound

The location of a maximum c

he zone of maximum low-level wi

of the low-level wind maxima in i

and London 1962; Bonner 1968). I

nitiation and enhancement of conv

contributions. The differential mo

Destabilization of the pre-convectiv

associated vertical motion lead to t

1955; Ucellini 1990). In this sectio

and synoptically-driven low-level w

n terminology that was mentioned

convection of the different types of

The characteristics of convecti

first. An attempt is made to relate

inematic properties of jets that are

followed by ways in which low-leve

convective environment.

1) GREAT PLAINS CONVECTION

The diurnal preference of low-l

as prompted researchers to speculat

and convective activity in the south

Bonner 1968). The agreement in the

different types of convective activity

phenomena. The bimodal seasonal v

Great Plains with a maximum in Sep

d. Convection Associated with Boundary-Layer Jets and Low-Level Jets

The location of a maximum of thunderstorm occurrence in the Great Plains north of the zone of maximum low-level wind frequency has prompted speculation about the role of the low-level wind maxima in initiating convective activity (Means 1954; Pitchford and London 1962; Bonner 1968). Low-level wind maxima are thought to affect the initiation and enhancement of convection through thermodynamic and kinematic contributions. The differential moisture and temperature advection promotes a destabilization of the pre-convective environment and low-level convergence and associated vertical motion lead to the release of convective instability (Beebe and Bates 1955; Uccellini 1990). In this section, the contributions of both boundary-layer forced and synoptically-driven low-level wind maxima will be discussed. Due to the confusion in terminology that was mentioned above, a distinction of the particular effects on convection of the different types of wind maxima is not possible.

The characteristics of convection in the southern Great Plains will be introduced first. An attempt is made to relate the convective activity to low-level wind fields. The kinematic properties of jets that are conducive to convection will be discussed next, followed by ways in which low-level wind maxima influence the thermodynamic convective environment.

1) GREAT PLAINS CONVECTION

The diurnal preference of low-level wind maxima for the nighttime hours has early on prompted researchers to speculate on a causal link between low-level wind maxima and convective activity in the southern Great Plains (Pitchford and London 1962; Bonner 1968). The agreement in the seasonal variation of low-level wind maxima and different types of convective activity also suggests some connection between the two phenomena. The bimodal seasonal variation of low-level wind maxima in the southern Great Plains with a maximum in September and a secondary maximum in May (Mitchell

et al. 1995), for instance, is also fou

al. 1994; Bradley and Smith 1994).

precipitation amounts are recorde

also been shown to be the peak tim

high winds in Oklahoma (Houze e

the month of most frequent Colora

and Horn 1981).

For extreme rain events, Brad

maxima in late spring and early fal

forcing and higher than average lev

variables that affect rainstorms, Br

factors: low-level winds and moistu

thunderstorm updraft and veering

occurred in convectively unstable e

course of the warm season. Based

distinguished between strong dynar

In both instances, 850-mb winds br

area. During strong dynamic forcin

toward the southern plains in the fo

mb level. A quasi-stationary front e

region. Large rainfall occurred ahea

dynamic forcing events, the strong

stationary front or a thunderstorm g

evident. This front served as a ramp

strong dynamic forcing events were

weak dynamic forcing events were m

availability and convective instabilit

et al. 1995), for instance, is also found in the frequency of extreme rainstorms (Smith et al. 1994; Bradley and Smith 1994). Furthermore, the highest monthly mean precipitation amounts are recorded in May (Bradley and Smith 1994). Springtime has also been shown to be the peak time for severe thunderstorms with tornadoes, hail and high winds in Oklahoma (Houze et al. 1990). Of the warm season months, May is also the month of most frequent Colorado cyclogenesis, followed by September (Whittaker and Horn 1981).

For extreme rain events, Bradley and Smith (1994) attributed the frequency maxima in late spring and early fall to a combination of relatively strong dynamic forcing and higher than average levels of moisture and instability. In addition to other variables that affect rainstorms, Bradley and Smith identified the following low-level factors: low-level winds and moisture, vertical shear of the horizontal winds, strength of thunderstorm updraft and veering of winds with height. While all extreme rainstorms occurred in convectively unstable environments, the synoptic patterns varied over the course of the warm season. Based on the synoptic patterns, Bradley and Smith distinguished between strong dynamic forcing events and weak dynamic forcing events. In both instances, 850-mb winds brought warm moist air from the south to the storm area. During strong dynamic forcing events, an upper-level disturbance was moving toward the southern plains in the form of a short-wave trough, or cut-off low, at the 500 mb level. A quasi-stationary front extended from the southern plains to the Great Lakes region. Large rainfall occurred ahead of the front in the warm sector. During weak dynamic forcing events, the strong upper-level disturbance was absent. A quasi-stationary front or a thunderstorm gust front, extending from east to west, was usually evident. This front served as a ramp for the low-level southerly wind. As expected, strong dynamic forcing events were more common in the spring and fall months while weak dynamic forcing events were more common during the summer when moisture availability and convective instability were higher (Bradley and Smith 1994).

In addition to the seasonal v

Plains shows considerable diurna

strong diurnal cycle of convection

(late-August). While severe conve

afternoon and early evening, thund

midnight and all rain events peake

region centered on Oklahoma City

rainfall to peak near 0300 LST, the

maximum low-level wind speed.

to include the entire six warm seas

predominantly nocturnal precipitat

observed an east-west gradient of a

frequency. If one considers the low

of convective activity, the east-west

inertial oscillation of the low-level w

undergo not only an oscillation in s

over the course of the night. The clo

the terminus of the jet in an eastward

hypothesis, Djuric and Damiani (19

were anticyclonically curved, which

2) Boundary-Layer Convergen

The boundary-layer convergen

resulting vertical velocity patterns ha

and prolonging convective activity (

and Schreiber 1986). Wilson and Sch

the organization and movement of se

In addition to the seasonal variability, the phasing of convection in the Great Plains shows considerable diurnal variability. Wallace (1975), for instance, noted a strong diurnal cycle of convection for the Central Plains during the summer months (June-August). While severe convective storms occurred most frequently during the late afternoon and early evening, thunderstorms showed a frequency maximum around midnight and all rain events peaked several hours after midnight (Wallace 1975). For a region centered on Oklahoma City, Smith et al. (1994) found the probability of all rainfall to peak near 0300 LST, the time Mitchell et al. (1995) give as the time of maximum low-level wind speed. When Balling (1985) extended Wallace's (1975) study to include the entire six warm season months (April - September), he also noted the predominantly nocturnal precipitation regime in the Central Plains. In addition, Balling observed an east-west gradient of approximately 1 h 100 km^{-1} in the timing of maximum frequency. If one considers the low-level wind to be a driving force behind the initiation of convective activity, the east-west gradient could be interpreted as a result of the inertial oscillation of the low-level wind. As discussed above, low-level wind maxima undergo not only an oscillation in speed but also a clockwise rotation of the wind vector over the course of the night. The clockwise rotation would move the convergence field at the terminus of the jet in an eastward direction during the night. In agreement with this hypothesis, Djuric and Damiani (1980), noted that the streamlines in a mature LLJs were anticyclonically curved, which would also display the terminus to the east.

2) BOUNDARY-LAYER CONVERGENCE

The boundary-layer convergence associated with a low-level wind maximum and resulting vertical velocity patterns have been recognized as important factors in initiating and prolonging convective activity (Pitchford and London 1962; Bonner 1966; Wilson and Schreiber 1986). Wilson and Schreiber (1986) pointed out that in certain instances the organization and movement of severe storms was more influenced by strong

low-level convergent features thar

Pitchford and London (1962) note

in regions of positive vertical mot

maximum. The decelerating leadi

horizontal wind field lead to ascer

region for release of convection by

Maddox and Doswell (1982) and

addition, noted that a region of co

axis, although the strongest conve

end of the jet where warm advecti

3) WARM ADVECTION

Maddox and Doswell (1982)

importance of strong southerly low

events. Bradley and Smith (1994)

direction between 135° and 225° in

southern Great Plains. All storms

convective storms developed withi

persistent lower-tropospheric warm

Particularly favorable conditions fo

warmest 850-mb temperatures lay

scenario was also reported by Mear

the highest mean temperatures to th

The amount of warm and moi

studied by Bonner (1966) for a 24 h

Plains. He found that the 850-mb t

the mixing ratio values increased by

low-level convergent features than by upper-level winds. For the Nebraska region, Pitchford and London (1962) noted that nocturnal thunderstorms were closely related to regions of positive vertical motion associated with convergence downstream of a LLJ maximum. The decelerating leading edge of a jet where strong convergence of the horizontal wind field lead to ascent of humid boundary-layer air was also given as a region for release of convection by Means (1954), Paegle and McLawhorn (1973), Maddox and Doswell (1982) and Nicolini et al. (1993). Beebe and Bates (1955), in addition, noted that a region of convergence was at times found to the left of the jet axis, although the strongest convergence was still thought to be located at the northern end of the jet where warm advection was greatest.

3) WARM ADVECTION

Maddox and Doswell (1982) and Bradley and Smith (1994) highlighted the importance of strong southerly low-level winds in generating significant convective events. Bradley and Smith (1994) found 850-mb winds in excess of 14 ms^{-1} from a direction between 135° and 225° in almost all investigated extreme rainstorms in the southern Great Plains. All storms in Maddox and Doswell's (1982) study of intense convective storms developed within regions that were characterized by strong and persistent lower-tropospheric warm advection and significant conditional instability. Particularly favorable conditions for severe storms development existed if the axis of the warmest 850-mb temperatures lay to the west of the 850-mb moisture axis. This scenario was also reported by Means (1954) for a heavy rain event where he observed the highest mean temperatures to the west of the low-level current.

The amount of warm and moist advection by a low-level wind maximum was studied by Bonner (1966) for a 24 h period during a thunderstorm event in the Great Plains. He found that the 850-mb temperatures rose by 4° C along the jet axis and that the mixing ratio values increased by 3 g kg^{-1} during the first 12 h (Bonner 1966). The

advected warm air can lead to pa
an inversion (Carlson 1983). Carl
initially prevents the release of lat
the lid or underrunning at the edg
subsequently lead to intense conv
congestus and hail days, noted tha
southerly flow were stronger. Als

4) VERTICAL MOTION AND LA

While LLJs may initially trigg
release may subsequently increase
jet itself (Nicolini et al. 1993). In a
rain was to increase the storm-relat
processes were thought to be strong
of the LLJ. Fuelberg and Buechler
They also noted that despite the fa
activity, its later development may
attributed the strengthening of the
as well as height falls.

5) MESOSCALE CONVECTIVE S

Mesoscale convective weather
the warm season (April - September
Rocky Mountains and the Mississip
As the warm season progresses, the
northward (Maddox et al. 1986).

advected warm air can lead to particularly explosive convection when it is capped by an inversion (Carlson 1983). Carlson pointed out that the capping inversion (lid) initially prevents the release of latent instability over large areas. The later removal of the lid or underrunning at the edges of the lid by moist boundary layer air can subsequently lead to intense convection. Mahrt (1977), in a comparison of cumulus congestus and hail days, noted that on hail days both the low-level inversion and the southerly flow were stronger. Also, low-level shear was stronger.

4) VERTICAL MOTION AND LATENT HEAT RELEASE

While LLJs may initially trigger nocturnal convection, the resulting latent heat release may subsequently increase the amount of vertical motion and thus strengthen the jet itself (Nicolini et al. 1993). In a model, Nicolini et al. showed that the effect of local rain was to increase the storm-relative inflow. The resulting cloud condensation processes were thought to be strong enough to almost double the nocturnal acceleration of the LLJ. Fuelberg and Buechler (1989) came to the same conclusion in their study. They also noted that despite the fact that the LLJ began to form prior to the convective activity, its later development may have been enhanced by the storm itself. They attributed the strengthening of the LLJ to enhanced low-level convergence west of the LLJ as well as height falls.

5) MESOSCALE CONVECTIVE SYSTEMS AND MESOSCALE CONVECTIVE COMPLEXES

Mesoscale convective weather systems (MCS) account for a significant amount of the warm season (April - September) precipitation over much of the region between the Rocky Mountains and the Mississippi River (Maddox et al. 1986; Fritsch et al. 1986). As the warm season progresses, the favored region of MCS development shifts slowly northward (Maddox et al. 1986).

Maddox (1983) noted that L

complexes (MCC), highly organiz

Maddox et al. (1986) pointed out

and the low-level wind field. MC

develop during the late afternoon

for hours. Maddox noted that MC

time when the nocturnal LLJ reach

component and is located closest

morning hours when low-level wi

During MCC development, l

apparently dominate the vertical

1984). Maddox et al. (1986) and

development is supported by a di

with the axis of a LLJ. Initial thun

convergence and lifting that is indu

time period from prior the MCC d

speed increases slightly, and subst

before and during the MCC, the 85

the low-level winds increase and v

shifts eastward across the Great Pl

to both the advance of a short-wav

decay, the LLJ is no longer present

have been observed to produce oth

strong winds, and intense electrica

Blanchard (1990), Houze et a

distinguished between different typ

(1990) examined meso-alpha scale a

Maddox (1983) noted that LLJs are recurrent features in mesoscale convective complexes (MCC), highly organized mesoscale convective systems. In a later study, Maddox et al. (1986) pointed out the apparent connection between MCC development and the low-level wind field. MCCs usually have their roots in thunderstorms that develop during the late afternoon. Under favorable conditions, MCCs are able to persist for hours. Maddox noted that MCCs reach maximum size around local midnight, the time when the nocturnal LLJ reaches its maximum strength, has the strongest westerly component and is located closest to the surface. Most often, MCCs weaken during the morning hours when low-level wind maxima should be backing and weakening.

During MCC development, lower-tropospheric forcing and convective instability apparently dominate the vertical circulations (Maddox 1983; Augustine and Caracena 1994). Maddox et al. (1986) and Cotton et al. (1989) pointed out that the convective development is supported by a distinct pocket of very unstable air that corresponded with the axis of a LLJ. Initial thunderstorms develop within a region of mesoscale convergence and lifting that is induced by the low-level warm advection. During the time period from prior the MCC development to the time of the MCC, the 850-mb wind speed increases slightly, and substantial veering is observed in the low levels. Both before and during the MCC, the 850-mb winds are stronger than the 500-mb winds. As the low-level winds increase and veer during the night, the warm advection pattern shifts eastward across the Great Plains. Maddox (1983) attributed the low-level veering to both the advance of a short-wave trough and inertial oscillation. At the time of MCC decay, the LLJ is no longer present (Maddox 1983). In addition to heavy rainfall, MCCs have been observed to produce other convective phenomena such as tornadoes, hail, strong winds, and intense electrical storms (Maddox et al. 1986).

Blanchard (1990), Houze et al. (1990) and Augustine and Caracena (1994) distinguished between different types of mesoscale convective systems. Blanchard (1990) examined meso-alpha scale and meso-beta scale occluding mesoscale convective

systems. Occluding mesoscale sy

the system and cold conveyor bel

rear-to-front flows across the syst

belt originated in a LLJ approxim

vertically in convective cells along

region of the system and turned c

occluding systems, two areas of c

convection developed first along

along the north-south cold front.

the intersection of the two lines.

moisture through greater depth, s

(Blanchard 1990).

Augustine and Caracena (1

They noted that while both large

level geostrophic wind maximum

had a stronger cyclonic turn to th

its counterpart in small MCSs. L

with stronger frontogenetic forcin

850-mb level, was located downs

maximum. Therefore, the noctur

north. The interaction of the LLJ

upward motion associated with t

convergence. In small MCSs, on

frontal boundary and the vertica

Houze et al. (1990) examin

rain events in Oklahoma. They f

systems with distinct "leading li

systems. Occluding mesoscale systems have warm conveyor belts to the front (east) of the system and cold conveyor belts to the rear (west) in addition to front-to-rear and rear-to-front flows across the system. In the investigated systems, the warm conveyor belt originated in a LLJ approximately 0.5-2.0 km AGL. Portions of the jet ascended vertically in convective cells along the gust front, while other parts ascended in the apex region of the system and turned cyclonically to flow toward the rear of the system. In occluding systems, two areas of convection were evident. An east-west line of convection developed first along a quasi-stationary front before convection was initiated along the north-south cold front. Stratiform precipitation subsequently began to form at the intersection of the two lines. Meso-alpha scale systems contained slightly more moisture through greater depth, stronger inflow and low-level veering of the wind (Blanchard 1990).

Augustine and Caracena (1994) distinguished between large and small MCSs. They noted that while both large and small MCSs matured north of a late afternoon low-level geostrophic wind maximum, the nocturnal surface geostrophic wind in large MCSs had a stronger cyclonic turn to the west of the location of the afternoon maximum than its counterpart in small MCSs. Large, heavy-rain producing MCSs were also associated with stronger frontogenetic forcing. A surface front, extending vertically through the 850-mb level, was located downwind of the late afternoon surface geostrophic wind maximum. Therefore, the nocturnal LLJ encountered a relatively deep boundary to the north. The interaction of the LLJ and the frontal boundary strengthened the pre-existing upward motion associated with the frontogenesis through warm advection and convergence. In small MCSs, on the other hand, the LLJ did not encounter a significant frontal boundary and the vertical motion was not focused.

Houze et al. (1990) examined different types of mesoscale organization of major rain events in Oklahoma. They first classified radar signatures into strongly classifiable systems with distinct "leading line /trailing stratiform" patterns, moderately to weakly

classifiable systems, and unclassi

symmetry in the systems. Their f

low-level environments for differ

line /trailing stratiform" pattern

unclassifiable systems, on the oth

frequently with symmetric, stron

tropospheric shear, a LLJ, and hi

typical of multi-cellular storm c

asymmetric, moderately to weak

a Bulk Richardson Number near

was observed in connection with

The low-level environment in thi

in the absence of a LLJ, with a Bu

6) SQUALL LINES

The existence of a low-leve

(Means 1954; Porter et al. 1955;

noted that low-level jets were pr

frequently oriented parallel to th

furthermore, attributed the obse

jet.

c. Summary

Low-level wind maxima in

different synoptic settings. Whil

[8] "Convective available potential e

the buoyant energy available to a

classifiable systems, and unclassifiable systems. Then they denoted the degree of symmetry in the systems. Their findings included varying mesoscale organizations and low-level environments for different weather events. The strongly classifiable "leading line /trailing stratiform" pattern was associated with a pronounced LLJ. The unclassifiable systems, on the other hand, lacked a LLJ. Flooding was observed most frequently with symmetric, strongly classifiable mesoscale patterns, weak-to-low mid tropospheric shear, a LLJ, and high Bulk Richardson Number (High CAPE[8] / low shear - typical of multi-cellular storm organization). Tornadic storms tended to occur with asymmetric, moderately to weakly classifiable patterns, stronger shear, a strong LLJ and a Bulk Richardson Number near the supercell range. Other severe weather (mostly hail) was observed in connection with an unclassifiable pattern of mesoscale organization. The low-level environment in this case was characterized by strong unidirectional shear in the absence of a LLJ, with a Bulk-Richardson Number well within supercell range.

6) SQUALL LINES

The existence of a low-level jet in squall lines has repeatedly been pointed out (Means 1954; Porter et al. 1955; Hoecker 1963; Raymond 1978). Porter et al. (1955) noted that low-level jets were present for 75 percent of squall lines. Squall lines are frequently oriented parallel to the jet axis (Means 1954; Kuettner 1971). Kuettner, furthermore, attributed the observed cloud deck to the linear organization caused by a jet.

e. Summary

Low-level wind maxima in the southern Great Plains have been reported in different synoptic settings. While early studies did not distinguish between different

[8] "Convective available potential energy (CAPE) is a measure of convective instability. It is the buoyant energy available to a parcel rising vertically through an undisturbed

types of low-level wind maxima

between low-level wind maxima

1988; Chen et al. 1994). Chen et

maxima fall into two categories:

PBL, and wind maxima above t

Both types of low-level wind ma

environment and boundary-layer

the traditional boundary-layer je

forcing mechanisms as described

pronounced diurnal oscillation in

distinct nocturnal frequency max

usually associated with well-defi

such as fronts and cyclones. Whi

nevertheless modified by diurnal

authors have similarly called for a

Stadtkovic and Kanter 1977), no co

wind maxima has been conducted

furthermore complicated by the fa

indiscriminately for both types of

conflicting findings about the diur

horizontal structure of low-level w

Low-level wind maxima hav

convective cycle of the central Plai

the region and initiating large-scale

types of low-level wind maxima ap

warm, moist air into regions of con

environment." (Bradley and Smith 19

types of low-level wind maxima, recent studies have recognized the need to differentiate between low-level wind maxima types in different settings (Uccellini 1980; Parish et al. 1988; Chen et al. 1994). Chen et al. (1994), for instance, suggested that low-level wind maxima fall into two categories: wind maxima within the planetary boundary layer (PBL) and wind maxima above the PBL, usually between the 900- and 600-mb levels. Both types of low-level wind maxima are the result of both the synoptic-scale environment and boundary-layer enhancement. The former type of wind maximum is the traditional boundary-layer jet (BLJ) in the absence of synoptic- or subsynoptic-scale forcing mechanisms as described by most early studies. It is characterized by a pronounced diurnal oscillation in wind speed, direction and height and it displays a distinct nocturnal frequency maximum. The latter type, wind maxima above the PBL, is usually associated with well-defined synoptic- or subsynoptic-scale weather systems, such as fronts and cyclones. While it lacks pronounced diurnal oscillations, it is nevertheless modified by diurnal changes in boundary-layer conditions. Although other authors have similarly called for a differentiation of low-level wind maxima (e.g. Sladkovic and Kanter 1977), no comprehensive study delineating the different types of wind maxima has been conducted. The distinction between the different types of jets is furthermore complicated by the fact that "low-level jet" has been applied indiscriminately for both types of wind maxima, leading to confusion and even conflicting findings about the diurnal and seasonal frequency, the vertical extent and the horizontal structure of low-level wind maxima, and their relation to convection.

Low-level wind maxima have been shown to be important components of the convective cycle of the central Plains due to their role in advecting warm, moist air into the region and initiating large-scale ascent through convergent flow patterns. While all types of low-level wind maxima appear to be important mechanisms for transporting warm, moist air into regions of convective activity, airflow patterns have been shown to

---

environment." (Bradley and Smith 1994, p. 1421).

vary considerably depending on

strength of the synoptic forcing.

3. Specific Objectives of Study

Although studies of low-le

questions remain. In an attempt

wind maxima, this study attemp

1. What impact does the definition
climatology of this phenomenon, spe

As shown above, since Bon

ncreasing body of literature has

pparent synoptic-scale influence

ubsynoptic scale environments

for example, found evidence for t

within an ascending anticyclonica

cyclones. Uccellini and Johnson

scale settings, lower-tropospheric

circulation in the exit region of up

the lower-tropospheric and upper

low-level wind maxima beyond th

definition of low-level wind maxi

850-mb level. A number of climat

his criteria. To fully understand th

mpact on convection, however, th

criteria on our interpretation of the

possible causes of jets need to be e

vary considerably depending on the synoptic- or subsynoptic-scale environment and the strength of the synoptic forcing.

3. Specific Objectives of Study

Although studies of low-level jets abound in the literature, a number of important questions remain. In an attempt to clarify some of the uncertainty surrounding low-level wind maxima, this study attempts to answer the following research questions:

1) What impact does the definition of low-level wind maxima have on our interpretation of the climatology of this phenomenon, specifically in the Central Plains?

As shown above, since Bonner's (1968) climatological study of the low-level jet, an increasing body of literature has suggested that, in addition to environments without apparent synoptic-scale influences, low-level jets are also found in synoptic-scale and subsynoptic scale environments such as cyclones and frontal systems. Carlson (1980), for example, found evidence for the existence of low-level wind maxima embedded within an ascending anticyclonically-curved airstream in the warm-sector of midlatitude cyclones. Uccellini and Johnson (1979), among others, point out that in certain large-scale settings, lower-tropospheric wind maxima are imbedded in the transverse circulation in the exit region of upper-tropospheric jet streaks. These linkages between the lower-tropospheric and upper-tropospheric wind fields imply a vertical extent of low-level wind maxima beyond the planetary boundary layer. Bonner's (1968) definition of low-level wind maxima, however, only allows for speed maxima up to the 850-mb level. A number of climatological studies followed Bonner's lead and adopted his criteria. To fully understand the different types of low-level wind maxima and their impact on convection, however, the effects of a relaxation of Bonner's speed and height criteria on our interpretation of the climatology of lower tropospheric jets and of the possible causes of jets need to be examined.

2) Is it possible to distinguish betw
tween (i.e., LLJs) lower troposphe
ccurrence? If so, are geographic va
LLJs in the Central Plains?

Although an increasing nu

wind maxima that appear to be

maxima that appear to be prima

1994), to date no comprehensive

frequency of different types of w

study, the speed and height crite

Bonner (1968) are relaxed to allo

In an attempt to isolate the temp

speed profiles of lower troposph

conducted for individual rawinso

the geographical differences in th

maxima. Geographical variations

based on the predominance of dif

wind maxima are observed most

from the occurrence of both boun

maxima. This region is located at

layer wind maxima are expected t

of the inertial oscillation with the

likely also located in the general vi

that it is situated east of the Color

have a less pronounced geographic

LLJs is expected to vary over the c

movement of dynamic forcing mec

2) Is it possible to distinguish between boundary-layer forced (i.e., BLJs) and synoptically-driven (i.e., LLJs) lower tropospheric wind maxima based on their height and time of occurrence? If so, are geographic variations evident in the frequency of warm season BLJs and LLJs in the Central Plains?

Although an increasing number of investigators are calling for a distinction between wind maxima that appear to be the result of boundary-layer influences and wind maxima that appear to be primarily driven by synoptic-scale influences (e.g. Chen et al. 1994), to date no comprehensive study has been undertaken to examine the relative frequency of different types of wind maxima. As a first step toward a comprehensive study, the speed and height criteria for low-level wind maxima as first applied by Bonner (1968) are relaxed to allow for the inclusion of a wider sample of wind maxima. In an attempt to isolate the temporal and height characteristics for BLJs and LLJs, the speed profiles of lower tropospheric wind maxima are analyzed. This analysis is conducted for individual rawinsonde stations across the Central Plains to investigate the geographical differences in the temporal and height characteristics of the wind maxima. Geographical variations in the frequency of BLJs versus LLJs are expected based on the predominance of different forcing mechanisms. The region where low-level wind maxima are observed most frequently, as identified by Bonner (1968), likely results from the occurrence of both boundary-layer forced and synoptically-driven wind maxima. This region is located at approximately 30° N, the latitude where boundary-layer wind maxima are expected to be most frequent based on the close correspondence of the inertial oscillation with the diurnal heating/cooling cycle. While some LLJs are likely also located in the general vicinity of Bonner's frequency maximum due to the fact that it is situated east of the Colorado cyclogenesis region, LLJs overall are expected to have a less pronounced geographic maximum. Rather, the geographical preference of LLJs is expected to vary over the course of the warm season due to the northward movement of dynamic forcing mechanisms during that time.

3) Are there distinct airflow config
zonal maxima in the Great Plains

Although the spatial config

explicitly studied previously, su

BLJs, for example, would be exp

LLJs, since BLJs are more geogra

studies have noted that BLJs are

LLJs, on the other hand, are in pa

cold frontal boundaries. Thus, th

distances and exhibit strong conv

1973; Sortais et al. 1993; Kotroni

4) How do moisture and temperatu

Low-level wind maxima in

strongly influenced by topograph

and dry southwest, while the moi

The temperature and moisture pa

of the different types of low-level

geographic preference.

5) How does the airflow configuratio
convection?

The spatial configurations of

location of any convergence and d

the location of any convection acco

studies have suggested that most

terminus of the jet due to speed co

1962; Astling et al. 1985). On the

display the strongest vertical motio

3) Are there distinct airflow configurations (and related convergence) associated with low-level wind maxima in the Great Plains and can these be related to BLJs and LLJs?

Although the spatial configurations of low-level wind maxima have not been explicitly studied previously, substantial variations between BLJs and LLJs are likely. BLJs, for example, would be expected to have shorter along-axis extent compared to LLJs, since BLJs are more geographically fixed in the Southern Plains. Also, previous studies have noted that BLJs are often strongly anticyclonically curved (Wexler 1961). LLJs, on the other hand, are in part forced by upper-level wind maxima or occur along cold frontal boundaries. Thus, these maxima would be expected to extend over long distances and exhibit strong convergence along their left flank (Browning and Pardoe 1973; Sortais et al. 1993; Kotroni et al. 1994).

4) How do moisture and temperature patterns differ among low-level wind maxima?

Low-level wind maxima in the Great Plains region are located in an area that is strongly influenced by topography. The warmest temperatures are observed over the hot and dry southwest, while the moisture source, the Gulf of Mexico, lies to the southeast. The temperature and moisture patterns are expected to reflect the spatial configuration of the different types of low-level wind maxima, their monthly preference, and their geographic preference.

5) How does the airflow configuration of low-level wind maxima influence the pattern of convection?

The spatial configurations of low-level wind maxima, including the existence and location of any convergence and deformation zones, are likely to have a large impact on the location of any convection accompanying the jet occurrence. For example, previous studies have suggested that most of the convection associated with BLJs occurs at the terminus of the jet due to speed convergence (Bonner et al. 1968; Pitchford and London 1962; Astling et al. 1985). On the other hand, LLJs associated with cold fronts should display the strongest vertical motion, and subsequently greatest convection, along the

left flank. The left flank is also a

with cyclones since the left flank

has the highest moisture content

area of convection is expected wh

a warm frontal boundary and ex

s: What are the typical synoptic-sca
ypical configurations and can the t
mportance of synoptic-scale forcing

Previous research suggests

greatly. All types of low-level wi

pressure gradient between a high

an area of low pressure over the

expected to be stronger for synop

consequence, the contributions of

are thought to be larger for LLJs t

wind components alone cannot e

associated with cyclogenesis, a pr

be a primary factor in inducing a

isallobaric wind component. Furt

the strength of the LLJ is proporti

streak. For BLJs, on the other han

component is expected to exceed

advective component of the ageos

pronounced under a surface high

the low-level flow had occurred d

1957).

In summary, this study exam

characteristics of low-level wind

left flank. The left flank is also an expected area of convection within LLJs associated with cyclones since the left flank of the ascending air stream (i.e. Warm Conveyor Belt) has the highest moisture content and the strongest lifting takes place there. A secondary area of convection is expected where a jet embedded within the conveyor belt rises over a warm frontal boundary and experiences additional lifting (Carlson 1980).

6) What are the typical synoptic-scale environments for low-level wind maxima with different spatial configurations and can the typical environments provide some insight into the relative importance of synoptic-scale forcing and boundary-layer forcing?

Previous research suggests that the typical synoptic environment should vary greatly. All types of low-level wind maxima are expected to be embedded within a pressure gradient between a high pressure cell over the southeastern United States and an area of low pressure over the western U.S., although that pressure gradient is expected to be stronger for synoptically-forced low-level wind maxima. As a consequence, the contributions of the geostrophic wind component to the actual wind are thought to be larger for LLJs than for BLJs. However, even for LLJs, the geostrophic wind components alone cannot explain the full variation in the actual wind. For LLJs associated with cyclogenesis, a pressure fall preceding the cyclone center is expected to be a primary factor in inducing a strong low-level current due to the contributions of the isallobaric wind component. Furthermore, Achtor and Horn (1986) have suggested that the strength of the LLJ is proportional to the magnitude of an upper-tropospheric jet streak. For BLJs, on the other hand, the relative contribution of the ageostrophic wind component is expected to exceed the geostrophic wind component. The inertial advective component of the ageostrophic wind is expected to be particularly pronounced under a surface high pressure system or ridge where strong retardation of the low-level flow had occurred during the day due to turbulent mixing (Blackadar 1957).

In summary, this study examines the temporal and spatial variations in the characteristics of low-level wind maxima in the Great Plains. One of the goals is to

identify the relative contribution

forcing to the formation of differ

to determine the spatial relations

tropospheric jets and convection

objectives are described in the fol

identify the relative contributions of boundary-layer conditions and synoptic-scale forcing to the formation of different types of low-level wind maxima. A second goal is to determine the spatial relationship between the airflow configuration of the lower tropospheric jets and convection. The data sets and methods used to accomplish these objectives are described in the following chapter.

D

The characteristics of low-le
the environments in which they o
rawinsonde observations and clou
describes the data sets, the study
analysis. The first section, the de
quality and the spatial and tempo
section is a brief description of th
methods applied to the different a
many objectives detailed in Chapt
clarity, the methods section is orga

1. Data

To examine the airflow config
environments and effect on convec
and temporal resolutions are used.
level wind maxima and to determi
sea-level pressure, temperature, an
To depict the location of convectiv
ground lightning observations ar
following, the rawinsonde observa
ground lightning observations.

Chapter 2

DATA AND METHODS

The characteristics of low-level wind maxima, their relationship to convection and the environments in which they occur are investigated with the help of two data sets, rawinsonde observations and cloud-to-ground lightning observations. This chapter describes the data sets, the study period, the study area, and the methods used for the analysis. The first section, the description of the data, focuses particularly on the quality and the spatial and temporal resolution of the two data sets. The second section is a brief description of the study period and study area. In the final section, the methods applied to the different analysis steps are described. In order to achieve the many objectives detailed in Chapter 1, a number of different methods are used. For clarity, the methods section is organized in the order of the subsequent chapters.

1. Data

To examine the airflow configuration of low-level wind maxima, their large-scale environments and effect on convection, two independent data sets with different spatial and temporal resolutions are used. Rawinsonde observations are used to identify low-level wind maxima and to determine the typical airflow, pressure, geopotential height, sea-level pressure, temperature, and moisture fields associated with the wind maxima. To depict the location of convective activity associated with the wind maxima, cloud-to-ground lightning observations are employed as surrogate for convection. In the following, the rawinsonde observations are discussed first, followed by the cloud-to-ground lightning observations.

1 Rawinsonde Observations

Routine upper-air rawinso

Climatic Data Center (NCDC) o

nformation on pressure, temper

speed. When interpreting the re

resolution of the National Weath

verage there is approximately o

contiguous U.S.. The station sep

Douglas and Stensrud 1996). To

resolution of a network of irregu

Great Plains region would result

results in a detectability of object

as a meso-alpha scale phenomen

the points of half-maximum winc

rawinsonde observations are able

weaker wind maxima, however, r

resolution.

Rawinsonde observations ar

data archive. While transmitted r

temperature and pressure values

significant levels[1], the archived da

and 25-mb increments (e.g., pseu

550, 450, and 350 mb always appe

values at these generated levels ar

[1] In a radiosonde observation, a sign
which values of pressure, temperatur
moisture-content data at that level ar
attention of the forecaster, or they are
radiosonde observation" (Huschke 19

a. Rawinsonde Observations

Routine upper-air rawinsonde observations were obtained from the National Climatic Data Center (NCDC) on CD-ROM. This archived data set contains information on pressure, temperature, dewpoint temperature, wind direction and wind speed. When interpreting the results of this study, one should remember that the spatial resolution of the National Weather Service upper-air network is rather coarse. On average there is approximately one to two rawinsonde stations per state in the contiguous U.S.. The station separation in the United States is between 350 and 450 km (Douglas and Stensrud 1996). Tobler's (1988) guidelines for determining the spatial resolution of a network of irregular points applied to this upper-air data set for the Great Plains region would result in a spatial resolution of approximately 370 km, which results in a detectability of objects twice that size. The Great Plains boundary-layer jet as a meso-alpha scale phenomenon has a width of approximately 600-700 km between the points of half-maximum wind speed (Bonner 1968; Raymond 1978). Therefore, the rawinsonde observations are able to depict the stronger low-level wind maxima. Some weaker wind maxima, however, may go unnoticed due to the coarse horizontal resolution.

Rawinsonde observations are reprocessed at NCDC before becoming part of the data archive. While transmitted real-time observations contain temperature, dewpoint temperature and pressure values for all mandatory (850, 700, 500, 300, 200 mb) and significant levels[1] , the archived data, additionally, contain "generated levels" at 50-mb and 25-mb increments (e.g., pseudo-"significant" levels at 950, 900, 800, 750, 650, 600, 550, 450, and 350 mb always appear in NCDC data). The temperature and humidity values at these generated levels are calculated using a logarithmic interpolation in

[1] In a radiosonde observation, a significant level is a "level (other than a mandatory level) for which values of pressure, temperature and humidity are reported because temperature and/or moisture-content data at that level are sufficiently important or unusual to warrant the attention of the forecaster, or they are required for the reasonably accurate reproduction of the radiosonde observation" (Huschke 1989).

pressure heights are computed h

originally transmitted wind data

o the mandatory levels, whereas

rom the original levels to the ma

his interpolation is often a smoo

originally transmitted winds (Sc

The vertical resolution of th

vestigation of low-level wind m

sharp 'jet noses' (i.e. strong increa

maximum wind and strong decre

f the 'jet nose' falls between the h

nterpolation schemes are unlikely

Thus, in addition to underreportin

likely that the strength of the spe

well.

The twice-daily (0000 and 1

comparison of the low-level wind

and the early morning hours. The

Standard Time (CST)), lies a few h

frequency for low-level wind max

wind maxima may therefore be mi

Although the rawinsonde da

spatial and temporal resolution, th

this nature. The advantages of usi

lie in their data accuracy, large are

variables. Rawinsondes provide t

most detailed (Schwartz and Dosw

pressure; heights are computed hydrostatically from the temperature profile. The originally transmitted wind data are available at 304 m (1,000 ft) increments in addition to the mandatory levels, whereas the wind data supplied by NCDC are interpolated from the original levels to the mandatory, significant, and generated levels. The result of this interpolation is often a smoothing of the wind profile when compared with the originally transmitted winds (Schwartz and Doswell 1991).

The vertical resolution of the wind observations has important implications for the investigation of low-level wind maxima. Low-level wind maxima frequently have very sharp 'jet noses' (i.e. strong increases in wind speed with height below the level of maximum wind and strong decreases in wind speed above the level of maximum wind). If the 'jet nose' falls between the height increments used in the data encoding, traditional interpolation schemes are unlikely to duplicate the full strength of the wind maximum. Thus, in addition to underreporting of the frequency of low-level wind maxima, it is likely that the strength of the speed maximum in some instances is underestimated as well.

The twice-daily (0000 and 1200 UTC) rawinsonde observations allow for a comparison of the low-level wind maxima and their environment *only* during the evening and the early morning hours. The morning observation time, 1200 UTC (0600 Central Standard Time (CST)), lies a few hours after the previously-reported time of maximum frequency for low-level wind maxima, 0900 UTC (Mitchell et al. 1995). Short-lived wind maxima may therefore be missed.

Although the rawinsonde data impose limitations on the study due to their coarse spatial and temporal resolution, they are still the best available data set for a study of this nature. The advantages of using rawinsonde observations over any other data set lie in their data accuracy, large areal coverage, and availability of different data variables. Rawinsondes provide the most accurate (Douglas and Stensrud 1996) and most detailed (Schwartz and Doswell 1991) account of the vertical atmospheric

thermodynamic structure. Also,

North America compared to the

upper-air measurement devices,

have a finer spatial and tempora

have other shortfalls besides limi

observations. Therefore, in order

maxima one would still need to i

its present configuration, the Wir

the lowest observation height to

This height is above the level of m

ets in the central and southern G

observations by profilers have bee

de Kamp 1988). Another concern

contamination by migratory birds

Cloud-to-Ground Lightning Obse

To depict the location of con

to-ground lightning observations v

National Lightning Detection Net

(GDS), Inc., of Tucson, Arizona. E

strength and multiplicity of the inc

period, three different lightning ne

lightning observations for the nort

Land Management sensors and for

Laboratory (NSSL). Sensors opera

remainder of the contiguous U.S.

thermodynamic structure. Also, the rawinsonde network covers the entire continent of North America compared to the limited areas of the Great Plains covered by alternative upper-air measurement devices, in particular the profiler network. While profiler data have a finer spatial and temporal data resolution than rawinsonde observations, they have other shortfalls besides limited areal coverage. For one, profilers only collect wind observations. Therefore, in order to characterize the environment of low-level wind maxima one would still need to include the coarser-scale rawinsonde data. Secondly, in its present configuration, the Wind Profiler Demonstration Network (WPDN) restricts the lowest observation height to 500 m above ground (Douglas and Stensrud 1996). This height is above the level of maximum wind speed in many summertime low-level jets in the central and southern Great Plains (Stensrud et al. 1990). Thirdly, wind observations by profilers have been shown to be unreliable in convective situations (van de Kamp 1988). Another concern when using profiler data is the likelihood of contamination by migratory birds (Wilczak et al. 1955).

b. Cloud-to-Ground Lightning Observations

To depict the location of convection relative to the low-level wind maxima, cloud-to-ground lightning observations were used. These observations were obtained from the National Lightning Detection Network (NLDN) operated by GeoMet Data Services (GDS), Inc., of Tucson, Arizona. Each observation includes the location, time, polarity, strength and multiplicity of the individual cloud-to-ground flashes. During the study period, three different lightning networks comprised the NLDN. Cloud-to-ground lightning observations for the northwestern U.S. were provided by the U.S. Bureau of Land Management sensors and for the south-central U.S. by the National Severe Storms Laboratory (NSSL). Sensors operated by the NLDN provided coverage for the remainder of the contiguous U.S.

Cloud-to-ground lightning

and are thus ideally suited for t

estimated at 80-90 percent for m

edges of the network may have

flashes that are detected only by

location accuracy is estimated fr

which is computed at the time o

estimated to be accurate to 0.1 m

and NSSL networks, the time of

(Cummins et al. 1992).

2. Study Area and Study Period

The Great Plains region (35

this climatology since it is the pre

level wind maxima to occur (Bonn

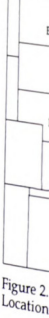

Figure 2.
Location

Cloud-to-ground lightning observations have a fine spatial and temporal resolution and are thus ideally suited for the analysis of convection. Detection efficiency is estimated at 80-90 percent for most of the conterminous U.S. Localized areas along the edges of the network may have lower detection efficiencies (60-70 percent) because flashes that are detected only by two sensors along a baseline are not reported. The location accuracy is estimated from 2-4 kilometers. The time of occurrence of flashes, which is computed at the time of the peak radiation field of the first return stroke, is estimated to be accurate to 0.1 milliseconds for the sensors run by GDS. For the BLM and NSSL networks, the time of occurrence is accurate to approximately 5 milliseconds (Cummins et al. 1992).

2. Study Area and Study Period

The Great Plains region (35-46° N/ 94-100° W) was chosen as the study area for this climatology since it is the preferred region in the United States for southerly low-level wind maxima to occur (Bonner 1968) (Figure 2.1).

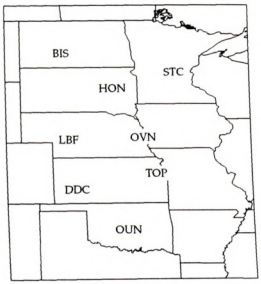

Figure 2.1. Central Plains Region with Location of Rawinsonde Stations.

A study period of April thr

variability of the different forcing

and LLJs. Two years of data, 19

differences in the large-scale circ

n the Great Plains whereas 1992

below-average temperatures and

3. Methods

As previously noted, this se

Within each subsection, the meth

described. The first subsection, t

Analysis of Characteristics of Low

utilized in Chapter 3. The metho

following three subsections, "Ana

Temperature and Humidity Fields

subsection, "Analysis of Lower-, M

the methods used in the analysis t

a. Identification of Low-Level Wind M
Maxima

1) RAWINSONDE SITES

The following eight rawinson

study area were used to identify oc

(DUN); Dodge City, KS (DDC); N

KS (TOP); Omaha, NE (OVN); and

stations form two approximate sou

TOP-OVN-STC. They were selecte

characteristics of the low-level wind

A study period of April through September was chosen to capture the seasonal variability of the different forcing mechanisms that are responsible for warm season BLJs and LLJs. Two years of data, 1991 and 1992, were analyzed to account for interannual differences in the large-scale circulation. The year 1991 was a fairly dry and warm year in the Great Plains whereas 1992 is remembered as the "year without a summer" with below-average temperatures and above-average precipitation for much of the region.

3. Methods

As previously noted, this section is ordered according to the following chapters. Within each subsection, the methods and analysis area that were employed are described. The first subsection, titled "Identification of Low-Level Wind Maxima and Analysis of Characteristics of Low-Level Wind Maxima", corresponds to the methods utilized in Chapter 3. The methods employed in Chapter 4 are described in the following three subsections, "Analysis of Airflow Configurations", "Analysis of Temperature and Humidity Fields", and "Analysis of Convection". The final subsection, "Analysis of Lower-, Mid- and Upper Tropospheric Environment" details the methods used in the analysis for Chapter 5.

a. Identification of Low-Level Wind Maxima and Analysis of Characteristics of Low-level Wind Maxima

1) RAWINSONDE SITES

The following eight rawinsonde stations in the previously-defined Great Plains study area were used to identify occurrences of low-level wind maxima: Norman, OK (OUN); Dodge City, KS (DDC); North Platte, NE (LBF); Bismarck, ND (BIS); Topeka, KS (TOP); Omaha, NE (OVN); and Huron, SD (HON) (see Figure 2.1). The eight stations form two approximate south-north transects: DDC-LBF-HON-BIS and OUN-TOP-OVN-STC. They were selected to enable a comparison of the frequency and characteristics of the low-level wind maxima both latitudinally and longitudinally within

the Great Plains. The analysis of

onducted on constant pressure s

tations in the southwest, DDC a

than the other six stations (Table

characteristics of the wind maxim

elevations.

Figure 2.2. Topography of the
above Mean Sea Level (MSL).

Table 2.1. Elevation of Raw

DDC	LBF	HON
790	849	393

2) DEFINITION OF A LOW-LE

As a first step in the selection

peed and wind direction were crea

the Great Plains. The analysis of the characteristics of low-level wind maxima was conducted on constant pressure surfaces with fixed cutoff heights. Since the two stations in the southwest, DDC and LBF, are located at considerably higher elevations than the other six stations (Table 2.1, Figure 2.2), the descriptive statistics of the characteristics of the wind maxima at these stations are biased toward higher elevations.

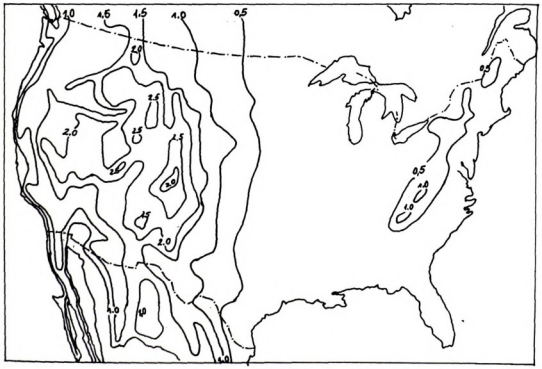

Figure 2.2. Topography of the Central United States. Elevation is in Kilometers above Mean Sea Level (MSL).

Table 2.1. Elevation of Rawinsonde Stations (in m MSL).

DDC	LBF	HON	BIS	OUN	TOP	OVN	STC
790	849	393	506	362	270	406	312

2) DEFINITION OF A LOW-LEVEL WIND MAXIMUM

As a first step in the selection of low-level wind maxima, vertical profiles of wind speed and wind direction were created for each of the eight rawinsonde stations for

each 0000 UTC and 1200 UTC ti
resulting in 5856 vertical profiles
nately ten percent (598 profiles)
erroneous data. These profiles w

The next step was to develo
low-level jet definitions were not
studies do not appear to have su
mpact of the horizontal, vertical
n the strength of low-level wind
boundary-layer wind maxima or
attempts to investigate both. As i
and low-level jets likely have diffe
Thus, a more comprehensive defin
definition used in this study was a
literature and by the inspection of
rawinsonde station (OUN). Below
are reviewed, and the criteria used
rotation used for depicting a jet's
described.

(i) Previous Jet Criteria

Boundary-layer jets have bee
Most frequently, a combination of
the jet level have been used as jet c
example, Bonner (1968), in his clas
depending on their strength. The w
AGL, and the wind speeds had to

each 0000 UTC and 1200 UTC time period during the warm-seasons of 1991 and 1992, resulting in 5856 vertical profiles. Out of the possible 5856 vertical profiles, approximately ten percent (598 profiles) were either absent, had insufficient data or obviously erroneous data. These profiles were not included in the subsequent analysis.

The next step was to develop a definition of a low-level wind maximum. Previous low-level jet definitions were not considered appropriate for two reasons. First, earlier studies do not appear to have sufficiently taken into account the previously-discussed impact of the horizontal, vertical and temporal resolution of rawinsonde observations on the strength of low-level wind maxima. Second, earlier studies were limited to either boundary-layer wind maxima or synoptically-driven low-level jets, whereas this study attempts to investigate both. As indicated in the literature review, boundary-layer jets and low-level jets likely have different speed, height, and vertical shear characteristics. Thus, a more comprehensive definition of a low-level wind maximum was needed. The definition used in this study was arrived upon by both a review of appropriate previous literature and by the inspection of 732 speed profiles for the entire study period for one rawinsonde station (OUN). Below the previous definitions of low-level wind maxima are reviewed, and the criteria used in this study are provided. Also, a shorthand notation used for depicting a jet's speed, height, and vertical shear characteristics is described.

(i) Previous Jet Criteria

Boundary-layer jets have been defined differently by almost every investigator. Most frequently, a combination of maximum speed and minimum speed decrease above the jet level have been used as jet criteria (e.g. Bonner 1968; Sjostedt et al. 1990). For example, Bonner (1968), in his classic study, divided wind maxima into four categories depending on their strength. The wind maxima could not be located higher than 1.5 km AGL, and the wind speeds had to decrease above the jet level, by 3 km AGL. Criterion

jets had maximum speeds ≥ 12

minimum or by 3 km. The corres

wind speeds ≥ 16 ms^{-1} (20 ms^{-1}) a

maxima that did not meet the mo

classified as criterion 0 (Bonner 1

Similarly, Sjostedt et al. (19

minimum decrease above the jet

minimum difference in wind spe

Bonner (1968). Sjostedt et al. (199

above the ground. In their study,

915 m and it had to exceed the su

wind velocity had to decrease by

maximum. To qualify as strong je

wind maximum exceed the surfac

speed not exceed 2 ms^{-1} and that

Blackadar (1957), unlike Bo

combination of wind speed profil

layer jets. To qualify as a signific

below 1000 m AGL, the wind spe

next higher minimum by ≥5 kts, a

maximum within the lowest 1000

Investigators of synoptically

selection criteria. Djuric and Lad

associated with winter cyclones, c

subsequently decrease in speed be

weaker LLJ-0 and the stronger LL

none. For the LLJ-0 type, the sma

1 jets had maximum speeds ≥ 12 ms^{-1} and decreased by ≥6 ms^{-1} to the next higher minimum or by 3 km. The corresponding conditions for criterion 2 (criterion 3) jets were wind speeds ≥ 16 ms^{-1} (20 ms^{-1}) and a decrease of ≥ 8 ms^{-1} (10 ms^{-1}). The remaining wind maxima that did not meet the more stringent conditions for criterion 1-3 jets were classified as criterion 0 (Bonner 1968).

Similarly, Sjostedt et al. (1990) used a combination of maximum speed and minimum decrease above the jet level as jet criteria. In addition, they required a minimum difference in wind speed between the surface and the jet level. Compared to Bonner (1968), Sjostedt et al. (1990) limited their selection of jet cases to a thinner layer above the ground. In their study, the maximum speed of a jet had to occur at or below 915 m and it had to exceed the surface speed by at least 10 ms^{-1}. Additionally, the wind velocity had to decrease by at least 4.5 ms^{-1} within 610 m above the wind maximum. To qualify as strong jets, Sjostedt et al. (1990) not only demanded that the wind maximum exceed the surface wind speed by 11 ms^{-1}, but also that the surface wind speed not exceed 2 ms^{-1} and that the 850 mb wind speed not exceed 4.5 ms^{-1}.

Blackadar (1957), unlike Bonner (1968) or Sjostedt et al. (1990), employed a combination of wind speed profile and temperature profile criteria to identify boundary-layer jets. To qualify as a significant jet maximum, the jet maximum had to be located below 1000 m AGL, the wind speed at the jet level had to exceed the wind speed at the next higher minimum by ≥5 kts, and the temperature had to increase up to a single maximum within the lowest 1000 m.

Investigators of synoptically-driven low-level jets have also employed various selection criteria. Djuric and Ladwig (1983), for instance, in their study of wind maxima associated with winter cyclones, demanded that the LLJ exceed 12 ms^{-1} and subsequently decrease in speed before 3 km AGL. They distinguished between their weaker LLJ-0 and the stronger LLJ-1 by the strength of the speed decrease above the jet nose. For the LLJ-0 type, the smallest permitted decrease was 2.5 ms^{-1}, whereas the

stronger LLJ-1 had to decrease b

On the other hand, Chen and Yu

ostachs on the 850- and 700-mb

alculated the deviation of the 85

mean value and investigated cas

Neither of these studies imposed

(a) *Current Jet Criteria*

The definition of low-level

with those of Bonner (1968), Dju

that it also applies a combination

ecrease below the jet level and m

compared to the earlier studies, th

compensate for the coarse data re

smoothed prior to archiving. Ad

upward to permit the identificati

layer forced jets. Southerly wind

of 6 ms^{-1} as well as a minimum dif

and the surface and between the le

were included in the analysis. No

this study since one of the foci of

level wind maxima and convection

level wind maxima has been show

activity (Pitchford and London 19

The amount of increase in wi

decrease above agrees in principle

used a difference in wind speed of

stronger LLJ-1 had to decrease by at least half the maximum wind speed before 3 km. On the other hand, Chen and Yu (1988) analyzed the axes of 12.5 ms^{-1} and 15 ms^{-1} isotachs on the 850- and 700-mb pressure surfaces, whereas Chen and Kpaeyeh (1993) calculated the deviation of the 850-mb daily-mean meridional wind from the seasonal mean value and investigated cases with deviations greater than one standard deviation. Neither of these studies imposed a minimum vertical shear.

(ii) Current Jet Criteria

The definition of low-level wind maxima adopted in this study has some similarity with those of Bonner (1968), Djuric and Ladwig (1983), and Sjostedt et al. (1990) in that it also applies a combination of criteria, including minimum speed, minimum increase below the jet level and minimum decrease above the jet level. However, compared to the earlier studies, the classification criteria have been relaxed somewhat to compensate for the coarse data resolution and the fact that the wind data were smoothed prior to archiving. Additionally, the height of the wind maxima was extended upward to permit the identification of synoptically-driven jets in addition to boundary-layer forced jets. Southerly wind maxima (from 90°-270°) that have a minimum speed of 8 ms^{-1} as well as a minimum difference of 4 ms^{-1} between the level of the jet maximum and the surface and between the level of the jet maximum and the next higher minimum were included in the analysis. Northerly wind maxima (270°-90°) were excluded from this study since one of the foci of this analysis was the spatial relationship between low-level wind maxima and convection. The advection of warm, moist air by southerly low-level wind maxima has been shown to be an important contributor to thunderstorm activity (Pitchford and London 1962; Bonner 1966).

The amount of increase in wind speed below the jet level and the amount of decrease above agrees in principle with other studies. Bonner (1968), for example, also used a difference in wind speed of one half the maximum wind speed when he devised

his speed criteria. While Bonner
level of maximum wind, a simila
ncluded in this study in order t
below (Figure 2.3). As previousl
maximum and the surface speed
Bonner's and Sjostedt's definitio
to the 700-mb level, as employed
maximum height, the level of mi
750 mb.

Figure 2.3.
Profile.

(iii) *Short-hand Description*

Visual inspection of the spee
types were evident among the stu
the jet maximum, the maximum sp
the wind maximum, a short-hand
zation of the vertical profile is inte

his speed criteria. While Bonner only specified the amount of speed decrease above the level of maximum wind, a similar difference in wind speed below the jet level is also included in this study in order to ensure a jet "nose" with vertical shear above and below (Figure 2.3). As previously noted, a decrease in wind speed between the wind maximum and the surface speed was also used by Sjostedt et al. (1990). Compared to Bonner's and Sjostedt's definition, the maximum height of the jet was expanded upward to the 700-mb level, as employed by Chen and Yu (1988). To accommodate this higher maximum height, the level of minimum wind above the jet also was extended upward to 550 mb.

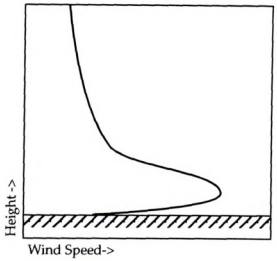

Figure 2.3. Schematic of Vertical Speed Profile.

(iii) Short-hand Description

Visual inspection of the speed profiles had shown that a number of distinct profile types were evident among the study cases. In order to quickly characterize the height of the jet maximum, the maximum speed and the amount of vertical shear above and below the wind maximum, a short-hand working description was developed. This characterization of the vertical profile is intended to add an additional dimension to the

description of the characteristics
resented in the following chapt

Three mutually-exclusive c
wind maxima. The level of the
Figures 2.3-2.6). Wind maxima
Figures 2.7-2.10), and wind ma
Figure 2.11). Classes A and B w
maximum wind speed of the jet
et level. Numerals are used to i
subtype, the minimum speed of
height of the jet nose. The amou
speed both above and below the
which the decrease in speed abov
n category A1 were located at or
they had an increase in wind spe
a decrease in speed above the jet
decrease above the jet level to one
Note that no minimum specificati
maxima that met some but not all
lowest level (A) were combined i
subclassified due to the comparati
category. Table 2.2 provides a su
that with increasing numbers, jets
profiles for the different categorie

description of the characteristics and environments of the low-level wind maxima that is presented in the following chapters.

Three mutually-exclusive classes are used to categorize the height of the low-level wind maxima. The level of the maximum wind for Class A jets occurs below 900 mb (Figures 2.3-2.6). Wind maxima falling in Class B are located between 900 and 800 mb (Figures 2.7-2.10), and wind maxima in Class C are found between 800 and 700 mb (Figure 2.11). Classes A and B were then subclassified based on the strength of the maximum wind speed of the jet and the amount of vertical shear above and below the jet level. Numerals are used to indicate the speed and shear characteristics. For each subtype, the minimum speed of the jet category is indicated in addition to the maximum height of the jet nose. The amount of vertical shear is defined by the difference in wind speed both above and below the wind maximum in addition to the upper boundary by which the decrease in speed above the wind maximum occurred. For example, jet cases in category A1 were located at or below 900 mb, their minimum speed was ≥ 12 ms^{-1}, they had an increase in wind speed of ≥ 8 ms^{-1} between the surface and the jet level and a decrease in speed above the jet level of at least one half the maximum speed. The decrease above the jet level to one half the maximum speed occurred below 850 mb. Note that no minimum specifications were made for category A5. Rather, the wind maxima that met some but not all the requirements for the other four categories at the lowest level (A) were combined in this category. The jet cases in Class C were not subclassified due to the comparatively small number of observations in that height category. Table 2.2 provides a summary of the different classes and subclasses. Note that with increasing numbers, jets are less pronounced in the vertical. Representative profiles for the different categories are provided in Figures 2.3 - 2.11.

Table 2.2–Classification Crite

Category	Maximum Height	Mir Sp
A1	900 mb	≥ 1
A2	900 mb	≥ 1
A3	900 mb	≥ 1
A4	900 mb	≥ 8
A5	900 mb	
B1	800 mb	≥ 1
B2	800 mb	≥ 1
B3	800 mb	≥ 1
B4	800 mb	≥ 8
C	700 mb	≥ 8

3) CHARACTERISTICS OF

Next, the spatial and tempo

level wind maxima were investig

times, jet noses were evident at m

height of the jet noses varied acro

jets were part of one or multiple a

included in the analysis, resulting

frequency, time of most frequent

directional, and speed characteris

examined in the hope of identifyi

synoptically-forced jets. Previous

different height and directional ch

that they were more closely affect

and temporal variations in the fre

Table 2.2.–Classification Criteria of Speed Profile Categories.

Category	Maximum Height	Minimum Speed	Vertical Shear Below Jet	Vertical Shear Above Jet	Upper Boundary
A1	900 mb	≥ 12 ms^{-1}	≥ 8 ms^{-1}	$\geq 1/2$ speed	850 mb
A2	900 mb	≥ 12 ms^{-1}	≥ 8 ms^{-1}	$\geq 1/2$ speed	700 mb
A3	900 mb	≥ 12 ms^{-1}	≥ 8 ms^{-1}	$< 1/2$ speed	700 mb
A4	900 mb	≥ 8 ms^{-1}	≥ 4 ms^{-1}	≥ 4 ms^{-1}	850 mb
A5	900 mb				
B1	800 mb	≥ 12 ms^{-1}	≥ 8 ms^{-1}	$\geq 1/2$ speed	550 mb
B2	800 mb	≥ 12 ms^{-1}	≥ 4 ms^{-1}	$\geq 1/2$ speed	550 mb
B3	800 mb	≥ 12 ms^{-1}	≥ 4 ms^{-1}	$< 1/2$ speed	550 mb
B4	800 mb	≥ 8 ms^{-1}	≥ 4 ms^{-1}	≥ 4 ms^{-1}	550 mb
C	700 mb	≥ 8 ms^{-1}	≥ 4 ms^{-1}	≥ 4 ms^{-1}	550 mb

3) CHARACTERISTICS OF LOW-LEVEL WIND MAXIMA

Next, the spatial and temporal variations in the characteristics of the 1522 low-level wind maxima were investigated across stations. For a number of observation times, jet noses were evident at more than one rawinsonde station. However, since the height of the jet noses varied across the stations, it could not be determined whether the jets were part of one or multiple airstreams. Thus, all the identified jet cases were included in the analysis, resulting in multiple jet cases for some time periods. The frequency, time of most frequent occurrence (0000 or 1200 UTC), and the height, directional, and speed characteristics, as indicated by the shorthand notation, were examined in the hope of identifying possible indicators for boundary-layer jets and synoptically-forced jets. Previous studies had suggested that boundary-layer jets had different height and directional characteristics compared to synoptically-driven jets and that they were more closely affected by latitude (see Literature Review). The spatial and temporal variations in the frequency of the jet cases is presented in Chapter 3.

150
200
Wavelength (nm)
Absorbance H2O2 OSC1:OSC2

150
200
Wavelength (nm)
Absorbance O2N OSC1:OSC2

150
200
Wavelength (nm)
Absorbance H2O OSC1:OSC2

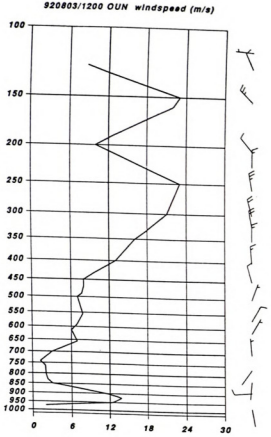

Figure 2.4. Example of Category a1 Wind Maximum.

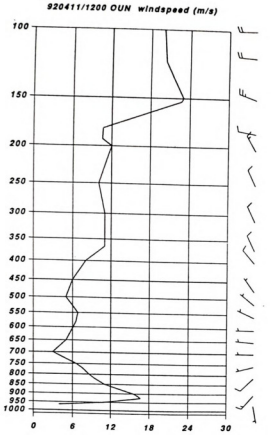

Figure 2.5. Example of Category a2 Wind Maximum.

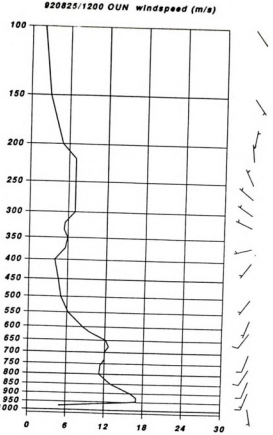

Figure 2.6. Example of Category a3 Wind Maximum.

(km) passenger km operated
100
150
200

(km) passenger km operated
100
150
200

(km) passenger km operated
100
150
200

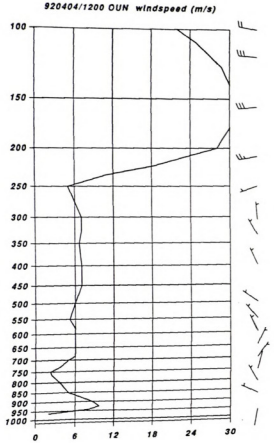

Figure 2.7. Example of Category a4 Wind Maximum.

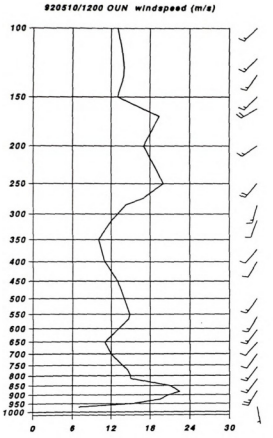

Figure 2.8. Example of Category b1 Wind Maximum.

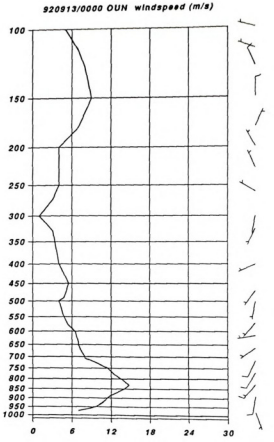

Figure 2.9. Example of Category b2 Wind Maximum.

100
150
200

100
150
200

100
150
200

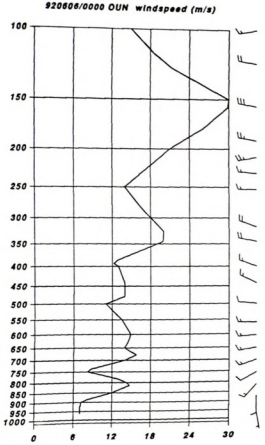

Figure 2.10. Example of Category b3 Wind Maximum.

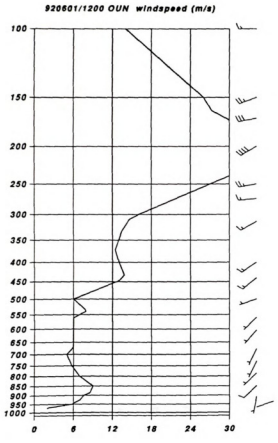

Figure 2.11. Example of Category b4 Wind Maximum.

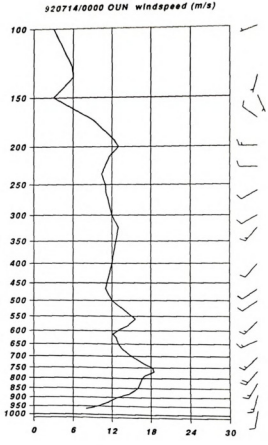

Figure 2.12. Example of Category C Wind Maximum.

1) MAPPING THE WIND F

The next step in the analy
season low-level wind maxima
interest as it is anticipated that
airflow pattern. Furthermore, w
form and/or occur in very differ
maxima can be represented by t
and the distribution of wind spe
fields were plotted on constant
low-level wind maxima identifie
rawinsonde stations.

The analysis region for this
Plains study area to include the
depict the airflow pattern along
the vicinity of the jet core. The n
this part of the analysis are depi
uniform across the analysis regio
portion of the analysis region du
Mexico. Another concern is the l
analysis region. Consequently, p
the earth's surface in the western
portion.

GEMPAK (Koch et al. 1981
used to interpolate and grid the w
isotach fields. GEMPAK first int
pressure level at each of the rawi

b. Analysis of Airflow Configurations

1) MAPPING THE WIND FIELDS

The next step in the analysis was to examine the spatial configuration of warm season low-level wind maxima in the Great Plains. The airflow configuration is of interest as it is anticipated that the distribution of convection is strongly related to the airflow pattern. Furthermore, wind maxima with different configurations are likely to form and/or occur in very different environments. The airflow configuration of the wind maxima can be represented by the instantaneous wind direction (i.e. streamline pattern) and the distribution of wind speed (i.e., isotach pattern). Thus, streamline and isotach fields were plotted on constant pressure surfaces for each of the 1522 cases of southerly low-level wind maxima identified during 1991 and 1992 at the eight Great Plains rawinsonde stations.

The analysis region for this part of the study was extended beyond the Great Plains study area to include the region from 20-60° N and from 70-120° W, in order to depict the airflow pattern along the entire axis of a jet, rather than the airflow only in the vicinity of the jet core. The number and location of the rawinsonde stations used for this part of the analysis are depicted in Figure 2.13. Note that the data coverage is not uniform across the analysis region. Coverage is particularly poor over the southeastern portion of the analysis region due to the lack of rawinsonde stations over the Gulf of Mexico. Another concern is the large increase in topography westward across the analysis region. Consequently, pressure surfaces will be located considerably closer to the earth's surface in the western portion of the region compared with the eastern portion.

GEMPAK (Koch et al. 1981), a meteorological analysis software package, was used to interpolate and grid the wind observations and to map the streamline and isotach fields. GEMPAK first interpolates the wind observation vertically to the desired pressure level at each of the rawinsonde locations. Next, the wind values are

Figure 2.13. Large
Stations.

interpolated horizontally from th

grid using the Barnes interpolat

interpolation schemes are descril

in this analysis was 1° latitude b

allow the extrapolation of the wi

was then performed a second tim

the wind maxima included for fu

scheme. Cases where obvious da

subsequent analyses. An import

which to plot the streamline and

wind field was plotted on the cor

the vertical profile. In cases whe

distance (in extreme cases severa

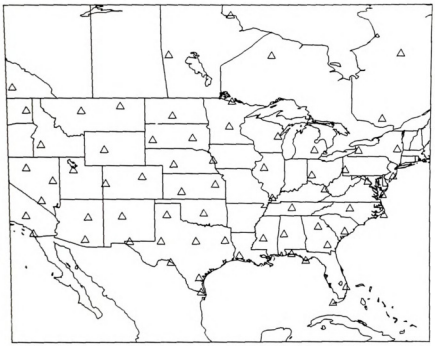

Figure 2.13. Large Study Area with Location of Rawinsonde Stations.

interpolated horizontally from the irregularly distributed station locations to a regular grid, using the Barnes interpolation scheme (Barnes 1973). The GEMPAK modules and interpolation schemes are described in more detail in Appendix A. The grid mesh used in this analysis was 1° latitude by 1° longitude. The interpolation scheme was set to allow the extrapolation of the wind field into data poor areas. However, the gridding was then performed a second time without extrapolation in order to ensure that none of the wind maxima included for further analysis were artifacts of the interpolation scheme. Cases where obvious data problems were evident were excluded from the subsequent analyses. An important decision was the choice of the pressure surface on which to plot the streamline and isotach fields. For each of the 1522 wind profiles, the wind field was plotted on the constant pressure surface through the jet nose evident on the vertical profile. In cases where the jet nose extended vertically for a considerable distance (in extreme cases several hundred millibars), plots were created for the lowest

and highest constant pressure l

changes in the airflow configur

For a particular day and

than one of eight rawinsonde s

occurred at different pressure l

particularly synoptically-driver

where the jet nose was observe

the jet nose was ≤ 1 mb, only o

created for the different pressur

the wind maximum was observ

isotach and streamline plot. Fo

station had to lie within the area

wind speed. This precaution wa

the vertical speed profile at a ra

actually part of the horizontal w

2) IDENTIFYING JET EVEN

The next step in the analys

time in order to identify "jet ever

that follow. A "jet event" differs

individual rawinsonde stations i

day and observation time. Howe

vertical level had been plotted fo

was retained for further analysis

same over all the plotted vertical

could be identified on the differe

retained. Multiple levels were pe

and highest constant pressure level within the isotach maximum in order to capture any changes in the airflow configuration that might have occurred over the vertical distance.

For a particular day and observation time, a jet nose often was observed at more than one of eight rawinsonde stations. Frequently, the jet nose at the different stations occurred at different pressure levels, which was expected given that wind maxima, particularly synoptically-driven low-level jets, often tilt upward with latitude. In cases where the jet nose was observed at more than one station, but the pressure difference of the jet nose was ≤ 1 mb, only one plot was constructed. Otherwise, separate plots were created for the different pressure levels. The location of the rawinsonde station where the wind maximum was observed in the speed profile was marked on the corresponding isotach and streamline plot. For that plot to be further considered in the analysis, the station had to lie within the area outlined by the isotach of one half of the maximum wind speed. This precaution was taken to ensure that the wind maximum observed in the vertical speed profile at a rawinsonde station, and used to identify the jet case, was actually part of the horizontal wind maximum evident on the constant pressure surface.

2) IDENTIFYING JET EVENTS AND MULTIPLE JET LEVELS

The next step in the analysis was to group the wind plots by day and observation time in order to identify "jet events" for the map typing and compositing procedures that follow. A "jet event" differs from the "jet cases" identified above for the individual rawinsonde stations in that now only one jet event is possible for a particular day and observation time. However, a jet event can have multiple levels. If only one vertical level had been plotted for a particular day and observation time, then that level was retained for further analysis if the airflow configuration remained essentially the same over all the plotted vertical levels. However, if several distinct airflow patterns could be identified on the different pressure surfaces, several levels (up to three) were retained. Multiple levels were permitted, as very likely the pattern of convection for

these jet events is a function of

maxima on the higher levels (b

closer to the surface. Also, the

displaced eastward with heigh

previously received little atten

the few investigators who have

different trajectories within dif

climatological analyses investig

Multiple jet levels may very like

spatial resolution (approximate

vertical resolution of 304 m. Al

implies that multiple jet events

the eight rawinsonde stations u

Finally, each jet event is as

i.e., 0000 or 1200 UTC). This a

resolution (i.e., 12 hours) of the

of the temporal evolution of low

The number of observation

Consequently, the maximum po

southerly low-level wind maxim

interest due to their advection o

maxima whose trajectories did n

the subsequent analysis. This de

events to convection is one of the

over the warm, moist Gulf of Me

activity. For this step, the stream

streamline plots for each event w

these jet events is a function of the airflow at the different levels. In general, the jet maxima on the higher levels (but still below 700 mb) are not as pronounced as those closer to the surface. Also, the jet cores for jet events with multiple levels tend to be displaced eastward with height. The existence of multiple levels for some jet events has previously received little attention. Kottmeier (1978) and Roth et al. (1989) are among the few investigators who have noted the existence of low-level wind maxima with different trajectories within different layers. However, I am not aware of any climatological analyses investigating low-level wind maxima with multiple cores. Multiple jet levels may very likely be underrepresented in this study, given the coarse spatial resolution (approximately 370 km) of the rawinsonde network, and the coarse vertical resolution of 304 m. Also, the eastward displacement of the jet core with height implies that multiple jet events may have been missed due to the limited areal extent of the eight rawinsonde stations used to identify jet cases.

Finally, each jet event is assumed to have a duration of only one observation time (i.e., 0000 or 1200 UTC). This assumption was necessary because the coarse temporal resolution (i.e., 12 hours) of the rawinsonde observations did not permit an investigation of the temporal evolution of low-level wind maxima.

The number of observation times during which jet cases were observed was 515. Consequently, the maximum possible number of jet events is 515. For this study, southerly low-level wind maxima with an 'open Gulf' connection were of particular interest due to their advection of warm, moist air into the Central U.S.. Therefore, wind maxima whose trajectories did not originate over the Gulf of Mexico were excluded from the subsequent analysis. This decision was made because the spatial relationship of jet events to convection is one of the primary foci of this study, and jet events that originate over the warm, moist Gulf of Mexico are more likely to be associated with convective activity. For this step, the streamlines were assumed to represent trajectories, and the streamline plots for each event were inspected to see whether the streamlines through the

jet core on the lowest pressure
originated over the Gulf of Me
Mexico connection (154 events
maxima were also excluded if
fact that only 'southerly' wind
were included in the first part
interpolated from a larger num
The number of jet events was f
the Great Plains region (11 eve
obviously erroneous data (19 e
unclassified (35 events). The fr

Table 2.3. The number of jet ev

Table 2.3. Frequency of Events

Events 260		
	154	
	No-Gulf 'connection'	N D

3) CLASSIFYING THE AIR

Next, the "open Gulf" case
their airflow configurations. Sy
descriptive tools for summarizin
Crane 1986). Yarnal (1984, 1993
(manual) and objective (automa
developed a semi-automated cla
Subjective classification techniqu
(Van Bebber and Köppen 1895;

jet core on the lowest pressure level (i.e., the pressure surface nearest the earth's surface) originated over the Gulf of Mexico. Southerly wind maxima that did not have a Gulf of Mexico connection (154 events) were excluded from the subsequent analysis. Wind maxima were also excluded if they had northerly streamlines (20 events). Despite the fact that only 'southerly' wind directions (90°-270°) for individual rawinsonde stations were included in the first part of the analysis, in a number of cases the streamlines, interpolated from a larger number of rawinsonde stations, had a northerly direction. The number of jet events was further reduced if they contained: 1) jet cores outside of the Great Plains region (11 events), 2) no discernible jet core (16 events), and 3) obviously erroneous data (19 events). Jet types with fewer than 10 jet events remained unclassified (35 events). The frequency of non-events is summarized by category in Table 2.3. The number of jet events retained for further analysis was 260.

Table 2.3. Frequency of Events and Non-Events.

Events	Non-Events					
260	255					
	154	20	11	16	19	35
	No-Gulf 'connection'	Northerly Direction	Outside of Area	No jet core	Data	Unclassified

3) CLASSIFYING THE AIRFLOW CONFIGURATIONS

Next, the "open Gulf" cases were subjectively typed based on the similarity of their airflow configurations. Synoptic typing schemes have a long tradition as descriptive tools for summarizing typical modes of atmospheric circulation (Key and Crane 1986). Yarnal (1984, 1993) grouped the various typing methods into subjective (manual) and objective (automated) procedures. Bardossy et al. (1995) subsequently developed a semi-automated classification for atmospheric circulation patterns. Subjective classification techniques have been in existence for over a century in Europe (Van Bebber and Köppen 1895; Baur et al. 1944; Hess and Brezowsky 1969) and about

half a century in the USA (Ya
high-speed computers brought
classification methods (Key ar
techniques or principal compo
synoptic classification (Barry 1
for their inherent subjectivity (
determined internal parameter
both correlation-based and pri
1966). Variations in sample siz
classification results in correla
Manually-derived synoptic cla
investigators because they are i
classification process complete

Subjective classifications
scales. The large-scale circulati
the concept of grosswetterlage
Schroeder (1950) and Brezowsk
region), while Muller (1977) inv
weather at a location. Mitchell
developed by Pielke et al. (199
cyclones, to documented the lar
low-level jet occurrence over the

In this study, a subjective,
objective scheme because of the
on both the streamline and isota
analysis (e.g. Kastendeuch and
[e.g. Klink 1986) to characterize

half a century in the USA (Yarnal and White 1987; Yarnal et al. 1988). The advent of high-speed computers brought with it the development of more 'objective' quantitative classification methods (Key and Crane 1986). These methods, based on correlation techniques or principal components analysis, were initially hailed as breakthrough in synoptic classification (Barry 1980). However, they are increasingly coming under fire for their inherent subjectivity (Yarnal and White 1987). Changes in subjectively-determined internal parameters, for example, result in varying classifications when using both correlation-based and principal components-based methodologies (Key and Crane 1986). Variations in sample size, number of grid points and random sampling will alter classification results in correlation-based classifications (Yarnal and White 1987). Manually-derived synoptic classifications are therefore still favored by many investigators because they are infinitely flexible and the investigator can control the classification process completely (Yarnal 1933).

Subjective classifications have been applied to research problems at a variety of scales. The large-scale circulation is emphasized in Lamb's (1972) weather types and the concept of grosswetterlagen (Baur et al. 1944; Hess and Brezowsky 1969). Schroeder (1950) and Brezowsky (1964) focus on a regional scale (e.g. the Great Lakes region), while Muller (1977) investigated the implications of synoptic types for the weather at a location. Mitchell et al. (1995) applied a subjective classification scheme developed by Pielke et al. (1991), which is based on the classical model of extratropical cyclones, to documented the large-scale circulation that was present during periods with low-level jet occurrence over the southern Great Plains.

In this study, a subjective, or manual, classification scheme was chosen over an objective scheme because of the difficulty in objectively classifying the windfield based on both the streamline and isotach patterns. Previous investigators have applied cluster analysis (e.g. Kastendeuch and Kaufmann 1997) and principal components analysis (e.g. Klink 1986) to characterize low-level wind vector fields. However, I am not aware

of any objective classification
direction but also regions of co
schemes have been shown to b
climatological studies (Yarnal
study because of its greater inh

The classification of the je
characteristics. For those event
pressure level was used in the

(i) Orientation. The direc
consideration. Inspection of th
not all low-level wind maxima
(1961) had described. Jet event
also observed.

(ii) Extent. The latitudina
distinction was made between
whose area of influence was so

(iii) Confluence zones. Co
been recognized as an importan
(Beebe and Bates 1955; Pitchfor
1986), thus jet events were also
present and, if so, on the orienta

(iv) Deformation zones. T
deformation fields. Pure stretch
hyperbolic streamlines. They ha
which the streamlines converge
which streamlines diverge asym
stretching deformation, areas of

of any objective classification method that distinguishes not only wind speed and wind direction but also regions of convergence and divergence. Since manual classification schemes have been shown to be generally as effective as automated schemes in synoptic-climatological studies (Yarnal 1993), a manual classification scheme was chosen for this study because of its greater inherent flexibility.

The classification of the jet events was based on the following airflow characteristics. For those events with multiple levels, the airflow pattern for the lowest pressure level was used in the classification procedure.

(i) Orientation. The direction and curvature of the airflow was taken into consideration. Inspection of the constant pressure plots for the jet events indicated that not all low-level wind maxima are anticyclonically curved, as Bonner (1968) and Wexler (1961) had described. Jet events with cyclonic curvature or even little curvature were also observed.

(ii) Extent. The latitudinal extent of the jet events varied considerably. A broad distinction was made between events that extended into Canada and those events whose area of influence was south of the Great Lakes.

(iii) Confluence zones. Convergence associated with low-level wind maxima has been recognized as an important factor initiating and prolonging convective activity (Beebe and Bates 1955; Pitchford and London 1962; Bonner 1966; Wilson and Schreiber 1986), thus jet events were also classified on whether distinct confluence zones were present and, if so, on the orientation of the confluence zones.

(iv) Deformation zones. The deformation zones in this study are *stretching* deformation fields. Pure stretching deformation fields are characterized by rectangular hyperbolic streamlines. They have two characteristic axes: an axis of dilatation toward which the streamlines converge asymptotically; and an axis of contraction from the which streamlines diverge asymptotically (Huschke 1989). Therefore, in a pure stretching deformation, areas of convergence are found along one axis, while areas of

divergence dominate the othe

the pattern of convection in th

were classified on whether a c

of the deformation zone.

(v) Diffluence or "splittin

was evident for a number of ev

that the characteristic intersec

was absent. In a deformation

converge are diffluent, whereas

The subjective classificati

identified via inspection of the

groups. Each group was then i

and the events were reclassifie

made to either the number of g

with ten or more members were

members are considered uncla

different airflow configuration

4) COMPOSITING THE WI

The wind fields were then

airflow identified configuration

of each type that can then be ea

parameters. Also, coherency of

adequacy of the subjective map

and isotach patterns, the conver

magnitude and sign of the conv

divergence dominate the other axis. The typical convergence along one axis likely affect the pattern of convection in the vicinity of low-level wind maxima. In this study, events were classified on whether a deformation zone was present, and if so, by the orientation of the deformation zone.

(v) Difluence or "splitting". Distinct difluence or "splitting" of the low-level jet was evident for a number of events. This splitting differed from a deformation zone in that the characteristic intersection of an axis of dilatation and an axis of contraction was absent. In a deformation zone both the southerly flow and the northerly flow that converge are difluent, whereas for 'splitters' only the southerly flow is difluent.

The subjective classification was an iterative process. Groups were initially identified via inspection of the constant pressure surface plots, and events placed in groups. Each group was then inspected for consistency. Groups were then redefined and the events were reclassified. The process stopped when no further changes were made to either the number of groups or the events placed in each group. Only groups with ten or more members were retained for further analysis. Groups with fewer members are considered unclassified. The 260 jet events were classified into twelve different airflow configuration types.

4) COMPOSITING THE WIND FIELD

The wind fields were then composited (i.e., averaged) for each of the twelve airflow identified configuration types. The composite fields provide a useful summary of each type that can then be easily related to the convection and the environmental parameters. Also, coherency of the composite patterns provides an indication of the adequacy of the subjective map typing procedure. In addition to compositing streamline and isotach patterns, the convergence field was also composited in order to quantify the magnitude and sign of the convergence associated with each airflow type.

To construct the compo

convergence fields were extra

the jet events. The subgrids w

pressure level and extended 1

grid (i.e. 1° latitude by 1° long

extracted subgrids were then

For those events with multipl

level. However, the same subg

earth's surface) was used for e

multiple jet airstreams.

Figure 2.14. Grid S

The subgrid extended beyo

events, particularly those at the

events, a missing value was subs

analysis area and the events wer

To construct the composite charts, subgrids of the streamline, isotach, and convergence fields were extracted from the larger constant pressure plots used to type the jet events. The subgrids were centered on the individual jet cores at the lowest pressure level and extended 17° latitude by 17° longitude. The grid spacing of the larger grid (i.e. 1° latitude by 1° longitude) was maintained for the subgrid (Figure 2.14). The extracted subgrids were then written to a file and averaged using FORTRAN programs. For those events with multiple levels, separate composite maps were prepared for each level. However, the same subgrid center (e.g., the center of the jet core closest to the earth's surface) was used for each level in order to depict the relative location of the multiple jet airstreams.

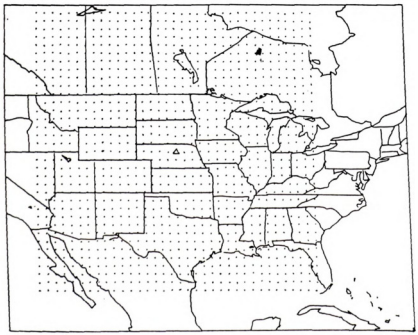

Figure 2.14. Grid Spacing in Analysis Grids.

The subgrid extended beyond the area of the larger analysis grid for a number of events, particularly those at the western and northern edges of the study area. For these events, a missing value was substituted for the gridpoint locations outside the larger analysis area and the events were not included in the gridpoint average. Thus, the

number of observations inclu

of the subgrid (see Figure 2.1

number of events also decrea

multiple levels. After the ave

GEMPAK for plotting and co

Figure 2.15.

c. Analysis of the Temperature an

Low-level wind maxima h

moisture advection. The transp

boundary-layer jets (Blackadar

and has important consequence

moisture and temperature patte

average mixing ratio and tempe

number of observations included in the gridpoint averages decreases towards the edges of the subgrid (see Figure 2.15 for an example of the number of cases per gridpoint). The number of events also decreases with increasing level, since not all events had distinct multiple levels. After the average fields were calculated, they were imported into GEMPAK for plotting and contouring.

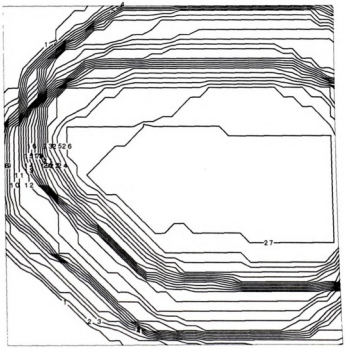

Figure 2.15. Example of Data Coverage.

c. Analysis of the Temperature and Moisture Fields

Low-level wind maxima have been shown to significantly increase temperature and moisture advection. The transport of warm, moist air is accomplished by both boundary-layer jets (Blackadar 1957; Modahl 1979) and low-level jets (Browning 1990) and has important consequences for thunderstorm development. In order to examine the moisture and temperature patterns of the different types of low-level wind maxima, average mixing ratio and temperature maps were calculated for the same subgrids

utilized for the airflow config

the individual jet cores

The temperature and m

750-mb, and 700-mb constant

to enable a quantitative comp

different types of wind maxir

and moisture patterns are sho

occurs at these levels.

3. Analysis of Convection

The location of convecti

examined using cloud-to-grou

defined as the occurrence of or

grid cell during the two-hour

1200 UTC) of the rawinsonde

were identified for the same 2

wind fields. The 35 x 35 cell su

summary maps were created b

lightning activity was observed

core. The summary grids were

Of concern in this part of

within jet types. Visual inspec

location of lightning activity re

composite lightning maps. In

composite patterns in term of t

[7] Trademark by Golden Software.

utilized for the airflow configuration composites. Again, the subgrids were centered on the individual jet cores

The temperature and moisture composites were calculated for the 900-mb, 850-mb, 750-mb, and 700-mb constant pressure surfaces rather than the level of maximum wind to enable a quantitative comparison of the temperature and moisture fields between the different types of wind maxima. However, only the 900-mb and 850-mb temperature and moisture patterns are shown in Chapter 3 since most of the between-type variation occurs at these levels.

d. Analysis of Convection

The location of convective activity relative to the low-level wind maxima is examined using cloud-to-ground lightning data. For this analysis, lightning periods were defined as the occurrence of one or more lightning flashes in a 1° latitude by 1° longitude grid cell during the two-hour period straddling the time of observation (i.e., 0000 and 1200 UTC) of the rawinsonde data. For each event, the grid cells with a lightning period were identified for the same 20-60° N and 70-120° W analysis region used to map the wind fields. The 35 x 35 cell subgrid was then centered on each jet event, and lightning summary maps were created by calculating the percentage of jet events for which lightning activity was observed in particular grid cells relative to the center of the jet core. The summary grids were then imported into SURFER[2] for contouring.

Of concern in this part of the study was the spatial variability of lightning activity within jet types. Visual inspection of the individual jet events indicated that the general location of lightning activity relative to the jet core is very well described by the composite lightning maps. In most instances, the individual events were similar to the composite patterns in term of the location of lightning with respect to the jet core.

---

[2] Trademark by Golden Software.

However, for a given ty

activity in the composite map

associated with lightning due

location of lightning activity r

activity, for example, might ra

areas of convection. Small va

zones from the grid cell at the

percentages for a given grid ce

Another factor that need

summary charts is the fact tha

were included in the analysis.

National Lightning Detection

complicate an interpretation o

Gulf of Mexico, for example, v

c. Analysis of Lower-, Mid- and

Low level wind maxima

settings. Therefore, the forcing

of air currents in the lower tro

environments associated with

prepared for a number of lowe

airflow composites, the environ

using the GEMPAK interpolati

environmental variables were c

appropriate 35 x 35 cell subgri

included in this analysis, and t

However, for a given type, the percentage of individual grid cells with convective activity in the composite map, however, is lower than the overall percentage of jet events associated with lightning due to some variability in the spatial extent and the exact location of lightning activity relative to the jet core. The areal extent of the lightning activity, for example, might range from individual lightning flashes to large continuous areas of convection. Small variations in the distance of confluence and convergence zones from the grid cell at the center of the jet core would similarly result in lower percentages for a given grid cell.

Another factor that needs to be considered when interpreting the lightning summary charts is the fact that only lightning flashes over the contiguous United States were included in the analysis. Since the decrease in the detection efficiency of the National Lightning Detection Network in areas outside the United States would complicate an interpretation of the lightning composite maps, lightning activity over the Gulf of Mexico, for example, was not included.

e. Analysis of Lower-, Mid- and Upper Tropospheric Environment

Low level wind maxima have been observed in a number of different large-scale settings. Therefore, the forcing mechanisms that aid in the formation and intensification of air currents in the lower troposphere are varied as well. To investigate the large-scale environments associated with the different configuration types, composite maps were prepared for a number of lower-, mid-, and upper-tropospheric parameters. As for the airflow composites, the environmental parameters were interpolated to a regular grid using the GEMPAK interpolation schemes described in Appendix A. Composites of the environmental variables were calculated by averaging, for each airflow type, the appropriate 35 x 35 cell subgrid centered on the individual jet cores. The parameters included in this analysis, and the rationale for their selection are presented below:

1) SURFACE PRESSURE A

Several earlier studies s

boundary-layer influences ar

In these situations, the large-s

the western Gulf Coast and a

1961; Hoecker 1963; Djuric a

wind maximum that forms w

forces imposed on the actual

1957; Wexler 1961; Hoecker 1

evaluating whether a particul

than synoptically-forced, is to

group to this described patter

On the other hand, one

synoptically-driven low-level

wind is a component of the ag

toward falling pressure. The

development has been shown

level wind maxima (Djuric 19

magnitude is proportional to t

surface pressure tendency wer

falls to the occurrence of the d

2) GEOSTROPHIC AND AG

Blackadar (1957) previou

maxima are not produced by

[1] An isallobar is a "line of equal c
interval" (Huschke 1989).

1) SURFACE PRESSURE AND SURFACE PRESSURE TENDENCY

Several earlier studies suggested that in the absence of large-scale disturbances, boundary-layer influences are the major contributing factors to low-level wind maxima. In these situations, the large-scale setting typically consists of a high pressure cell along the western Gulf Coast and a warm, low pressure area to the west (Means 1954; Wexler 1961; Hoecker 1963; Djuric and Damiani 1980; Djuric and Ladwig 1983). The low-level wind maximum that forms within this environment is thought to be the result of inertial forces imposed on the actual wind at the time of release of surface friction (Blackadar 1957; Wexler 1961; Hoecker 1963; Parish et al. 1988). Thus, a possible means of evaluating whether a particular airflow type is primarily boundary-layer driven, rather than synoptically-forced, is to compare the composite sea-level pressure pattern for that group to this described pattern.

On the other hand, one factor that has been suggested as a contributor to synoptically-driven low-level wind maxima is the isallobaric wind. The isallobaric[1] wind is a component of the ageostrophic wind. It is directed normal to the isallobars toward falling pressure. The isallobaric wind component associated with cyclone development has been shown to be an important contributor to the development of low-level wind maxima (Djuric 1981; Djuric and Ladwig 1983; Parish et al. 1988). Its magnitude is proportional to the pressure tendency gradient. Composite maps of surface pressure tendency were created in order to examine the contribution of pressure falls to the occurrence of the different airflow configuration types.

2) GEOSTROPHIC AND AGEOSTROPHIC WIND COMPONENTS

Blackadar (1957) previously noted that boundary-layer forced low-level wind maxima are not produced by diurnal oscillations in the pressure fields, but rather are the

[1] An isallobar is a "line of equal change in atmospheric pressure during a specified time interval" (Huschke 1989).

result of an oscillation of t

later modeling study, show

maximum can be about 50

minimum eddy viscosity.

found that the magnitude

with latitude. Bonner (196

component reaches a maxi

of the geostrophic wind, in

pressure forces. Composit

were created for the level c

contribution of the pressur

the formation of low-level

3) 500-MB GEOPOTEN

Low-level wind maxi

midtropospheric height pa

midtropospheric environm

maxima was located under

trough-ridge pattern. This

forcing. The area upstream

divergence (Moran and M

falls and cyclone developm

linked to surface pressure

Djuric and Ladwig 1983; F

midtropospheric support,

individual types of low-lev

result of an oscillation of the ageostrophic wind vector. Paegle and Rasch (1973), in a later modeling study, showed that at 30° latitude, the magnitude of the low-level wind maximum can be about 50 percent larger than the geostrophic wind at the time of minimum eddy viscosity. In other words, the wind is supergeostrophic. They also found that the magnitude of the oscillation of the ageostrophic wind vector diminishes with latitude. Bonner (1968) pointed out that the ageostrophic v (i.e., north-south) wind component reaches a maximum downstream of the jet core. Its direction, toward the left of the geostrophic wind, indicates the production of kinetic energy through work done by pressure forces. Composite maps of the geostrophic and ageostrophic wind components were created for the level of the maximum wind in order to investigate the relative contribution of the pressure gradient force versus the ageostrophic wind components to the formation of low-level wind maxima.

3) 500-MB GEOPOTENTIAL HEIGHT

Low-level wind maxima have been identified under distinctly different midtropospheric height patterns (Uccellini 1980). Uccellini identified two types of midtropospheric environments for low-level wind maxima. One type of low-level wind maxima was located under a midtropospheric ridge. The other type was found under a trough-ridge pattern. This trough-ridge pattern is generally associated with synoptic forcing. The area upstream of a midtropospheric ridge is characterized by upper-level divergence (Moran and Morgan 1986). Thus, it provides support for surface pressure falls and cyclone development. As previously noted, low-level wind maxima are closely linked to surface pressure falls associated with cyclone development (Djuric 1981; Djuric and Ladwig 1983; Parish et al. 1988). To investigate the degree of midtropospheric support, the 500-mb geopotential height fields are examined for the individual types of low-level wind maxima.

4) 200-MB WIND FIELD

The importance of the

tropospheric jet streak to the

attention (Beebe and Bates 1

field of upper-level jet streak

and right-rear quadrants of t

rear quadrants (Beebe and B

associated with cyclogenesis,

quadrant of an upper-level je

superimposed on lower-tropo

instability develops when the

advection by the upper- and

Johnson 1979). Uccellini and

low-level jets. They noted tha

lower branch of an indirect tr

streak, directed up sloped ise

toward the cyclonic side of th

was observed in the entrance

flow (Sechrist and Whittaker

the 200-mb isotach and strear

convergence field. Similar to

for each variable, centered on

f. Summary

To summarize, the first

characteristics of low-level wi

United States. The goal was t

4) 200-MB WIND FIELD AND 200-MB CONVERGENCE

The importance of the interaction of an upper-tropospheric jet streak with a lower-tropospheric jet streak to the generation of severe weather has received considerable attention (Beebe and Bates 1955; Newton 1967; Chen and Kpaeyeh 1993). The kinetic field of upper-level jet streaks results in areas of upper-level divergence in the left-front and right-rear quadrants of the jet streak and in convergence in the right-front and left-rear quadrants (Beebe and Bates 1955). During the formation of a low-level jet associated with cyclogenesis, the low-level wind maximum intersects the left front quadrant of an upper-level jet streak such that upper-tropospheric divergence is superimposed on lower-tropospheric convergence (Newton 1967). The greatest instability develops when the jet axes are orthogonal and the intensity of the differential advection by the upper- and lower-tropospheric jets is maximized (Uccellini and Johnson 1979). Uccellini and Johnson also investigated the link between the upper- and low-level jets. They noted that a southerly low-level jet is frequently embedded in the lower branch of an indirect transverse circulation in the exit region of an upper-level jet streak, directed up sloped isentropic surfaces (from the 950- to the 750-mb level) toward the cyclonic side of the upper-level jet. Similarly, a direct transverse circulation was observed in the entrance region of the jet streak resulting in a northerly low-level flow (Sechrist and Whittaker 1979). To characterize the upper-tropospheric wind field, the 200-mb isotach and streamline patterns were analyzed, together with the 200-mb convergence field. Similar to the other analysis variables, composite maps were created for each variable, centered on the individual jet cores.

f. Summary

To summarize, the first part of this study investigates the temporal and spatial characteristics of low-level wind maxima at individual rawinsonde stations across the United States. The goal was to investigate whether boundary-layer forced and

synoptically-driven low-leve
vertical speed profiles. In th
configurations of the wind n
that was evident in the airfl
compositing approach was u
the average large-scale lowe
In the next chapter, the first
the characteristics of southe

synoptically-driven low-level wind maxima can be differentiated on the basis of their vertical speed profiles. In the second part of the analysis, the horizontal airflow configurations of the wind maxima were examined. To describe the spatial variation that was evident in the airflow configuration patterns, a manual classification and compositing approach was used. For each of the resulting airflow configuration types, the average large-scale lower-, mid- and upper-tropospheric environment was examined. In the next chapter, the first part of the analysis, the temporal and spatial variation in the characteristics of southerly jet cases, is discussed.

FREQUENCY

1. Temporal Variations in t

a. Monthly Variations

The number of low-lev

during the warm seasons of

individual rawinsonde static

Bonner (1968) for the warm

observations for this study c

stringent selection criteria en

direction.

The monthly distributio

monthly distribution describ

et al. noted a primary frequer

maximum in jet frequency fr

with frequency maxima in M

However, unlike the findings

approximately equal in streng

maximum toward the end of

Interestingly, monthly v

the jet nose is considered. As

Category A cases if the jet no

was between 900 and 800 mb

Chapter 3

FREQUENCY OF SOUTHERLY LOW-LEVEL WIND MAXIMA

1. Temporal Variations in the Frequency of Southerly Low-level Wind Maxima

a. Monthly Variations

The number of low-level wind maxima identified at the eight rawinsonde stations during the warm seasons of 1990 and 1991 was 1522 cases. The number of jet cases at individual rawinsonde stations is higher than the number of low-level jets identified by Bonner (1968) for the warm seasons of 1959 and 1960. The larger number of jet observations for this study can be explained, as noted in Chapter 2, by the more stringent selection criteria employed by Bonner, both in terms of speed criteria and direction.

The monthly distribution of low-level wind maxima agrees fairly well with the monthly distribution described by Mitchell et al. (1995) but not that of Bonner. Mitchell et al. noted a primary frequency maximum in September and a weaker secondary maximum in jet frequency from April to May. For this study, a bimodal distribution, with frequency maxima in May and again in September, is evident (Figure 3.1). However, unlike the findings of Mitchell et al., the two frequency maxima are approximately equal in strength. On the one hand, Bonner noted only a single frequency maximum toward the end of the warm season.

Interestingly, monthly variations in frequency are also observed when the level of the jet nose is considered. As described in Chapter 2, jet observations were identified as Category A cases if the jet nose was below 900 mb, as Category B cases if the jet nose was between 900 and 800 mb, and as Category C cases if it was between 800 and 700

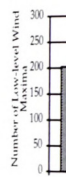

Figure 3.1.
Wind Maxi

mb Category A and Categor

the warm season, except dur

proportion of the total numb

far the least frequent. They s

Figure 3.2 that the increase i

May (seen in Figure 3.1) is th

observations. In contrast, th

Category A jets, and the incr

The differences in the month

Figure 3.2. Mont
Wind Maxima by

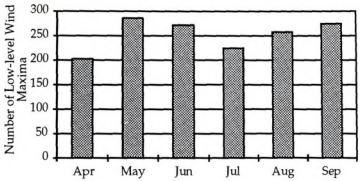

Figure 3.1. Monthly Frequency of Southerly Low-Level Wind Maxima.

mb. Category A and Category B observations are approximately equally frequent during the warm season, except during August when Category A events comprise a larger proportion of the total number of jet observations (Figure 3.2). Category C cases are by far the least frequent. They show a frequency maximum in May and June. Note from Figure 3.2 that the increase in the total number of low-level wind maxima in April and May (seen in Figure 3.1) is the result of an increase in the frequency of all categories of jet observations. In contrast, the increase in jet frequency in August is due to an increase in Category A jets, and the increase in September is due to an increase in Category B jets. The differences in the monthly jet frequencies between this study and previous studies

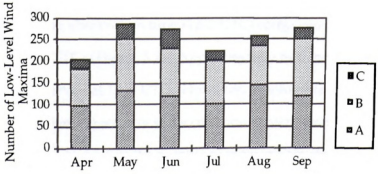

Figure 3.2. Monthly Frequency of Southerly Low-Level Wind Maxima by Height

(e.g., Bonner 1968 and Mitch

and some Category B jets in

jet occurrences to 1500 m ab

presents are dominated by

The frequency maximu

attributed by previous auth

likelihood of synoptic envir

wind maxima (Mitchell et al

cyclones affecting the Great

explanation based on the sy

maximum as well. Whittak

frequency increases from Ap

until a minimum in July.

b. Diurnal Variations

Although rawinsonde

per day, a comparison of the

UTC observation times can p

wind maxima. As expected,

frequently at the morning ob

observation time (0000 UTC

wind maxima were observed

frequent compared to mornin

during the warm season. In

the earlier months. This incr

on the other hand, are most f

low-level wind maxima rema

(e.g., Bonner 1968 and Mitchell et al. 1995) likely is due to the omission of Category C and some Category B jets in the previous studies. For example, Bonner's study limited jet occurrences to 1500 m above ground level. Thus, the frequency diagrams Bonner presents are dominated by Category A jets.

The frequency maximum of low-level wind maxima in September has been attributed by previous authors to a decrease in moisture availability and a greater likelihood of synoptic environments that are conducive to the development of low-level wind maxima (Mitchell et al. 1995). From August to September, the number of Colorado cyclones affecting the Great Plains increases (Whittaker and Horn 1981). An explanation based on the synoptic environment can be used for the spring frequency maximum as well. Whittaker and Horn noted that, for the warm season, cyclone frequency increases from April to May, after which the number of cyclones decreases until a minimum in July.

b. Diurnal Variations

Although rawinsonde observations are available for only two observation times per day, a comparison of the frequency of low-level wind maxima for the 0000 and 1200 UTC observation times can provide some insight on the diurnal variations of low-level wind maxima. As expected, warm season low-level wind maxima are observed more frequently at the morning observation time (1200 UTC) compared to the evening observation time (0000 UTC) (Figure 3.3). Approximately two thirds of all the low-level wind maxima were observed at 1200 UTC. However, evening jets, although less frequent compared to morning jets, are still a common occurrence in the Great Plains during the warm season. In August the number of morning jets increases, compared to the earlier months. This increase is followed by a decrease in September. Evening jets, on the other hand, are most frequent in May and September. The percentage of morning low-level wind maxima remains fairly constant from April through July (Table 3.1). A

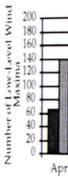

Figure 3.3. M
Maxima by T

maximum in the percentage

decrease to a minimum in Se

Table 3.1.

Apr	
68	

The more frequent occu

been attributed by previous

conditions, in particular to f

Parish et al. 1988). Uccellini

associated with cyclones and

is so typical of boundary-lay

during the evening and morn

related to cyclogenesis and o

jets in August is probably du

September, the diurnal patte

favorable, while at the same

low-level jet development.

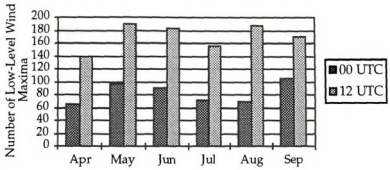

Figure 3.3. Monthly Frequency of Southerly Low-Level Wind Maxima by Time of Day.

maximum in the percentage of morning jets is evident in August and a subsequent decrease to a minimum in September.

Table 3.1. Percentage of Morning (1200 UTC) Jets.

Apr	May	Jun	Jul	Aug	Sep
68	66	67	69	73	62

The more frequent occurrence of low-level wind maxima in the morning hours has been attributed by previous authors to temporal variations in boundary-layer conditions, in particular to frictional decoupling at night (Hoecker 1965; Hoxit 1975; Parish et al. 1988). Uccellini (1980), on the other hand, noted that low-level jets associated with cyclones and frontal boundaries often lack the diurnal oscillation which is so typical of boundary-layer jets. The increases during May in the number of jets both during the evening and morning hours likely reflect the effects of both upper-level forcing related to cyclogenesis and of boundary-layer forcing, whereas the increase in morning jets in August is probably due to more favorable boundary-layer conditions. In September, the diurnal pattern suggests that boundary-layer conditions are less favorable, while at the same time the synoptic environment becomes more favorable for low-level jet development.

2. Spatial Variations in the

The rawinsonde statio

transects (Figure 3.4). The w

Kansas, northward to North

and to Bismarck (BIS), Nort

(OUN), Oklahoma, to Tope

Saint Cloud (STC), Minneso

trends in the frequency of lo

four stations on the left hand

transect (i.e., DDC to BIS), a

easternmost transect (i.e., O

Fig
Sta

A general decrease with

evident along both transects

at OVN compared to the stat

dependence of the frequency

2. Spatial Variations in the Frequency of Low-Level Wind Maxima

The rawinsonde stations included in the analysis roughly form two south-to-north transects (Figure 3.4). The westernmost transect extends from Dodge City (DDC), Kansas, northward to North Platte (LBF), Nebraska, to Huron (HON), South Dakota, and to Bismarck (BIS), North Dakota. The easternmost transect extends from Norman (OUN), Oklahoma, to Topeka (TOP), Kansas, to Omaha (OVN), Nebraska, and to Saint Cloud (STC), Minnesota. These transects were used to investigate the spatial trends in the frequency of low-level wind maxima. On the figures presented below, the four stations on the left hand side of the horizontal axis represent the westernmost transect (i.e., DDC to BIS), and the four stations on the right hand side represent the easternmost transect (i.e., OUN to STC).

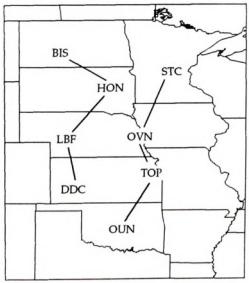

Figure 3.4. Transects of Rawinsonde Stations.

A general decrease with latitude in the total number of low-level wind maxima is evident along both transects (Figure 3.5). The only exception is the larger number of jets at OVN compared to the stations to the north and south. In general, the latitude-dependence of the frequency of low-level wind maxima is most pronounced for the 1200

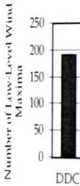

Figure 3.5. Freq
Station.

UTC observation time (Fig

UTC steadily decreases nor

excellent agreement with Bo

low-level wind maxima occ

Figure 3.6. Diurnal
Rawinsonde Statio

Evening low-level win

compared to the western tra

transect in the frequency of

0000 UTC wind maxima are

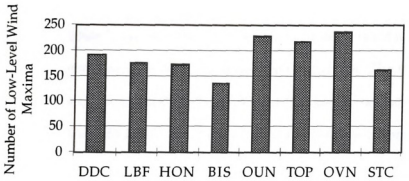

Figure 3.5. Frequency of Low-Level Wind Maxima by Rawinsonde Station.

UTC observation time (Figure 3.6). The frequency of low-level wind maxima at 1200 UTC steadily decreases northward along both transects. This northward decrease is in excellent agreement with Bonner's (1968) findings that the highest percentage of morning low-level wind maxima occurs near 35° N.

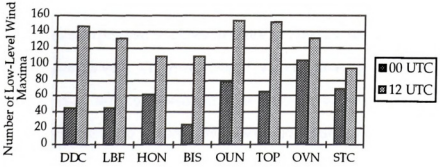

Figure 3.6. Diurnal Variation of Low-Level Wind Maxima by Rawinsonde Station.

Evening low-level wind maxima are more frequent along the eastern transect compared to the western transect. Little latitudinal variation is evident along either transect in the frequency of 0000 UTC low-level wind maxima. Figure 3.6 indicates that 0000 UTC wind maxima are particularly numerous for OVN.

3 Spatial Variations in th

As noted in Chapter

strongly influenced by the

observations are biased to

mean sea level (MSL), due

transmitted at 304 m (1000

nb increments. Therefore,

these levels (Table 3.2). O

an intervening height. Wh

terms of pressure rather th

(Figure 3.7). Note in Figur

stations and both observat

are evident at 3000 and 40

readers should keep in mi

individual jet types, expre

the fixed observation level

that needs to be taken into

Table 2.1), as low-level wi

Table 3.2.

Height
2,000
3,000
4,000
5,000
6,000
7,000
8,000
9,000
10,00
all othe

3. Spatial Variations in the Height of Low-Level Wind Maxima

As noted in Chapter 2, the recorded height of the low-level wind maxima is strongly influenced by the rawinsonde data collection procedures. The strongest wind observations are biased toward 2000, 3000, 4000 feet (ft), and so on, heights above mean sea level (MSL), due to the fact that the original rawinsonde observations are transmitted at 304 m (1000 ft) intervals. Additional levels are generated at 50- and 25-mb increments. Therefore, a significant proportion of wind maxima are observed at these levels (Table 3.2). Of the 1522 low-level wind maxima, only 145 were recorded at an intervening height. When the height of the low-level wind maxima is expressed in terms of pressure rather than distance above mean sea level, similar biases are evident (Figure 3.7). Note in Figure 3.7 that most of the wind maxima, when summed over all stations and both observations times, were observed at 2000 ft, although smaller peaks are evident at 3000 and 4000 ft. A secondary peak is evident at 6000 ft. Consequently, readers should keep in mind that the average height values presented below for the individual jet types, expressed in either distance or pressure units, are biased toward the fixed observation levels. The mean height was also investigated by station. A factor that needs to be taken into consideration is the elevation of the rawinsonde stations (see Table 2.1), as low-level wind maxima are believed to occur at a constant level above the

Table 3.2. Height of Wind Maxima.

Height (ft)	Height(m)	Frequency
2,000	610	456
3,000	914	271
4,000	1,219	308
5,000	1,524	64
6,000	1,829	119
7,000	2,134	71
8,000	2,438	51
9,000	2,743	29
10,000	3,048	8
all others	all others	145

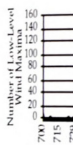

Figure 3.7. Pre

ground surface (Bonner 196

factor are DDC and LBF wh

other rawinsonde locations.

at both 0000 UTC and 1200

elevation differences appear

height shows little spatial va

HON, even though HON is

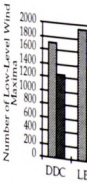

Figure 3.8. Mean

At all locations, mean

considerably larger than thos

is on the order of several hu

findings (1968) that the mea

hours compared to the eveni

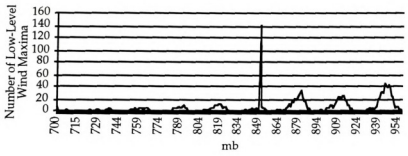

Figure 3.7. Pressure Levels of Wind Maxima.

ground surface (Bonner 1968). However, the only stations where this appears to be a factor are DDC and LBF which have considerably higher elevations compared to the other rawinsonde locations. Note that the mean heights of the low-level wind maxima at both 0000 UTC and 1200 UTC are also considerably higher (Figure 3.8). However, elevation differences appear to have little impact for the other stations, where the mean height shows little spatial variation. The only exception is the lower mean heights for HON, even though HON is not located at the lowest elevation.

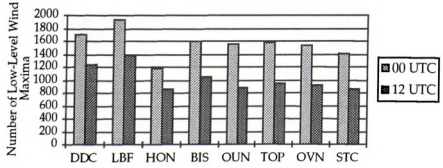

Figure 3.8. Mean Height of Wind Maxima (MSL).

At all locations, mean heights for the 0000 UTC low-level wind maxima are considerably larger than those for the morning jets. The difference in height is on the order of several hundred meters. This finding is consistent with Bonner's earlier findings (1968) that the mean heights of low-level wind maxima are lower in the morning hours compared to the evening hours. The number of wind maxima in the individual

height categories also reflec

morning (Figures 3.9 and 3.

1200 to 0000 UTC, the num

However, most of the diurn

(wind maxima below 900 m

diurnal influences there ext

ets suggests that diurnally-

below 900 mb, whereas litt

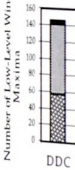

Figure 3.9. Lo

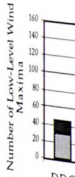

Figure 3.10. L

height categories also reflects an increase in height for the evening hours compared to the morning (Figures 3.9 and 3.10). Note that, despite the decrease in total frequency from 1200 to 0000 UTC, the number of wind maxima in categories B and C is increasing. However, most of the diurnal variation in the frequency of jets is confined to Category A (wind maxima below 900 mb). Due to the higher station elevation at HON and LBF, diurnal influences there extend up to 800 mb. The pronounced difference in Category A jets suggests that diurnally-varying boundary-layer conditions are particularly influential below 900 mb, whereas little variation is evident above 900 mb.

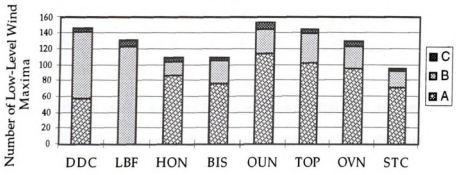

Figure 3.9. Low-Level Wind Maxima by Station by Category, 1200 UTC.

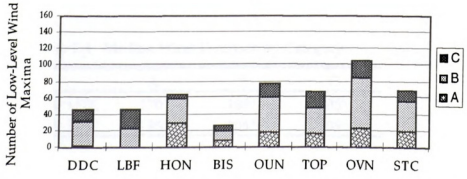

Figure 3.10. Low-Level Wind Maxima by Station by Category, 0000 UTC.

4. Speed and Direction of

A well-documented f

diurnal oscillation with gre

3.3). For this study, large

0000 LTC for Category A a

maxima, the mean wind sp

observation times.

Table 3.3.

0000 UTC	
1200 UTC	

A diurnal oscillation

Category B low-level wind

direction veers by 25 degre

slightly less, only 20 degre

veering with time is evider

Table 3.4.

0000 UTC	
1200 UTC	

5. Summary

The temporal and spa

eight rawinsonde stations a

part of the analysis was to

4. Speed and Direction of Low-Level Wind Maxima

A well-documented feature of boundary-layer forced low-level wind maxima is the diurnal oscillation with greater wind speeds occurring in the early morning hours (Table 3.3). For this study, large mean wind speeds are observed at 1200 UTC compared to 0000 UTC for Category A and Category B jet cases. For Category C low-level wind maxima, the mean wind speed is almost identical for the 0000 UTC and 1200 UTC observation times.

Table 3.3. Mean Wind Speed (in ms^{-1}) by Category.

	A	B	C
0000 UTC	13.1	14.6	15.3
1200 UTC	14.8	16.1	15.2

A diurnal oscillation is also evident in the wind direction for Category A and Category B low-level wind maxima (Table 3.4) For Category A jets, the median wind direction veers by 25 degrees from 0000 UTC to 1200 UTC. The amount of veering is slightly less, only 20 degrees for Category B low-level wind maxima. Note that no veering with time is evident for Category C jets (Table 3.4) .

Table 3.4. Median Wind Direction by Category

	A	B	C
0000 UTC	170°	185°	205°
1200 UTC	195°	205°	205°

5. Summary

The temporal and spatial variations in the frequency of low-level wind maxima at eight rawinsonde stations across the Great Plains were analyzed. The objective of this part of the analysis was to determine whether distinct characteristics were evident in the

vertical speed profiles of lo

tion between boundary-lay

s indicate that considerabl

Plains in terms of frequenc

both types of low-level wir

The frequency distrib

distribution with maxima i

from August to September

mb, which would support

the month with the most fr

number of wind maxima at

when a large-scale surface

conditions over the southe

below 900 mb.

Other indications for

the fact that the diurnal os

height. The oscillations th

and 900 mb and are non-e

vertical speed profiles of low-level wind maxima that allowed for a broad differentiation between boundary-layer forced and synoptically driven jets. The results of Chapter 3 indicate that considerable variation is evident for wind maxima across the Great Plains in terms of frequency, speed, height, and direction. These variations suggest that both types of low-level wind maxiina are present in the observational sample.

The frequency distribution of all jets combined displays a bimodal frequency distribution with maxima in May and September. The increase in the frequency of jets from August to September is largely a result of an increase in wind maxima above 800 mb, which would support the claim of favorable synoptic environments. During May, the month with the most frequent Colorado cyclogenesis during the warm season, the number of wind maxima above 800 mb is similarly high. August, on the other hand, when a large-scale surface high pressure area sets up favorable boundary-layer conditions over the southern Plains, has the largest percentage of low-level wind maxima below 900 mb.

Other indications for the existence of different types of wind maxima are given by the fact that the diurnal oscillations in speed and direction decrease with increasing height. The oscillations that are observed below 900 mb show a decrease between 800 and 900 mb and are non-existent above 800 mb.

A
AND TI

1. Introduction and Over

In this chapter the ty
Great Plains are identified
patterns are related to the
and convection.

As a first step, "jet e
the previous chapter. Unl
and observation time. Onl
Mexico were included in th
can have multiple levels, if
height. The jet events were
instantaneous wind direct
closest to the earth's surfac
orientation and latitudinal
of confluence, deformation

The subjective typing
distinct airflow groups wit
isotach fields were then co
found to be unique and col
procedure. Below, the dist
composite airflow patterns

Chapter 4

AIRFLOW CONFIGURATION TYPES AND THEIR RELATIONSHIP TO CONVECTION

1. Introduction and Overview

In this chapter the typical airflow configurations of low-level wind maxima in the Great Plains are identified and described. In addition, the airflow configuration patterns are related to the spatial distributions of convergence, temperature, moisture, and convection.

As a first step, "jet events" were identified from the 1522 "jet cases" described in the previous chapter. Unlike jet cases, only one jet event is possible for a particular day and observation time. Only those jet events with trajectories originating over the Gulf of Mexico were included in the subsequent analysis. As described in Chapter 2, a jet event can have multiple levels, if the orientation of the low-level wind maxima shifts with height. The jet events were subjectively classified on the basis of their streamline (i.e., instantaneous wind direction) and isotach (i.e., wind speed) patterns for the level closest to the earth's surface. The key features used to classify the events were the orientation and latitudinal extent of the wind maximum, and the existence and location of confluence, deformation, and difluence zones.

The subjective typing of jet events with a Gulf 'connection' resulted in twelve distinct airflow groups with at least 10 members each. Composite streamline and isotach fields were then computed for each of the twelve groups. The composites were found to be unique and coherent and provided evidence of the adequacy of the typing procedure. Below, the distinctions between groups are discussed with respect to the composite airflow patterns. Also, the composite airflow configuration is overlaid on

composite distributions o

the spatial interrelations

Each airflow confi

smaller latitudinal exter

that extend to higher la

discussed in order of de

type, the airflow config

the typical temperature

convection with that ai

2. AC_EW Jets (Anti

a. *Airflow Configuration*

The first type of

in the southern portio

southeastern United S

4.3). The average flo

s^{-1})[1] north of the isota

an east-west directio

immediately west ar

referred to as anticy

confluence zone (sh

The AC_EW je

altitudinal, seasona

have very shallow,

mb) for the pressu

911 mb. Thirteen

[1] Note that the figu

composite distributions of temperature, moisture, and convection for each group, and the spatial interrelationships of the different parameters are discussed.

Each airflow configuration type is described in turn. The six airflow types with smaller latitudinal extents are described first, followed by the six types of wind maxima that extend to higher latitudes (i.e., into Canada). Within each group the types are discussed in order of decreasing anticyclonic (increasing cyclonic) curvature. For each type, the airflow configuration and convergence fields are discussed first, followed by the typical temperature and moisture fields, concluding with the typical distribution of convection with that airflow type.

2. AC_EW Jets (Anticyclonically curved jet with Confluence oriented East-West)

a. Airflow Configuration and Convergence

The first type of low-level wind maximum is characterized by an isotach maximum in the southern portion of the Great Plains embedded within anticyclonic flow over the southeastern United States (Figure 4.1; for reference to geographic location consult Figure 4.3). The average flow pattern is characterized by strong speed convergence (3.78×10^{-5} s^{-1})[1] north of the isotach maximum in the vicinity of a confluence zone that is oriented in an east-west direction (Figure 4.2). A second, weaker convergence zone is located immediately west and southwest of the isotach maximum. This configuration type is referred to as anticyclonic low-level wind maximum with an east-west oriented confluence zone (shorthand notation: *AC_EW* Jets).

The *AC_EW* jets appear to be primarily boundary-layer phenomena, based on their altitudinal, seasonal and geographical preferences (Tables 4.1 and 4.2). *AC_EW* jets have very shallow, pronounced jet noses with a median (mean) height of 942 mb (928 mb) for the pressure surface closest to the ground. Only one event had an altitude above 911 mb. Thirteen of the fourteen jet events in this configuration type are Category A jets

[1] Note that the figures show values of divergence, instead of convergence.

Fig
Lev
lin

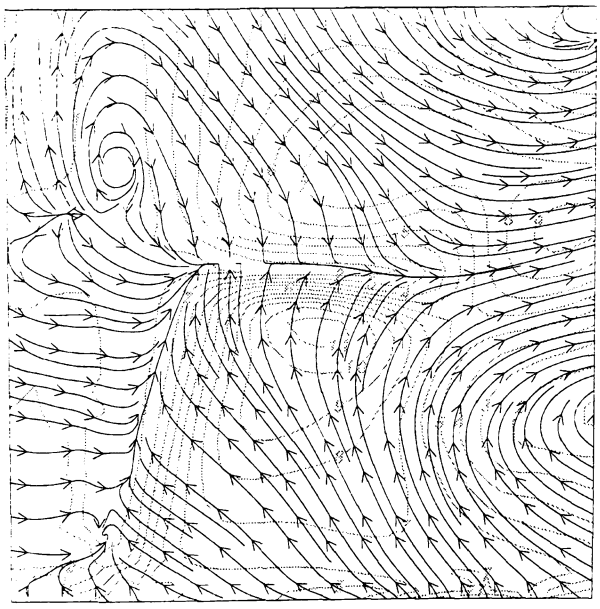

Figure 4.1. Composite Isotachs and Streamlines, Level 1 – *AC_EW Jets*. Solid black lines are streamlines, dotted gray lines are isotachs.

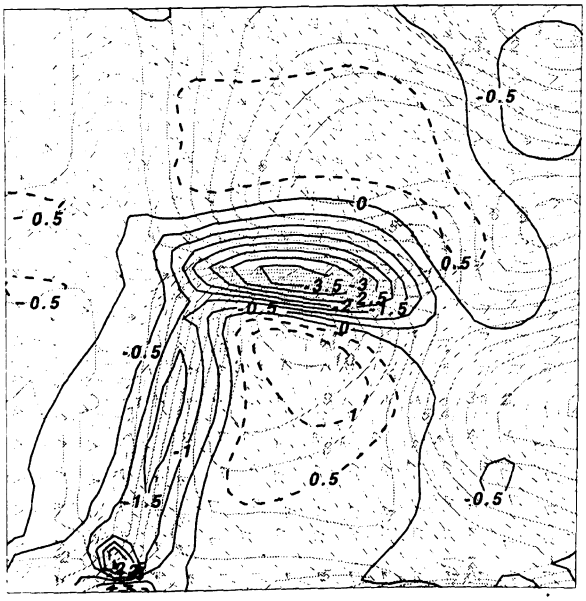

Figure 4.2. Composite Divergence, Level 1 – *AC_EW* Jets. Light dashed lines are streamlines, light solid lines are isotachs, heavy lines represent divergence field.

Table 4.1. N
– AC_EW J

Level 1
Level 2

(i.e., wind maximum oc

maxima have speeds ≥

decreases above the sp

instances, the decrease

diurnal signature. All

slight preference for th

also that the centers of

median location of 36°

centered on the media

Table 4.2. Characteri

Number of observations	Diur varia
Level 1: 14	0000
Level 2: 3	1200

[1] Median Value
[2] Average Value

[2] 'Strong' jets have ma
of maximum wind of
designations correspo
[3] 'Less pronounced' je
wind speed above the

Table 4.1. Number of Events by Speed Profile Category -- *AC_EW* Jets.

	'Strong' Jets[2]	'Less Pronounced'[3] Jets
Level 1	a1: 1 a2: 9 b1: 1	a4: 1 a5: 2
Level 2	a2: 2 b1: 1	

(i.e., wind maximum occurs below 900 mb). In addition the majority of the wind maxima have speeds ≥ 12 ms^{-1} (i.e. subtypes a1, a2, b1). Also, the wind speed decreases above the speed maximum by at least one half (i.e., 'strong' jets). In most instances, the decrease in speed occurs below 700 mb. The *AC_EW* jets display a strong diurnal signature. All events occurred at the 1200 UTC observation time. There is a slight preference for the months of July and August, the height of the warm season. Note also that the centers of the isotach maxima are geographically clustered around the median location of 36°N/102°W in the Texas Panhandle (Figure 4.3). The subgrid is centered on the median location. The centroids of the wind maxima are found in a

Table 4.2. Characteristics of *AC_EW* Jets.

Number of observations	Diurnal variation	Seasonal variation	Annual variation	Height (mb)	Median location
Level 1: 14 Level 2: 3	0000 Z: 0 1200 Z: 14	Apr: 3 May: 0 Jun: 1 Jul: 4 Aug: 4 Sep: 2	1991: 4 1992: 10	Level 1: Med*: 942 Ave$^{\nabla}$: 926 Level 2: Med: 904 Ave 877	36°N/102°W

* Median Value
$^{\nabla}$ Average Value

[2] 'Strong' jets have maximum speeds in excess of 12 ms^{-1} and a minimal decrease above the level of maximum wind of at least one half the maximum wind speed. The alphanumeric designations correspond to the vertical speed profile categories discussed in Chapter 2.
[3] 'Less pronounced' jets either have maximum velocities of less than 12 ms^{-1} and/or a decrease in wind speed above the wind maximum of less than one half the maximum wind speed.

narrow band between s

displaced somewhat to

level wind maxima dete

the majority of the *AC_*

Very few *AC_EW*

included in the calculat

Remember that the mai

configurations that are

Fig
- *A*

orientation. Due to t

of the observed patte

level for the three cas

(877 mb). The stream

of the first level. Als

level jet core. The co

than the correspond

narrow band between southeastern Colorado and central Texas. The centers are displaced somewhat to the southwest compared with the climatological location of low-level wind maxima determined by Bonner (1968). Finally, it is interesting to note that the majority of the *AC_EW* events occurred during 1992, the "year without a summer."

Very few *AC_EW* jets had distinct upper levels, and only three events were included in the calculations of the composites for the second level (Figure 4.4). Remember that the main criterion for the inclusion of higher levels is airflow configurations that are distinctly different from that of the lower levels in terms of

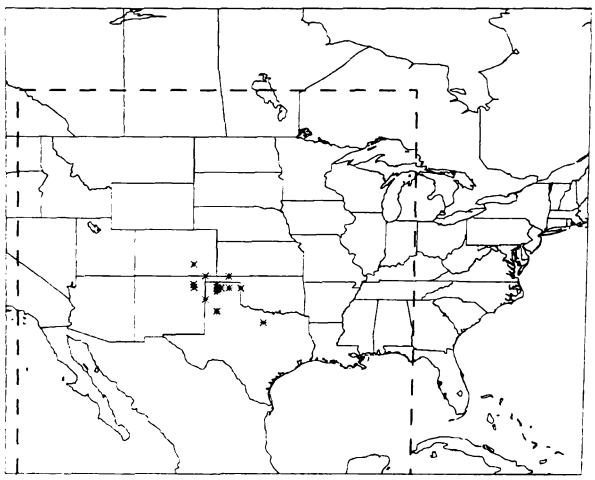

Figure 4.3. Geographical Centers of Isotach Maxima - - *AC_EW* Jets.

orientation. Due to the small number of observations, only a qualitative interpretation of the observed pattern for the second analysis level should be attempted. The second level for the three cases is fairly shallow with a median (mean) height of only 904 mb (877 mb). The streamlines for the second level are slightly more anticyclonic than those of the first level. Also, the wind maximum is located farther east compared to the first-level jet core. The confluence zone and resulting convergence (Figure 4.5) are weaker than the corresponding first level features and are also displaced to the east.

Figure
Leve

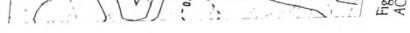

Figure
AC

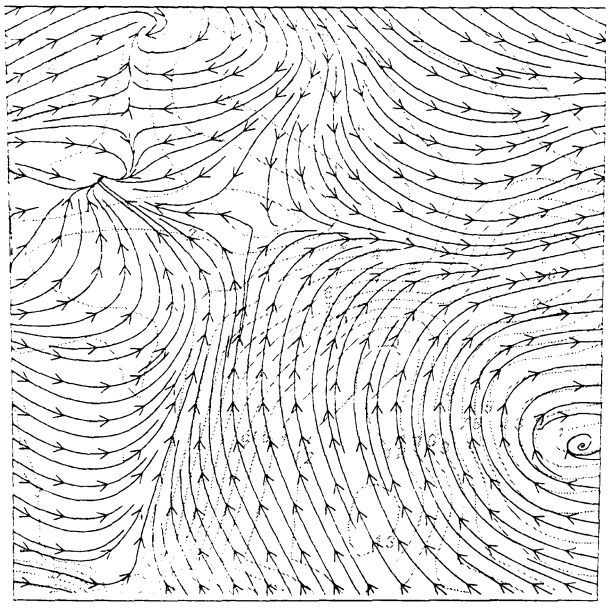

Figure 4.4. Composite Isotachs and Streamlines, Level 2 -- *AC_EW* Jets. As in Figure 4.1.

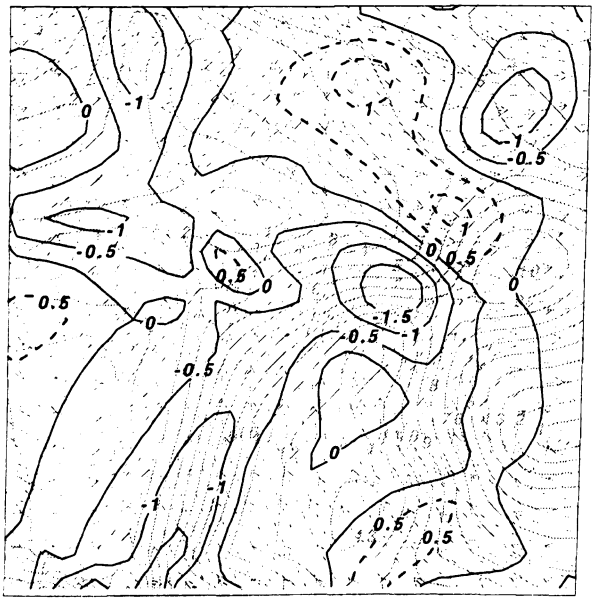

Figure 4.5. Composite Divergence, Level 2 -- *AC_EW* Jets. As in Figure 4.2.

b. Temperature and Mo

As described in

the temperature and r

650 mb surface was ch

events. While the me

or 850 mb, standard le

temperature and mois

For *AC_EW* jets,

maximum at both the

feature is a trough in t

the southern portion o

northward from the h

lines of equal mixing

moisture that is adve

orientation of the moi

temperatures (≥22°C)

location of a dryline (

maximum appears to

temperature pattern,

the direction of the co

In Figure 4.7, th

overlaid onto the com

However, keep in mi

three cases. The 850-

influence by the wind

northeastward over th

southwestern U.S.. T

b. Temperature and Moisture

As described in Chapter 2, the 900 mb pressure surface was chosen to represent the temperature and moisture distributions for the first level of the jet events, and the 850 mb surface was chosen to represent these distributions for the second level of the events. While the mean height of the jet events does not always correspond to 900 mb or 850 mb, standard levels were chosen to permit a quantitative comparison of the temperature and moisture variables among the airflow configuration types.

For *AC_EW* jets, a strong temperature gradient is evident north of the isotach maximum at both the 900- and 850-mb levels (Figures 4.6 and 4.7). A conspicuous feature is a trough in the thermal field located northwest of the wind maximum. Within the southern portion of the composite area, a ridge of higher temperatures extends northward from the hot, dry southwestern United States. At both levels, isohumes (i.e., lines of equal mixing ratio) clearly identify the Gulf of Mexico as the source area for the moisture that is advected into the area. Note in particular the northwest-southeast orientation of the moisture tongue. At the 900-mb level, the ridge of warmest temperatures (≥22°C) coincides with a strong moisture gradient, likely indicating the location of a dryline (Figure 4.6). The advective influence of the low-level wind maximum appears to be more important for the moisture distribution compared with the temperature pattern, as indicated by bulge of the 12 g kg^{-1} and the 11 g kg^{-1} isohumes in the direction of the composite streamlines.

In Figure 4.7, the average temperature and moisture pattern for the 850 mb level is overlaid onto the composite airflow configuration at the second analysis level. However, keep in mind that the airflow composite for the second level is based on only three cases. The 850-mb temperature pattern (Figure 4.7) suggests a stronger advective influence by the wind maximum compared to the 900 mb pattern, as the isotherm bulge northeastward over the center of the composite region from a source area in the southwestern U.S.. The moisture gradient at the 850-mb level is considerably weaker

Fig
hea
das
Co
are
co

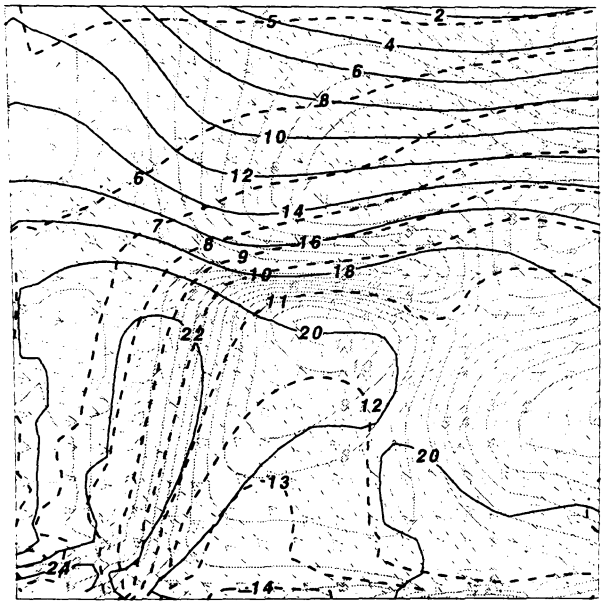

Figure 4.6. Composite 900-mb Temperature (°C; heavy solid lines) and Mixing Ratio (g kg^{-1} heavy dashed lines) plotted on Level 1 Composite Airflow Configuration – *AC_EW Jets*. The light dashed lines are the composite streamlines, the light solid lines are composite isotachs.

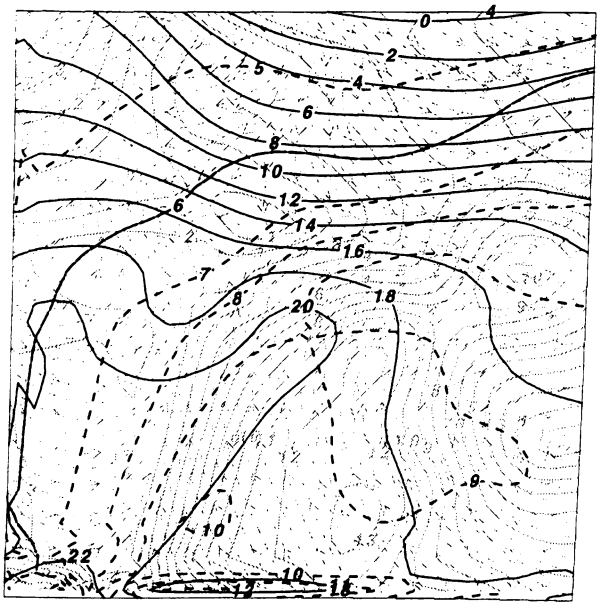

Figure 4.7. Composite 850-mb Temperature (°C) and Mixing Ratio (g kg^{-1}) plotted on Level 2 Composite Airflow Configuration -- *AC_EW Jets*. As in Figure 4.6.

than at the 900-mb leve

at 850-mb are only 9 g

c. Convection

Cloud-to-ground

jets. All of the AC_EW

Figures 4.8 and 4.9 da

were observed in a gi

rawinsonde observat

system applied to th

An important obser

The distribution of l

configuration. Rela

most frequent light

west oriented confl

As indicated

general location of

However, despite

activity, the larges

50 percent. The s

location of lightni

extent of the ligh

lightning strikes,

the two-hour per

the individual ev

[4] A lightning per
a particular grid

than at the 900-mb level and the mixing ratio values at the center of the composite map at 850-mb are only 9 g kg^{-1} compared to 11 g kg^{-1} for the 900 mb surface.

c. Convection

Cloud-to-ground lightning, as a surrogate for convection, is common with *AC_EW* jets. All of the *AC_EW* jets included were associated with one or more lightning flashes. Figures 4.8 and 4.9 depict the percentages of jet events during which lightning flashes were observed in a given grid cell during the two-hour period straddling the time of the rawinsonde observations. The lightning periods[4] were accumulated in the same grid system applied to the rawinsonde observations and divided by the number of jet events. An important observation is that cloud-to-ground lightning flashes are very localized. The distribution of lightning flashes corresponds closely to the composite airflow configuration. Relative to the wind maximum at the first analysis level, the location of most frequent lightning activity is offset to the east along and to the north of the east-west oriented confluence zone (Figure 4.8).

As indicated in Chapter 2, the lightning composite maps very well represent the general location of lightning activity of individual jet events relative to the jet core. However, despite the fact that all *AC_EW* jet events were associated with lightning activity, the largest percentage for any particular grid cell in the composite map is only 50 percent. The smaller percentage (< 100 percent) is due to slight variations in the location of lightning flashes relative to the jet core as well as variations in the areal extent of the lightning activity. Some jet events were accompanied by only a few lightning strikes, while for other jet events an extensive area experienced lightning during the two-hour period. In general, however, the visual inspection of the lightning plots for the individual events suggests that the lightning composite maps very well represent the

[4] A lightning period is defined as an analysis time period during which lightning is observed in a particular grid cell. In this study the analysis time periods are equal to two hours.

R
A
C

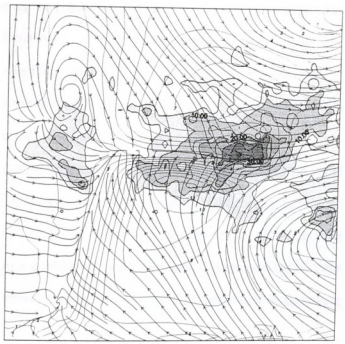

Figure 4.8. Percentage of Jet Events with Lightning Activity in Individual Grid Cells plotted on Level 1 Composite Airflow Configuration -- *AC_EW* Jets.

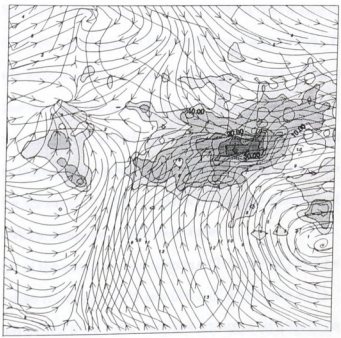

Figure 4.9. Percentage of Jet Events with Lightning Activity plotted on Level 2 Composite Airflow Configuration -- *AC_EW* Jets.

general location of ligh
lightning flashes occur
convergence zone slig
downstream of the wi
pressure level, near a

Keep in mind w
only three cases. Ho
airflow configuration
when explaining the
common for this airf

3. AC_SWNE Jets (
oriented SouthWe

a. Airflow Configura

The second fl
anticyclonic flow o
the *AC_EW* jets en
west confluence zo
AC_EW jets is abs
west of the wind r
ease of reference,
zone oriented **SW**

The magnit
the *AC_SWNE* je
convergence out
northwest of the
of the isotach ma

general location of lightning activity relative to the jet core for this jet type. Most lightning flashes occur north of the wind maximum along the east-west oriented convergence zone slightly offset to the east. This area, however, is also located directly downstream of the wind maximum at the wind maximum evident on the second pressure level, near a confluence zone (Figure 4.9).

Keep in mind when interpreting this pattern that the airflow composite is based on only three cases. However, the excellent spatial relationship between convection and the airflow configuration at the second level suggests 1) that all levels need to be considered when explaining the location of convection, and 2) that multiple levels may be more common for this airflow configuration type than indicated in this study.

3. AC_SWNE Jets (Anticyclonically curved wind maximum with Confluence zone oriented SouthWest-NorthEast)

a. Airflow Configuration and Convergence

The second flow type resembles the *AC_EW* jets in that it also is embedded in the anticyclonic flow over the southeastern United States (Figure 4.10). The resemblance to the *AC_EW* jets ends with the anticyclonic curvature, however. The distinctive east-west confluence zone north of the isotach maximum that is so pronounced for the *AC_EW* jets is absent in the *AC_SWNE* jets. Rather, a confluence zone is located to the west of the wind maximum and oriented in a southwesterly-northeasterly direction. For ease of reference, the acronym *AC_SWNE* (**A**nticyclonically-curved with **C**onfluence zone oriented **SW-NE**) is assigned to this flow type.

The magnitude of the resulting convergence ($0.95 \times 10^{-5}\ s^{-1}$) is considerably less for the *AC_SWNE* jets than for the *AC_EW* jets ($3.8 \times 0^{-5}\ s^{-1}$)(Figure 4.11). The area of convergence outlined by the $0.5 \times 10^{-5}\ s^{-1}$ isopleth includes an area of confluence to the northwest of the isotach maximum as well as an area of speed convergence downstream of the isotach maximum.

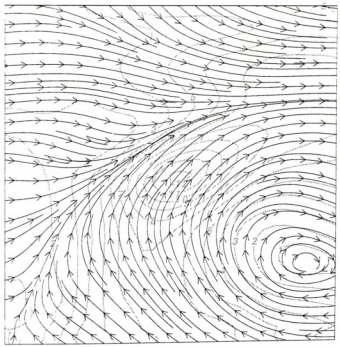

Figure 4.10. Composite Isotachs and Streamlines, Level 1 -- *AC_SWNE* Jets. As in Figure 4.1.

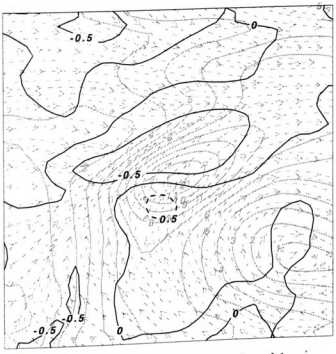

Figure 4.11. Composite Divergence, Level 1 – *AC_SWNE* Jets. As in Figure 4.2.

Table 4.3. Characteri

Number of observations	Diur variat
Level 1: 31	0000 2
Level 2: 4	1200 2
Level 3: 2	

Compared wit

higher elevations w

(Table 4.3). There i

(Table 4.4). At the

subsequent decreas

a weaker maximur

distinctions were n

In addition t

jets also differ fro

preferences (Table

Table
AC_S

Leve
Lev
Lev

Table 4.3. Characteristics of *AC_SWNE* Jets.

Number of observations	Diurnal variation	Seasonal variation	Annual variation	Height (mb)	Median location
Level 1: 31 Level 2: 4 Level 3: 2	0000 Z: 13 1200 Z: 8	Apr: 3 May: 1 Jun: 3 Jul: 12 Aug: 5 Sep: 7	1991: 21 1992: 10	Level 1: Med: 878 Ave: 874 Level 2: Med: 862 Ave: 837 Level 3: Med: 817 Ave: 817	38°N/97°W

Compared with the *AC_EW* jets, the *AC_SWNE* jets are located at considerably higher elevations with a median (mean) height of 878 mb (874 mb) for the first level (Table 4.3). There is also a higher proportion of jets with a less pronounced jet nose (Table 4.4). At the first level, 16 cases have a maximum speed of 12 ms^{-1} and a subsequent decrease of one half the maximum speed or more, while 10 cases have either a weaker maximum speed or smaller vertical shear. For the five cases above 800 mb, no distinctions were made regarding the shape of the speed profile.

In addition to differences in the height and speed characteristics, the *AC_SWNE* jets also differ from the *AC_EW* jets in terms of their temporal and geographical preferences (Table 4.3). The *AC_SWNE* jets lack the pronounced diurnal signature

Table 4.4. Number of Events by Speed Profile Category -- *AC_SWNE* Jets.

	'Strong' Jets	'Less Pronounced' Jets	Other
Level 1	a1: 2 a2: 3 b1: 10 b2: 1	a3: 1 a4: 2 a5: 1 b3: 4 b4: 2	c: 5
Level 2	b1: 2 b2: 1	b3: 1	
Level 3	b1: 1	b3: 1	

of the AC_EW jets. Al
the evening hours (000
located farther northea
centers has considerabl
AC_EW jets (Figure 4.1
from Texas into Wisco
distribution of jet core
cases in his study (Bo
height, diurnal and sp
scale forcing mechani
majority of AC_SWN
were observed during
different large-scale s
however, the AC_SW
season (i.e., in July)

of the *AC_EW* jets. Almost half of the *AC_SWNE* jets (42 percent) were observed during the evening hours (0000 UTC). Additionally, the median center of the *AC_SWNE* jets is located farther northeast, in central Kansas, and the location of the individual isotach centers has considerably greater variance about the median than observed for the *AC_EW* jets (Figure 4.12). The individual jet cores are found in a broad area extending from Texas into Wisconsin. The distribution of the centroids strongly resembles the distribution of jet cores presented by Bonner (1968). The median location of the jet cases in his study (Bonner 1968, Figure 13) was also found in central Kansas. The height, diurnal and spatial characteristics combined suggest a stronger influence of large-scale forcing mechanisms as compared to boundary-layer influences. Note also that the majority of *AC_SWNE* jets were observed during 1991, whereas most of the *AC_EW* jets were observed during 1992. The annual preferences would corroborate the notion that different large-scale settings are needed for the two jet types. Similar to the *AC_EW* jets, however, the *AC_SWNE* jets also have a frequency maximum at the height of the warm season (i.e., in July) (Table 4.3).

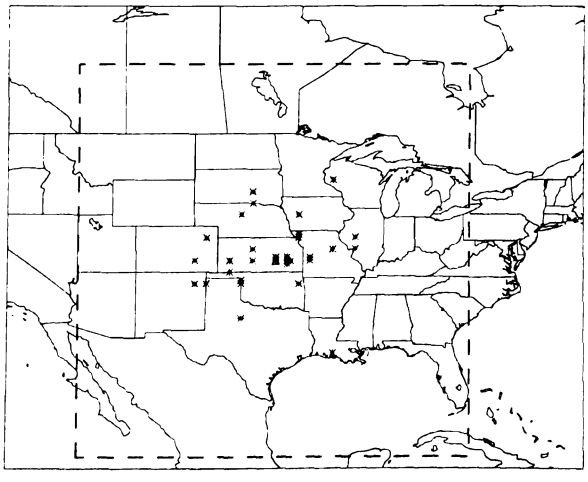

Figure 4.12. Geographical Centers of Isotach Maxima - - *AC_SWNE* Jets.

The streamline an
also displays a confluen
4.13). The isotach max
first-level, but it is disp
considerably less antic
The composite converg
While a broad area of
to the first level, small
north of the isotach ma
areas surpasses the ma
explanation for the hig
four cases included in
(see Table 4.3).

Only two cases
for the third level (se
section because it giv
maxima and convect
attempted here. One
third level (Figure 4.
evident downstream

b. Temperature and M

Similar to the
a respectable tempe
4.18), although the
north of the *AC_EW*
northeastward from

The streamline and isotach composite for the second level (based on four cases) also displays a confluence zone along the left flank of the isotach maximum (Figure 4.13). The isotach maximum at the second level is of equal magnitude as that of the first-level, but it is displaced downstream (i.e., to the northeast) and displays considerably less anticyclonical curvature. Backing of the wind with height is implied. The composite convergence pattern differs slightly from the first level (Figure 4.14). While a broad area of convergence is located to the left of the isotach maximum, similar to the first level, smaller areas of strong convergence are evident to the southwest and north of the isotach maximum. The magnitude of the convergence in these localized areas surpasses the maximum convergence values at the first level. A possible explanation for the higher values of convergence at the second level is that three of the four cases included in the composite for the second level had very strong speed maxima (see Table 4.3).

Only two cases were included in the calculation of the composite *AC_SWNE* jets for the third level (see Table 4.3). This composite was nevertheless included in this section because it gives important insight into the spatial relationship of low-level wind maxima and convection. However, only a qualitative assessment of the airflow is attempted here. One feature worth mentioning is the lack of a confluence zone at the third level (Figure 4.15). However, a fairly pronounced area of speed convergence is still evident downstream of the wind maximum (Figure 4.16).

b. Temperature and Moisture

Similar to the *AC_EW* jets, the temperature pattern for the *AC_SWNE* jets displays a respectable temperature gradient north of the isotach maximum (Figures 4.17 and 4.18), although the gradient is not as pronounced and it lacks the thermal trough to the north of the *AC_EW* isotach maximum. Again, the warmest temperatures extend northeastward from the southwestern corner of the composite area. At the 900-mb

Figu
Lev

Fi
A

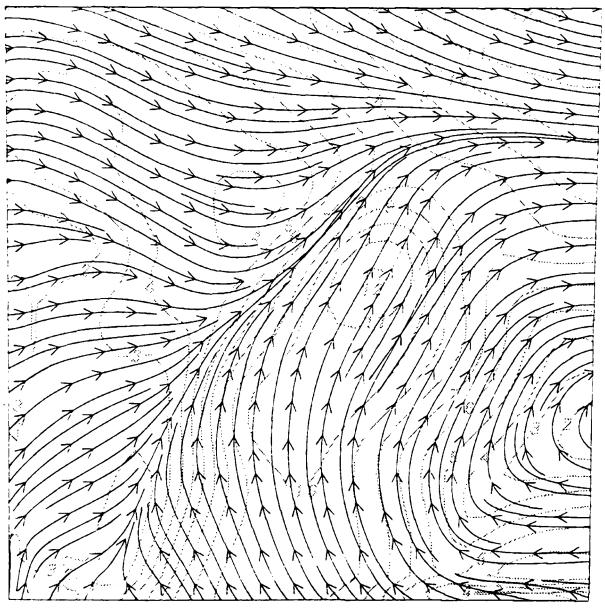

Figure 4.13. Composite Isotachs and Streamlines, Level 2 -- *AC_SWNE* Jets. As in Figure 4.1.

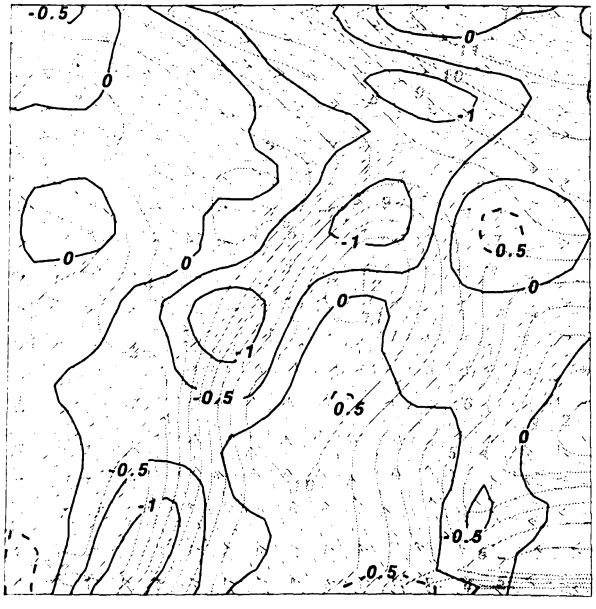

Figure 4.14. Composite Divergence, Level 2 -- *AC_SWNE* Jets. As in Figure 4.2

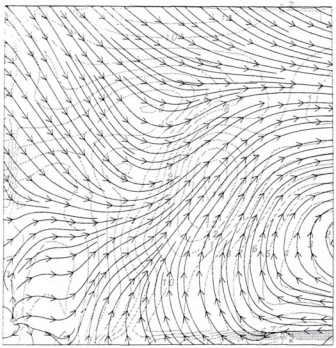

Figure 4.15. Composite Isotachs and Streamlines, Level 3 -- *AC_SWNE* Jets. As in Figure 4.1.

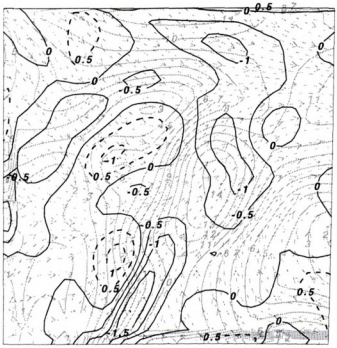

Figure 4.16. Composite Divergence, Level 3 -- *AC_SWNE* Jets. As in Figure 4.2.

level, an elongated area

with a moderate to stron

mixing ratio values in th

AC_EW jets (11 g kg^{-1}),

level. The 900-mb mea

C in the case of AC_EW

southwestern corner is

explanation is that AC_

variation in the relative

weaker composite grad

The 850 mb temp

level wind maxima, ra

elevation of AC_SWN

the isohumes (note the

composite first-level v

to those for the AC_E

environment. Similar

corner of the compos

900-mb level, an indi

c. Convection

Lightning activ

Of the 31 events, onl

to AC_EW events, w

confluence zone, the

widespread. Two lo

of the low-level win

level, an elongated area of high temperatures, outlined by the 24°C isotherm, coincides with a moderate to strong moisture gradient in the southwest (Figure 4.17). While the mixing ratio values in the center of the composite map are comparable with those of the *AC_EW* jets (11 g kg^{-1}), the environment of the *AC_SWNE* jets is warmer at the 900-mb level. The 900-mb mean temperatures at the center of the composite map are barely 20° C in the case of *AC_EW* jets, but ≥ 22°C for *AC_SWNE* jets. The moisture gradient in the southwestern corner is weaker for *AC_SWNE* jets compared to *AC_EW* jets. A likely explanation is that *AC_SWNE* jets are more dispersed geographically and the greater variation in the relative distance between the dryline and the jet centers results in a weaker composite gradient.

The 850 mb temperature pattern is probably reflective of advection from the first level wind maxima, rather than the second level maxima, given the relatively high mean elevation of *AC_SWNE* jets. The bulges in the isotherms (note the 20° C isotherm) and the isohumes (note the 10 g kg^{-1} isohume) coincide nicely with the streamlines of the composite first-level wind maximum. The 850 mb average temperatures are comparable to those for the *AC_EW* jets; however *AC_SWNE* jets are accompanied by a more humid environment. Similar to the *AC_EW* jets, the moisture gradient in the southwestern corner of the composite map is considerably weaker at the 850-mb level compared to the 900-mb level, an indication of the rather shallow nature of the dryline in that region.

c. Convection

Lightning activity is less frequent with *AC_SWNE* jets compared with *AC_EW* jets. Of the 31 events, only 26 (84 percent) were associated with lightning flashes. In contrast to *AC_EW* events, where the lightning is confined to a fairly small area along the confluence zone, the lightning activity during *AC_SWNE* events is considerably more widespread. Two locations of frequent lightning activity are evident along the left flank of the low-level wind maxima. One frequency maximum is located downstream of the

Figu
and
Cor
Jets

F
a
C
J

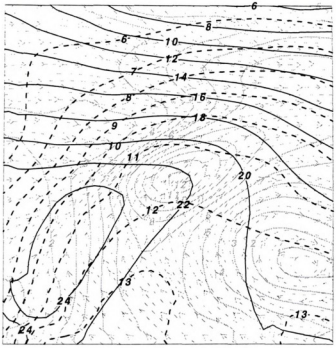

Figure 4.17. Composite 900-mb Temperature (°C) and Mixing Ratio (g kg^{-1}) plotted on Level 1 Composite Airflow Configuration -- *AC_SWNE* Jets. As in Figure 4.6.

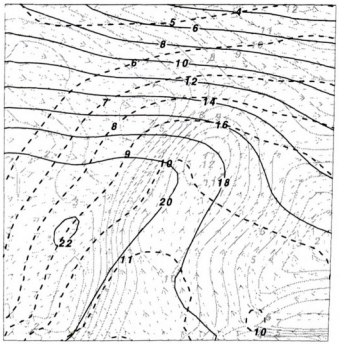

Figure 4.18. Composite 850-mb Temperature (°C) and Mixing Ratio (g kg^{-1}) plotted on Level 2 Composite Airflow Configuration -- *AC_SWNE* Jets. As in Figure 4.6.

wind maximum and so

This maximum also coi

levels (Figure 4.20 and

level confluence zone t

moisture gradient. The

flashes, however, whic

known 'ring of fire' arc

Fig
Ac
Co

wind maximum and south of the confluence zone evident at the first level (Figure 4.19). This maximum also coincides with areas of convergence at the second and third analysis levels (Figure 4.20 and 4.21). A second frequency maximum is evident along the first-level confluence zone to the southwest of the jet core, a region characterized by a strong moisture gradient. The area between those frequency maxima is not devoid of lightning flashes, however, which gives the spatial pattern of lightning the appearance of the well-known 'ring of fire' around a high pressure system.

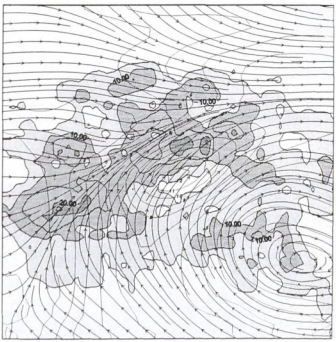

Figure 4.19. Percentage of Jet Events with Lightning Activity plotted on Level 1 Composite Airflow Configuration -- *AC_SWNE* Jets.

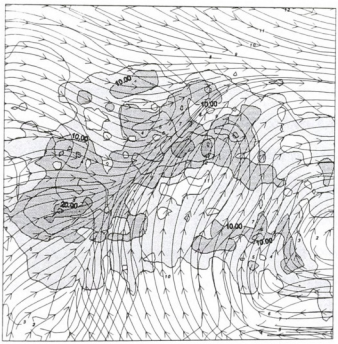

Figure 4.20. Percentage of Jet Events with Lightning Activity plotted on Level 2 Composite Airflow Configuration -- *AC_SWNE* Jets.

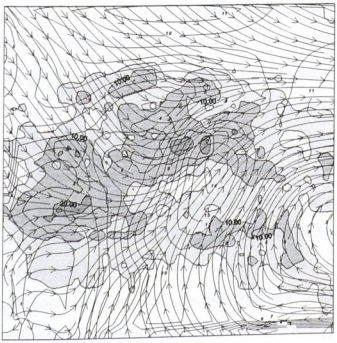

Figure 4.21. Percentage of Jet Events with Lightning Activity plotted on Level 3 Composite Airflow Configuration -- *AC_SWNE* Jets.

4. KC_SWNE Jets (wind maxima with "Kurl" and Confluence oriented SouthWest-NorthEast)

a. Airflow Configuration and Convergence

The third airflow configuration type, like the two previously described types, is characterized by anticyclonically-curved airflow over the southern Great Plains (Figure Confluence oriented **SW-NE**). Like the *AC_EW* jets, this flow type is found at very low altitudes with a median (mean) height of 942 mb (931 mb) at the lowest level (Table 4.5). The *KC_SWNE* jets are similar to *AC_EW* jets in a number of other respects, as well. Like the *AC_EW* jets, *KC_SWNE* jets have an area of strong convergence to the northwest of the isotach maximum (2.92×10^{-5} s^{-1}) (Figure 4.23). They also have a strong diurnal preference. Eleven out of twelve events occurred in the early morning hours (1200 UTC). Remember that the *AC_SWNE* jets, on the other hand, are located at considerably higher elevations, their areas of convergence are less pronounced, and they lack a pronounced diurnal signature. Similar to the *AC_EW* jets, but unlike the *AC_SWNE* jets, the centers of the *KC_SWNE* jets are fairly clustered about a median location on the Oklahoma/Kansas border (Figure 4.24). The majority of jet cores is found from the Texas panhandle into central Kansas. The strength of the *KC_SWNE* jets is quite large; the composite wind speed for the first level is 16 ms^{-1}. However, there is not as large a proportion of strong vertical profiles (i.e., a1, a2, b1, b2 categories) as was the case for *AC_EW* and *AC_SWNE* types (Table 4.6). Also, unlike the previously discussed types, *KC_SWNE* show a seasonal preference for the end of the warm season (September) and were equally frequent in 1991 and 1992 (Table 4.5).

A fairly high percentage of the *KC_SWNE* jets have multiple levels. At the second level, seven events (58 percent) were included in the composite. Since there was only one event with three levels, no composite was created for a third level. At the second level, the airflow is still anticyclonically curved (Figure 4.25) but differs from the first level airflow in several respects. The isotach maximum is displaced to the northeast and

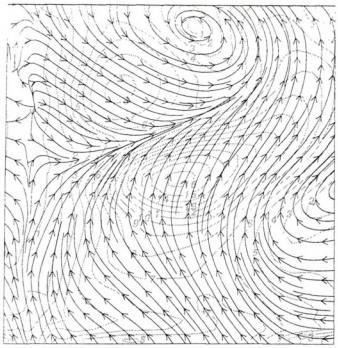

Figure 4.22. Composite Isotach and Streamlines, Level 1 -- *KC_SWNE* Jets. As in Figure 4.1.

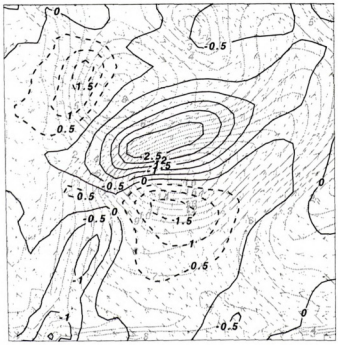

Figure 4.23. Composite Divergence, Level 1 -- *KC_SWNE* Jets. As in Figure 4.2.

Table 4.5. Characteristics of *KC_SWNE* Jets.

Number of observations	Diurnal variation	Seasonal variation	Annual variation	Height (mb)	Median location
Level 1: 12	0000 Z: 1	Apr: 1	1991: 6	Level 1:	37°N/101°W
Level 2: 7	1200 Z: 11	May: 1	1992: 6	Med: 942	
		Jun: 3		Ave: 931	
		Jul: 1		Level 2:	
		Aug: 1		Med: 850	
		Sep: 5		Ave: 863	

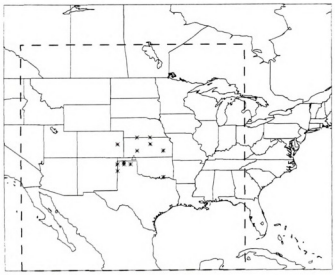

Figure 4.24. Geographical Centers of Isotach Maxima -- *KC_SWNE* Jets.

Table 4.6. Number of Events by Speed Profile Category -- *KC_SWNE* Jets.

	'Strong' Jets	'Less Pronounced' Jets	Others
Level 1	a1: 1 a2: 5 b2: 1	a3: 5	
Level 2	a1: 1 a2: 1 b1: 2 b2: 1	a3: 1 b3: 1	
Level 3			c: 1

its average speed is lower. It is embedded in an airstream that is more strongly anti-cyclonically curved and that does not have a closed cyclonic circulation downstream of the jet core. As for the first level, a confluence zone is evident along the left flank of the wind maximum, but the airstreams join at a smaller angle. Individual areas of larger convergence are evident along the left flank (1.34×10^{-5} s^{-1}) and downstream (1.04×10^{-5} s^{-1}) of the wind maximum (Figure 4.26), similar to the *AC_SWNE* jets. It is interesting to note that the airflow configurations for the second level are similar for the *AC_SWNE* and *KC_SWNE* jets even though the first level airflow configurations are extremely different and the two jet types have very different diurnal and seasonal characteristics.

b. Temperature and Moisture

KC_SWNE jets set themselves apart from the other low-level wind maxima discussed so far in that their environment is considerably warmer and more humid to a greater depth. Although 900 mb temperatures in the southwestern corner of the composite area are not quite as warm as those for *AC_SWNE* jets, the area outlined by the 20°C isotherm is considerably larger than for any other type (Figure 4.27). The 20°C isotherm extends some distance northeast of the average location of the jet core. Note the apparent advective influence of the low-level wind maximum in the orientation of the isotherms. At the 900-mb level, the center of the composite area lies in a region with average mixing ratio values of ≥ 12 g kg^{-1}. The strongest moisture gradient is again located in the southwestern corner of the composite map, in the same location as the ridge of warmest temperatures. The strong advective influence of the wind maximum is continued at the 850-mb level (Figure 4.28). Note the ridge of elevated temperature and moisture values in the direction of the streamlines. At the 850-mb level, the center of the composite area has an average temperature and mixing ratio values of 20°C and 10 g kg^{-1}, respectively.

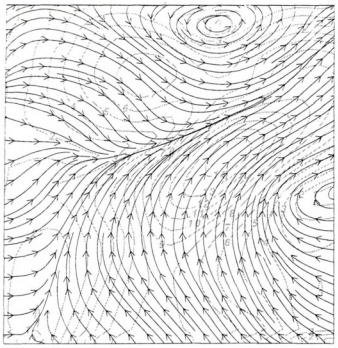

Figure 4.25. Composite Isotachs and Streamlines, Level 2 -- *KC_SWNE* Jets. As in Figure 4.1.

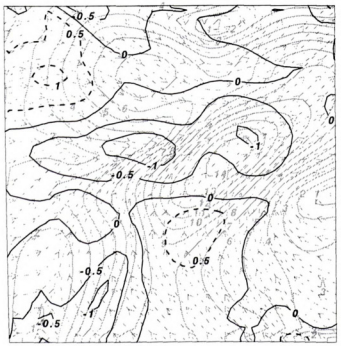

Figure 4.26. Composite Divergence, Level 2 -- *KC_SWNE* Jets. As in Figure 4.2.

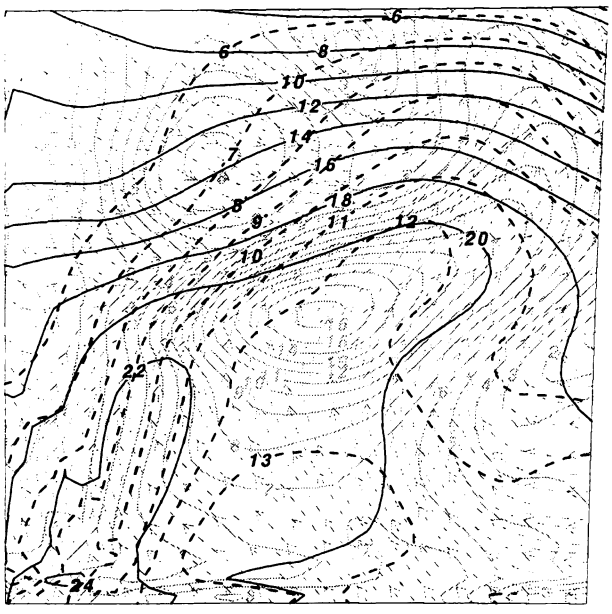

Figure 4.27. Composite 900-mb Temperature (°C) and Mixing Ratio (g kg^{-1}) plotted on Level 1 Composite Airflow Configuration -- *KC_SWNE* Jets. As in Figure 4.6.

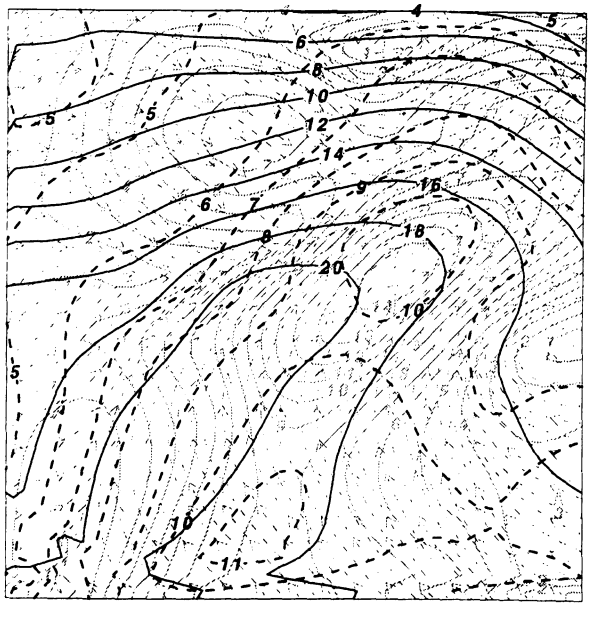

Figure 4.28. Composite 850-mb Temperature (°C) and Mixing Ratio (g kg^{-1}) plotted on Level 2 Composite Airflow Configuration -- *KC_SWNE* Jets. As in Figure 4.6.

c. Convection

The spatial pattern of lightning during *KC_SWNE* events bears some resemblance to the pattern for *AC_EW* jets in that the area of most frequent lightning activity is confined to a fairly localized region downstream of the jet core along the confluence zone (Figure 4.29). The general area of high lightning occurrence extends eastward into an area of convergence at the second analysis level (Figure 4.30). Despite the fairly localized pattern, lightning is frequent with the *KC_SWNE* airflow configuration type. Of the twelve events that were recorded during the warm seasons of 1991 and 1992, eleven (92 percent) were associated with cloud-to-ground lightning. The largest percentage of lightning occurrence in any individual grid cell in the composite map was 58 percent.

5. SD_SWNE Jets (low-level wind maximum with "Split' airflow and Deformation zone oriented SouthWest-NorthEast)

a. Airflow Configuration and Convergence

The anticyclonic flow over the southeastern United States is again present in the fourth airflow configuration type. However, while the isotach maximum is embedded in the anticyclonic flow, the broader-scale flow "splits" downstream of the wind maximum and a pronounced deformation zone is located to the northwest of the isotach maximum (Figure 4.31). Consequently, this airflow type is designated *SD_SWNE* (**S**plit with **D**eformation Zone oriented **SW-NE**). Convergence is largest just south of the deformation zone (Figure 4.32). The average values of convergence are slightly larger (1.37×10^{-5} s^{-1}) than the values for the *AC_SWNE* jets but smaller than the values for the *AC_EW* and *KC_SWNE* jets. *SD_SWNE* jets fall between *AC_SWNE* jets, on the one hand, and *AC_EW* and *KC_SWNE* jets, on other hand, with respect to their temporal preferences, as well (Table 4.7). *SD_SWNE* jets are most frequent during the morning hours; seventy-one percent of the jet events occurred at 1200 UTC. The comparable

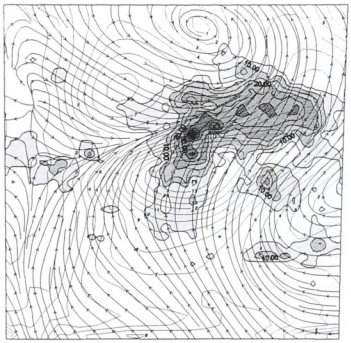

Figure 4.29. Percentage of Jet Events with Lightning Activity plotted on Level 1 Composite Airflow Configuration -- *KC_SWNE* Jets.

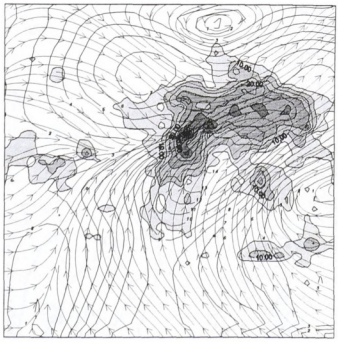

Figure 4.30. Percentage of Jet Events with Lightning Activity plotted on Level 2 Composite Airflow Configuration -- *KC_SWNE* Jets.

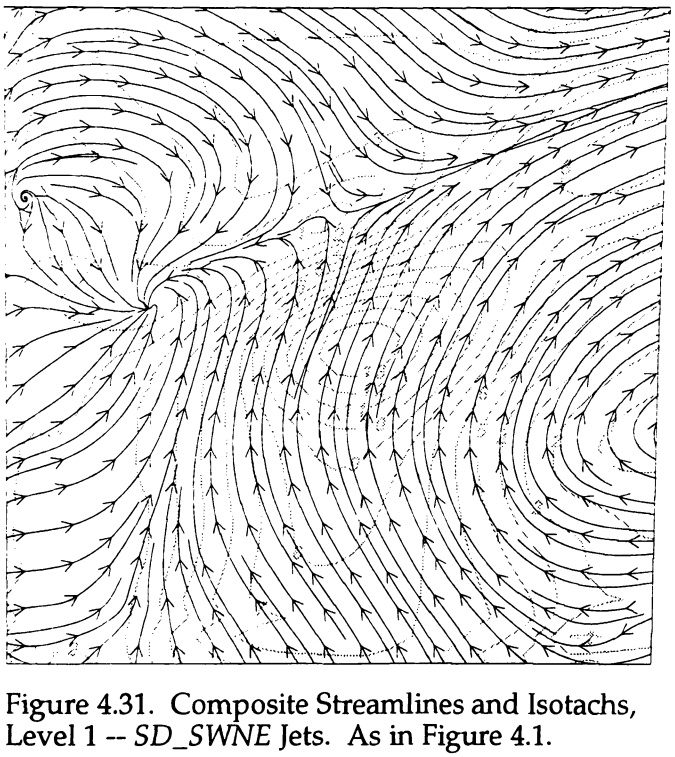

Figure 4.31. Composite Streamlines and Isotachs, Level 1 -- *SD_SWNE* Jets. As in Figure 4.1.

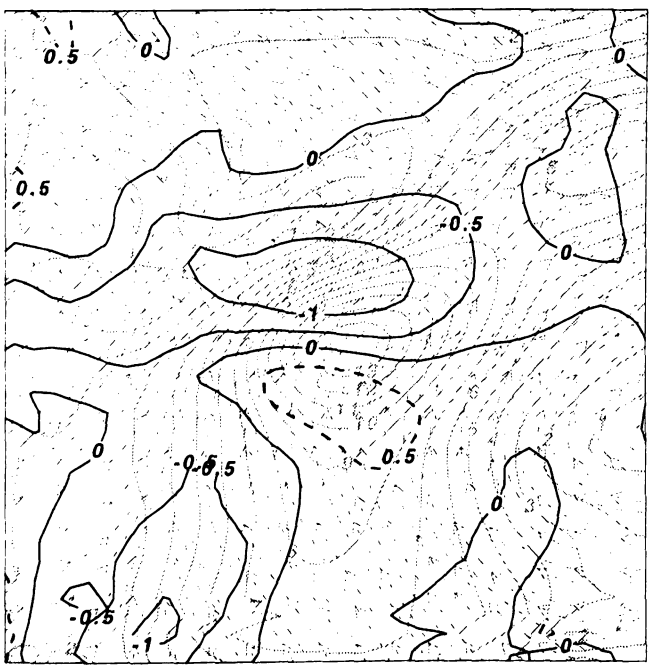

Figure 4.32. Composite Divergence, Level 1 -- *SD_SWNE* Jets. As in Figure 4.2.

Table 4.7. Characteristics of *SD_SWNE* Jets.

Number of observations	Diurnal variation	Seasonal variation	Annual variation	Height (mb)	Median location
Level 1: 17	0000 Z: 5	Apr: 3	1991: 9	Level 1:	38°N/100°W
Level 2: 9	1200 Z: 12	May: 4	1992: 8	Med: 850	
		Jun: 3		Ave: 877	
		Jul: 1		Level 2:	
		Aug: 3		Med: 850	
		Sep: 3		Ave: 839	

percentages are 58 percent for *AC_SWNE* jets and 100 and 92 percent for *AC_EW* and *KC_SWNE* jets, respectively. Unlike *AC_SWNE* jets and *AC_EW* jets which are most frequent at this time, *SD_SWNE* jets are least frequent in July. The average (median) height for *SD_SWNE* jets of 877 mb (850 mb) is comparable with that of the *AC_SWNE* jets (mean: 874 mb / median: 878 mb), but is generally higher than that of *AC_EW* and *KC_SWNE* jets. The geographic distribution of the isotach centers and the amount of dispersion about the center also resembles that of the *AC_SWNE* jets (Figure 4.33). The

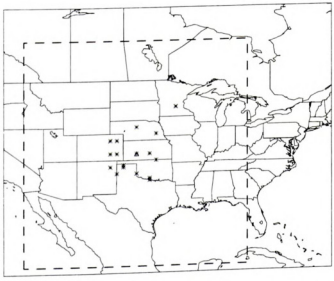

Figure 4.33. Geographical Centers of Isotach Maxima - - *SD_SWNE* Jets.

median location for both the *SD_SWNE* and the *AC_SWNE* jets is found in Kansas at approximately 38° latitude, compared to the median locations of 36° N and 37° N for *AC_EW* and *KC_SWNE* jets, respectively. Similar to the *AC_SWNE* configuration type, the location of the individual *SD_SWNE* jet cores are found in a broad swath between the Texas Panhandle and Wisconsin. The *SD_SWNE* jets are distinct from the three previously-discussed types in that they have more 'weak' than 'strong' profiles types at the first level (Table 4.8). Nine of the seventeen cases have either maximum speeds of less than 12 ms^{-1} or a vertical shear of less than one half of the maximum speed.

Table 4.8. Number of Events by Speed Profile Category -- *SD_SWNE* Jets.

	'Strong' Jets	'Less Pronounced' Jets	Others
Level 1	a1: 1 a2: 2 b1: 5 b2: --	a3: 4 b3: 3 b4: 2	
Level 2	a2: 2 b1: 4	b3: 2	c: 1

The number of cases (9 or 53 percent) included in the calculation of the composites for the second level is relatively large compared to the number of the other configuration types discussed so far. The most obvious difference between the composite airflow patterns for the two levels is that the "split" evident on the pressure surfaces closest to the ground is absent at the second level (Figure 4.34). The broad anticyclonically-curved airstream evident on the second level composite most resembles the airflow for AC_SWNE jets. While a weak confluence zone is evident along the left flank of the second-level jet core, it is not reflected in the composite map of convergence (Figure 4.35). Rather, the largest convergence is located downstream of the jet core.

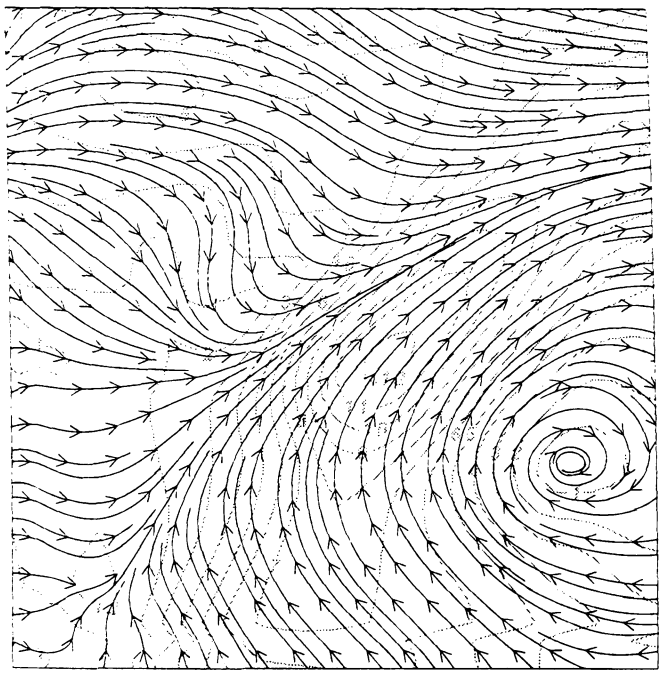

Figure 4.34. Composite Isotachs and Streamlines, Level 2 -- *SD_SWNE* Jets. As in Figure 4.1.

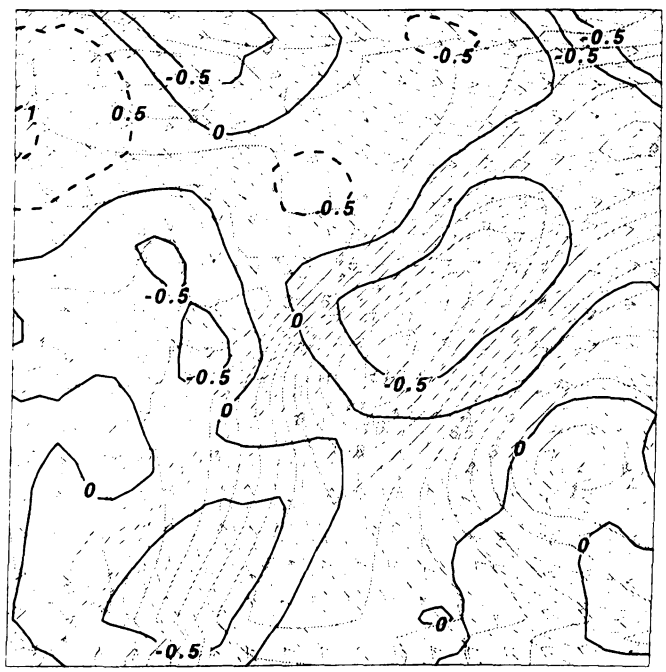

Figure 4.35. Composite Divergence, Level 2 -- *SD_SWNE* Jets. As in Figure 4.2.

b. Temperature and Moisture

The *SD_SWNE* jets occur in a comparatively cool and dry environment. Mean temperatures at the 900-mb level in the vicinity of the jet core are only ≥ 18° C compared to mean temperatures ≥ 20-22° C for the three previously-discussed configuration types (Figure 4.36). The tongue of higher temperatures extending northward from the southwestern corner of the study area is less pronounced than that for the other three types. Also, the average mixing ratio at 900 mb is lower for *SD_SWNE* jets, particularly in the region of the jet core. Another difference is the strength of the moisture gradient southwest of the jet core. At the 900-mb level, this gradient is comparable in magnitude to the mean gradient observed for the *AC_SWNE* jets, but weaker than the gradients observed for the *AC_EW* and *KC_SWNE* jets. As suggested earlier, the strength of the moisture gradient is likely a reflection of the geographic preference of the jet cores. *AC_EW* and *KC_SWNE* jets are more clustered about their median location near the Texas panhandle compared to the *AC_SWNE* or *SD_SWNE* jets which are more geographically dispersed.

The tendency for a cooler environment extends up to the 850-mb level (Figure 4.37). While average temperatures of 20° were recorded in the center of the composite map for the previous types, *SD_SWNE* jets have average temperatures of only approximately 18° C. The amount of moisture at 850 mb, on the other hand, is similar for all four configuration types.

c. Convection

Cloud-to-ground lightning flashes were reported with 94 percent of the *SD_SWNE* jets. The influence of the configuration pattern on the location of the lightning flashes is evident (Figures 4.38 and 4.39). In terms of the first level airflow, lightning is most frequent along the left flank of the jet core, just south of the deformation zone. The spatial association between lightning activity and airflow is even more evident for the

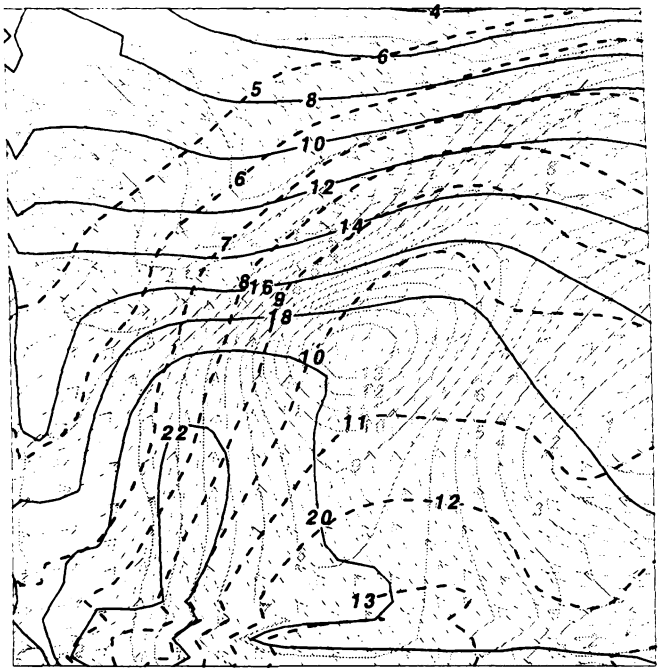

Figure 4.36. Composite 900-mb Temperature (°C) and Mixing Ratio (g kg^{-1}) plotted on Level 1 Composite Airflow Configuration --*SD_SWNE* Jet. As in Figure 4.6.

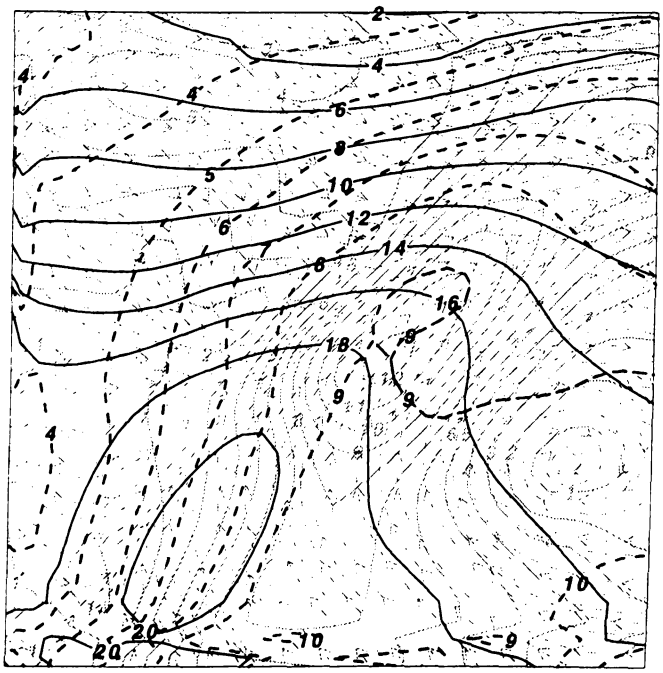

Figure 4.37. Composite 850-mb Temperature (°C) and Mixing Ratio (g kg^{-1}) plotted on Level 2 Composite Airflow Configuration --*SD_SWNE* Jet. As in Figure 4.6.

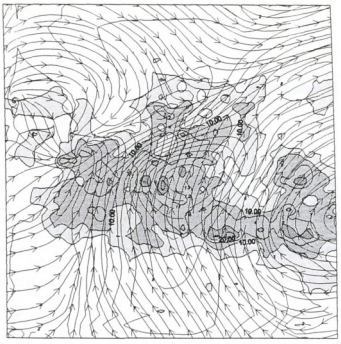

Figure 4.38. Percentage of Jet Events with Lightning Activity plotted on Level 1 Composite Airflow Configuration -- *SD_SWNE* Jets.

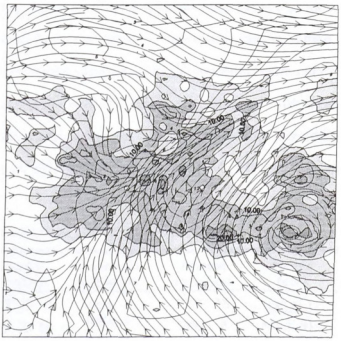

Figure 4.39. Percentage of Jet Events with Lightning Activity plotted on Level 2 Composite Airflow Configuration -- *SD_SWNE* Jets.

second level composite, where lightning is most frequent along the confluence zone west of the jet core.

6. SD_NWSE Jets (low-level wind maxima with "Split" flow and Deformation zone oriented NorthWest-SouthEast)

a. Airflow Configuration and Convergence

The next configuration type is similar to the *SD_SWNE* type, except that the deformation zone is oriented in a northwest-southeast direction, rather than the southwest-northeast orientation observed for *SD_SWNE* jets (Figure 4.40). Also, the "split" in the airflow for *SD_NWSE* jets (Split with Deformation Zone oriented NorthWest-SouthEast) is located downstream of the isotach center rather than to the west of the center, as was the case for *SD_SWNE* jets. For both types the largest convergence is observed downstream of the "split", and is of approximately equal magnitude (1.28×10^{-5} s^{-1}) (Figure 4.41).

The temporal, height and geographical characteristics of the *SD_NWSE* jets suggest that boundary-layer conditions are important factors in their formation. *SD_NWSE* jets have a strong preference for the morning hours with 76 percent of the events having occurred at 1200 UTC (Table 4.9). They are most frequently observed at the height of the warm season, in July. Their height is fairly low with an average (median) elevation of 900 mb (913 mb). Like the *AC_EW* jets, their median latitude

Table 4.9. Characteristics of *SD_NWSE* Jets.

Number of observations	Diurnal variation	Seasonal variation	Annual variation	Height (mb)	Median location
Level 1: 21	0000 Z: 5	Apr: 1	1991: 15	Level 1:	36°N/100°W
Level 2: 6	1200 Z: 16	May: 1	1992: 6	Med: 913	
		Jun: 4		Ave: 900	
		Jul: 9		Level 2:	
		Aug: 2		Med: 833	
		Sep: 4		Ave: 824	

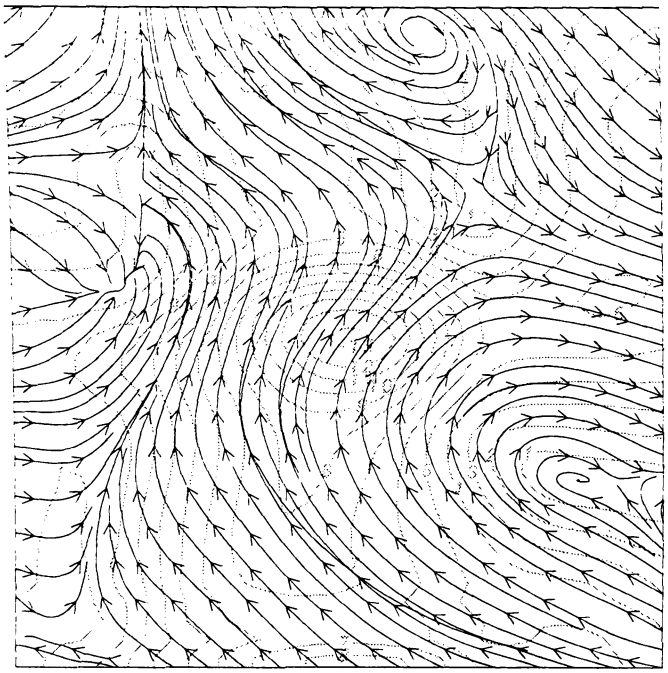

Figure 4.40. Composite Isotachs and Streamlines, Level 1 – *SD_NWSE* Jets. As in Figure 4.1.

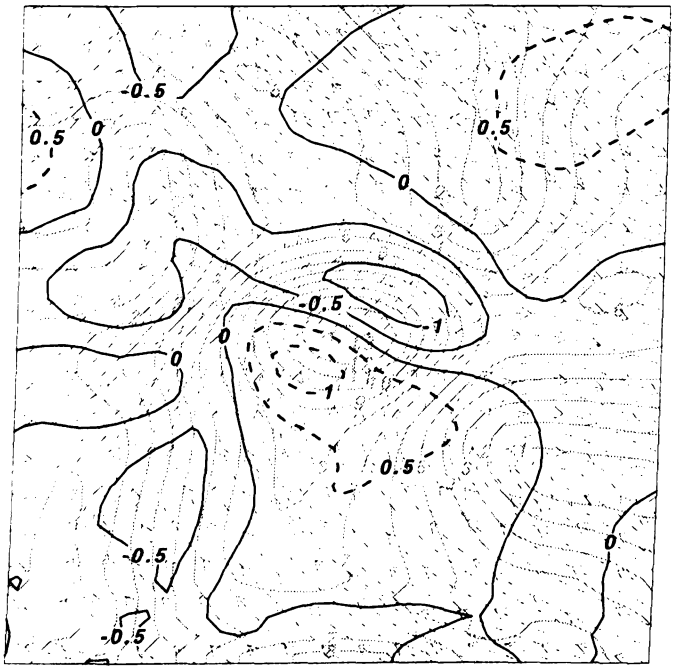

Figure 4.41. Composite Divergence, Level 1 -- *SD_NWSE* Jets. As in Figure 4.2.

is 36° N. The median jet core is found on the Oklahoma/Texas border (Figure 4.42). The amount of scattering about the median is moderate for *SD_NWSE* jets. Individual centroids are found in a fairly narrow band from the Texas Panhandle into Missouri.

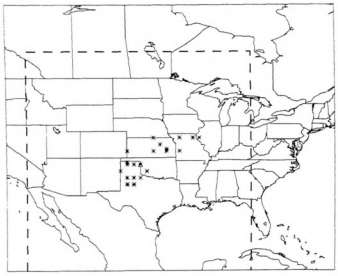

Figure 4.42. Geographical Centers of Isotach Maxima -- *SD_NWSE* Jets.

Unlike other jets types that appear to be strongly influenced by boundary-layer conditions (i.e. *AC_EW* jets and *KC_SWNE* jets), *SD_NWSE* jets 1) were most frequent in 1991 when 71 percent of the events were recorded and 2) lack a predominance of 'strong' speed profile types (Table 4.10).

Table 4.10. Number of Events by Speed Profile Category-- *SD_NWSE* Jets.

	'Strong' Jets	'Less Pronounced' Jets	Others
Level 1	a1: 3 a2: 4 b1: 3	a3: 2 a4: 1 a5: 3 b3: 2 b4: 2	c: 1
Level 2	a2: 1 b1: 1	b3: 1 b4: 2	c: 1

At the second level of the *SD_NWSE* jets, the split in the airflow is still present, unlike the pattern observed for *SD_SWNE* jets (Figure 4.43). The branch that curves cyclonically is considerably less pronounced than the similar branch at the lower level, however. While the split at the first level is located downstream of the isotach maximum, the split at the second level is shifted to the west of the streamline through the isotach center. Unlike the previously-discussed types, the isotach center at the second level for the *SD_NWSE* jets is displaced slightly to the west of the center at the first level. At both levels, the primary area of convergence is located downstream of the isotach maximum and is similar in magnitude (1.23×10^{-5} s^{-1}) (Figure 4.44). Since the curvature of the airstreams at the second level is more anticyclonic than the first level airflow, the area of convergence at the second level is located to the south of the convergence zone at the first level. The magnitude of the convergence at the second level for *SD_NWSE* jets is larger than that for *SD_SWNE* jets. Due to the fact that only one event with a distinct airflow was identified at a third level, no third level will be discussed.

b. Temperature and Moisture

The environment of *SD_NWSE* jets is relatively warm and humid compared to *SD_SWNE* jets. At the 900-mb level, the mean temperature and humidity near the jet core is ≥ 22°C and 12 g kg-1, respectively (Figure 4.45). In the southwestern corner of the composite map, mean temperatures exceed 24° C, and a strong humidity gradient is evident. The advective influence of the difluent airstream is clearly evident in the shape of the isotherms and isohumes. Note in particular the shape of the isohumes northward of the jet core, which are generally aligned with the streamlines.

The influence of the left branch of the split airstream is also evident in the shape and orientation of the isotherms and isohumes at the 850-mb level (Figure 4.46). Note the bulge in the direction of the streamlines, particularly for the mixing ratio isopleths.

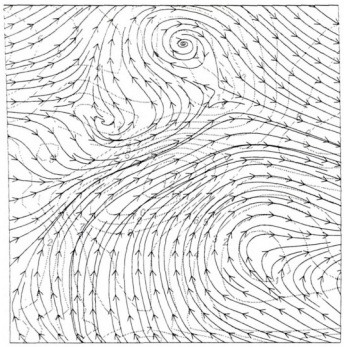

Figure 4.43. Composite Isotachs and Streamlines, Level 2 -- *SD_NWSE* Jets. As in Figure 4.1.

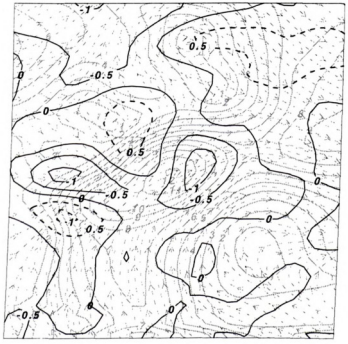

Figure 4.44. Composite Divergence, Level 2 -- *SD_NWSE* Jets. As in Figure 4.2.

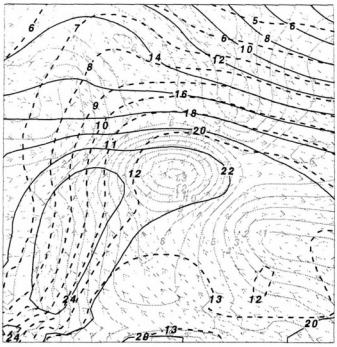

Figure 4.45. Composite 900-mb Temperature (°C) and Mixing Ratio (g kg^{-1}) plotted on Level 1 Composite Airflow Configuration – *SD_NWSE* Jets. As in Figure 4.6.

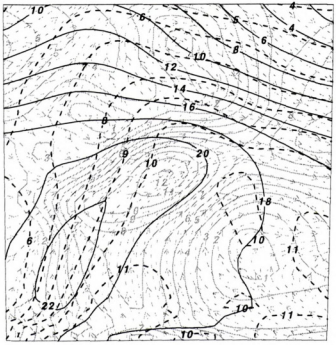

Figure 4.46. Composite 850-mb Temperature (°C) and Mixing Ratio (g kg^{-1}) plotted on Level 2 Composite Airflow Configuration – *SD_NWSE* Jets. As in Figure 4.6.

This bulge suggests that the left branch of the split flow is stronger for *SD_NWSE* jets compared to *SD_SWNE* jets. Recall that the left branch is evident on both the first and second level airflow composites for *SD_NWSE* jets but only on the first level for *SD_SWNE* jets. Thus, the advective influence of the low-level wind maxima into the region northwest of the jet core is considerably larger for *SD_NWSE* jets.

c. Convection

The strength of the left branch of the airflow is also evident in the spatial pattern of lightning. Areas of frequent lightning activity are aligned along both branches of the split flow on the upstream side of the deformation zone (Figures 4.47 and 4.48). Within those general areas of convection, individual centers are evident, particularly in the western branch of the airstream.

7. CC (Cyclonically-curved wind maxima with Confluence zone)

a. Airflow Configuration and Convergence

The final airflow configuration for the low-level wind maxima that do not extend beyond the latitude of the Great Lakes shows a distinct cyclonic, rather than anticyclonic, curvature (CC -- confluent cyclonically curved) (Figure 4.49). A distinct confluence zone along with pronounced convergence of 2.18×10^{-5} s^{-1} is located to the west and northwest of the isotach maximum (Figure 4.50).

Although this configuration type is found at fairly low elevations (average [median] height of 923 mb [939 mb]) (Table 4.11), the wind maxima do not display the same temporal and geographical preferences as the other configuration types with low altitude. The CC events are more frequent during the evening hours (0000 UTC) rather than the morning hours (1200 UTC) and they are more common during late spring/early summer. Approximately an equal number of events were reported 1991 and 1992. Also, the median jet core of the CC jets is located farther north (at 39° N along the Kansas /

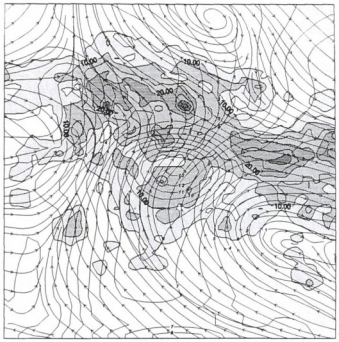

Figure 4.47. Percentage of Jet Events with Lightning Activity plotted on Level 1 Composite Airflow Configuration -- *SD_NWSE* Jets.

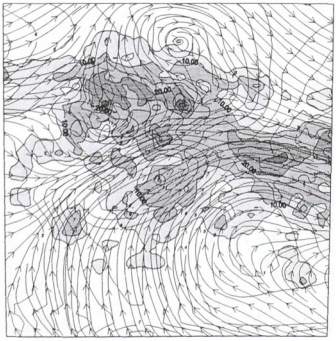

Figure 4.48. Percentage of Jet Events with Lightning Activity plotted on Level 2 Composite Airflow Configuration -- *SD_NWSE* Jets.

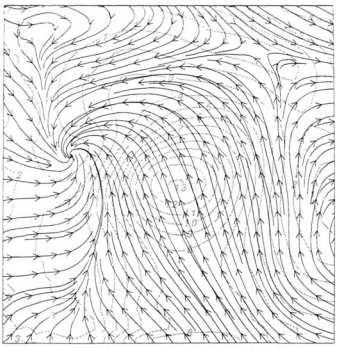

Figure 4.49. Composite Isotachs and Streamlines, Level 1 -- CC Jets. As in Figure 4.1.

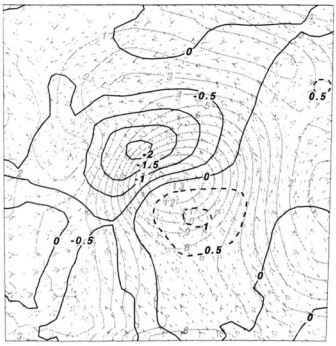

Figure 4.50. Composite Divergence, Level 1 -- CC Jets. As in Figure 4.2.

Table 4.11. Characteristics of *CC* Jets.

Number of Observations	Diurnal variation	Seasonal variation	Annual variation	Height (mb)	Median location
Level 1: 38 Level 2: 27 Level 3: 3	0000 Z: 22 1200 Z: 16	Apr: 6 May: 11 Jun: 11 Jul: 3 Aug: 3 Sep: 4	1991: 18 1992: 20	Level 1: Med: 939 Ave: 923 Level 2: Med: 846 Ave: 838 Level 3: Med: 850 Ave: 809	39°N/102°W

Colorado border) compared to the other low-altitude jets (Figure 4.51). The axis of most frequent activity has a northward extension into Wyoming and South Dakota rather than the northeastward orientation observed for the other types. 'Strong' and 'weak' wind profile categories are equally frequent for *CC* low-level wind maxima (Table 4.12).

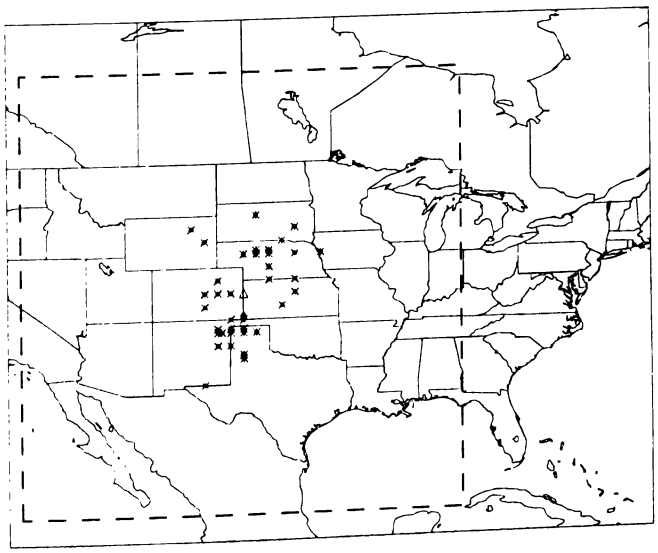

Figure 4.51. Geographical Centers of Isotach Maxima - - *CC* Jets.

Table 4.12. Number of Events by Speed Profile Category -- CC jets.

	'Strong' Jets	'Less Pronounced' Jets	Others
Level 1	a1: 2 a2: 10 b1: 2 b2: 2	a3: 7 a4: 2 a5: 9 b3: 1 b4: 3	
Level 2	a2: 1 b1: 9 b2: 1	a3: 1 a5: 4 b3: 4 b4: 2	c: 5
Level 3	a2: 1	b3: 1	c: 1

A second level was observed for the majority (71 percent) of the CC cases, and the airflow configuration for this level is distinctly different from that of the first level (Figure 4.52). The cyclonically-curved airflow at the first level is replaced by anticyclonically-curved flow upstream of the jet maximum and split flow downstream of the jet maximum. The change in the main direction of the flow from the first to the second level implies strong veering of the wind with height. The convergence downstream of the wind maximum covers a fairly extensive region (Figure 4.53), however, compared with other convergence values at the second level, the CC jets have fairly weak convergence (0.92×10^{-5} s^{-1}).

The composite streamline and isotach pattern of the third level will only be discussed briefly, as only three events were included in the calculations. The source area for the streamlines on the third level composite airflow map appears to be the southwestern United States instead of the Gulf of Mexico (Figure 4.54). The third-level composites for CC jets and the AC_SWNE jets (the only other configuration type thus far for which third level composites were computed) suggest that these jets are embedded in an open wave. Convergence at this level, although generally weak, is greatest downstream of the wind maximum (Figure 4.55).

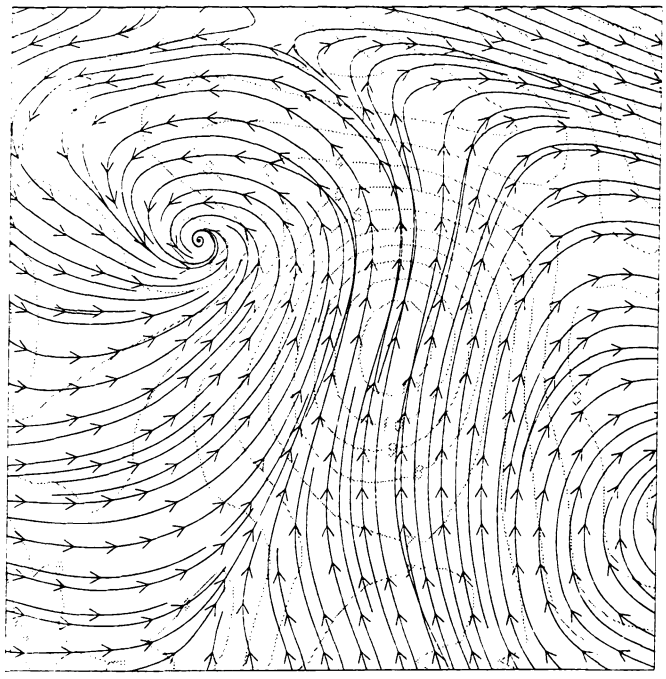

Figure 4.52. Composite Isotachs and Streamlines, Level 2 – CC Jets. As in Figure 4.1.

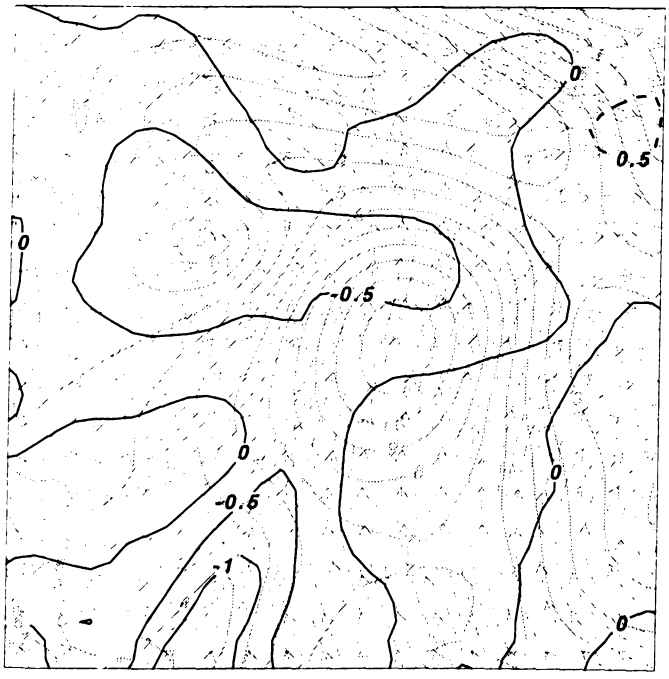

Figure 4.53. Composite Divergence, Level 2 – CC Jets. As in Figure 4.2.

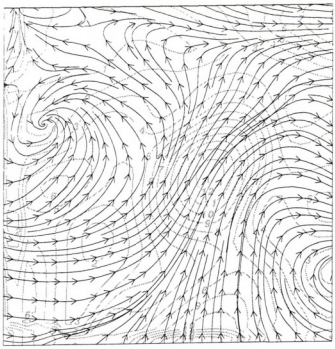

Figure 4.54. Composite Isotachs and Streamlines, Level 3 -- CC Jets. As in Figure 4.1.

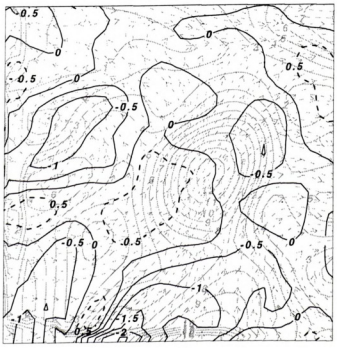

Figure 4.55. Composite Divergence, Level 3 -- CC Jets. As in Figure 4.2.

b. Temperature and Moisture

Like *SD_SWNE* jets, *CC* wind maxima are embedded within a relatively cool and dry environment. At the 900-mb level, average temperatures of 20°C and mean mixing ratio values of 10 g kg^{-1} are evident over the jet core (Figure 4.56). While the warmest temperatures in the southwest are in excess of 24°C and comparable to other flow types, the temperature gradient extending north from the southwestern corner of the composite area is considerably stronger than for other types. Similar to other types, a strong moisture gradient is evident but it is located farther east, closer to the jet core. Remember that the geographic locations of the jet cores for the *CC* type are farthest west compared with the locations for the other low-level wind maximum types. This would translate into a closer proximity of the jet core for *CC* events to the geographically preferred location of the dryline. Notice again the bulge in the mixing ratio isopleths to the northwest of the jet core, indicating the advective influence of the wind maximum. The temperature and moisture patterns for the 850-mb level do not vary much from those of the 900-mb level (Figure 4.57). The mean temperature at the center of the composite area is 18°C and the mean mixing ratio 9 g kg^{-1}.

c. Convection

Convection associated with *CC* jets is a frequent and widespread phenomenon. Not only were 36 out of the 38 *CC* events (95 percent) associated with lightning, but the spatial extent of the lightning activity is greater than for any other type of low-level wind maximum. The center of most frequent lightning activity is located downstream and slightly to the east of the jet core for the first level (Figure 4.58). That region also coincides with an area of convergence at the second analysis level (Figure 4.59). The airstreams at the third level also appear to have an influence on the spatial distribution the lightning activity. Notice the area of increased lightning frequency downstream of the third-level jet core (Figure 4.60).

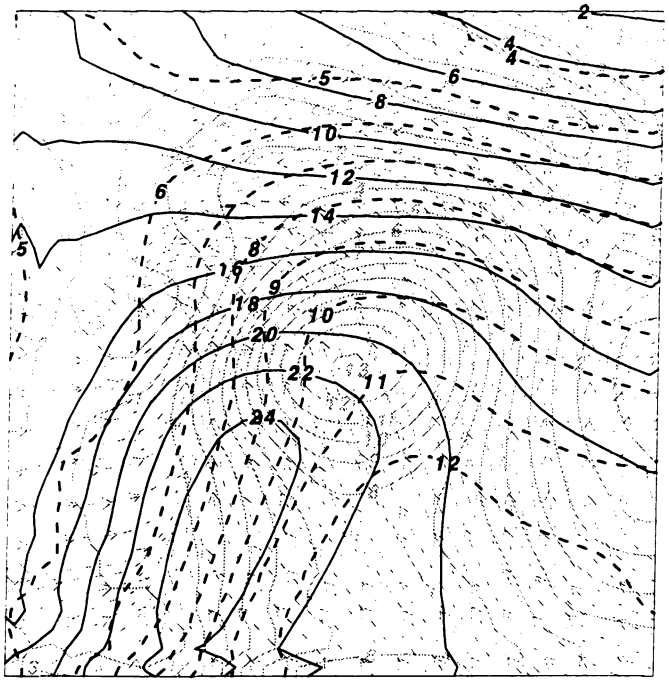

Figure 4.56. Composite 900-mb Temperature (°C) and Mixing Ratio (g kg^{-1}) plotted on Level 1 Composite Airflow Configuration -- *CC* Jets. As in Figure 4.6.

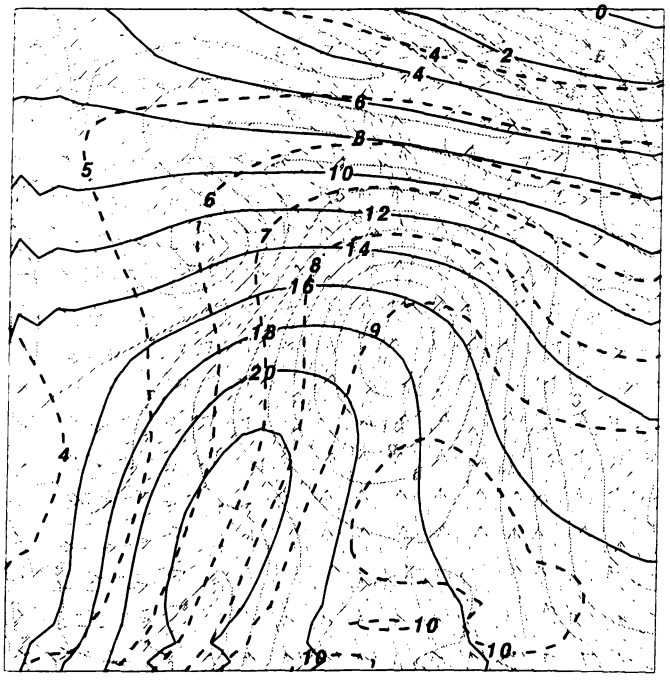

Figure 4.57. Composite 850-mb Temperature (°C) and Mixing Ratio (g kg^{-1}) plotted on Level 2 Composite Airflow Configuration -- *CC* Jets. As in Figure 4.6.

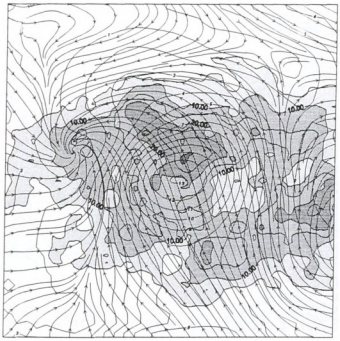

Figure 4.58. Percentage of Jet Events with Lightning Activity plotted on Level 1 Composite Airflow Configuration -- *CC* Jets.

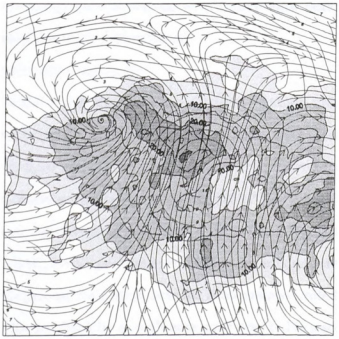

Figure 4.59. Percentage of Jet Events with Lightning Activity plotted on Level 2 Composite Airflow Configuration -- *CC* Jets.

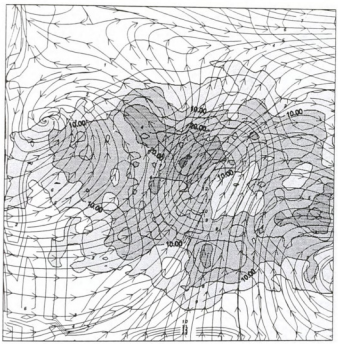

Figure 4.60. Percentage of Jet Events with Lightning Activity plotted on Level 3 Composite Airflow Configuration – *CC* Jets.

8. LAC_SWNE Jets (Long wind maximum with Anticyclonic curvature and Confluence oriented SouthWest-NorthEast)

a. Airflow Configuration and Convergence

This jet type is the first of the remaining six types that have greater horizontal extents (i.e., the wind maxima extend beyond the latitude of the Great Lakes). The composite airflow pattern for the first level resembles the pattern for the *AC_SWNE* configuration type, therefore the designation *LAC_SWNE* (Long **A**nticyclonically curved with **C**onfluence zone **S**outh**W**esterly-**N**orth**E**asterly) is used (Figure 4.61). Like the *AC_SWNE* jets, the *LAC_SWNE* jets are embedded in the anticyclonically-curved flow around a closed anticyclonic circulation over the southeastern United States and they are bounded along the left flank by a confluence zone oriented in a southwest-northeast direction. However, compared with the *AC_SWNE* jets, the *LAC_SWNE* jets extend farther north and the confluence zone to the northwest of the wind maximum is

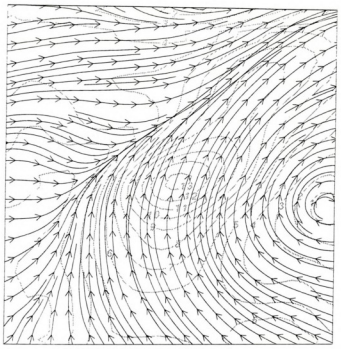

Figure 4.61. Composite Isotachs and Streamlines, Level 1 -- *LAC_SWNE* Jets. As in Figure 4.1.

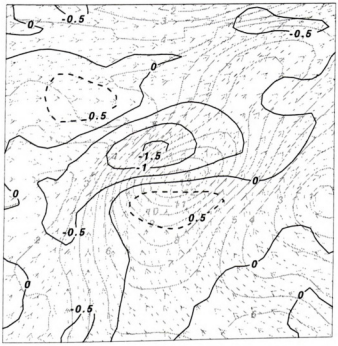

Figure 4.62. Composite Divergence, Level 1 -- *LAC_SWNE* Jets. As in Figure 4.2.

considerably stronger (1.57×10^{-5} s^{-1}) (see Figure 4.62). Also, the vertical speed profiles for *LAC_SWNE* jets do not have predominantly 'strong' jet noses. At the first level, only 41 percent of the wind maxima have speed profiles with either wind speeds exceeding 12 ms^{-1} or a vertical shear above the level of maximum wind of at least one half of the wind speed (Table 4.13).

Table 4.13. Number of Events by Speed Profile Category -- *LAC_SWNE* Jets.

	'Strong' Jets	'Less Pronounced' Jets	Others
Level 1	a2: 6 b1: 5	a3: 7 a5: 4 b3: 1 b4: 3	c: 1
Level 2	b1: 2	a5: 3 b3: 1	c: 3
Level 3	b1: 1		

The mean (median) altitude of *LAC_SWNE* jets is 888 mb (904 mb), which is slightly lower than the median elevation for the *AC_SWNE* jets (Table 4.14). Both types are slightly more frequent at 0000 UTC, and both occurred more often in 1991 compared to 1992. However, the seasonal preferences of the two types differ. Most *LAC_SWNE* jets occur in May, the early part of the warm season, whereas *AC_SWNE* jets are more frequent in July. The northerly median location (40°N, along the Kansas/Nebraska border) for *LAC_SWNE* jets (Figure 4.63) is similar to the median location observed for

Table 4.14. Characteristics of *LAC_SWNE* Jets.

Number of observations	Diurnal variation	Seasonal variation	Annual variation	Height (mb)	Median location
Level 1: 27 Level 2: 9 Level 3: 1	0000 Z: 11 1200 Z: 16	Apr: 1 May: 8 Jun: 6 Jul: 4 Aug: 3 Sep: 5	1991: 15 1992: 12	Level 1: Med: 904 Ave: 888 Level 2: Med: 780 Ave: 792	40°N/99°W

AC_SWNE jets. The dispersion about the median is fairly large with some jet cores being located as far north as southern Canada.

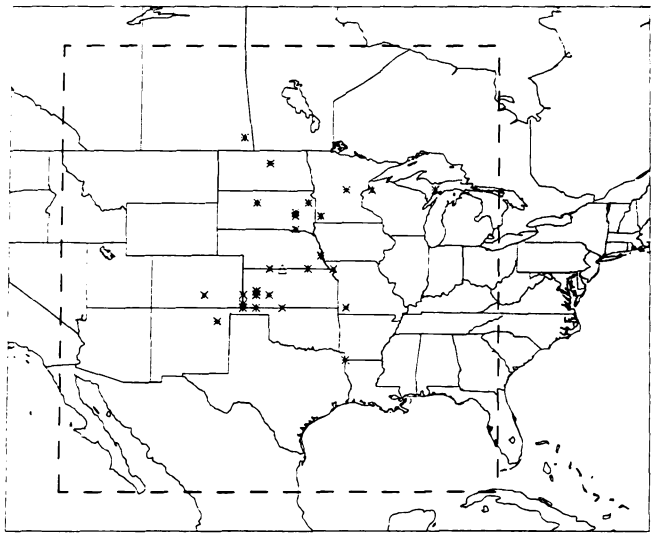

Figure 4.63. Geographical Centers of Isotach Maxima - - *LAC_SWNE* Jets

As was observed for several other types, the composite airstream for the second level is more anticyclonically curved than the first-level airflow (Figure 4.64).

The pronounced confluence zone at the first level is considerably less evident at the upper level. Consequently, the mean convergence values are fairly small (0.90×10^{-5} s^{-1}) for the second level (Figure 4.65). The vertical speed profiles are also predominantly weak. Only two out of the nine wind maxima included in the second-level composite had maximum winds ≥ 12 ms^{-1}.

b. Temperature and Moisture

Compared with its 'short' counterpart, the *LAC_SWNE* type is located in a cooler and dryer environment. This is an expected result, since *LAC_SWNE* jet cores are found farther north than their 'short' cousins. In the vicinity of the jet core, average temperatures of 20° C are found in combination with average mixing ratio values of 11 g kg^{-1}. At the 900-mb level, the moisture gradient to the southwest of the jet core is not as

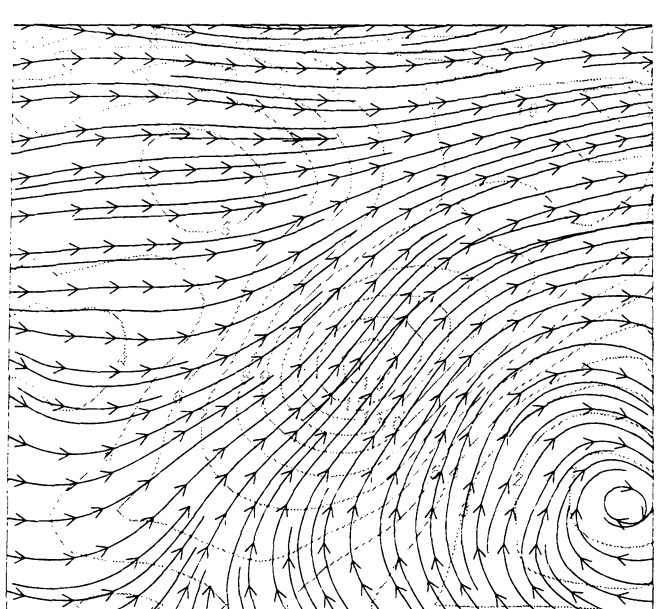

Figure 4.64. Composite Isotachs and Streamlines, Level 2 -- *LAC_SWNE* Jets. As in Figure 4.1.

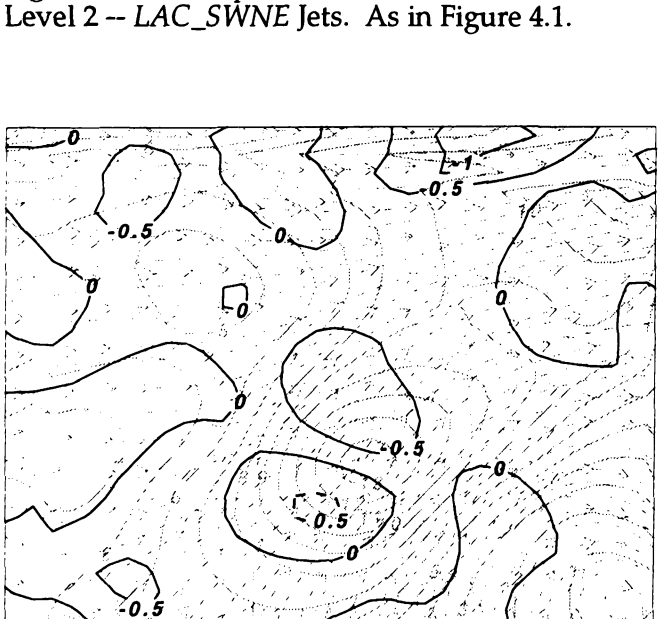

Figure 4.65. Composite Divergence, Level 2 -- *LAC_SWNE* Jets. As in Figure 4.2.

strong as observed for some of the other jet types (Figure 4.66). As for the previous types, the isotherms and isohumes are bent in the direction of the streamlines, indicating the importance of the low-level wind maxima in modifying their environment. The bend in the isohumes and isotherms is even more pronounced at the 850-mb level (Figure 4.67). The elongated shape of the low-level wind maximum is reflected very well in the southwest-northeast oriented temperature and moisture ridge. At the 850-mb level, the southwestern moisture gradient is even less pronounced.

c. Convection

The spatial pattern of lightning in association with *LAC_SWNE* jets has some similarities with the "ring of fire" pattern earlier observed for the *AC_SWNE* jets. The region of most frequent lightning activity extends in a broad swath from the southwest toward the northeast. The convergence zones generated by the airflow configuration at the individual analysis levels again determine the location of cloud-to-ground lightning activity for *LAC_SWNE* jets. For the first level, lightning is most frequent along the jet core (Figure 4.68). This region coincides with maximum convergence at both the first and second analysis levels (Figure 4.69).

9. L2A Jets (Long wind maximum with 2 Anticyclonic circulation centers)

a. Airflow Configuration and Convergence

The next airflow configuration type is unique. Instead of being embedded in anticyclonic flow around a single circulation center, the members of this low-level wind maximum type are embedded within the return flow around two centers of closed anticyclonic circulation (Figure 4.70). Therefore, the shorthand designation is *L2A* (Long with 2 Anticyclonic Circulation centers). This airflow configuration type does not have a corresponding "short" type. The jet cores for the events classified as *L2A* types were found in two different locations relative to the centers of anticyclonic circulation. They

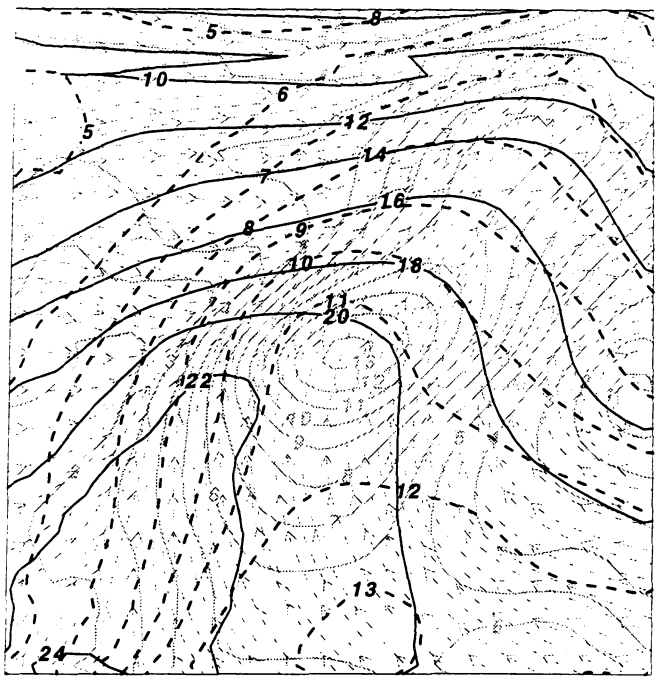

Figure 4.66. Composite 900-mb Temperature (°C) and Mixing Ratio (g kg^{-1}) plotted on Level 1 Composite Airflow Configuration – *LAC_SWNE* Jets. As in Figure 4.6.

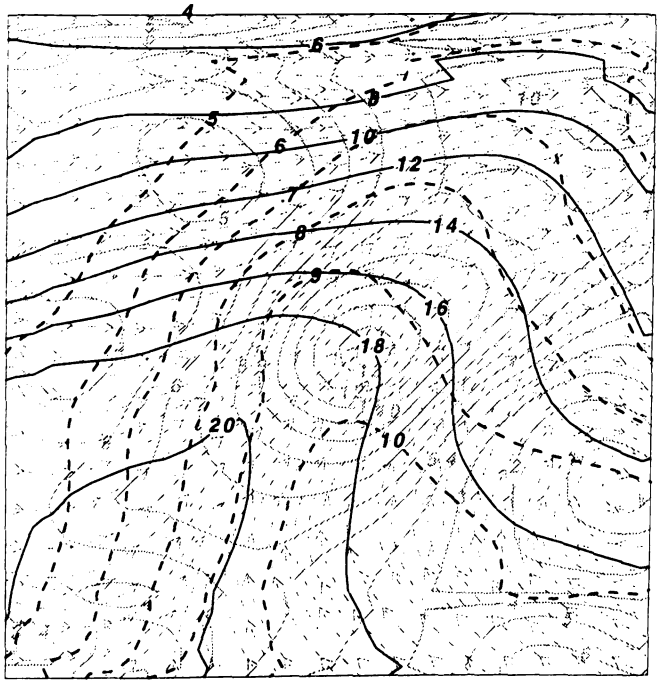

Figure 4.67. Composite 850-mb Temperature (°C) and Mixing Ratio (g kg^{-1}) plotted on Level 2 Composite Airflow Configuration – *LAC_SWNE* Jets. As in Figure 4.6.

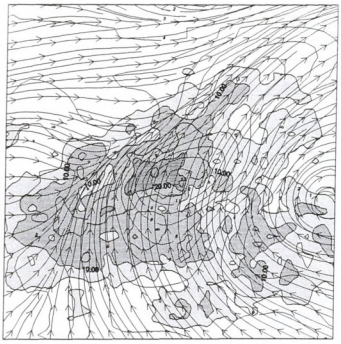

Figure 4.68. Percentage of Jet Events with Lightning Activity plotted on Level 1 Composite Airflow Configuration -- *LAC_SWNE* Jets.

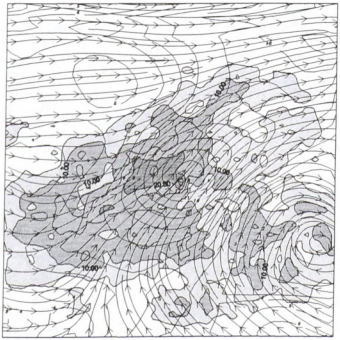

Figure 4.69. Percentage of Jet Events with Lightning Activity plotted on Level 2 Composite Airflow Configuration -- *LAC_SWNE* Jets.

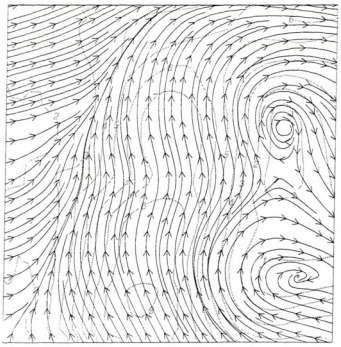

Figure 4.70. Composite Isotachs and Streamlines, Level 1 – *L2A* Jets. As in Figure 4.1.

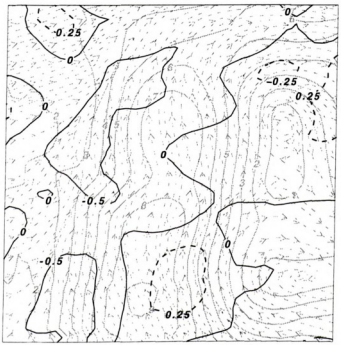

Figure 4.71. Composite Divergence, Level 1 – *L2A* Jets. As in Figure 4.2.

were located either immediately to the west of the southernmost circulation center or immediately west of the northernmost circulation center. Consequently, the procedure for centering the subgrid for the composite analysis needed to be modified. For this configuration type only, the subgrid is centered on a streamline west of the two anticyclonic centers, approximately equidistant between both centers. Because the composite grid is not centered on the jet core, as was the case for the other types, the mean wind speed and convergence for *L2A* jets is relatively weaker (see Figure 4.71).

The larger number of *L2A* jet occurrences at 1200 UTC suggests at least some boundary-layer forcing, although the average (median) height of 891 mb (895 mb) is higher than that for the other jet types with predominantly morning events (Table 4.15). *L2A* jets are most fequent in July and August, and about 71 percent of the events were recorded during 1992. The geographical preference of L2A jets is very similar to the other 'long' types. The median location is found in central Kansas at 29° latitude (Figure 4.72).

Table 4.15. Characteristics of *L2A* Jets.

Number of observations	Diurnal variation	Seasonal variation	Annual variation	Height (mb)	Median location
Level 1: 24	0000 Z: 9	Apr: 4	1991: 17	Level 1:	39°N/99°W
Level 2: 15	1200 Z: 15	May: 1	1992: 7	Med: 895	
Level 3: 3		Jun: 3		Ave: 891	
		Jul: 7		Level 2:	
		Aug: 7		Med: 850	
		Sep: 2		Ave: 834	
				Level 3:	
				Med: 792	
				Ave: 811	

Compared with other flow types, the amount of dispersion about the median is fairly large. Individual isotach centers are dispersed from central Texas into South Dakota. The vertical profiles of *L2A* are predominantly 'weak', i.e., either their

maximum speeds are less than 12 ms^{-1} or the vertical decrease in speed is less than one half the maximum value (Table 4.16).

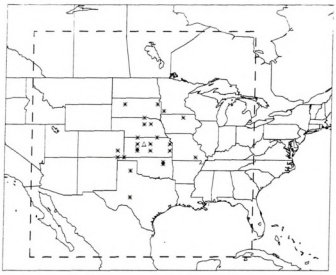

Figure 4.72. Geographical Centers of Isotach Maxima -- *L2A* Jets.

Table 4.16. Number of Events by Speed Profile Category -- *L2A* Jets.

	'Strong' Jets	'Less Pronounced' Jets	Others
Level 1	a1: 1 a2: 3 b1: 1	a3: 5 a5: 5 b3: 2 b4: 6	c: 1
Level 2	a2: 1 b1: 2 b2: 1	a5: 1 b3: 4 b4: 4	c: 2
Level 3		a4: 1	c: 2

A second level wind maximum was evident for 63 percent of the L2A events. Although the anticyclonic centers west of the wind maxima remain evident at the second level, the second-level composite jet core is located north of the maximum observed at the first level, and the airflow is more anticyclonic (Figure 4.73). Also, the confluence zone for the second level is located farther east and is weaker ($0.5 \times 10^{-5} s^{-1}$) (Figure

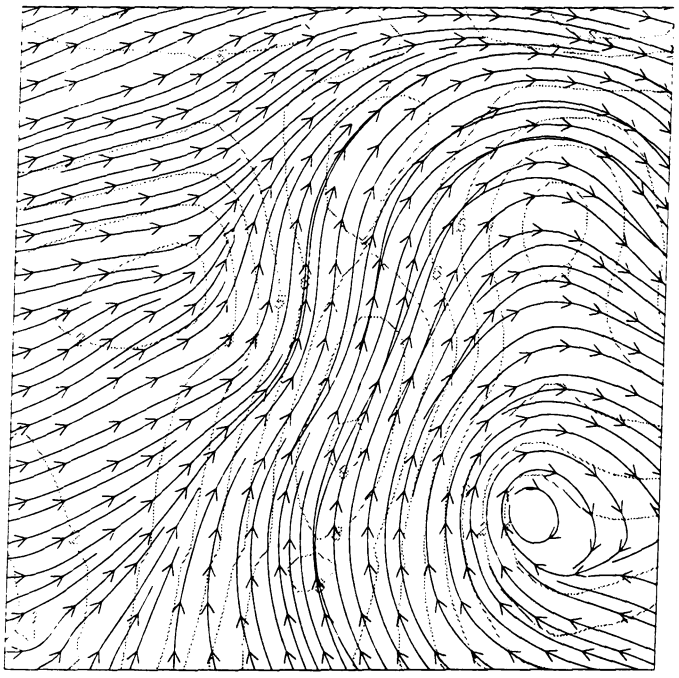

Figure 4.73. Composite Isotachs and Streamlines, Level 2 – *L2A* Jets. As in Figure 4.1.

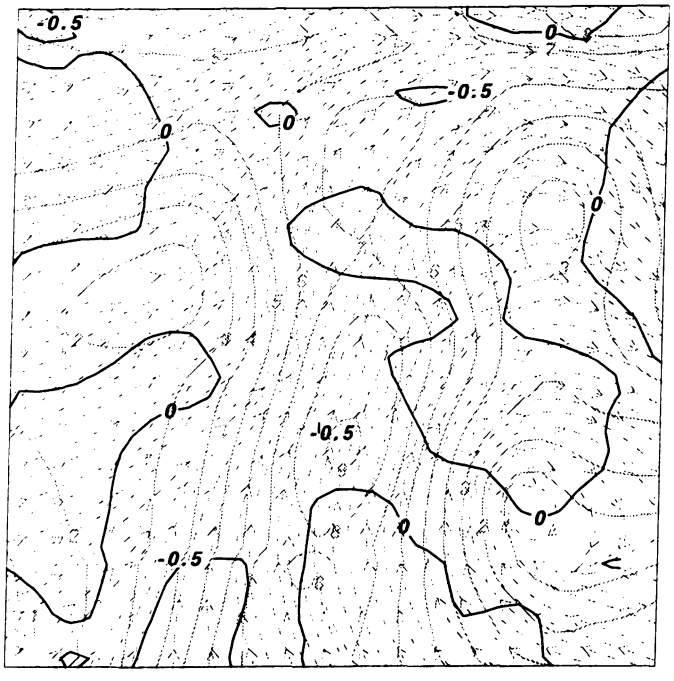

Figure 4.74. Composite Divergence, Level 2 – *L2A* Jets. As in Figure 4.2.

4.74). Few (only four out of fifteen) of the jet profiles for the second level were categorized as 'pronounced' (see Table 4.16). The trend toward a more anticyclonic flow pattern with height is also evident for the third level (Figure 4.75), although the few cases (3) included in this composite only permit a qualitative assessment of the flow pattern. The convergence at the third level is strongest southwest of the maximum (Figure 4.76).

b. Temperature and Moisture

Pronounced temperature and moisture ridges are associated with the *L2A* jets (Figures 4.77 and 4.78). The southwestern region of the composite area displays the now familiar pattern of an area of high temperatures superimposed onto a strong moisture gradient. The rotation of the wind direction with height is evident in the mixing ratio isopleths at the 850-mb level (Figure 4.78); the bulge in the isohumes at the 850-mb level is displaced to the east of the bulge at the 900-mb level. Another notable feature of the composite temperature and moisture patterns is that the southwestern moisture gradient remains strong over a much deeper atmospheric layer compared with other jet types.

c. *Convection*

One of the preferred locations for lightning activity associated with *L2A* jets is in the vicinity of the southwestern temperature ridge and strong moisture gradient (Figure 4.79). This region is also characterized by confluence at the first airstream level. A second area of frequent lightning activity is observed in the center of the composite lightning map. This region is located downstream and slightly to the east of the first-level jet core and within the area of speed convergence downstream of the second-level (Figure 4.80) and third-level (Figure 4.81) wind maxima.

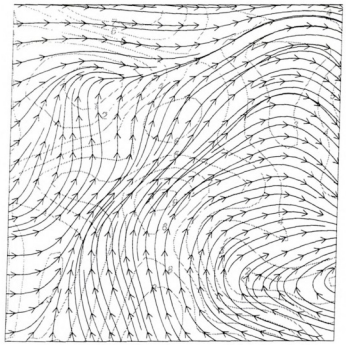

Figure 4.75. Composite Isotachs and Streamlines, Level 3 -- *L2A* Jets. As in Figure 4.1.

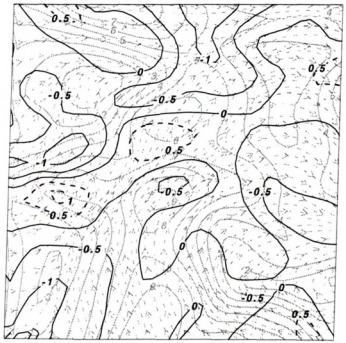

Figure 4.76. Composite Divergence, Level 3 -- *L2A* Jets. As in Figure 4.2.

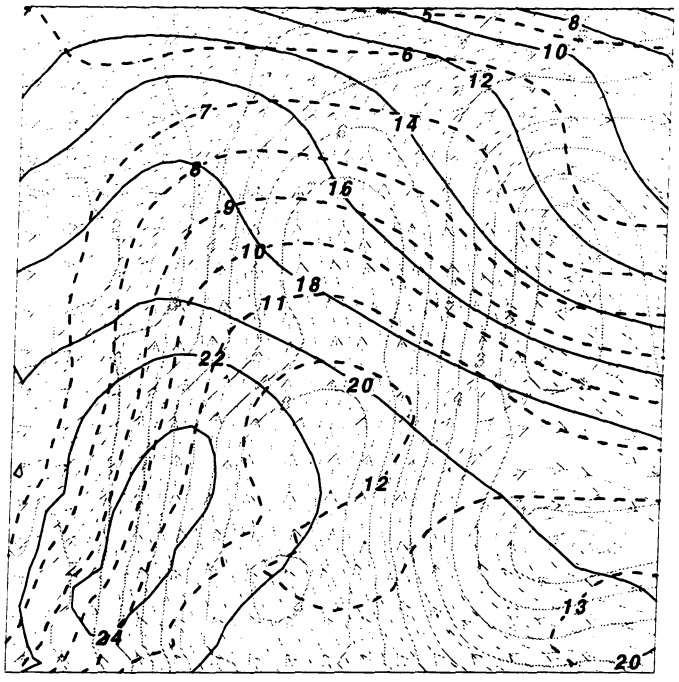

Figure 4.77. Composite 900-mb Temperature (°C) and Mixing Ratio (g kg^{-1}) plotted on Level 1 Composite Airflow Configuration -- *L2A* Jets. As in Figure 4.6.

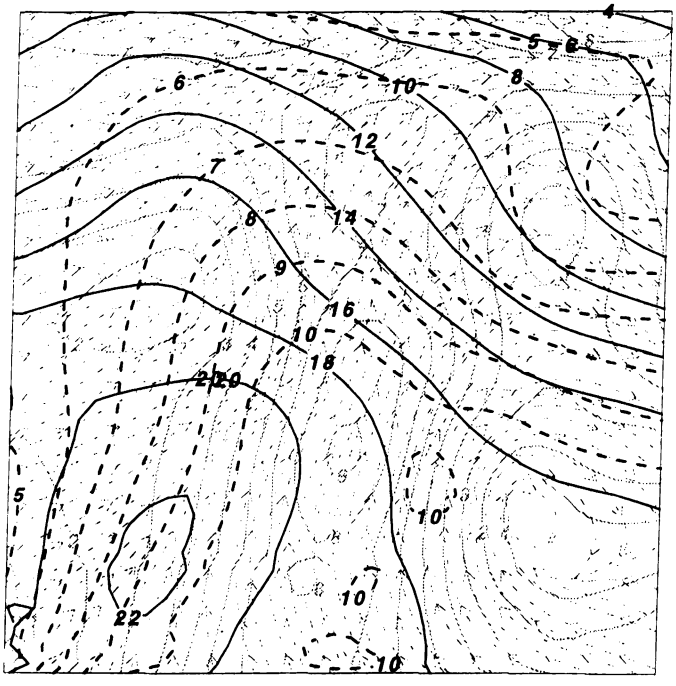

Figure 4.78. Composite 850-mb Temperature (°C) and Mixing Ratio (g kg^{-1}) plotted on Level 2 Composite Airflow Configuration -- *L2A* Jets. As in Figure 4.6.

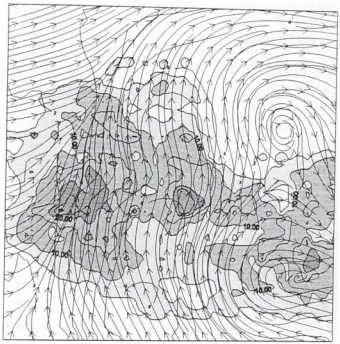

Figure 4.79. Percentage of Jet Events with Lightning Activity plotted on Level 1 Composite Airflow Configuration – *L2A* Jets.

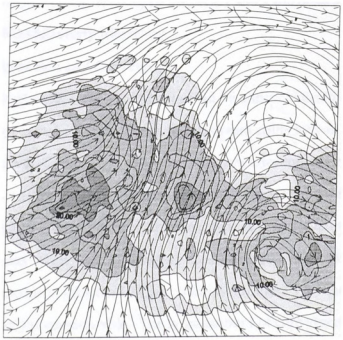

Figure 4.80. Percentage of Jet Events with Lightning Activity plotted on Level 2 Composite Airflow Configuration – *L2A* Jets.

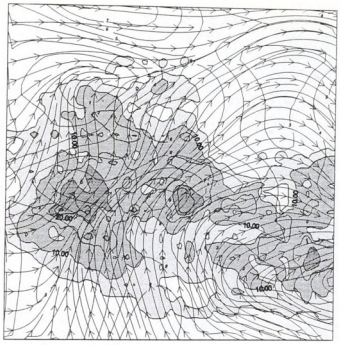

Figure 4.81. Percentage of Jet Events with Lightning Activity plotted on Level 3 Composite Airflow Configuration -- *L2A* Jets.

10. LSKC_SWNE Jets (Long with Split and Kurl and Confluence zone oriented in SouthWesterly-NorthEasterly direction)

a. Airflow Configuration and Convergence

The next 'long' airflow type is characterized by anticyclonically-curved airflow upstream of the jet core, but downstream the airstream splits into an anticyclonic branch and a cyclonic branch (Figure 4.82). The cyclonic, or westernmost, branch terminates in a closed cyclonic circulation. Another distinct feature is a strong confluence zone along the left flank of the jet core. Therefore, this flow type is referred to as *LSKC_SWNE* (**L**ong with **S**plit and "**K**url" and **C**onfluence zone oriented in **S**outh**W**esterly-**N**orth**E**asterly direction). Like the *L2A* jets, there is no 'short' counterpart. The average wind speed (16 ms^{-1}) is considerable. The large amount of convergence (1.99 x 10^{-5} s^{-1}) is likely due to the combined effects of confluence and speed convergence (Figure 4.83).

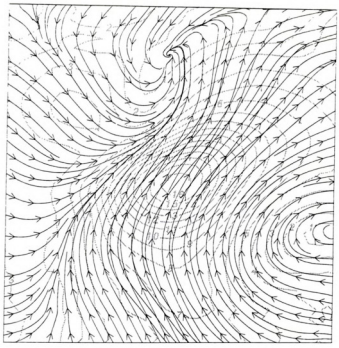

Figure 4.82. Composite Isotachs and Streamlines, Level 1 -- *LSKC_SWNE* Jets. As in Figure 4.1.

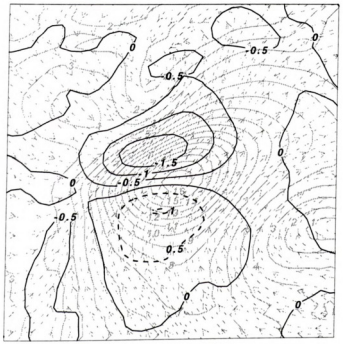

Figure 4.83. Composite Divergence, Level 1 -- *LSKC_SWNE* Jets. As in Figure 4.2.

magnitude and location. Similar to the *LAC_SWNE* and the *L2A* jets, 'less pronounced' vertical profiles are more frequent than 'pronounced profiles' (Table 4.17). In addition, the average and median heights for the *LSKC_SWNE* jets are comparable to the average values for the *LAC_SWNE* and *L2A* jets, the three types share the same preference for the morning hours, the median latitudes (39-40° N) are similar, and the amount of dispersion about the median location is comparable (Table 4.18, Figure 4.84). However, *LSKC_SWNE* jets lack a distinct seasonal preference and, unlike the *LAC_SWNE* and *L2A* jets were more frequent during 1992 than during 1991.

Table 4.17. Number of Events by Speed Profile Category -- *LSKC_SWNE* Jets.

	'Strong' Jets	'Less Pronounced' Jets	Others
Level 1	a1: 2 a2: 6 b1: 3	a3: 4 a5: 2 b3: 4 b4: 3	
Level 2	a2: 1 b1: 2 b2: 1	a5: 2 b3: 5	c: 2

Table 4.18. Characteristics of *LSKC_SWNE* Jets.

Number observations	Diurnal variation	Seasonal variation	Annual variation	Height (mb)	Median location
Level 1: 24 Level 2: 13	0000 Z: 9 1200 Z: 15	Apr: 6 May: 4 Jun: 2 Jul: 5 Aug: 2 Sep: 5	1991: 8 1992: 16	Level 1: Med: 892 Ave: 889 Level 2: Med: 822 Ave: 826	40°N/98°W

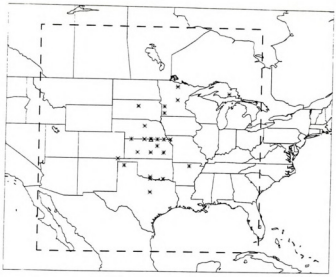

Figure 4.84. Geographical Centers of Isotach Maxima - - *LSKC_SWNE* Jets.

The second level of the LSKC_SWNE jets lacks the cyclonic branch of the first level and in general the curvature of the second-level airflow is more anticyclonic than that of the first level (Figure 4.85). Also, the confluence zone along the left flank of the wind maximum is considerably weaker at the second level. The average speed at the second level is large, but due to the weaker confluence zone, the magnitude of the convergence is smaller than that observed for the first level. The region of maximum convergence is located immediately downstream of the wind maximum (Figure 4.86).

b. Temperature and Moisture

Surprisingly, the average temperature and moisture values associated with the *LSKC_SWNE* jets type are comparable with those for most 'short' airflow configuration types that are located farther south. At the 900-mb level, the composite jet core is located in an area with average temperatures of ≥20°C and average mixing ratio values of ≥11 g kg^{-1} (Figure 4.87). The source area for the warmest temperatures is clearly evident from the ridge of high temperatures located to the southwest. The bend in the isotherms and isohumes in the direction of the streamlines is much more pronounced at

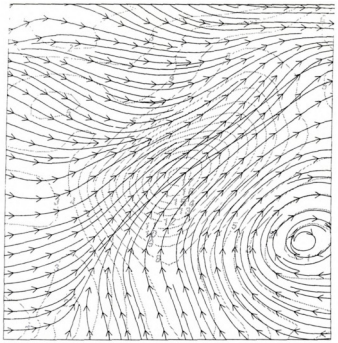

Figure 4.85. Composite Isotachs and Streamlines, Level 2 -- *LSKC_SWNE* Jets. As in Figure 4.1.

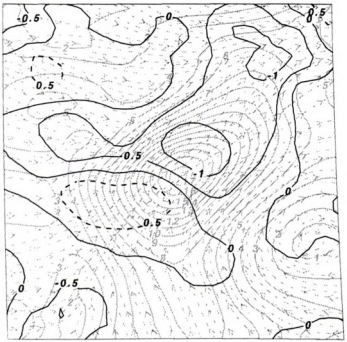

Figure 4.86. Composite Divergence, Level 2 -- *LSKC_SWNE* Jets. As in Figure 4.2.

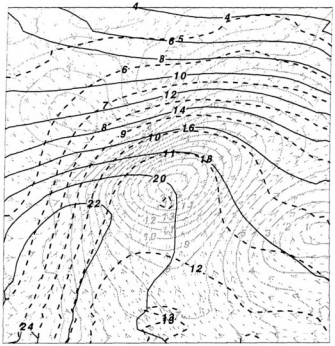

Figure 4.87. Composite 900-mb Temperature (°C) and Mixing Ratio (g kg^{-1}) plotted on Level 1 Composite Airflow Configuration -- *LSKC_SWNE* Jets. As in Figure 4.6.

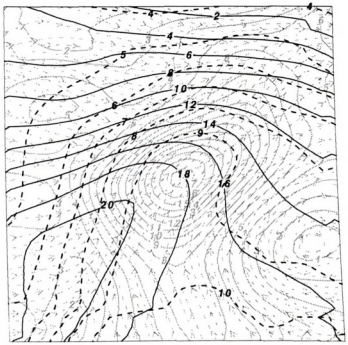

Figure 4.88. Composite 850-mb Temperature (°C) and Mixing Ratio (g kg^{-1}) plotted on Level 2 Composite Airflow Configuration -- *LSKC_SWNE* Jets. As in Figure 4.6.

the 850-mb level compared with the 900-mb level (see Figure 4.88). Thus, the 850-mb temperature and moisture pattern appears to be influenced by the low-level wind maximum. The strength of the advective pattern is not surprising considering that *LSKC_SWNE* jets, except for *KC_SWNE* jets, have the highest average wind speed of the different configuration types. The vertical extent of the dryline is somewhat limited, as indicated by the weaker moisture gradient at the 850-mb level.

c. Convection

The pattern of convection associated with *LSKC_SWNE* jets is clearly related to the kinematic fields. Frequent lightning activity (100 percent of jet events) is located primarily downstream of the wind maximum and along the confluence zones. The highest lightning frequency is located downstream of the jet core as depicted on the first analysis level (Figure 4.89). This area is characterized by the convergence at both the first and second analysis levels (Figure 4.90). The veering of the wind with height likely contributes to the eastward extension of lightning activity, as this area is located immediately downstream of the second-level wind maximum. The spatial pattern of lightning for *LSKC_SWNE* jets bears some resemblance with the spatial pattern of lightning ("ring of fire") associated with *AC_SWNE* and *LAC_SWNE* jets.

It is interesting to note that for all these types lightning is not only found downstream of the wind maximum and along the confluence zone to the left of the wind maximum, but also along the confluence zone associated with the moisture gradient southwest of the jet core. Thus, the vertical motion associated with the dryline may also be an important mechanism in triggering lightning.

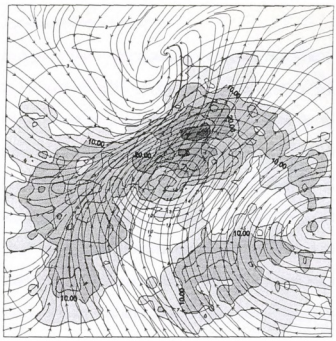

Figure 4.89. Percentage of Jet Events with Lightning Activity plotted on Level 1 Composite Airflow Configuration -- *LSKC_SWNE* Jets.

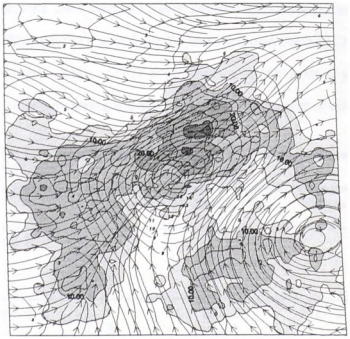

Figure 4.90. Percentage of Jet Events with Lightning Activity plotted on Level 2 Composite Airflow Configuration -- *LSKC_SWNE* Jets.

11. LSPLIT Jets (Long with "Split")

a. Airflow Configuration and Convergence

The next flow type is also characterized by a split in the airflow downstream of the wind maximum. Unlike the *LSKC_SWNE* jets, however, the *LSPLIT* jets (Long with Split) lack a pronounced confluence zone along the left flank of the wind maximum and the closed cyclonic circulation in the left branch (Figure 4.91). The *LSPLIT* jets also set themselves apart from the 'short' *SD_NWSE* and *SD_SWNE* jets in that the split in their airstream is not associated with a strong deformation zone. Similar to the *LSKC_SWNE* jets, but unlike the two 'short' configuration types with split flow (i.e., *SD_NWSE* and *SD_SWNE* jets), the strongest convergence is not observed downstream of the wind maximum (Figure 4.92). Rather, the area of strongest convergence is located northwest of the isotach maximum, similar to the convergence pattern of *LSKC_SWNE* jets although the magnitude (1.32×10^{-5} s^{-1}) is smaller.

The *LSPLIT* jets differentiate themselves from the previously-discussed 'long' airflow types in that they are found at a lower altitude with a mean (median) height of 904 mb (908 mb), although their speed profile and temporal characteristics resemble those of other flow types. Most *LSPLIT* events have a 'weak' vertical speed profile (Table 4.19) and they occur during the morning hours (77 percent of all events recorded

Table 4.19. Number of Events by Speed Profile Category -- *LSPLIT* Jets.

	'Strong' Jets	'Less Pronounced' Jets	Others
Level 1	a1: 2 a2: 9 b1: 3 b2: 1	a3: 6 a5: 3 b3: 3 b4: 4	
Level 2	a2: 1 b1: 5 b2: 1	a3: 1 a4: 1 a5: 1 b3: 7 b4: 3	c: 2
Level 3	b2: 1		

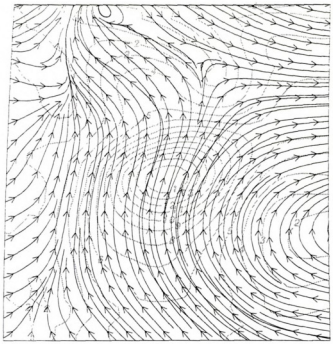

Figure 4.91. Composite Isotachs and Streamlines Level 1 – *LSPLIT* Jets. As in Figure 4.1.

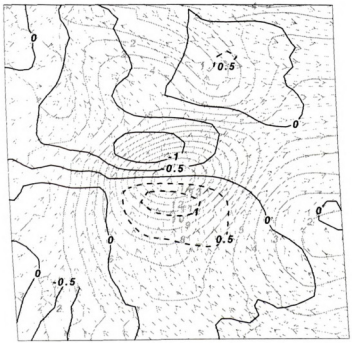

Figure 4.92. Composite Divergence, Level 1 – *LSPLIT* Jets. As in Figure 4.2.

at 1200 UTC) (Table 4.20).

Like the *LAC_SWNE* jets and the *L2A* jets, they were more frequent during 1991, and, like the *LAC_SWNE* jets, they have a seasonal preference for the early part of the warm season (i.e., May). The spatial distribution of the jet cores resembles that of the *L2A* and *LSKC_SWNE* jets (Figure 4.93). The median center is again located in Kansas at a latitude of 40° N. Individual centroids are scattered from central Texas northeastward into Ontario.

Table 4.20. Characteristics of *LSPLIT* Jets.

Number of obs in composite	Diurnal variation	Seasonal variation	Annual variation	Height (mb)	Median location °N/°W
Level 1: 31 Level 2: 22 Level 3: 1	0000 Z: 7 1200 Z: 24	Apr: 0 May: 9 Jun: 6 Jul: 5 Aug: 5 Sep: 6	1991: 18 1992: 13	Level 1: Med: 908 Ave: 904 Level 2: Med: Ave:	39/100

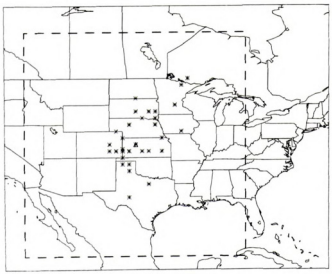

Figure 4.93. Geographical Centers of Isotach Maxima - - *LSPLIT* Jets.

The second level of the LSPLIT jets shows no evidence of a split in the airflow (Figure 4.94). A similar pattern was observed for the 'short' configuration types with split airflow (i.e., *SD_SWNE* and *SD_SWNE* jets). Convergence at the second level is very small (0.49×10^{-5} s^{-1}) for LSPLIT jets. (Figure 4.95).

b. Temperature and Moisture

The temperature and moisture fields at the 900-mb level during *LSPLIT* events are comparable to the other 'long' airflow configuration types. Again, the influence of the difluent flow in shaping the isotherm and isohume patterns is evident (Figure 4.96). Notice the bends in the mixing ratio isopleths to the west and to the east of the jet core in the direction of the streamlines. The advective influence on the temperature field is more pronounced along the eastern branch of the split flow compared with the western branch. Compared with other low-level wind maxima, however, the mixing ratio gradient in the southwest is rather relaxed. The 850-mb environment for *LSPLIT* jets is warmer and has more moisture compared to other 'long' airflow configuration types (Figure 4.97). Mean temperatures of close to 20° C and mean mixing ratio values of 10 g kg^{-1} are observed in the vicinity of the jet core at 850 mb.

c. Convection

Ninety-four percent of the *LSPLIT* jet events were associated with lightning. Two areas of preferred lightning activity are evident from Figure 4.98. The first area occurs west of the jet core along the pronounced confluence zone evident on the first-level airflow composite. This region coincides with the temperature ridge and strong moisture gradient observed on the 900 and 850 mb composite surfaces. The second region of frequent lightning activity extends in either direction along the difluence zone. The small values of convergence for the second level suggest that the pattern of convection for *LSPLIT* jets is not strongly related to the airflow configuration at this level (Figure 4.99).

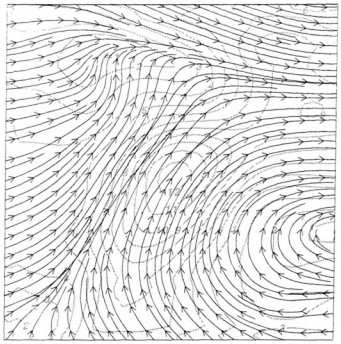

Figure 4.94. Composite Isotachs and Streamlines, Level 2 -- *LSPLIT* Jets. As in Figure 4.1.

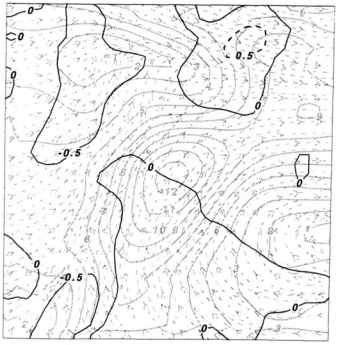

Figure 4.95. Composite Divergence, Level 2 -- *LSPLIT* Jets. As in Figure 4.2.

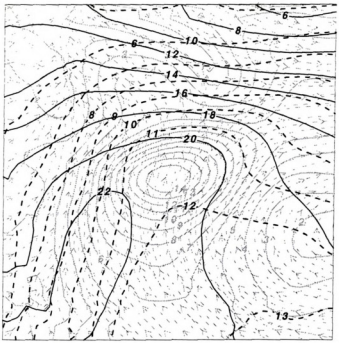

Figure 4.96. Composite 900-mb Temperature (°C) and Mixing Ratio (g kg^{-1}) plotted on Level 1 Composite Airflow Configuration -- *LSPLIT* Jets. As in Figure 4.6.

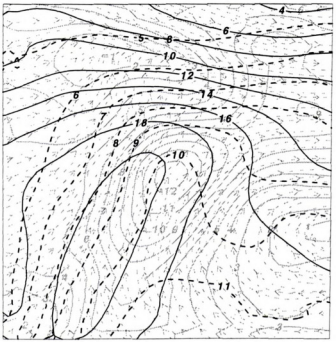

Figure 4.97. Composite 850-mb Temperature (°C) and Mixing Ratio (g kg^{-1}) plotted on Level 2 Composite Airflow Configuration -- *LSPLIT* Jets. As in Figure 4.6.

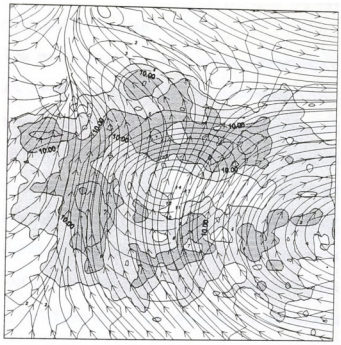

Figure 4.98. Percentage of Jet Events with Lightning Activity plotted on Level 1 Composite Airflow Configuration -- *LSPLIT* Jets.

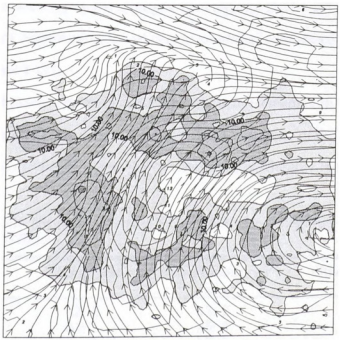

Figure 4.99. Percentage of Jet Events with Lightning Activity plotted on Level 2 Composite Airflow Configuration -- *LSPLIT* Jets.

12. LKC_SWNE Jets (Long with **K**url and **C**onfluence in **SW-NE** direction)

a. Airflow Configuration and Convergence

Yet another flow type with a 'split' in the airflow downstream of the wind maximum is the *LKC_SWNE* (**L**ong with **K**url and **C**onfluence in **SW-NE** direction) jets (Figure 4.100). Similar to the *KC_SWNE* jets, the wind maximum is embedded in a broad airstream that curves anticyclonically upstream of the isotach maximum and then reverses its orientation into a cyclonic curvature downstream of the jet maximum. *LKC_SWNE* jets have some common features with *LSKC_SWNE* and *LSPLIT* jets. Like *LSKC_SWNE* jets and *LSPLIT* jets, difluent flow is evident downstream of the jet core and, like *LSKC_SWNE* jets, a cyclonic circulation is evident downstream on the left flank. Unlike *LSKC_SWNE* jets and *LSPLIT* jets, however, the streamlines are not difluent downstream of the jet core, but rather they are cyclonically curved and the 'split' is displaced to the east.

At the first level, this airflow type has a fairly strong average wind speed of 14 ms^{-1}. Similar to other types, the strongest convergence (1.51×10^{-6} s^{-1}) is found along the confluence zone northwest of the jet core in an area of confluence and speed decrease (see Figure 4.101).

Strong speed profile types are in the minority in agreement with the other 'long' types discussed so far (Table 4.21). The eleven observed cases of the *LKC_SWNE* jets differ from the other jet types in that they are located considerably farther north (Figure

Table 4.21. Number of Events by Speed Profile Category -- *LKC_SWNE* Jets.

	'Strong' Jets	'Less Pronounced' Jets	Others
Level 1	a2: 2 b1: 1	a3: 2 a5: 3 b3: 2 b4: 1	
Level 2		b3: 1 b4: 3	c: 2

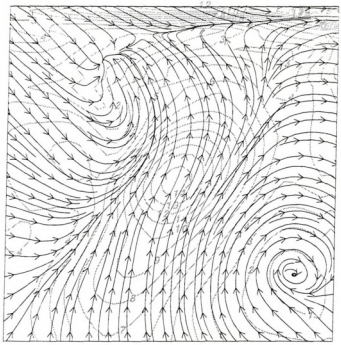

Figure 4.100. Composite Isotachs and Streamlines, Level 1 – *LKC_SWNE* Jets. As in Figure 4.1.

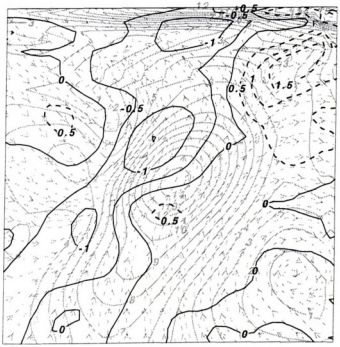

Figure 4.101. Composite Divergence, Level 1 – *LKC_SWNE* Jets. As in Figure 4.2.

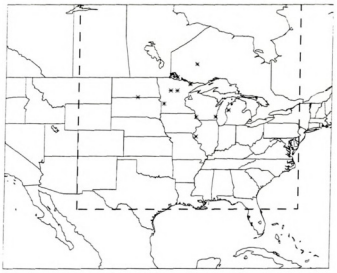

Figure 4.102. Geographical Centers of Isotach Maxima -- *LKC_SWNE* Jets.

Table 4.22 summarizes the temporal and altitudinal characteristics of the *LKC_SWNE* jets. *LKC_SWNE* jets are most frequently observed during the evening. In fact, they have the highest percentage of evening observations of any jet configuration type. The majority of *LKC_SWNE* events (seven out of eleven cases) occurred in 1991. *LKC_SWNE* jets appear to have a slight preference for the beginning and the end of the warm season. In terms of their height characteristics, *LKC_SWNE* jets strongly resemble *LAC_SWNE* jets with a median (average) height of 902 mb (885 mb).

Table 4.22. Characteristics of *LKC_SWNE* Jets.

Number of Observations	Diurnal variation	Seasonal variation	Annual variation	Height (mb)	Median location
Level 1: 11	0000 Z: 7	Apr: 3	1991: 4	Level 1:	46°N/92°W
Level 2: 6	1200 Z: 4	May: 3	1992: 7	Med: 902	
		Jun: 1		Ave: 885	
		Jul: 1		Level 2:	
		Aug: 1		Med: 800	
		Sep: 2		Ave: 799	

Once again, the cyclonic branch of *LKC_SWNE* jets is replaced by anticyclonic airflow at the second level (Figure 4.103). Two areas of convergence are notable at the second level (Figure 4.104). First, as in previous types, an area of convergence (0.70 x 10^{-5} s^{-1}) is observed downstream of the isotach maximum. Secondly, an area of stronger convergence is found considerably southwest of the jet core along a confluence zone.

b. Temperature and Moisture

Due to the northern location of *LKC_SWNE* jets, the average temperature and moisture values are the lowest for any type of low-level wind maximum. The temperatures in the center of the composite map only reach a mean value of 16° C, and the mean mixing ratio in the area is only 9 g kg^{-1} for *LKC_SWNE* jets. In broad strokes, the main features of the temperature and moisture fields for LKC_SWNE jets correspond to those of the other jets with a temperature ridge in the west and a moisture ridge to the east of the temperature ridge. The warmest temperatures are again observed in the southwestern corner of the composite. A fairly strong moisture gradient at 900-mb is also observed in this region (Figure 4.105). The moisture pattern, in particular the isohumes at the center of the composite map, clearly reflects the advective influence of the low-level wind maximum, in particular into the center of the composite map. The isotherms, on the other hand, do not display as strong a bend in the direction of the streamlines as the mixing ratio isopleths.

At the 850-mb level, the curvature of the isohumes distinctly follows the streamlines at the second analysis level (Figure 4.106). The 850-mb moisture ridge has a southwest-northeast orientation compared to the more north-south orientation evident on the 900-mb composites. These differences indicate that in order to gain an understanding of the environment of the low-level wind maxima, one needs to consider the advective influences of the individual airstreams at both the first and second composites.

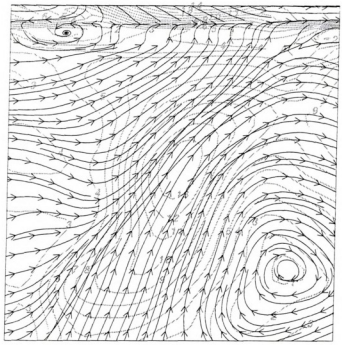

Figure 4.103. Composite Isotachs and Streamlines, Level 2 -- *LKC_SWNE* Jets. As in Figure 4.1.

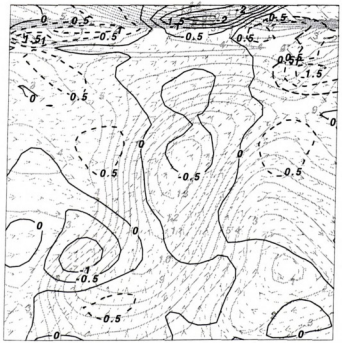

Figure 4.104. Composite Divergence, Level 2 -- L*KC_SWNE* Jets. As in Figure 4.2.

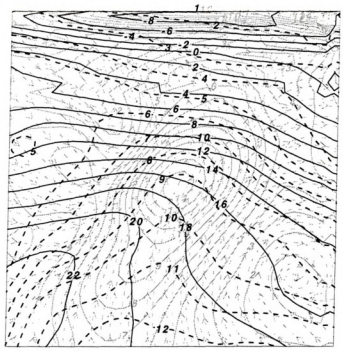

Figure 4.105. Composite 900-mb Temperature (°C) and Mixing Ratio (g kg^{-1}) plotted on Level 1 Composite Airflow Configuration -- *LKC_SWNE* Jets. As in Figure 4.6.

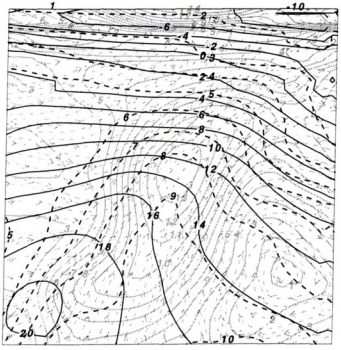

Figure 4.106. Composite 850-mb Temperature (°C) and Mixing Ratio (g kg^{-1}) plotted on Level 2 Composite Airflow Configuration -- *LKC_SWNE* Jets. As in Figure 4.6.

c. Convection

Despite the more northerly location of *LKC_SWNE* jets, lightning is frequent. Of the 11 cases that were assigned to this flow type, 10 were associated with cloud-to-ground lightning activity (91 percent). The location of convective activity is in the same preferred areas evident for many of the other jet types. That is, areas of frequent lightning activity are located downstream of the wind maximum and along the confluence zone west of the jet core. Both areas are characterized by convergence at the first and second analysis levels (Figures 4.107 and 4.108). The area that is affected by lightning is relatively smaller compared to other types. However, keep in mind that only eleven jet events were classified as *LKC_SWNE* jets.

13. LCC Jets (Long with Cyclonic Flow and Confluence)

a. Airflow Configuration and Convergence

The final airflow configuration type that extends to higher latitudes is characterized by a broad area of cyclonic flow (Figure 4.109). This flow type is called *LCC* (**L**ong with **C**yclonic Flow and **C**onfluence). Unlike its 'short' counterpart (i.e. the *CC* type), the cyclonic flow does not culminate in a closed cyclonic circulation. The speed maximum for *LCC* jets is weaker than that for the *CC* jets and the other 'long types, with average speeds of 12 ms^{-1}. The convergence values resulting from this flow configuration are quite respectable (1.94×10^{-5} s^{-1}), although not as strong as for the *CC* jets (Figure 4.110). Convergence is largest northwest of the isotach center, similar to the pattern of *CC* jets. The vertical speed profiles indicate that the majority of *LCC* jets have fairly pronounced jet noses at low altitudes (Table 4.23). Nine out of ten jet events had maximum speeds $\geq$12 ms^{-1} and a vertical decrease of at least one half the maximum speed. In addition, eight out of the ten cases had a speed maximum located below 900 mb. These height values result in a median (average) height for the first level of 915 mb (919 mb) (Table 4.24). Therefore, among the 'long' jet types, the *LCC* jets are found at

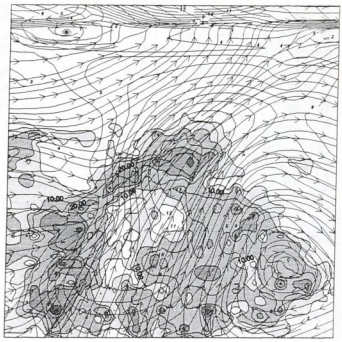

Figure 4.107. Percentage of Jet Events with Lightning Activity plotted on Level 1 Composite Airflow Configuration -- *LKC_SWNE* Jets.

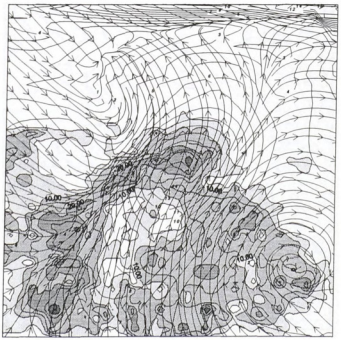

Figure 4.108. Percentage of Jet Events with Lightning Activity plotted on Level 2 Composite Airflow Configuration -- *LKC_SWNE* Jets.

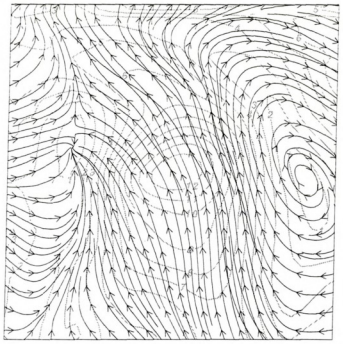

Figure 4.109. Composite Isotachs and Streamlines, Level 1 -- *LCC* Jets. As in Figure 4.1

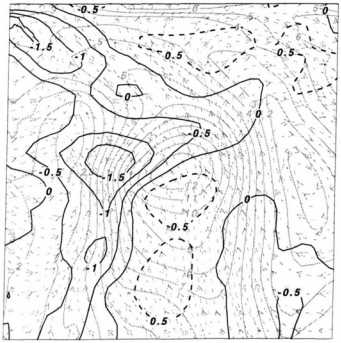

Figure 4.110. Composite Divergence, Level 1 -- *LCC* Jets. As in Figure 4.2.

Table 4.23. Number of Events by Speed Profile Category -- *LCC* Jets.

	'Strong' Jets	'Less Pronounced' Jets	Others
Level 1	a1: 2 a2: 5 b1: 1 b2: 1	a3: 1	
Level 2	b1: 2	a3: 3 a5: 1 b3: 1 b4: 2	
Level 3	b1: 1 b2: 1		c: 1

the lowest elevation. In agreement with their shallow height, *LCC* jets have a clear preference for the morning hours (1200 UTC). *LCC* jets are most common at the end of the warm season, during September. Their geographical preference of the *LCC* jets is the western Great Plains (median 42°N/101°W, western Nebraska), similar to that of *CC* jets (Figure 4.111). Centroids are dispersed from southeastern Colorado to North Dakota.

Table 4.24. Characteristics of *LCC* Jets.

Number observations	Diurnal variation	Seasonal variation	Annual variation	Height (mb)	Median location
Level 1: 10 Level 2: 9 Level 3: 3	0000 Z: 2 1200 Z: 8	Apr: 1 May: 1 Jun: 1 Jul: 2 Aug: 1 Sep: 4	1991: 7 1992: 3	Level 1: Med: 915 Ave: 919 Level 2: Med: 881 Ave: 869 Level 3: Med: 850 Ave: 841	42°N/101°W

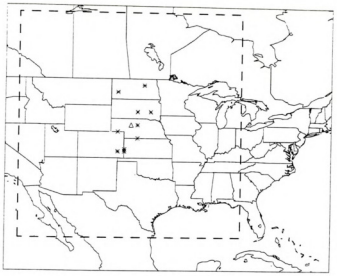

Figure 4.111. Geographical Centers of Isotach Maxima – *LCC* Jets.

At the second level, which is also found at relatively low altitudes, the cyclonic curvature north of the isotach maximum, evident at the first level is overlaid by anticyclonic flow (Figure 4.112). Unlike the second levels for other jet types, the strongest convergence is not located immediately downstream of the jet maximum but rather is found along the confluence zone located northwest of the wind maximum (Figure 4.113). The average convergence values are rather weak (0.68×10^{-5} s^{-1}) compared to the second-level convergence for other jet types. A large number of jet events had a second level (90 percent).

The jet core at the third analysis level is displaced to the east compared with the second-level core (Figure 4.114). The trend toward less cyclonic curvature is continued at the third level. A fairly strong confluence zone is located along the left flank of the wind maximum (Figure 4.115).

b. Temperature and Moisture

The *LCC* jets, due to their first-level cyclonic curvature are associated with strong temperature and moisture advection into the northwestern portion of the study area. At

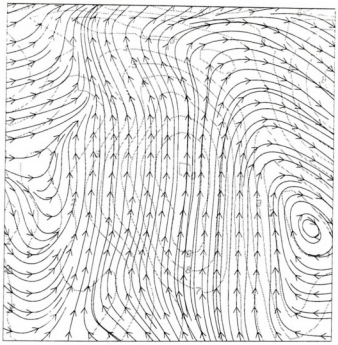

Figure 4.112. Composite Isotachs and Streamlines, Level 2 -- *LCC* Jets. As in Figure 4.1

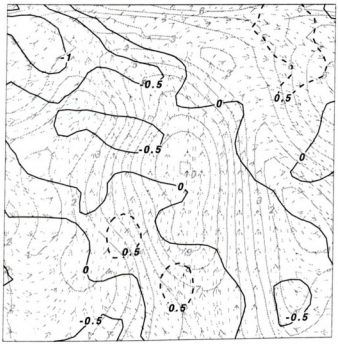

Figure 4.113. Composite Divergence, Level 2 -- *LCC* Jets. As in Figure 4.2

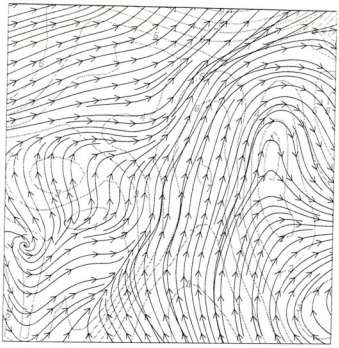

Figure 4.114. Composite Isotachs and Streamlines, Level 3 -- *LCC* Jets. As in Figure 4.1.

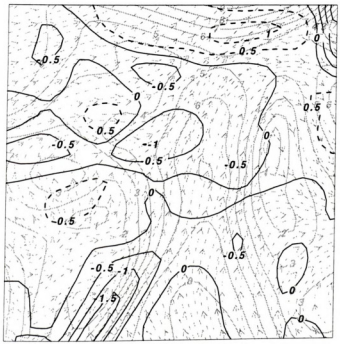

Figure 4.115. Composite Divergence, Level 3 -- *LCC* Jets. As in Figure 4.2

the 900-mb level, notice the pronounced temperature and moisture ridge in the western portion of the study are (Figure 4.116). Unlike the other jet types, the temperature and moisture ridge for *LCC* jets are collocated. The temperature and moisture values are fairly low compared with other types, which is not too surprising considering the northerly location of the jet core. The temperature and moisture pattern does not change much with height. At the 850-mb level, the pronounced temperature and moisture ridge is still evident (Figure 4.117). A slight shift eastward of the ridge axes is noticeable, however, indicative of the change in wind direction with height.

c. Convection

While the number of events (10) is fairly small, all *LCC* jets were associated with lightning activity. Compared with their short counterparts, the *CC* jets, the spatial pattern of lightning activity is much more confined. The area of most frequent lightning activity is located upstream of the jet cores evident at the first, second and third analysis levels (Figures 4.118-4.120). A secondary frequency maximum is evident along the confluence zone to the west.

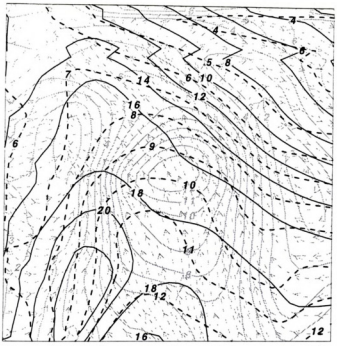

Figure 4.116. Composite 900-mb Temperature (°C) and Mixing Ratio (g kg^{-1}) plotted on Level 1 Composite Airflow Configuration -- *LCC* Jets. As in Figure 4.6.

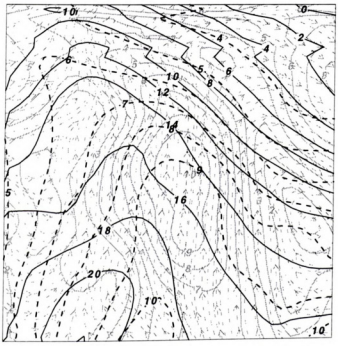

Figure 4.117. Composite 850-mb Temperature (°C) and Mixing Ratio (g kg^{-1}) plotted on Level 2 Composite Airflow Configuration -- *LCC* Jets. As in Figure 4.6.

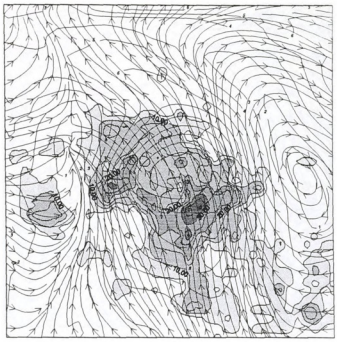

Figure 4.118. Percentage of Jet Events with Lightning Activity plotted on Level 1 Composite Airflow Configuration -- *LCC* Jets.

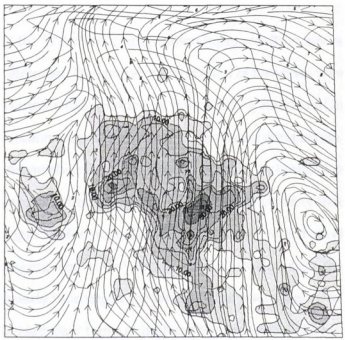

Figure 4.119. Percentage of Jet Events with Lightning Activity plotted on Level 2 Composite Airflow Configuration -- *LCC* Jets.

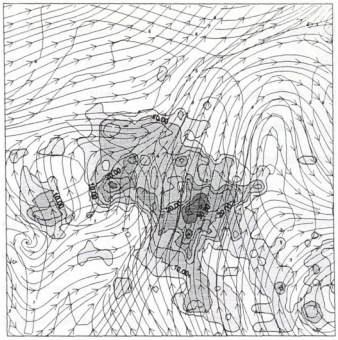

Figure 4.120. Percentage of Jet Events with Lightning Activity plotted on Level 3 Composite Airflow Configuration -- *LCC* Jets.

14. Summary

The analysis of the 12 airflow configuration types results in a number of major findings. First and foremost, the spatial configuration of low-level wind maxima is considerably more complex than previously portrayed. A number of airflow configuration types (summarized in Figure 4.121 for easier comparison) were identified which differentiate themselves from one another not only in terms of their isotach and streamline patterns and resulting convergence, but also in terms of their temporal, geographical and height preferences (Table 4.25). A broad spectrum of configuration types is observed ranging from a very localized, shallow flow type that is primarily observed during the early morning at the height of the warm season to more geographically dispersed flow types at higher altitudes with different temporal preferences.

Another major finding of this study is the existence of multiple airstreams for some jet events. The individual airstreams are found at different heights and distinguish themselves by a change in the orientation with height. Generally, the airstreams assume increasingly more anticyclonic curvature with height. The effects of the multiple airstreams are evident in the temperature and moisture pattern associated with the jet events and in the pattern of convection. Thus, the area ultimately affected by the wind maxima is larger than the lowest level would indicate.

The convergence fields associated with the configuration types vary. At the lowest level, the strongest convergence is frequently observed along a confluence zone to the northwest of the isotach center. At higher levels, the strongest convergence is most frequently located immediately downstream of the wind maximum. A secondary area of convergence at the second level is frequently found along the confluence zone to the west of the isotach maximum, similar to that for the first level.

The composite temperature and mixing ratio patterns for all types of low-level wind maxima highlight the fact that the topography of the Central Plains sets the stage for the geographically preferred location for convection. The composite maps, centered on the isotach maxima, displayed a ridge of higher temperatures originating over the hot and dry regions of the southwestern United States. This ridge extends from the southwestern corner of the composites and intersects a moisture ridge extending northward from the Gulf of Mexico. However, variations of that scheme are observed due to the different configurations of the wind maxima.

This study also shows that wind maxima that do not fit the more stringent selection criteria of Bonner (1968) and other authors, nevertheless, have important impacts on convective activity. Between 84 and 100 percent of the jet events assigned to individual jet types in this study were associated with cloud-to-ground lightning activity.

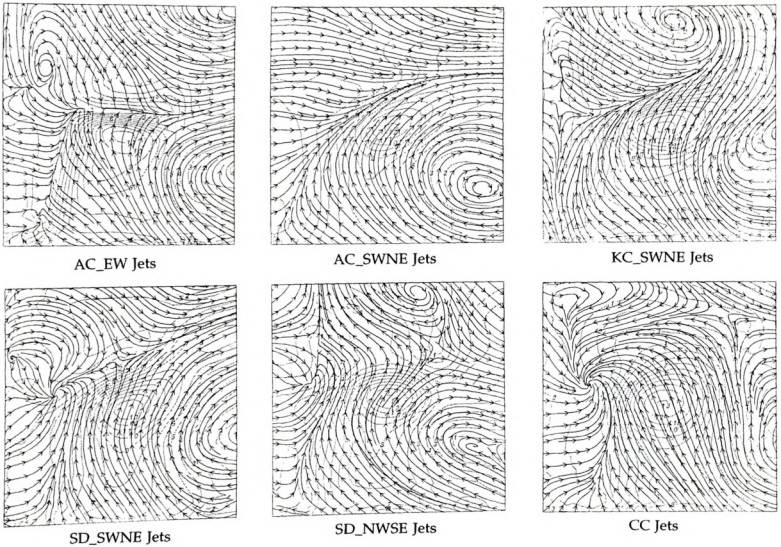

Figure 4.121. Airflow Configuration Types.

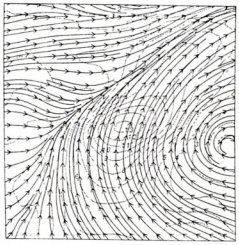

LAC_SWNE Jets

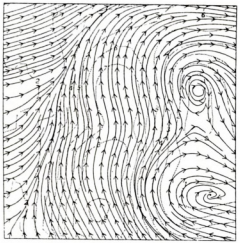

L2A Jets

LSKC_SWNE Jets

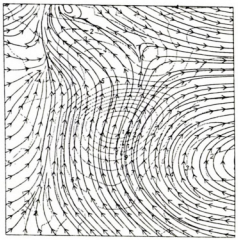

LSPLIT Jets

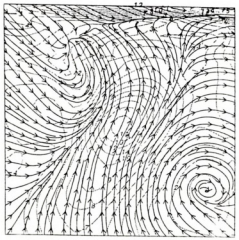

LKC_SWNE Jets

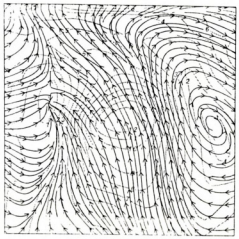

LCC Jets

Figure 4.121 (cont'd).

Table 4.25. Temporal, Geographical, Height, Speed Profile and Convergence Pattern Characteristics of the Airflow Configuration Types

	AC_EW	AC_ SWNE	KC_ SWNE	SD_ SWNE	SD_ NWSE	CC	LAC_ SWNE	L2A	LSKC_ SWNE	LSPLIT	LKC_ SWNE	LCC
Number of Observations												
L1	14	31	12	17	21	38	27	24	24	31	11	10
L2	3	4	7	9	6	27	9	15	13	22	6	9
L3	-	2	-	-	-	3	1	3	-	1	-	3
Temporal Preference												
% 12 Z	100	58	92	71	76	42	59	63	63	77	36	80
month	Jul/Aug	Jul	Sep	min Jul	Jul	May/Jun	May	Jun/Jul	Apr	May	Apr/May	Sep
% 1992	71	32	50	47	29	53	44	29	67	42	64	30
Geographical Preference												
med loc.[1]	36/102	38/97	37/101	38/100	36/100	39/102	40/99	39/99	40/98	39/100	46/92	42/101
Height (mb):												
L1: med[2]	942	878	942	850	913	939	904	895	892	908	902	915
L1: ave[3]	928	874	931	877	900	923	888	891	889	904	885	919
L2: med	904	862	850	850	833	846	780	850	822	849	800	881
L2: ave	877	837	863	839	824	838	792	834	826	833	799	869
L3: med	-	817	-	-	-	850	-	792	-	-	-	850
L3: ave	-	817	-	-	-	809	-	811	-	-	-	841

[1] Median location of geographical centers of isotach maxima (latitude and longitude in °N and °W).
[2] Median Value.
[3] Average Value

Table 4.25 (cont'd).

	AC_EW	AC_ SWNE	KC_ SWNE	SD_ SWNE	SD_ NWSE	CC	LAC_ SWNE	L2A	LSKC_ SWNE	LSPLIT	LKC_ SWNE	LCC
% 'Strong' Speed Profiles												
L1	79	52	58	47	48	42	41	21	46	48	27	90
L2	100	75	71	67	33	41	22	27	31	32	0	22
L3	-	75	-	-	-	33	-	0	-	-	-	67
Average Speed (ms^{-1})												
L1	13	12	16	13	13	13	13	9	16	14	14	12
L2	11	12	14	12	12	11	13	9	17	12	13	10
L3	-	14	-	-	-	12	-	9	-	-	-	10
Maximum Convergence[4] ($10^{-5}s^{-1}$)												
L1	3.78 ds/cf	0.95 nw/cf	2.92 nw/cf	1.37 lft/spl	1.28 ds	2.18 ds/lft	1.57 nw/cf	0.83 lft	1.99 nw/cf	1.32 nw	1.51 nw/cf	1.94 ds/lft
L2	1.97 ds	1.37 sw 1.22 ds	1.34 sw 1.04 ds	0.96 ds	1.23 ds	0.92 ds/lft	0.90 ds/lft	0.5 lft	1.34 ds	0.49 ds	0.70 ds/cf	0.64 nw/cf
L3	- -	1.20 ds	- -	- -	- -	1.02 ds/rght	- -	0.62 ds	- -	- -	- -	1.01 lft/cf

[4] Abbreviations used:
nw: to northwest of jet core
sw: to southwest of jet core
lft: along left flank
rght: along right flank
cf: along confluence zone
ds: downstream of jet maximum
spl: near split

The differences in the geographical distribution of the individual types have important implications for identifying areas that are affected by the low-level wind maxima. Depending on the configuration type, the area downstream of the jet core may be located as far west as Wyoming or as far east as Michigan. The geographical distribution of the jet cores, in turn, is an indication that different synoptic situations are prerequisites for the different wind maxima. In the next chapter, the lower-, mid-, and upper-tropospheric large-scale setting for the different airflow configurations is investigated.

MICHIGAN STATE UNIV. LIBRARIES
31293013947423

THESIS

LIBRARY
Michigan State University

PLACE IN RETURN BOX to remove this checkout from your record.
TO AVOID FINES return on or before date due.

DATE DUE	DATE DUE	DATE DUE
JAN 1 6 2005		

MSU Is An Affirmative Action/Equal Opportunity Institution
c:\circ\datedue.pm3-p.1

A SYNOPTIC CLIMATOLOGY OF WARM-SEASON LOW LEVEL WIND MAXIMA IN THE GREAT PLAINS AND THEIR RELATIONSHIP TO CONVECTION

VOLUME II

By

Claudia K. Walters

A DISSERTATION

Submitted to
Michigan State University
in partial fulfillment of the requirements
for the degree of

DOCTOR OF PHILOSOPHY

Department of Geography

1997

Chapter 5

THE LOWER, MID- AND UPPER TROPOSPHERIC ENVIRONMENTS OF LOW-LEVEL WIND MAXIMA

In the previous chapter, the airflow configurations for 12 types of low-level wind maxima were introduced. Considerable variation in the composite airflow and convergence patterns was noted between the individual types. Although the composite temperature and moisture fields for the different types did not show as much variation, quantitative differences were evident. An important finding of Chapter 4 was the existence of multiple airstreams for some jet events. The multiple airstreams, in turn, have important implications for the pattern of convection. The superposition of multiple airstreams is often mirrored in the spatial distribution of convection.

In this chapter, the lower, mid- and upper tropospheric environments are discussed for the individual types of low-level wind maxima. For each type, the large-scale lower tropospheric environment is introduced first by means of the composite surface pressure and 12-h surface pressure tendency patterns. The resultant pressure-gradient forcing on the low-level wind maxima is examined by means of the geostrophic wind field at the level of maximum wind. Other lower tropospheric factors that might influence the formation of the low-level wind maxima are examined by means of the ageostrophic wind field. To investigate mid- and upper-tropospheric influences, the average 500-mb geopotential height fields and the 200-mb kinematic patterns are provided. Similar to the low-level wind field, the 200-mb kinematic patterns are investigated by means of composite isotach and streamline patterns and convergence fields. The individual airflow configuration types are discussed in the same order as in the previous chapter, starting with the six types of wind with limited horizontal extents,

followed by the remaining six that extend to higher latitudes. Within these two broad groups, the configuration types are discussed in order of increasingly less anticyclonic curvature.

In the Chapter it will be shown that the individual airflow configuration types are associated with considerably different large-scale pressure and height environments. Consequently, the mechanisms that lead to the formation of low-level wind maxima are suspected to vary with the different airflow types.

1. AC_EW Jets

a. Surface Pressure and Surface Pressure Tendency

In keeping with the same order as the previous chapter, the *AC_EW* jet type, which is composed of strongly anticyclonically-curved, 'short' jet events is discussed first. Remember that *AC_EW* jets have fairly strong temporal and geographical signatures. All events were observed during the early morning hours and their jet cores were strongly clustered around the Texas Panhandle.

The surface pressure pattern during *AC_EW* events takes on the shape of a 'col', formed by low pressure centers in the northeastern (minimum pressure of 1012 mb) and southwestern (minimum pressure of 1012 mb) portions of the composite region and two centers of high pressure in the southeast (maximum pressure of 1016 mb) and northwest (maximum pressure of 1020 mb) (Figure 5.1). The strongest of these surface features appears to be the high-pressure system to the northwest. The composite pressure tendency field suggests that the two centers to the northwest and northeast are strengthening (Figure 5.2). During the previous 12 h, the region to the northwest of the wind maximum witnessed on average a pressure rise of 11 mb, while the cyclone to the northeast underwent a moderate pressure fall (2 mb). An interesting observation is that the composite jet core is not located in the center of the col but rather is embedded within the weak pressure gradient between the southwest low and the southeast high.

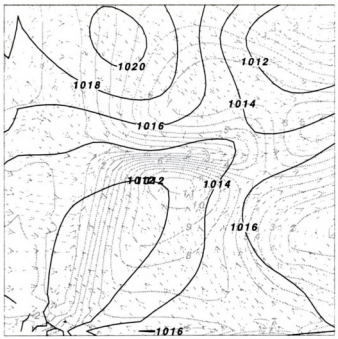

Figure 5.1. Composite Surface Pressure plotted on Level 1 Composite Airflow Configuration -- *AC_EW* Jets. Dark solid lines are isobars (in mb), light dashed lines are streamlines, light solid lines are isotachs.

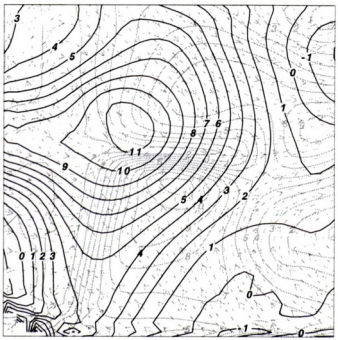

Figure 5.2. Composite 12-h Surface Pressure Tendency plotted on Level 1 Composite Airflow Configuration -- *AC_EW* Jets. Dark lines are lines of equal 12-h pressure change (in mb). Light dashes lines are streamlines, light solid lines are isotachs.

b. Geostrophic and Ageostrophic Wind

The low-level wind maximum during *AC_EW* events cannot be attributed to a local maximum in the pressure gradient in the vicinity of the jet core. Note that the geostrophic wind, which is proportional to the strength of the pressure gradient, is considerably weaker than the actual wind in the jet core (Figure 5.3). The actual wind in the jet core, therefore, has supergeostrophic velocities. Surprisingly, the strongest geostrophic wind is not found at the center of the composite jet core, but rather is observed to the southwest and southeast of the jet core.

In order to explain the location of the jet core and the speed of the actual wind, one needs to consider the ageostrophic component of the wind (Figure 5.4). As noted above, the ageostrophic wind is defined as the vector difference between the observed and the geostrophic wind. Unlike the geostrophic component, the ageostrophic component is fairly strong in the vicinity of the jet core. The strength of the ageostrophic wind and the agreement of the ageostrophic wind direction with the actual wind direction highlight the fact that the actual wind speeds are considerably supergeostrophic for *AC_EW* jets in the vicinity of the jet core. The strongest ageostrophic wind vectors, however, are somewhat off to the west of the jet core. The ageostrophic wind component of *AC_EW* jets is likely the result of a number of different factors. Due to the fact that the *AC_EW* jets are exclusively early morning phenomena (1200 UTC), the inertial component of the ageostrophic wind vector may be a significant contributor to the ageostrophic wind pattern. The veering of the ageostrophic wind vectors with latitude through the jet core can be interpreted as additional support for the notion that at least part of the ageostrophic wind vector is due to the inertial component, as the inertial component of the ageostrophic wind vector is influenced by the Coriolis parameter. The direction of the ageostrophic wind vector is expected to become increasingly more westerly with latitude. Another possible explanation for the

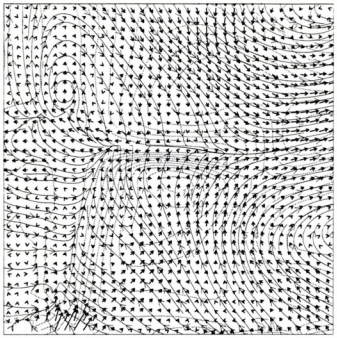

Figure 5.3. Composite Geostrophic Wind, Level 1 -- *AC_EW* Jets. The length of the scale arrow is 10 ms^{-1}.

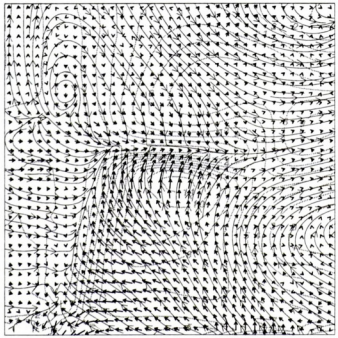

Figure 5.4. Composite Ageostrophic Wind, Level 1 -- *AC_EW* Jets. The length of the scale arrow is 10 ms^{-1}.

change in wind direction of the ageostrophic component through the jet core is related to the transverse circulation in the entrance and exit regions of jet streaks. Upstream of a jet maximum, the ageostrophic component is oriented toward the area of lower pressure to the left of the jet core while downstream of a jet maximum, the ageostrophic component is oriented toward the area of higher pressure to the right of the jet core.

The isallobaric component of the ageostrophic wind offers another possible explanation for the enhanced wind speed in the jet core. Despite the fact that the 12-h surface pressure tendency composite displays a region of pressure rises to the northwest of the wind maximum, the possibility of an isallobaric component in connection with a confluence/cold frontal zone cannot be discounted. The pressure rises to the northwest of the jet core would suggest that the high pressure system is increasing in intensity and probably advancing eastward. Consequently, a confluence/frontal zone along its leading edge is suspected to be fairly strong as well. The orientation of the ageostrophic wind vector toward the confluence zone to the north of the wind maximum would suggest a transverse circulation about a cold front and pressure falls associated with the approach of the front could contribute to the strengthening of the ageostrophic component. Unfortunately, the resolution of the rawinsonde observation does not permit a detailed analysis. Therefore, any prefrontal pressure falls may go undetected. Another interesting feature in the spatial pattern of the ageostrophic wind vectors is the region of strong ageostrophic wind in the southwestern portion of the composite. The orientation of the wind vectors toward the west suggests possible frictional influences. Since *AC_EW* are fairly shallow phenomena, the southwestern corner of the composite area is close to the earth's surface. Therefore, the ageostrophic wind vectors may be caused by a deflection and slowing of the geostrophic wind by friction.

c. Mid-tropospheric Heights and Upper Tropospheric Wind Field

As previously suggested, boundary-layer influences may dominate for *AC_EW* jets, as the large-scale surface pressure gradient is not the primary driving force behind this type of low-level wind maximum nor do large-scale pressure falls appear to contribute to the formation of *AC_EW* jets. Instead, a likely driving mechanism is the inertial component of the ageostrophic wind. The 500-mb pattern also suggests that large-scale forcing is not very important (Figure 5.5). *AC_EW* jets are located near a 500-mb ridge, just south of a fairly strong 500-mb height gradient. To the north, a 500-mb shortwave trough is evident. This trough and the upstream ridge support, respectively, the northeastern low pressure center and northwestern high pressure center evident on the composite pressure pattern.

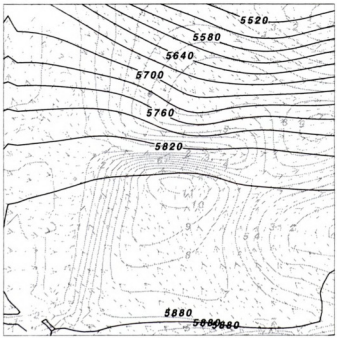

Figure 5.5. Composite 500-mb Geopotential Height plotted on Level 1 Composite Airflow Configuration -- *AC_EW* Jets. Dark solid lines represent geopotential height (in meters), light dashed lines are streamlines, light solid lines are isotachs.

The only indication of mid- and upper-tropospheric large-scale forcing is an upper-tropospheric (i.e., 200 mb) jet streak north of the jet core (Figure 5.6). Note that the upper-level jet streak is located over the strongest 500-mb height gradient. Researchers have shown that the 'right rear' quadrants of jet streaks are areas of divergence (Beebe and Bates 1955), thus upper-level divergence is likely located immediately to the north of the *AC_EW* jets. This suggests a possible linkage between the upper and lower tropospheric wind maxima, as the upper-level divergence would be compensated by low-level inflow/convergence (Figure 5.7).

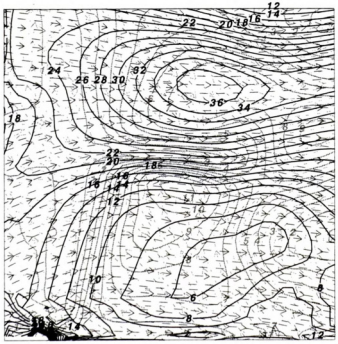

Figure 5.6. Composite 200-mb Isotachs and Streamlines -- *AC_EW* Jets. Dark solid lines are 200 mb isotachs (in m s^{-1}); dark dashed lines are 200 mb streamlines; light dashed lines are low-level streamlines; light solid lines are low-level isotachs.

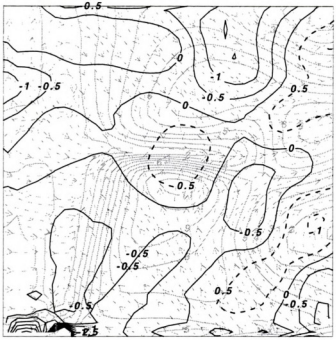

Figure 5.7. Composite 200-mb Divergence plotted on Level 1 Composite Airflow Configuration -- *AC_EW* Jets. Dark solid lines represent 200-mb divergence (10^{-5} s^{-1}); light dashed lines are low-level streamlines; light solid lines are low-level isotachs.

2. AC_SWNE Jets

a. Surface Pressure and Surface Pressure Tendency

Similar to *AC_EW* jets, the composite surface pressure pattern for *AC_SWNE* jets can be characterized as a 'col' (Figure 5.8). However, the two northern pressure features, the high to the northwest and the low to the northeast, are considerably weaker. Instead, the dominant feature for the *AC_SWNE* jets is the high pressure system (central pressure of 1018 mb) southeast of the jet core. As a result, the pressure gradient across the southern portion of the composite region is considerably stronger for *AC_SWNE* jets. The jet core is embedded within the return flow around this anticyclone. Note, too, that the jet core is located along the western edge of the pressure gradient between the southeastern anticyclone and the weak surface pressure trough to the

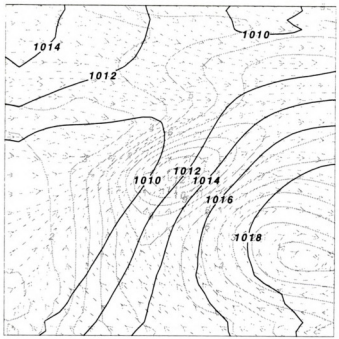

Figure 5.8. Composite Surface Pressure plotted on Level 1 Composite Airflow Configuration -- *AC_SWNE* Jets. As in Figure 5.1.

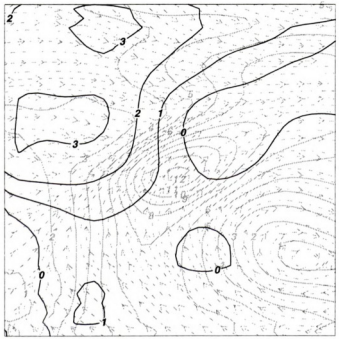

Figure 5.9. Composite 12-h Surface Pressure Tendency plotted on Level 1 Composite Airflow Configuration -- *AC_SWNE* Jets. As in Figure 5.2.

southwest. Similar to *AC_EW* jets, surface pressure has risen during the previous 12 h over much of the composite region, although the pressure increases are considerably smaller than those for the *AC_EW* jets (see Figure 5.9).

b. Geostrophic and Ageostrophic Wind

In concert with the stronger pressure gradient force, the geostrophic forcing is greater than the ageostrophic forcing for *AC_SWNE* jets (Figures 5.10 and 5.11). The area of largest geostrophic wind vectors is in agreement with the location of the jet core, suggesting that the local maximum in the pressure gradient is a dominant forcing mechanism. However, the *AC_SWNE* jets, like the *AC_EW* jets, are supergeostrophic, although the ageostrophic vectors are not nearly as large as those for the *AC_SWNE* jets. A possible explanation for the weaker along-flow ageostrophic component can be inferred from the differences in the diurnal preference of the two jet types. The *AC_EW* jets are exclusively early morning phenomena, which is the time of day when the inertial component is expected to be strongest. The *AC_SWNE* jets, on the other hand, are approximately equally frequent during the early morning and evening hours. Thus, the average inertial component would not be as pronounced.

It is interesting to note that, as was the case for *AC_EW* jets, two centers of strong ageostrophic wind, one in the vicinity of the jet core and the other in the southwestern portion of the composite grid, are again present for *AC_SWNE* jets. In the vicinity of the jet core, the ageostrophic wind vectors are directed toward the confluence zone located west/northwest of the jet core. As described earlier, this ageostrophic component can be hypothesized to be at least partially the result of cross-frontal circulation. The cross-frontal circulation would be expected to be weaker, and hence the ageostrophic component would be weaker, for the *AC_SWNE* jets, since the northwestern high pressure system and the magnitude of the pressure rises for the *AC_SWNE* jets are not as strong as those observed for the *AC_EW* jets.

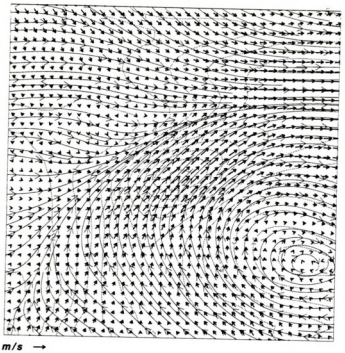

Figure 5.10. Composite Geostrophic Wind, Level 1 – *AC_SWNE* Jets. As in Figure 5.3.

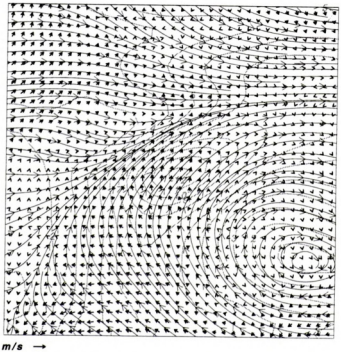

Figure 5.11. Composite Ageostrophic Wind, Level 1 – *AC_SWNE* Jets. As in Figure 5.3.

Note, too, that the direction of the ageostrophic wind through the jet core for the *AC_SWNE* jets veers with latitude, similar to the latitudinal veering observed for the *AC_EW* jets. This shift in wind direction may be a manifestation of the effect of the Coriolis parameter on the ageostrophic wind or it may be the result of transverse circulations in the entrance and exit regions of the low-level wind maximum. Relatively stronger ageostrophic wind components, likely due to friction, are again observed in the southwestern portion of the composite region. However, the ageostrophic component in this region is generally smaller than that for the *AC_EW* jets, which corresponds well with the higher median height of *AC_SWNE* jets compared to the height of *AC_EW* jets.

c. Mid-tropospheric Heights and Upper-tropospheric Wind Field

AC_SWNE jets are located under a 500-mb ridge, similar to the midtropospheric pattern observed for *AC_EW* jets (Figure 5.12). However, the height gradient north of

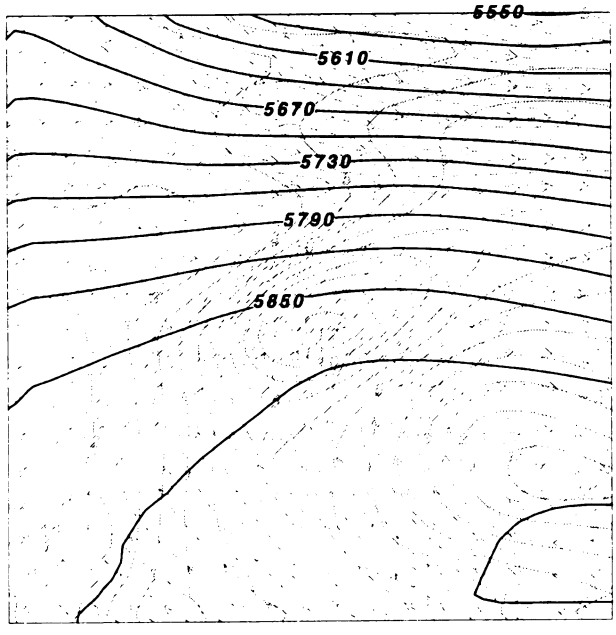

Figure 5.12. Composite 500-mb Geopotential Height plotted on Level 1 Composite Airflow Configuration– *AC_SWNE* Jets. As in Figure 5.5.

the jet core is somewhat weaker for the *AC_SWNE* jets, the ridge is better defined, and the northern shortwave trough is not evident. Surprisingly, *AC_SWNE* jets are directed toward the right front quadrant of a jet streak evident on the 200-mb airflow composite (Figure 5.13). This is a region of upper-level convergence that would be expected to suppress any rising motion. Thus, there is little indication of a link between the upper-level jet and the *AC_SWNE* wind maximum. Also, the 200-mb composite convergence pattern supports the contention that upper-level dynamical support is weak or absent for *AC_SWNE* jets (Figure 5.14). Note that upper-level divergence is not evident on the composite.

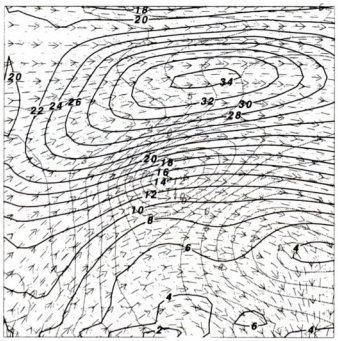

Figure 5.13. Composite 200-mb Isotachs and Streamlines plotted on Level 1 Composite Airflow Configuration – *AC_SWNE* Jets. As in Figure 5.6.

The large-scale setting for *AC_SWNE* jets suggests that this airflow configuration type is similar to the jet described earlier by Wexler (1961). Features in common include a 500-mb ridge, an anticyclone over the southeastern U.S., and a strongly

anticyclonically-curved low-level wind maximum embedded in the return flow around the anticyclone.

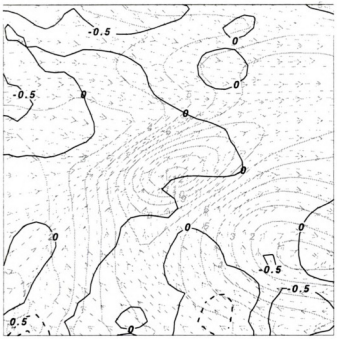

Figure 5.14. Composite 200-mb Divergence plotted on Level 1 Composite Airflow Configuration -- *AC_SWNE* Jets. As in Figure 5.7.

3. KC_SWNE Jets

a. Surface Pressure and Surface Pressure Tendency

The third airflow configuration type, *KC_SWNE* jets, is anticyclonically curved upstream of the wind maximum, but downstream of the jet core, the airflow reverses direction into a closed cyclonic circulation. The surface pressure features differ from the *AC_EW* and *AC_SWNE* types in that the previously-noted southwestern and northeastern low pressure centers are replaced by an elongated trough of low pressure (Figure 5.15). The lowest pressure values are observed north of the jet core, just southeast of the closed cyclonic circulation. This region of low pressure resembles an 'Alberta Clipper', i.e. a low pressure system that developed in the Alberta cyclogenesis

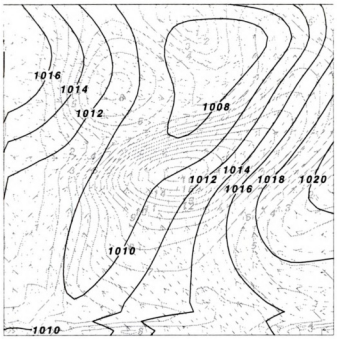

Figure 5.15. Composite Surface Pressure plotted on Level 1 Composite Airflow Configuration -- *KC_SWNE* Jets. As in Figure 5.1.

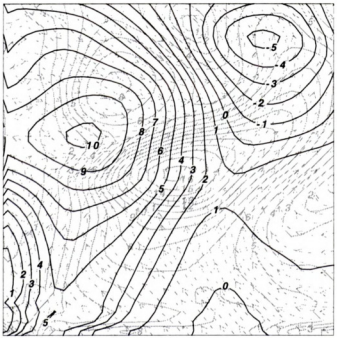

Figure 5.16. Composite 12-h Surface Pressure Tendency plotted on Level 1 Composite Airflow Configuration -- *KC_SWNE* Jets. As in Figure 5.2.

region. The composite surface pressure features are all fairly pronounced. Strong pressure areas to the southeast (central pressure of 1020 mb) and northwest (cer pressure of 1016), in combination with a fairly strong low pressure trough (centr pressure of 1008 mb), result in a strong pressure gradient along the eastern edge study area. Similar to the previous types, the jet core is located along the wester of the pressure gradient, immediately ahead of the trough of low pressure. In the previous 12 h, the surface pressure features have undergone considerable change Figure 5.16). Similar to *AC_EW* jets, the largest pressure increases occurred in connection with a strengthening (12 h change of 10 mb) of the high pressure area northwest of the jet core. In addition, the low pressure trough deepened (12 h ch 5 mb). Anothersignificant difference between the two types is the orientation of KC_SWNE jets toward the region of greatest pressure fall. This implies an isallo wind component.

b. Geostrophic and Ageostrophic Wind

The strong pressure gradient along the eastern edge of the composite area r a strong geostrophic wind component (Figure 5.17). Surprisingly, however, the s geostrophic wind speeds are not observed in the location of the low-level wind maximum. Rather, the highest speeds are displaced to the northeast of the jet co Unlike either of the two previously-discussed types, the ageostrophic componen *KC_SWNE* jets is equally strong as the geostrophic component (Figure 5.18). Thu the pressure gradient sets the stage for a strong wind maximum, the ageostrophi component appears to be important in determining the location of the jet core ar wind direction. A surprising feature of *KC_SWNE* jets is the orientation of the geostrophic wind, rather than the ageostrophic component, toward the region of scale pressure falls in the northeast. The ageostrophic component does not appe

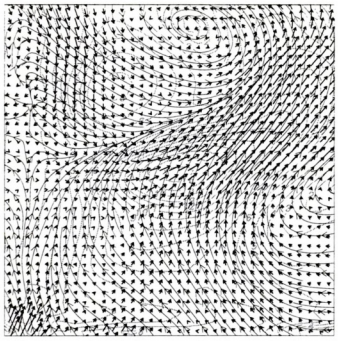

Figure 5.17. Composite Geostrophic Wind, Level 1 – *KC_SWNE* Jets. As in Figure 5.3.

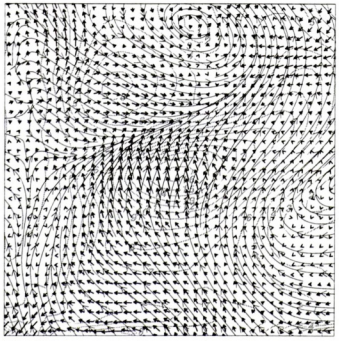

Figure 5.18. Composite Ageostrophic Wind, Level 1 – *KC_SWNE* Jets. As in Figure 5.3.

reaches a minimum between the locations of the jet core and the pressure fall.

Similar to the other two types, the ageostrophic wind vectors near the jet core are oriented toward the confluence zone with the largest vectors extending northwest from the jet core. Thus, it appears that the confluence/frontal zone plays an important role in generating the ageostrophic wind component. The existence of an inertial component of the ageostrophic wind cannot be ruled out, however. Remember that the jet cores for *KC_SWNE* jets are clustered about the Texas Panhandle, similar to the spatial distribution of *AC_EW* jets. Furthermore, *KC_SWNE* jets have a diurnal preference for the morning hours. Since the inertial component of the ageostrophic wind is thought to decrease with latitude, the location of the jet core is likely strongly influenced by the contributions of this ageostrophic component. Other pieces of evidence pointing to the existence of an inertial component can be found in the rotation of the wind vector through the jet core. As mentioned above, the inertial component is thought to be acted upon by the Coriolis parameter, thus it should veer with latitude. To the southwest of the jet core, the ageostrophic wind vectors display the now familiar orientation toward the west.

c. Mid-tropospheric Heights and Upper-tropospheric Wind Field

The mid- and upper tropospheric large-scale patterns for *KC_SWNE* jets differ substantially from the environments of the two previously-discussed airflow configuration types. At the 500-mb level, the ridge axis is located considerably east of the low-level wind maximum core (Figure 5.19). Upstream of the jet is a fairly well-defined 500-mb trough. This trough provides upper-level support for the southwest-northeast oriented surface pressure trough noted above. The 500-mb ridge supports the surface anticyclone evident in the extreme eastern portion of the composite region.

The jet streak at the 200-mb level is located considerably farther east than the jet streaks for the other two types (Figure 5.20). Consequently, the exit region of the jet

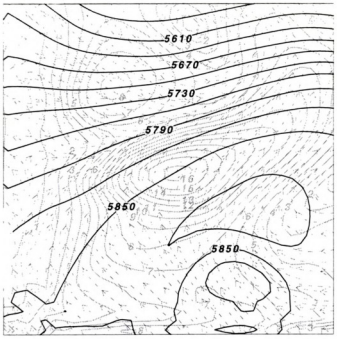

Figure 5.19. Composite 500-mb Geopotential Height plotted on Level 1 Composite Airflow Configuration -- *KC_SWNE* Jets. As in Figure 5.5.

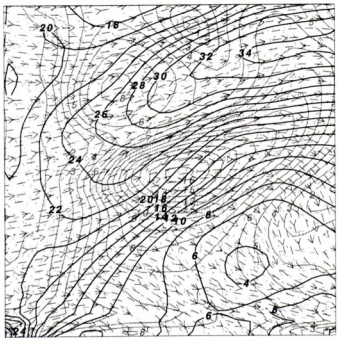

Figure 5.20. Composite 200-mb Isotachs and Streamlines plotted on Level 1 Composite Airflow Configuration -- *KC_SWNE* Jets. As in Figure 5.6.

streak is beyond the limits of the composite area. The low-level flow is oriented toward the right entrance region, however, a region of upper-level divergence. The notion of upper-level support for *KC_SWNE* jets is supported by the orientation the low-level flow is toward a local maximum in the 200-mb divergence field (Figure 5.21).

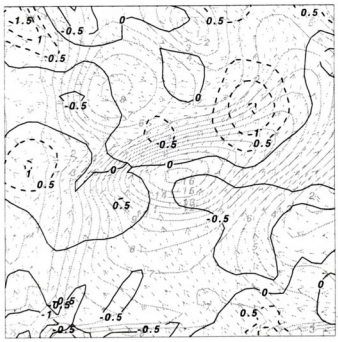

Figure 5.21. Composite 200-mb Divergence plotted on Level 1 Composite Airflow Configuration -- *KC_SWNE* Jets. As in Figure 5.7.

Considering the large-scale setting, it therefore appears that the exceptionally strong wind speeds for the *KC_SWNE* jets need to be explained by a combination of upper-level dynamics and boundary-layer support. In terms of large-scale support, the low-level wind maximum is oriented toward a low-pressure system, and is aligned parallel to a confluence/frontal boundary. On the other hand, the jet core is displaced to the south of the large-scale pressure gradient maximum, likely due to the influence of boundary-layer conditions.

4. SD_SWNE Jets

a. Surface Pressure and Surface Pressure Tendency

Next, the first "short" airflow configuration type with split flow downstream of the jet core is discussed. The composite surface pressure pattern is very similar to that for the *KC_SWNE* events, with a southwest-northeast oriented surface trough covering much of the composite region (Figure 5.22). Two anticyclones, one located in the extreme east and another located in the northeast portion of the composite region, are also evident. However, the "closed isobar" within the surface trough is located southeast, rather than northeast, of the jet core. Another important difference is that the large pressure falls northeast of the jet core evident for *KC_SWNE* events are missing on the pressure tendency composite for the *SD_SWNE* jets, although the pressure rises west of the jet core are evident (Figure 5.23). The jet core is found in its now familiar location along the western edge of the pressure gradient between the surface trough and the eastern anticyclone. This pressure gradient is comparable in strength to the gradients observed earlier for the *KC_SWNE* and *AC_SWNE* jets.

b. Geostrophic and Ageostrophic Wind

The geostrophic wind speeds for the *SD_SWNE* jets are comparable to the speeds for the *KC_SWNE* and *AC_SWNE* jets, but weaker than those for the *AC_EW* jets (Figure 5.24). There is good agreement between the location of the largest geostrophic wind vectors and the jet core for *SD_SWNE* jets, as was the case for *AC_SWNE* jets. However, contrary to the *AC_SWNE* jets, the ageostrophic component is as strong as the geostrophic component, thus leading to strongly supergeostrophic wind speeds (Figure 5.25). As for the other three configuration types, two areas of large ageostrophic wind are evident. An ageostrophic wind component directed toward the confluence/frontal zone, as in the case of *AC_EW* and *KC_SWNE* jets, is not evident, similar to *AC_SWNE* jets. These findings support the notion that the ageostrophic component directed

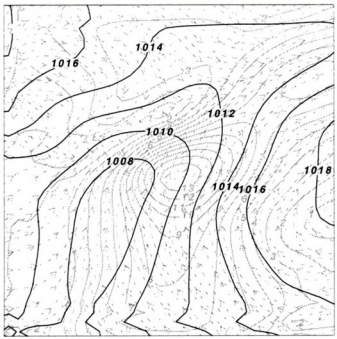

Figure 5.22. Composite Surface Pressure plotted on Level 1 Composite Airflow Configuration -- *SD_SWNE* Jets. As in Figure 5.1.

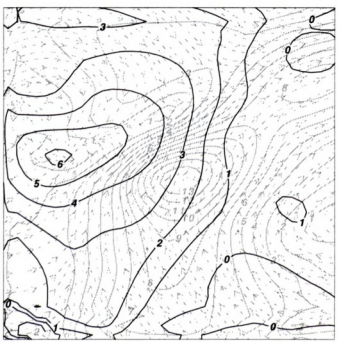

Figure 5.23. Composite 12-h Surface Pressure Tendency plotted on Level 1 Composite Airflow Configuration -- *SD_SWNE* Jets. As in Figure 5.2.

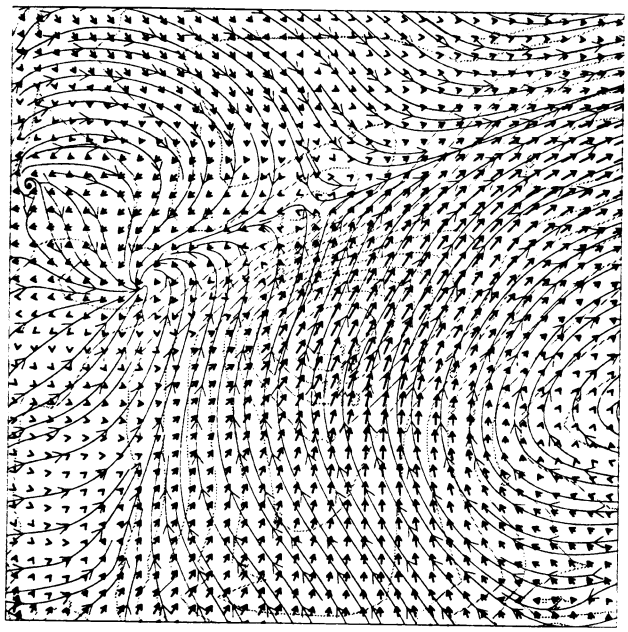

Figure 5.24. Composite Geostrophic Wind, Level 1 – *SD_SWNE*. As in Figure 5.3.

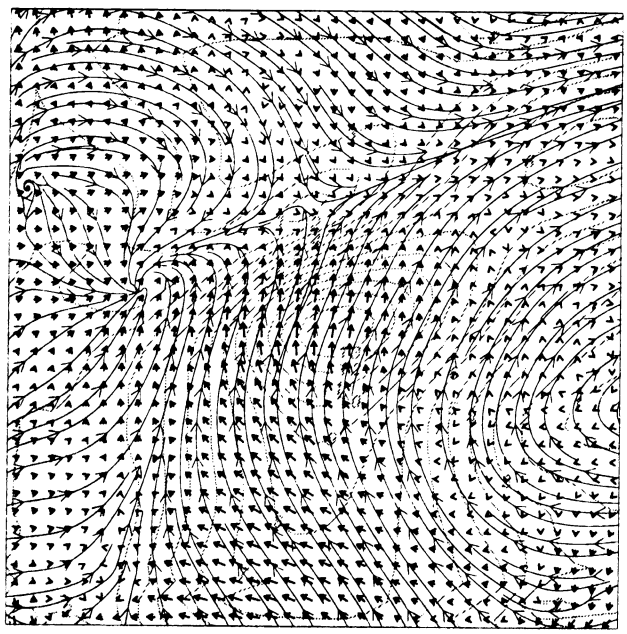

Figure 5.25. Composite Ageostrophic Wind, Level 1 – *SD_SWNE* Jets. As in Figure 5.3.

toward the confluence zone is proportional to the strength of the frontal zone, which in turn is related to the amount of pressure increase over the northwestern portion of the composite region. It is also interesting to note for *SD_SWNE* jets that the largest geostrophic wind vector is associated with the right, or east, branch, whereas the ageostrophic component is equally large for the left and right branches. Also, both the geostrophic and ageostrophic components are weak in the vicinity of the deformation zone. As with the other types, the ageostrophic vectors veer with latitude, particularly upstream of the jet core.

c. Mid-tropospheric Heights and Upper-tropospheric Wind Field

The 500-mb composite pattern for *SD_SWNE* events most resembles that of the *KC_SWNE* jets (Figure 5.26). A trough is located in the western portion of the analysis region, and a ridge is located to the east. However, the trough is more amplified for the

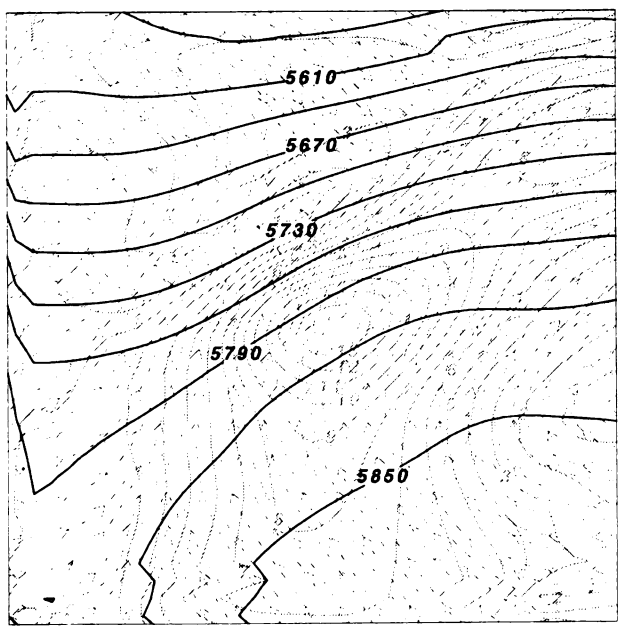

Figure 5.26. Composite 500-mb Geopotential Height plotted on Level 1 Composite Airflow Configuration -- *SD_SWNE* Jets. As in Figure 5.5

SD_SWNE events, and the trough axis extends farther south and southwest. The extension of the trough into the southwestern portion of the composite region helps explain the closed isobar observed on the pressure composite south of **the** low-level wind maximum core. Note that the low-level wind maximum is located immediately downwind of the 500-mb trough axis in a region of southwesterly 500-mb airflow.

Similar to the *KC_SWNE* jets, the right entrance region of an upper-tropospheric jet streak (Figure 5.27), and the resulting area of upper-level divergence (Figure 5.28), is located immediately north/northwest of the jet core. This composite pattern suggests a linkage between the upper-level jet and the left or westernmost branch of the *SD_SWNE* jets.

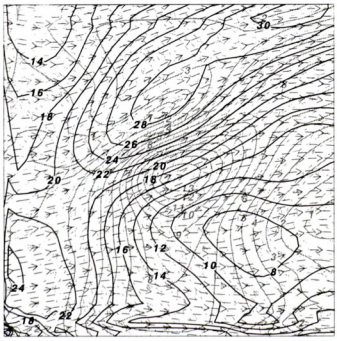

Figure 5.27. Composite 200-mb Isotachs and Streamlines plotted on Level 1 Composite Airflow Configuration -- *SD_SWNE* Jets. As in Figure 5.6.

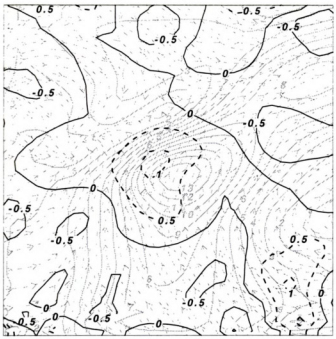

Figure 5.28. Composite 200-mb Divergence plotted on Level 1 Composite Airflow Configuration -- *SD_SWNE* Jets. As in Figure 5.7.

5. SD_NWSE Jets

a. Surface Pressure and Surface Pressure Tendency

The composite pressure pattern is weaker for difluent low-level wind maxima with deformation zones oriented northwest-southeast (i.e., *SD_NWSE* jets) compared to difluent jets with southwest-northeast deformation zones (i.e., *SD_SWNE* jets) (Figure 5.29). The trough of low pressure located in the western portion of the composite region for the *SD_NWSE* jets has a north-south orientation, in contrast to the pressure troughs observed for the previously-discussed jet types, which were oriented southwest-northeast. Similar to the other types, an anticyclone is present in the southeastern portion of the composite region. However, the composite central pressure (1016 mb) is smaller than for all but the *AC_EW* jets. As expected, given the weak character of the pressure systems, the pressure gradient is also weak, although note that the strongest gradient is located over or slightly to the east of the composite jet core. The pressure

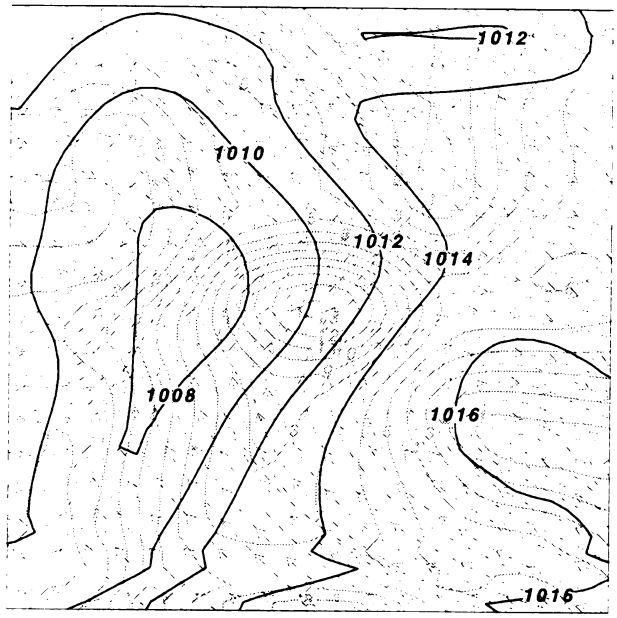

Figure 5.29. Composite Surface Pressure plotted on Level 1 Composite Airflow Configuration -- *SD_NWSE* Jets. As in Figure 5.1.

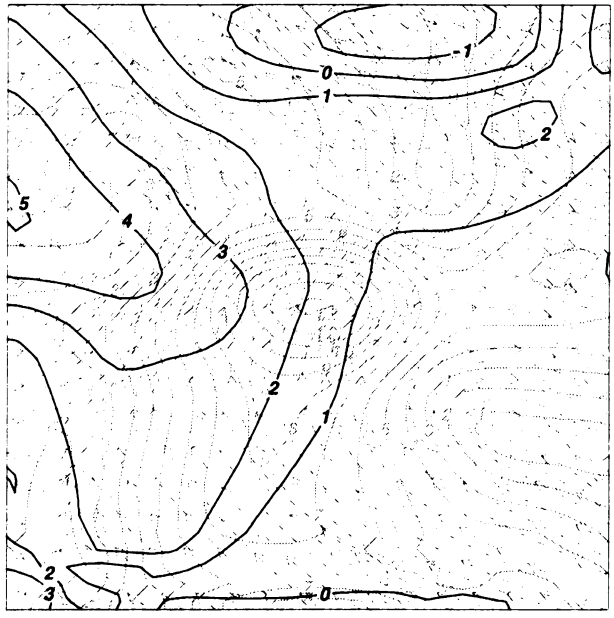

Figure 5.30. Composite 12-h Surface Pressure Tendency plotted on Level 1 Composite Airflow Configuration -- *SD_NWSE* Jets. As in Figure 5.2.

change over the previous 12 h is not very strong either (see Figure 3.30); although, in agreement with other types, pressures have risen to the northwest of the wind maximum. Similar to the *AC_EW* and *KC_SWNE* jets, pressure falls, although small, are evident northeast of the jet core.

b. Geostrophic and Ageostrophic Wind

Similar to *AC_EW* jets, the geostrophic wind component for *SD_NWSE* jets is weaker than the ageostrophic component (Figure 5.31). This pattern was expected given the very weak pressure gradient associated with *SD_NWSE* jets. As for all the previous jet types, the largest geostrophic wind vectors are co-located with the composite jet core. Also, the spatial pattern of the ageostrophic wind component is almost identical to that of the previous types (Figure 5.32). The ageostrophic wind is fairly strong near the jet core, resulting in supergeostrophic winds. The familiar rotation of the ageostrophic wind with latitude through the jet core is evident on the *SD_NWSE* composites, and, in the southwestern portion of the composite region, the ageostrophic wind vectors are deflected to the west.

c. Mid-tropospheric Heights and Upper-tropospheric Wind Field

The composite 500-mb geopotential height field for *SD_NWSE* differs from the field for all the previously-discussed airflow configuration types (Figure 5.33). A strong ridge is evident to the east of the jet core. The low-level wind maximum is found in a region of a weak 500-mb height gradient, although immediately north of the jet core the gradient increases substantially. An upper-level jet streak is associated with the northern height gradient, as indicated by the isotach maximum on the 200-mb airflow composite (Figure 5.34). A possible connection between the upper-tropospheric and lower-tropospheric wind maxima is suggested. The low-level wind maximum is again located underneath the right entrance region of a jet streak and south of a region of

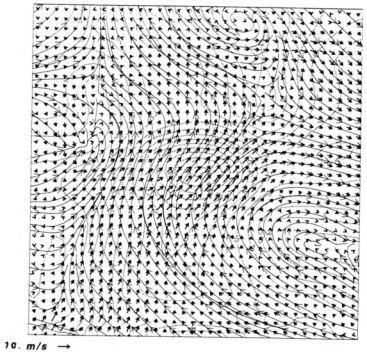

Figure 5.31. Composite Geostrophic Wind, Level 1 – *SD_NWSE* Jets. As in Figure 5.3.

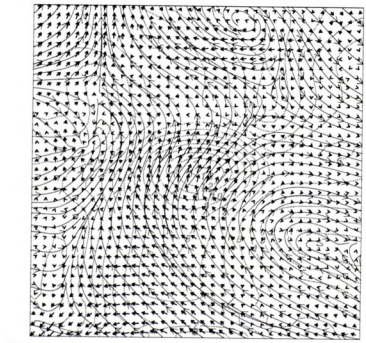

Figure 5.32. Composite Ageostrophic Wind, Level 1 – *SD_NWSE* Jets. As in Figure 5.3.

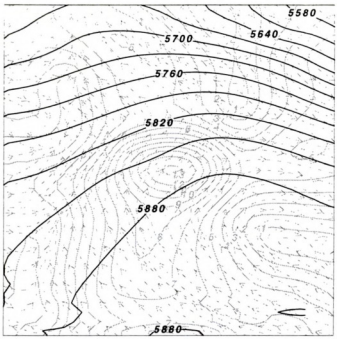

Figure 5.33. Composite 500-mb Geopotential Height plotted on Level 1 Composite Airflow Configuration -- *SD_NWSE* Jets. As in Figure 5.5.

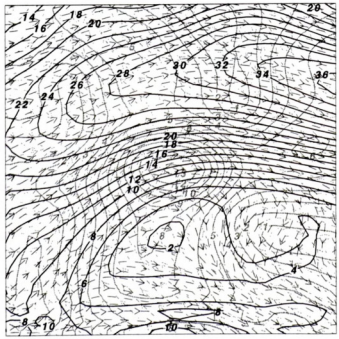

Figure 5.34. Composite 200-mb Isotachs and Streamlines plotted on Level 1 Composite Airflow Configuration -- *SD_NWSE* Jets. As in Figure 5.6.

upper-level divergence (Figure 5.35). The largest upper-level divergence is found downstream of the jet core, in the vicinity of the "split" in the low-level wind maximum. This region also experiences frequent convective activity, as shown in Chapter 4.

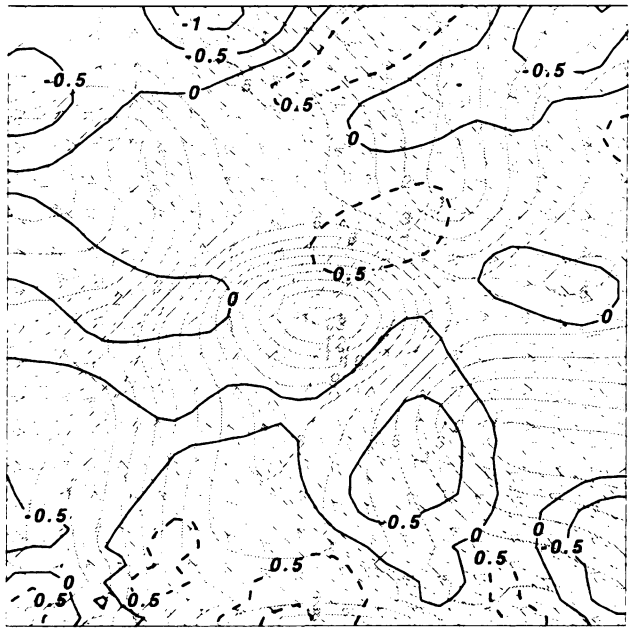

Figure 5.35. Composite 200-mb Divergence plotted on Level 1 Composite Airflow Configuration -- *SD_NWSE* Jets. As in Figure 5.7.

6. CC Jets

a. Surface Pressure and Surface Pressure Tendency

The sea-level pressure composite for *CC* jets is dominated by a large, fairly intense (central pressure of 1004 mb) low pressure system (Figure 5.36). The eastern anticyclone, a key feature of the pressure composites of the other types, is confined to the extreme eastern portion of the composite area and is shifted farther north such that the anticyclone center is located at approximately the same latitude as the jet core. Absent from the pressure composites for the *CC* jets is an anticyclone located northwest of the jet core. The composite jet core is again located along the western edge of the strong pressure gradient between the cyclone and the eastern anticyclone. The changes

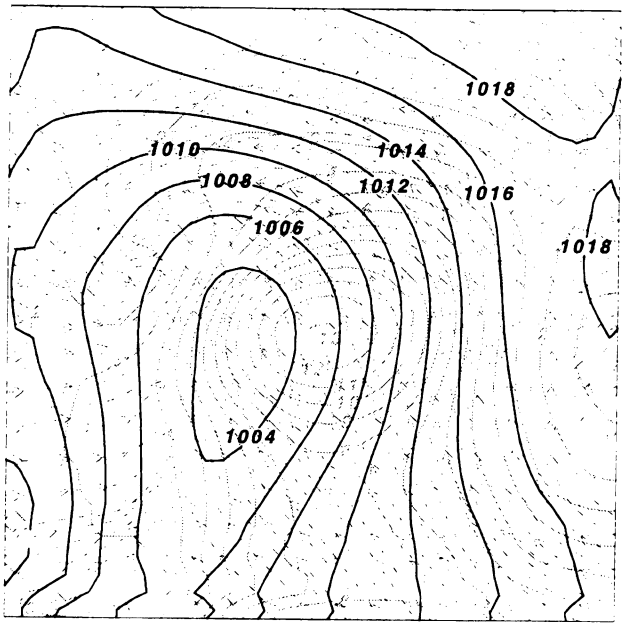

Figure 5.36. Composite Surface Pressure plotted on Level 1 Composite Airflow Configuration -- *CC* Jets. As in Figure 5.1.

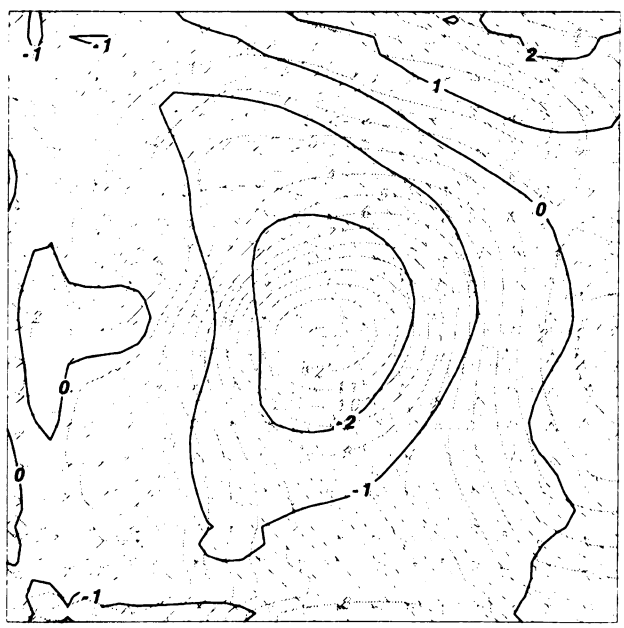

Figure 5.37. Composite 12-h Surface Pressure Tendency plotted on Level 1 Composite Airflow Configuration -- *CC* Jets. As in Figure 5.2.

in the pressure pattern during the previous 12 h also differ significantly from the other airflow configuration types (see Figure 5.37). The center of the low-level wind maximum is located in an area that had experienced a pressure fall of 2 mb in the previous 12 h. Unlike any other type, an area of pressure rise is evident in the northeast.

b. Geostrophic and Ageostrophic Wind

Despite the strong pressure gradient, the ageostrophic wind speeds for *CC* jets exceed the geostrophic wind speeds (Figures 5.38 and 5.39). The spatial pattern of the geostrophic wind supports the contention that pressure gradient forcing is not the primary mechanism behind this type of wind maximum. The local maximum of the geostrophic wind is displaced to the east and north of the jet core. Instead, one must consider the ageostrophic wind in order to explain the location of the jet core and the wind speeds within the core. The along-wind component of the ageostrophiccomponent is stronger than the cross-wind component, supporting the notion that the wind speeds are considerably ageostrophic. Like the previously-discussed types with a strong ageostrophic wind component (i.e., *AC_EW*, *KC_SWNE*), the strongest ageostrophic wind is observed to the left of the jet core. Strong ageostrophic winds in the southwestern portion of the analysis area are again present. For *CC* jets, however, the magnitude of the ageostrophic wind near the jet core clearly exceeds that of the ageostrophic wind southwest of the jet core. Unlike the previous types, the rotation of the ageostrophic wind vectors through the jet core is less pronounced upstream, and absent downstream of the jet core. An explanation for the absence of the rotation downstream of the wind maximum can possibly be found in the diurnal preference of *CC* jets. *CC* jets are primarily evening phenomena. Thus, the inertial component in the composite ageostrophic pattern is expected to be relatively weak. However, the existence of a strong ageostrophic wind component for wind maxima that occur primarily in the evening hours is an interesting finding. Possible reasons for the strong

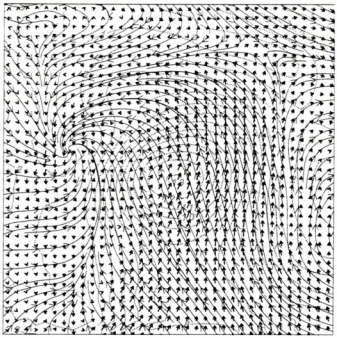

Figure 5.38. Composite Geostrophic Wind, Level 1 – CC Jets. As in Figure 5.3.

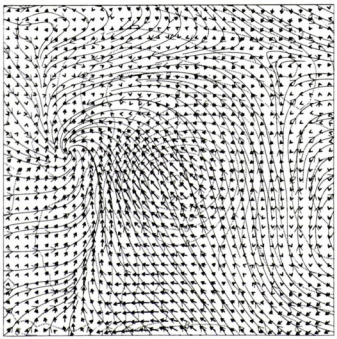

Figure 5.39. Composite Ageostrophic Wind, Level 1 – CC Jets. As in Figure 5.3.

ageostrophic component include cross-frontal airflow, as a strong confluence/frontal zone is present west of the jet core. A second reason may be an isallobaric wind component directed toward the region of largest pressure falls.

c. Mid-tropospheric Heights and Upper-tropospheric Wind Field

The composite 500-mb heights display a pronounced trough-ridge pattern, similar to that observed earlier for the *SD_SWNE* type (Figure 5.40). The trough west of the jet core supports the strong surface cyclone, and the jet core is observed downstream of the trough axis. As for the other "short" types, with the exception of the *AC_SWNE* jets, the low-level wind maximum is directed toward the right rear quadrant of an upper-level jet streak (Figure 5.41) and an area of upper-level divergence (Figure 5.42). However, the 200-mb airflow composite is more complex than that for the other types, as a second upper-level jet streak is observed in the extreme southeastern portion of the

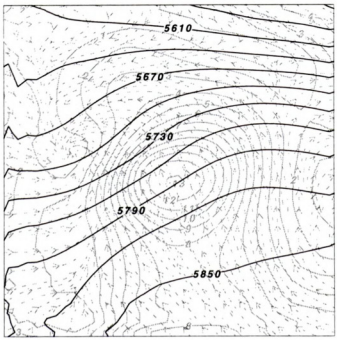

Figure 5.40. Composite 500-mb Geopotential Height plotted on Level 1 Composite Airflow Configuration -- CC Jets. As in Figure 5.5.

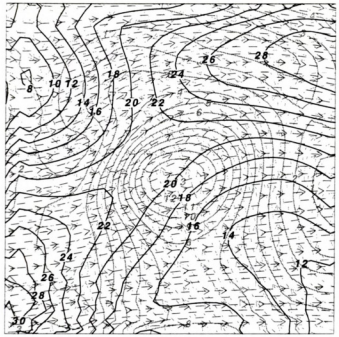

Figure 5.41. Composite 200-mb Isotachs and Streamlines plotted on Level 1 Composite Airflow Configuration -- CC Jets. As in Figure 5.6.

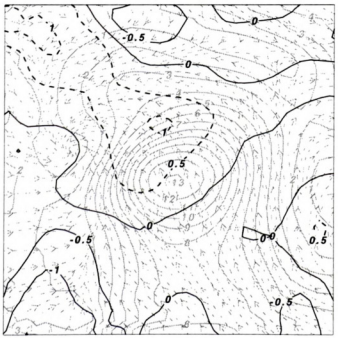

Figure 5.42. Composite 200-mb Divergence plotted on Level 1 Composite Airflow Configuration -- CC Jets.

analysis region. At the time of the composite, it appears that the low-level wind maximum is being influenced by the right front quadrant of this second jet streak. This pattern of an upper-level jet streak rotating through the "bottom" of a trough is the classic pattern for cyclogenesis (Hovanec and Horn 1975, and others), and provides further evidence that *CC* jets are associated with well organized, and probably intensifying, surface cyclones.

7. LAC_SWNE Jets

a. Surface Pressure and Surface Pressure Tendency

LAC_SWNE are the 'long' counterpart of the *AC_SWNE* jets. Not surprisingly, the 500-mb composites for the two jet types have a number of features in common (Figures 5.8 and 5.43). For both types, the most prominent surface feature is a high pressure system over the eastern portion of the analysis region. An important difference, however, is that for the *LAC_SWNE* jets the center of the high is located at approximately the same latitude as the jet core, whereas for the *AC_SWNE* jets the center of the high is found southeast of the jet core. Also, the average central pressure is slightly higher for *LAC_SWNE* jets (1020 mb) compared to *AC_SWNE* jets (1018 mb). Another feature the two types share is a southwest-northeast oriented trough of low pressure to the west of the wind maximum. However, the trough is slightly more intense for *LAC_SWNE* events, and furthermore only one closed isobar, located just west of the jet core, is present. In contrast, two centers of minimum pressure are observed for the *AC_SWNE* jets, one in the southwestern portion of the composite region and the other in the northwestern corner of the composite grid. Although marked pressure gradients are observed for both jet types, the gradient is somewhat stronger for the *LAC_SWNE* jets due to the more intense surface systems (i.e., stronger anticyclone and deeper pressure trough) for the *LAC_SWNE* events compared to the *AC_SWNE* jets. As expected, the jet core for the *LAC_SWNE* jets is located along the western edge of the pressure gradient.

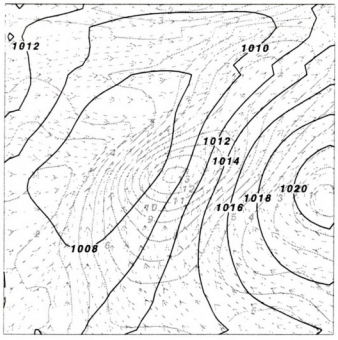

Figure 5.43. Composite Surface Pressure plotted on Level 1 Composite Airflow Configuration -- *LAC_SWNE* Jets. As in Figure 5.1.

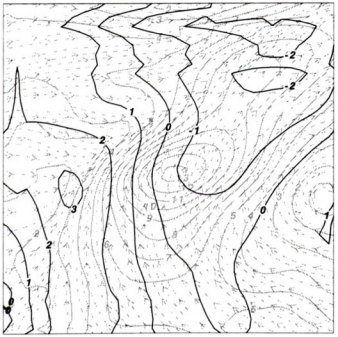

Figure 5.44. Composite 12-h Surface Pressure Tendency plotted on Level 1 Composite Airflow Configuration -- *LAC_SWNE* Jets. As in Figure 5.2.

Differences in the pressure tendency composite are also observed between the two jet types. While the main feature for the *AC_SWNE* jets (see Figure 5.44) is the weak pressure rises northwest of the jet core, the main feature for the *LAC_SWNE* events is the pressure falls northeast of the jet core.

b. Geostrophic and Ageostrophic Wind

The spatial pattern of the wind components is similar for the *LAC_SWNE* jets and *AC_SWNE* jets, in that the geostrophic wind is stronger than the ageostrophic wind (Figures 5.45 and 5.46). Large geostrophic components are associated with strong pressure gradients evident for both jet types. For the *LAC_SWNE* jets, the geostrophic wind speeds are largest north of the wind maximum where the geostrophic wind vector is aligned with the actual wind. Although the geostrophic component is still fairly respectable near the jet core, the direction is more westerly than the actual wind. On the other hand, the ageostrophic component in the vicinity of the jet core is southeasterly and is directed toward the confluence zone. This orientation occurs in spite of the lack of pressure rises northwest of the confluence zone. It appears that the pressure fall associated with the passage of a confluence/frontal boundary has an effect on the ageostrophic wind component even though the pressure changes suggest that the front is not undergoing any strengthening.

c. Mid-tropospheric Heights and Upper-tropospheric Wind Field

LAC_SWNE jets have greater mid- and upper-tropospheric support compared to *AC_SWNE* jets. Whereas the *AC_SWNE* jets have little dynamic support, as suggested by their location near a 500 mb ridge and their inconclusive relationship with a 200 mb jet streak, *LAC_SWNE* jets are located downstream of a pronounced 500 mb longwave trough (Figure 5.47) and near the right entrance region of a 200 mb jet streak (Figure

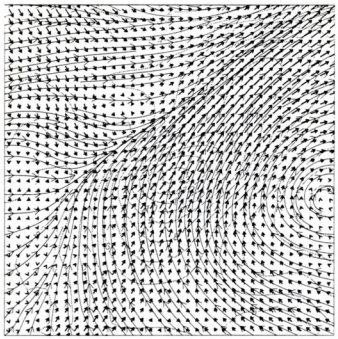

Figure 5.45. Composite Geostrophic Wind, Level 1 – *LAC_SWNE* Jets. As in Figure 5.3.

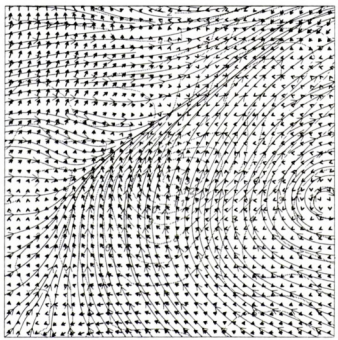

Figure 5.46. Composite Ageostrophic Wind, Level 1 – *LAC_SWNE* Jets. As in Figure 5.3.

5.48). The upper-level divergence generated by the jet streak is located immediately downstream of the jet core (Figure 5.49).

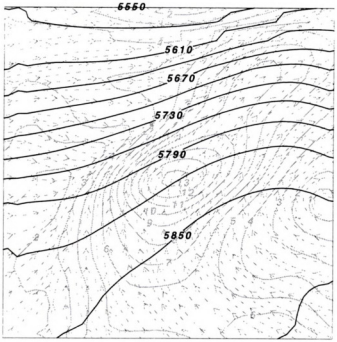

Figure 5.47. Composite 500-mb Geopotential Height plotted on Level 1 Composite Airflow Configuration -- *LAC_SWNE* Jets. As in Figure 5.5.

8. 2LA Jets

a. Surface Pressure and Surface Pressure Tendency

As described in Chapter 4, the airflow configuration of *L2A* jets consists of two closed anticyclonic centers, and the jet core is found either to the west of the northern closed circulation, to the west of the southern closed circulation, or in-between the two centers. In order to preserved the airflow configuration, the wind maxima were composited relative to the two closed circulations rather than with respect to the jet core. This approach makes the low-, mid-, and upper-tropospheric composites more difficult to interpret compared to the other jet types, as the center of the composite map does not reflect the location of the jet core. Instead, it represents the area west of the

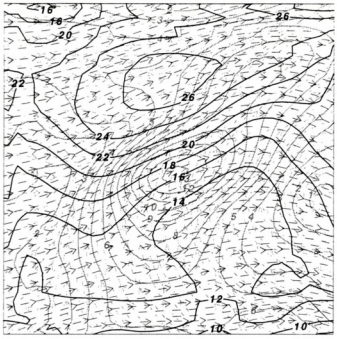

Figure 5.48. Composite 200-mb Isotachs and Streamlines plotted on Level 1 Composite Airflow Configuration -- *LAC_SWNE* Jets. As in Figure 5.6.

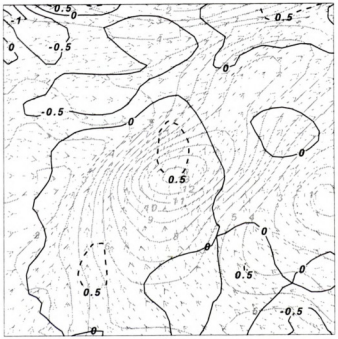

Figure 5.49. Composite 200-mb Divergence plotted on Level 1 Composite Airflow Configuration -- *LAC_SWNE* Jets. As in Figure 5.7.

two closed anticyclonic circulations, about equidistant between the two centers. An extensive high pressure ridge is evident across the eastern portion of the composite sea-level pressure map (Figure 5. 50). The northern portion of this ridge is more intense, as indicated by the closed isobars (central pressure of 1020 mb). Note that the closed anticyclonic circulation on the airflow composite agrees well with the location of the center of the northern high. The pressure ridge is not as strong to the south, and a closed isobar is not present. Another important feature of the pressure composite is the north-south oriented low-pressure (central pressure of 1008 mb) across the western portion of the composite. A fairly strong pressure gradient between the latitudinally-extensive eastern ridge and western trough is observed over the central portion of the composite grid. Pressure falls are greatest immediately east of the pressure trough, whereas pressure rises are observed over the extreme western and eastern portions of the analysis region (Figure 5.51).

b. Geostrophic and Ageostrophic Wind

The pressure gradient between the western pressure trough and eastern pressure ridge sets the stage for strong geostrophic winds (Figure 5.52). The *L2A* jets resemble the *AC_SWNE* jets in that their geostrophic wind is considerably stronger than the ageostrophic wind (Figure 5.53). The ageostrophic component throughout most of the central portion of the map is oriented toward the west, and is weak. A noteworthy area of stronger ageostrophic winds is again found in the southwest. The orientation, towards the west, suggests possible frictional or thermal influences.

c. Mid-tropospheric Height and Upper-tropospheric Wind Field

A ridge is evident over the eastern third of the composite map of 500-mb geopotential height (Figure 5.54). Surprisingly, given the well-defined surface pressure trough, only a slight indication of upper-level troughing is evident on the 500-mb

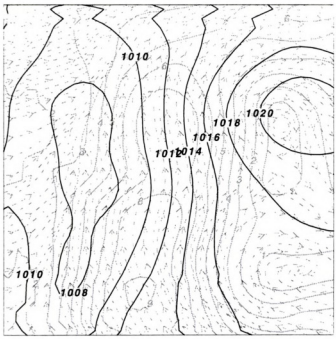

Figure 5.50. Composite Surface Pressure plotted on Level 1 Composite Airflow Configuration -- *L2A* Jets. As as in Figure 5.1.

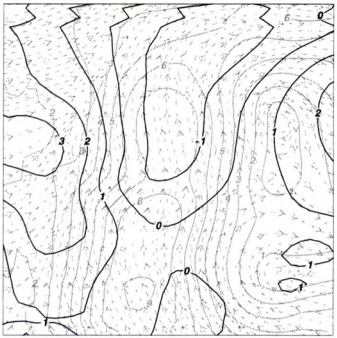

Figure 5.51. Composite 12-h Surface Pressure Tendency plotted on Level 1 Composite Airflow Configuration -- *L2A* Jets. As in Figure 5.2.

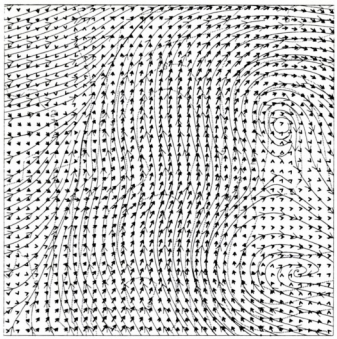

10. m/s →

Figure 5.52. Composite Geostrophic Wind, Level 1 – *L2A* Jets. As in Figure 5.3.

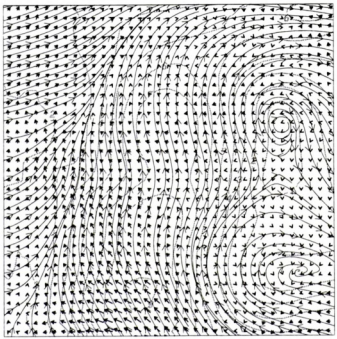

10. m/s →

Figure 5.53. Composite Ageostrophic Wind, Level 1 – *L2A* Jets. As in Figure 5.3.

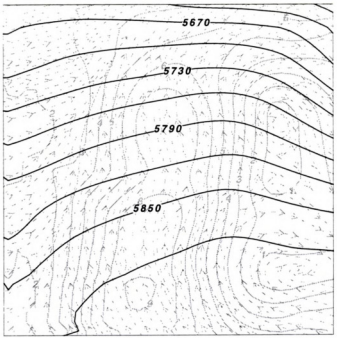

Figure 5.54. Composite 500-mb Geopotential Height plotted on Level 1 Composite Airflow Configuration -- *L2A* Jets. As in Figure 5.5.

composite. The 500-mb height gradient over the northern portion of the composite region is considerably weaker than the gradients observed for any of the previous jet types. However, the weaker gradient may be an artifact of the method used to center the composite. The 200-mb kinematic pattern follows a now familiar pattern. The highest low-level wind speeds is located south of the entrance region of an upper-tropospheric jet streak (Figure 5.55) Upper-level divergence is evident immediately downstream of the low-level wind maximum (Figure 5.56).

9. LSKC_SWNE Jets

a. Surface Pressure and Surface Pressure Tendency

The next airflow configuration type to be discussed, *LSKC_SWNE* jets, is the 'long' counterpart of the *KC_SWNE* jets. Both jet types are associated with a southwest-northeast oriented surface pressure trough located to the west of the jet core and with an

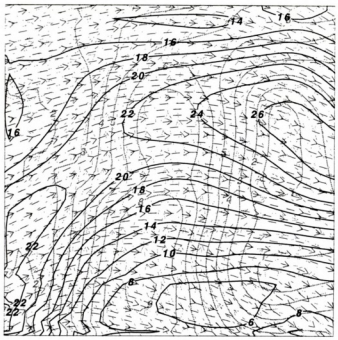

Figure 5.55. Composite 200-mb Isotachs and Streamlines plotted on Level 1 Composite Airflow Configuration -- *L2A* Jets. As in Figure 5.6.

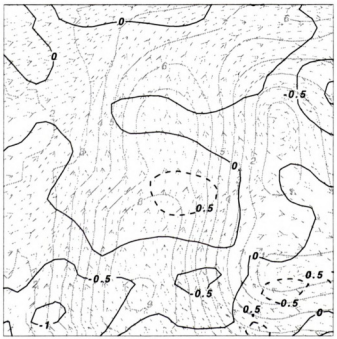

Figure 5.56. Composite 200-mb Divergence plotted on Level 1 Composite Airflow Configuration -- *L2A* Jets. As in Figure 5.7

eastern pressure ridge (Figures 5.57 and Figure 5.15). The strength of the pressure gradient between these two features is similar for the two jet types, although the pressure trough is more intense for the *LSKC_SWNE* events and the ridge is stronger for the *KC_SWNE* jets. A second high pressure system is observed in the northwest portion of the composite grid for both types, although this high is not as strong for the *LSKC_SWNE* jets. An important difference between the two types, however, is the location of the closed isobar within the surface pressure trough. For the *LSKC_SWNE* jets, the closed isobar to the west/southwest of the jet core, whereas for the *KC_SWNE* jets it is located north/northeast of the jet core.

For both types, large pressure rises over the past 12 h are found west and northwest of the jet core, although the average increase for *LSKC_SWNE* jets is only 6 mb compared to 10 mb for *KC_SWNE* jets. The pattern of pressure falls differs substantially, however (Figure 5.58). The average pressure falls are smaller for the *LSKC_SWNE* jets (only - 2 mb) compared to the *KC_SWNE* jets (- 5 mb). Also, the largest pressure falls for the *LSKC_SWNE* jets are located immediately northeast of the jet core, whereas the largest falls for the *KC_SWNE* jets are found in the extreme northeastern portion of the composite grid.

b. Geostrophic and Ageostrophic Wind

Substantial differences in the geostrophic and ageostrophic wind fields are observed between *LSKC_SWNE* and *KC_SWNE* jets. For both types, the strongest geostrophic wind vectors are located over and northeast of the jet core (Figures 5.59 and 5.17). However, the vectors for the *LSKC_SWNE* jets have a southwesterly orientation in comparison to the west-southwesterly orientation for the *KC_SWNE* jets. For the *LSKC_SWNE* jets, the ageostrophic component is weaker than the geostrophic component, whereas the ageostrophic and geostrophic components for *KC_SWNE* jets have similar magnitudes. For the *LSKC_SWNE* jets, the ageostrophic component in the

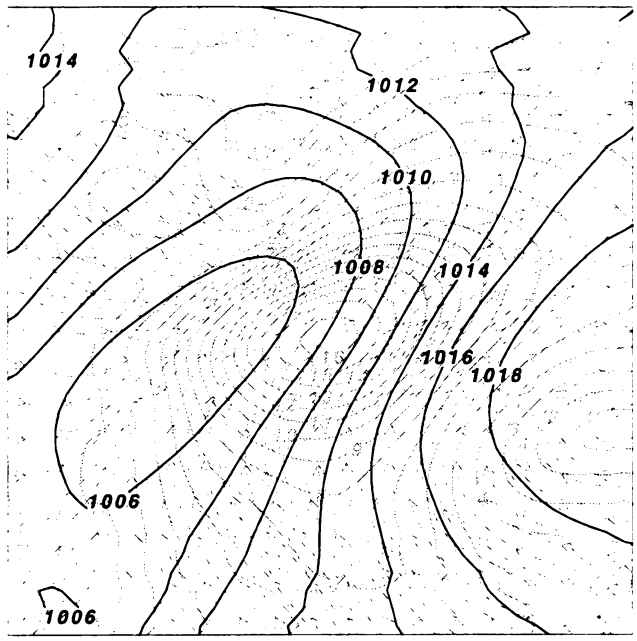

Figure 5.57. Composite Surface Pressure plotted on Level 1 Composite Airflow Configuration -- *LSKC_SWNE* Jets. As in Figure 5.1.

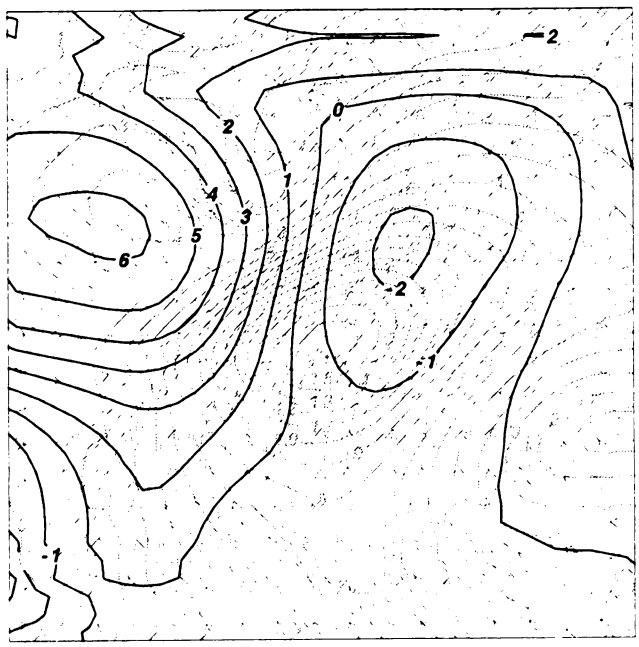

Figure 5.58. Composite 12-h Surface Pressure Tendency plotted on Level 1 Composite Airflow Configuration – *LSKC_SWNE* Jets. As in Figure 5.2.

vicinity of the jet core is directed to the north, whereas it is directed to the north/northwest for the *KC_SWNE* jets (Figures 5.60 and 5.11). For both types there is a fairly small area west of the jet core where the ageostrophic wind speeds are large and directed toward the confluence/frontal zone.

Possible explanations for the weaker ageostrophic wind for the *LSKC_SWNE* jets can be found in the differences in the diurnal preferences for the two jet types. *KC_SWNE* jets are almost exclusively observed during the early morning hours when the inertial component of the ageostrophic wind is expected to contribute to strongly supergeostrophic wind speeds. On the other hand, only two-thirds of the *LSKC_SWNE* jets were observed at 2100 UTC. Also, the confluence/frontal boundary is suspected to be stronger for the *KC_SWNE* jets due to the large 12 h pressure rises west of the confluence zone.

c. Mid-tropospheric Heights and Upper-tropospheric Wind Field

The mid- and upper-tropospheric environment appears to play a role in the development of *LSKC_SWNE* low-level wind maxima, similar to *KC_SWNE* jets. At the 500-mb level, the geopotential height field is almost identical to that for *KC_SWNE* jets with a trough in the west and a ridge in the east (Figure 5.61). Upper-level jet streaks are found in similar locations relative to the two types of low-level wind maxima. The *LSKC_SWNE* jets are also found underneath the right entrance region of the upper-level jet (Figure 5.62). Despite the fact that the speed of the upper-level jet is higher for *KC_SWNE* jets, the 200-mb divergence field downstream of the low-level jet core is stronger for *LSKC_SWNE* jets (Figure 5.63).

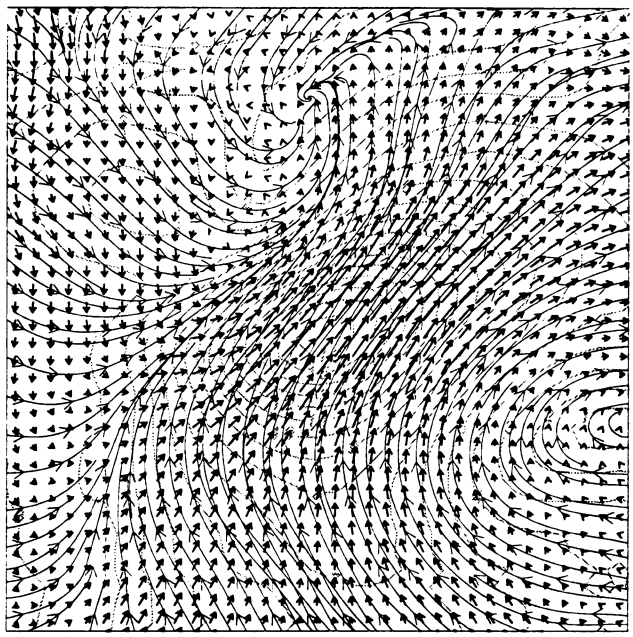

10. m/s →

Figure 5.59. Composite Geostrophic Wind, Level 1 – *LSKC_SWNE* Jets. As in Figure 5.3.

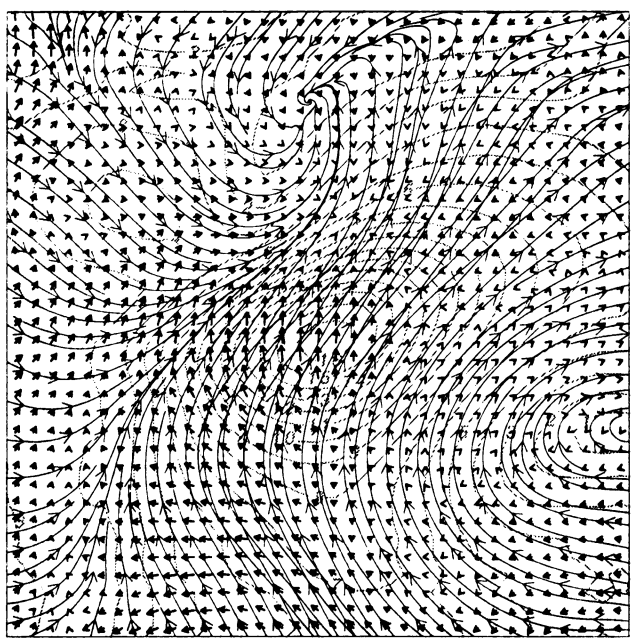

10. m/s →

Figure 5.60. Composite Ageostrophic Wind, Level 1 – *LSKC_SWNE* Jets. As in Figure 5.3.

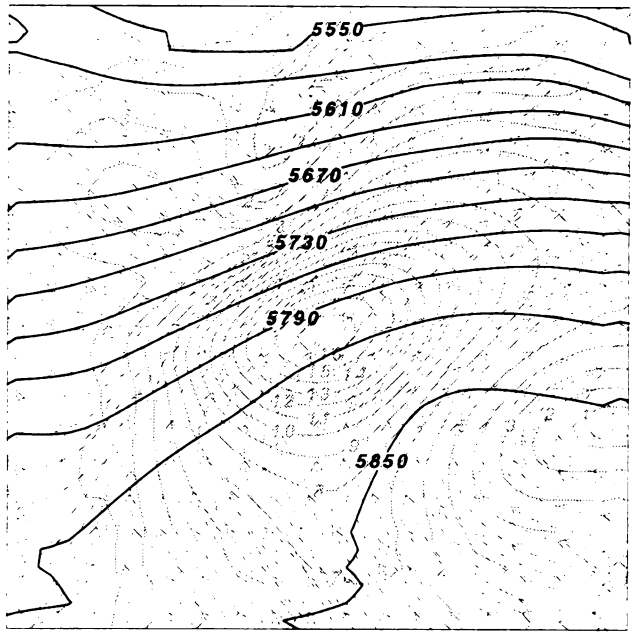

Figure 5.61. Composite 500-mb Geopotential Height plotted on Level 1 Composite Airflow Configuration -- *LSKC_SWNE* Jets. As in Figure 5.5.

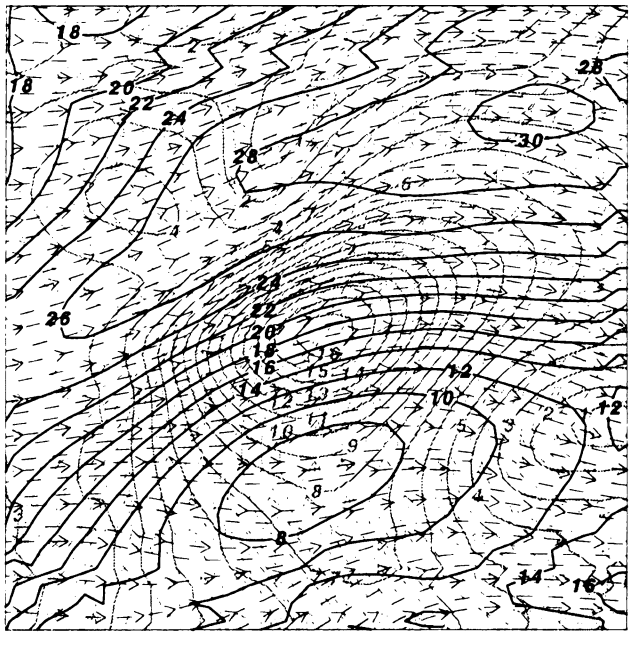

Figure 5.62. Composite 200-mb Isotachs and Streamlines plotted on Level 1 Composite Airflow Configuration -- *LSKC_SWNE* Jets. As in Figure 5.6.

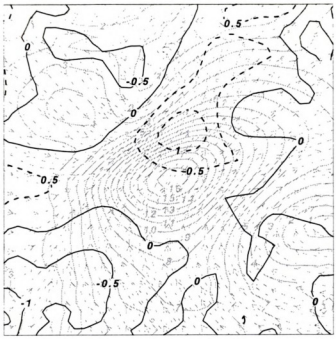

Figure 5.63. Composite 200-mb Divergence plotted on Level 1 Composite Airflow Configuration -- *LSKC_SWNE* Jets. As in Figure 5.7.

10. LSPLIT Jets

a. Surface Pressure and Surface Pressure Tendency

The three remaining types of low-level wind maxima have fairly similar surface pressure patterns. Unlike the more complex pattern of most of the 'short' patterns, they are characterized by a single center of low pressure to the west and a single center of high pressure to the east. *LSPLIT* jets, for example, have a moderate pressure gradient between a low (central pressure of 1008 mb) to the west and a high (central pressure of 1018 mb) to the east (Figure 5.64). The jet core, as in the previously-discussed cases, is located along the western edge of that pressure gradient. The surface pressure tendency over the previous 12 h sets the *LSPLIT* jets apart from all the other jet configuration types. While the jet center is located in an area that had experienced a minimal rise in pressure, two areas, one to the southwest (4 mb) and another to the northeast (6 mb) of

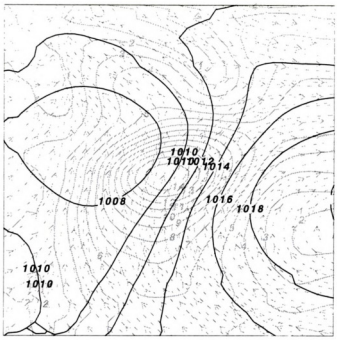

Figure 5.64. Composite Surface Pressure plotted on Level 1 Composite Airflow Configuration -- *LSPLIT* Jets. As in Figure 5.1.

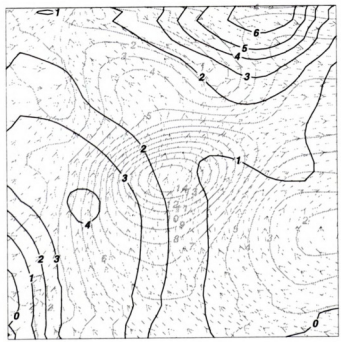

Figure 5.65. Composite 12-h Surface Pressure Tendency plotted on Level 1 Composite Airflow Configuration -- *LSPLIT* Jets. As in Figure 5.2.

the wind maximum, have experienced larger rises in pressure (see Figure 5.65). No area of pressure falls is evident for *LSPLIT* jets.

b. Geostrophic and Ageostrophic Wind

The ageostrophic wind component of *LSPLIT* jets is as strong as the geostrophic wind component (Figures 5.66 and 5.67), unlike the three previously-discussed "long" configuration types where the geostrophic wind was dominant. For the *LSPLIT* events, the geostrophic wind is strongest northwest of the jet core. A distinct "split" in the geostrophic wind vectors is evident along the western and eastern branches of the *LSPLIT* jets. In terms of the ageostrophic component, the primary region of strong values is located west of the jet core and a secondary area is located in the southwestern portion of the composite grid. This pattern is similar to that of the majority of the jet types. The ageostrophic wind vectors near the jet core are directed toward the low pressure system to the west. Farther south, the vectors are not evident from the ageostrophic wind vectors. The rotation of the ageostrophic wind vector with latitude is only observed upstream of the jet core.

c. Mid-tropospheric Heights and Upper-tropospheric Wind Field

LSPLIT jets are located downstream of a 500-mb trough, although the trough is not as strong as for other types of jets (Figure 5.68). Also, *LSPLIT* jets occur underneath the right entrance quadrant of a 200-mb jet streak (Figure 5.69). Similar to the three 'long' types described above, an area of 200-mb divergence is located immediately downstream of the jet core (Figure 5.70).

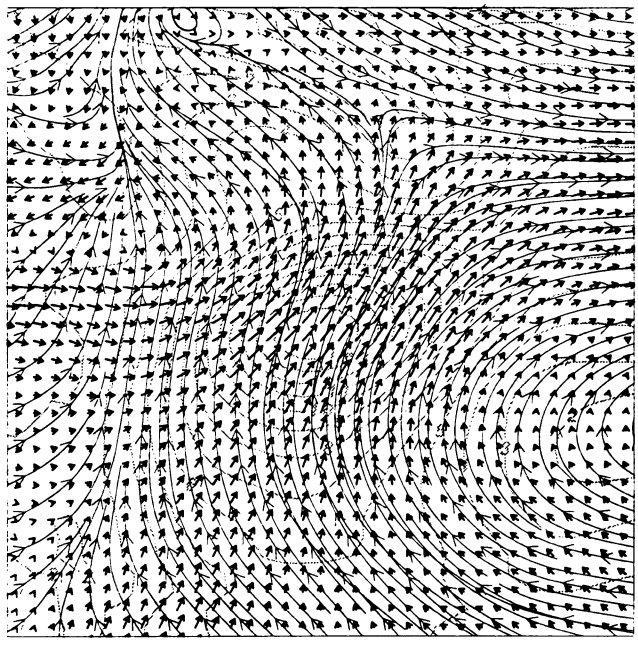

Figure 5.66. Composite Geostrophic Wind, Level 1 – *LSPLIT* Jets. As in Figure 5.3.

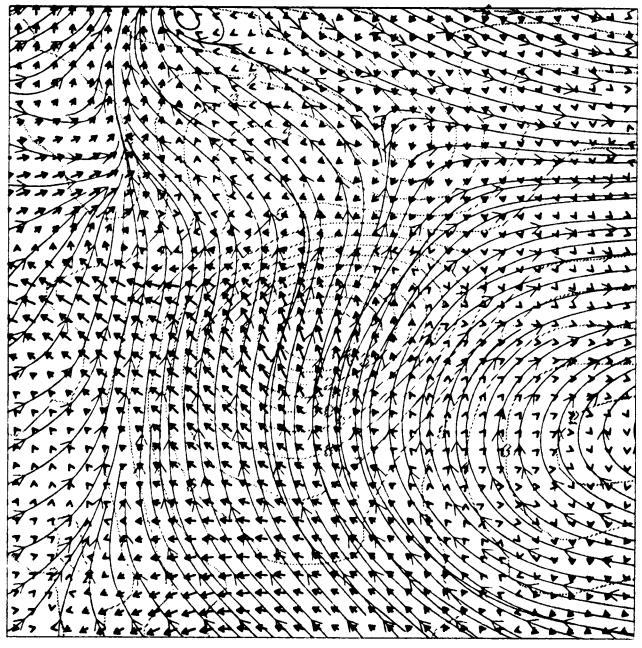

Figure 5.67. Composite Ageostrophic Wind, Level 1 – *LSPLIT* Jets. As in Figure 5.3.

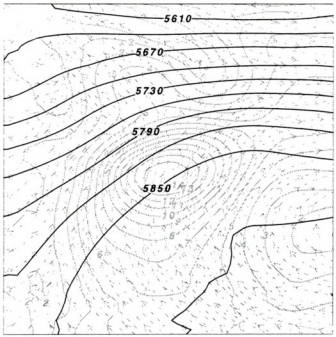

Figure 5.68. Composite 500-mb Geopotential Height plotted on Level 1 Composite Airflow Configuration -- *LSPLIT* Jets. As in Figure 5.5.

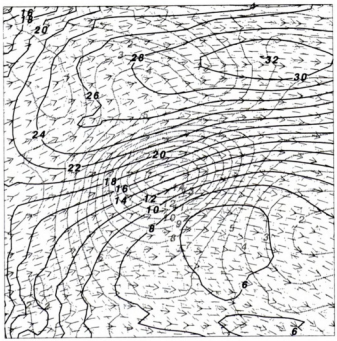

Figure 5.69. Composite 200-mb Isotachs and Streamlines plotted on Level 1 Composite Airflow Configuration -- *LSPLIT* Jets. As in Figure 5.6.

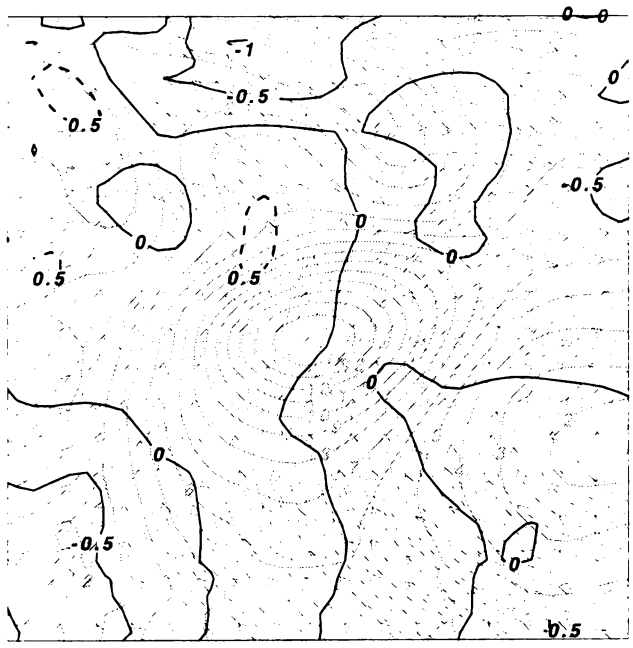

Figure 5.70. Composite 200-mb Divergence plotted on Level 1 Composite Airflow Configuration – *LSPLIT* Jets. As in Figure 5.7.

11. LKC_SWNE Jets

a. Surface Pressure and Surface Pressure Tendency

The next to the last airflow configuration type, *LKC_SWNE* jet is characterized by a mean surface pressure pattern with very distinct pressure cells. A strong low-pressure system (central pressure of 1004 mb) is located southwest of the wind maximum, while a strong high (central pressure of 1020 mb) is found along the eastern margin of the composite area (Figure 5.71). The pressure gradient in the vicinity of the jet core is stronger for *LKC_SWNE* jets than for any other type. The low pressure system appears to have advanced eastward during the previous 12 hours, resulting in large (6 mb) pressure falls (6 mb) downstream of the low-level wind maximum within the left branch of the split flow (Figure 5.72).

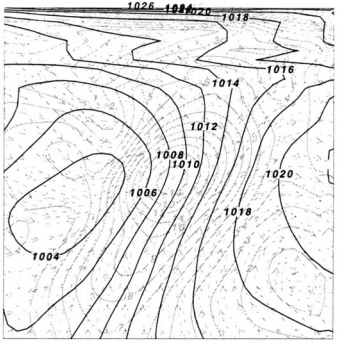

Figure 5.71. Composite Surface Pressure plotted on Level 1 Composite Airflow Configuration -- *LKC_SWNE* Jets. As in Figure 5.1.

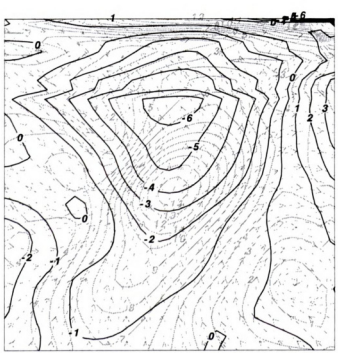

Figure 5.72. Composite 12-h Surface Pressure Tendency plotted on Level 1 Composite Airflow Configuration -- *LKC_SWNE* Jets. As in Figure 5.2.

b. Geostrophic and Ageostrophic Wind

As a result of the strong pressure gradient, the geostrophic component of the wind is the dominant contributor to the observed airflow pattern for *LKC_SWNE* jets. geostrophic winds are observed in the vicinity of the jet core (Figure 5.73). The strongest geostrophic winds are observed in the vicinity of the jet core, and the spatial pattern of the geostrophic wind vectors roughly duplicates the split flow of the observed wind. The ageostrophic component for *LKC_SWNE* jets is considerably smaller than the geostrophic component. Thus, the speed of *LKC_SWNE* jets is only slightly supergeostrophic. As in previous types, the contribution of ageostrophic to the actual wind consists in to deflect the actual wind to the left of the geostrophic wind (Figure 5.74). The strongest ageostrophic wind components are observed to the north and northeast of the jet core, and are oriented into a region of maximum pressure falls north of the jet core. Consequently, the isallobaric contribution to the actual wind appears to be large for *LKC_SWNE* jets.

c. Mid-tropospheric Heights and Upper-tropospheric Wind Field

LKC_SWNE jets are located immediately upstream of a 500 mb ridge axis (Figure 5.75). Further upstream, a strong upper-level trough is present. The geopotential height gradient north of the jet core is very strong, and the 200 mb jet streak is faster (42 ms-1) for the *LKC_SWNE* jets than for any other type (Figure 5.76). The superposition of the two jets places the low-level wind maximum, particularly the left branch of the split flow, underneath the right entrance region of the upper-level jet streak (Figure 5.77). An extended area of upper-level divergence is located to the north and northeast of the low-level wind maximum core. Centers of larger divergence are evident immediately to the north of the wind maximum in the left branch and to the east in the right branch.

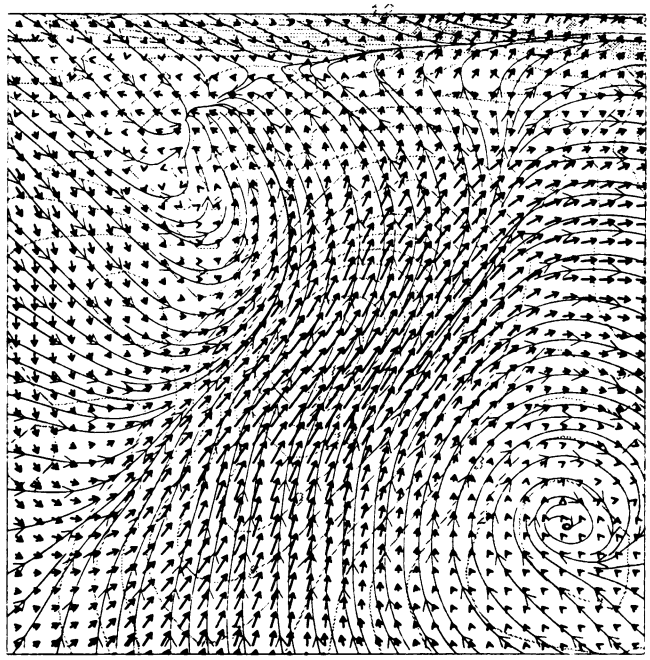

Figure 5.73. Composite Geostrophic Wind, Level 1 – *LKC_SWNE* Jets. As in Figure 5.3.

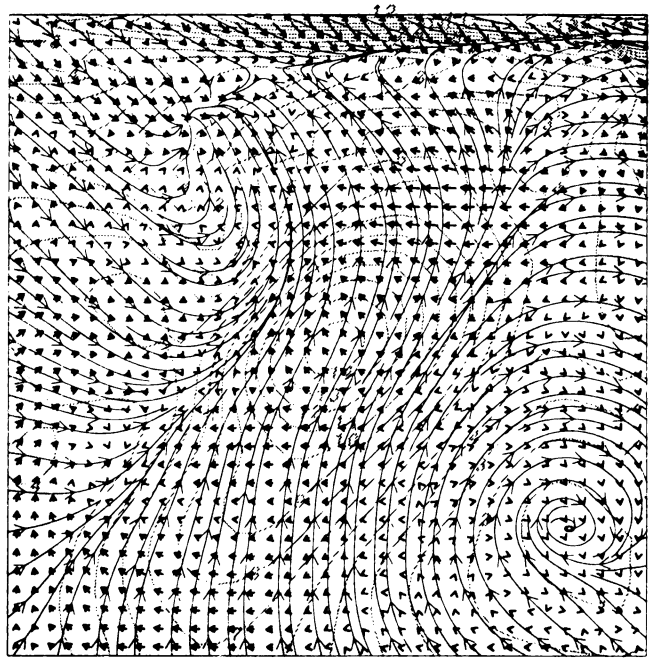

Figure 5.74. Composite Ageostrophic Wind, Level 1 – *LKC_SWNE* Jets. As in Figure 5.3.

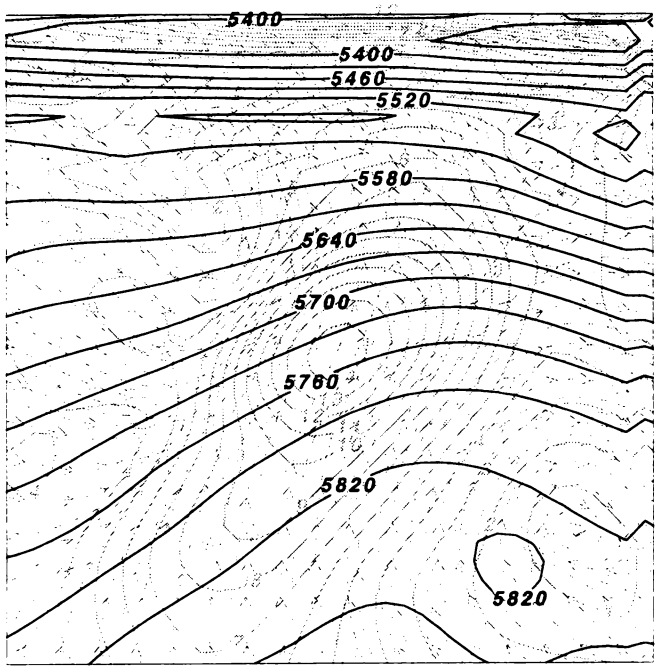

Figure 5.75. Composite 500-mb Geopotential Height plotted on Level 1 Composite Airflow Configuration -- *LKC_SWNE* Jets. As in Figure 5.5.

very strong. At the 200-mb level, a strong jet streak is evident (42 ms^{-1}) (Figure 5.76). The superposition of the two features places the low-level wind maximum, particularly the left branch of the split flow, underneath its right entrance region. Thus, an extended area of upper-level divergence is located to the north and northeast of the jet core (Figure 5.77). Centers of stronger divergence are evident immediately to the north of the wind maximum in the left branch and to the east in the right branch.

12. LCC Jets

a. Surface Pressure and Surface Pressure Tendency

The final low-level wind maximum type, *LCC* jets, also is embedded in a fairly simple surface pressure configuration (Figure 5.78). A trough of low pressure extends north along the western edge of the wind maximum and a distinct high pressure cell is evident to the east. Compared with the previous types, the high pressure area is located

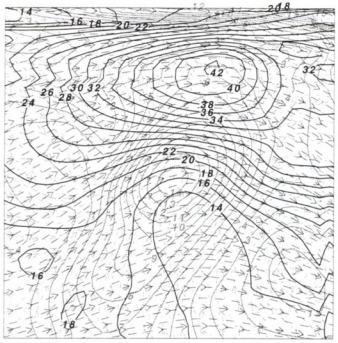

Figure 5.76. Composite 200-mb Isotachs and Streamlines plotted on Level 1 Composite Airflow Configuration -- *LKC_SWNE* Jets. As in Figure 5.6

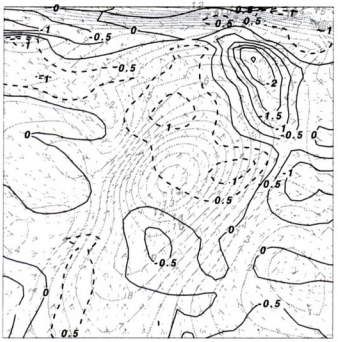

Figure 5.77. Composite 200-mb Divergence plotted on Level 1 Composite Airflow Configuration -- *LKC_SWNE* Jets. As in Figure 5.7.

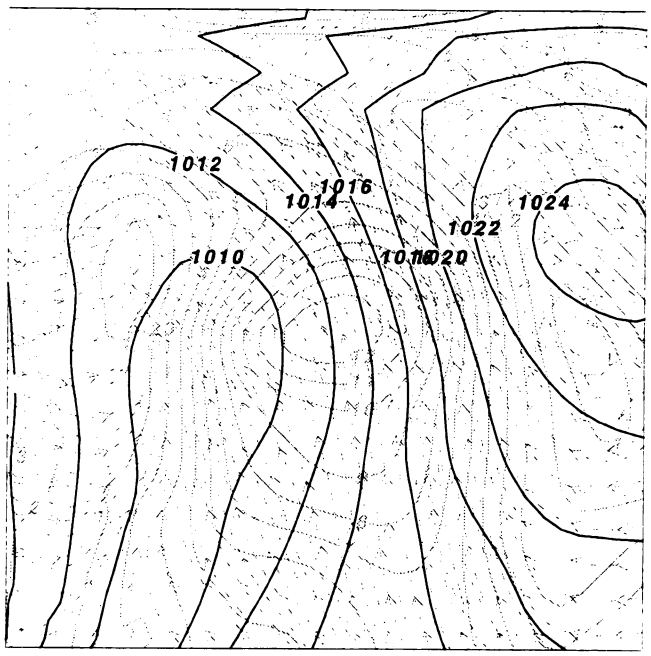

Figure 5.78. Composite Surface Pressure plotted on Level 1 Composite Airflow Configuration -- *LCC* Jets. As in Figure 5.1

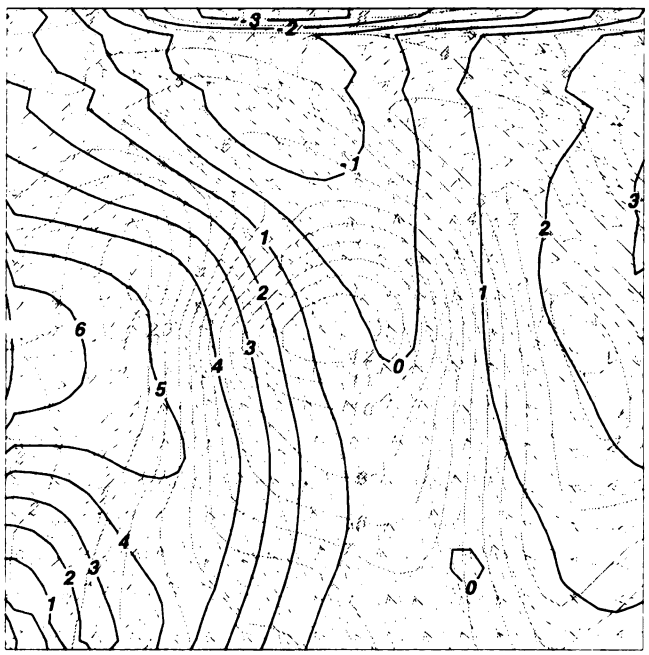

Figure 5.79. Composite 12-h Surface Pressure Tendency plotted on Level 1 Composite Airflow Configuration – *LCC* Jets. As in Figure 5.2.

considerably farther north. Only for the *L2A* types is the latitude of the high pressure cell as far north, relative to the wind maximum, as that for the *LCC* jets. Another difference between *LCC* jets and all the other types is that the ridge of surface high pressure, in which the high pressure cell is located, has a northwest-southeast orientation, rather than a north-south or southwest-northeast orientation. The jet core is found in its familiar location – the western edge of the pressure gradient between the low to the west and the high to the east. The pressure pattern has undergone moderate changes in the previous 12 h (Figure 5.79). An area of pressure falls is evident north of the wind maximum. It is bounded by two areas that experienced a rise in pressure over the previous time period. The pressure rise in the west is stronger (6 mb) compared to the pressure rise in the east (3 mb).

b. Geostrophic and Ageostrophic Wind

The mean pressure pattern produces an elongated zone of strong geostrophic winds east of the low-level wind maximum (Figure 5.80). Similar to a number of other jet types, the strongest geostrophic wind vectors are not collocated with the jet core. Rather they are displaced to the northeast. Compared with the geostrophic wind, strong ageostrophic wind components are confined to either (1) the area just west of the jet core, or (2) the southwestern portion of the analysis region (Figure 5.81). Within the jet core itself, the geostrophic and ageostrophic components have similar magnitudes, but very large differences in orientation are evident. The geostrophic component is directed toward the north, whereas the ageostrophic component is directed toward the confluence center located northwest of the jet core.

c. Mid-tropospheric Heights and Upper-tropospheric Wind Field

The 500-mb mean geopotential height pattern for *LCC* jets set itself apart from any other jet type (Figure 5.82). A distinct split-flow pattern is evident with a cut-off low

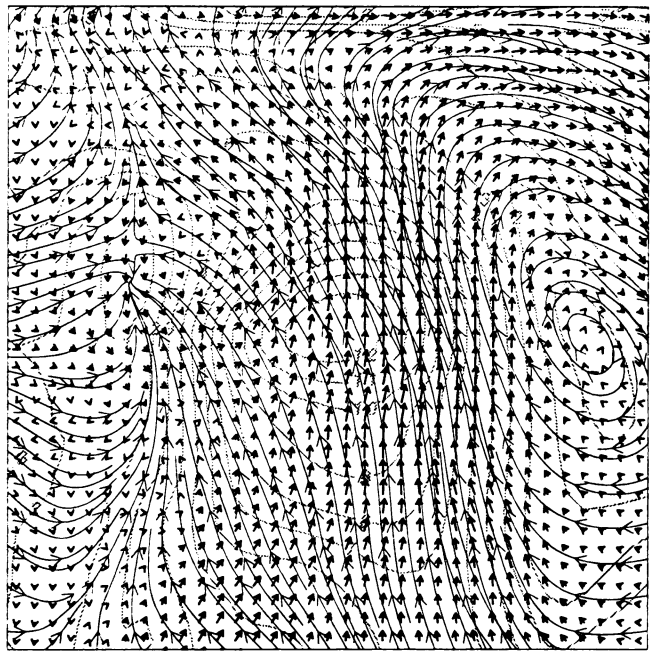

Figure 5.80. Composite Geostrophic Wind, Level 1 – *LCC* Jets. As in Figure 5.3.

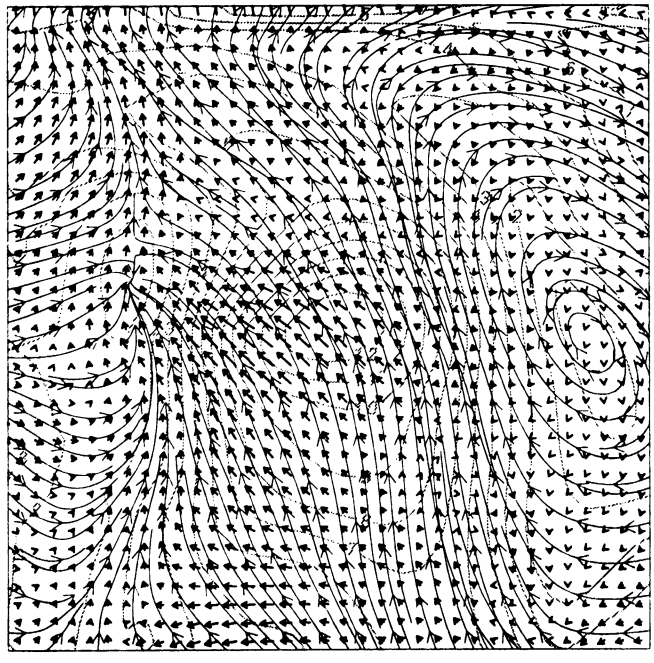

Figure 5.81. Composite Ageostrophic Wind, Level 1 – *LCC* Jets. As in Figure 5.3.

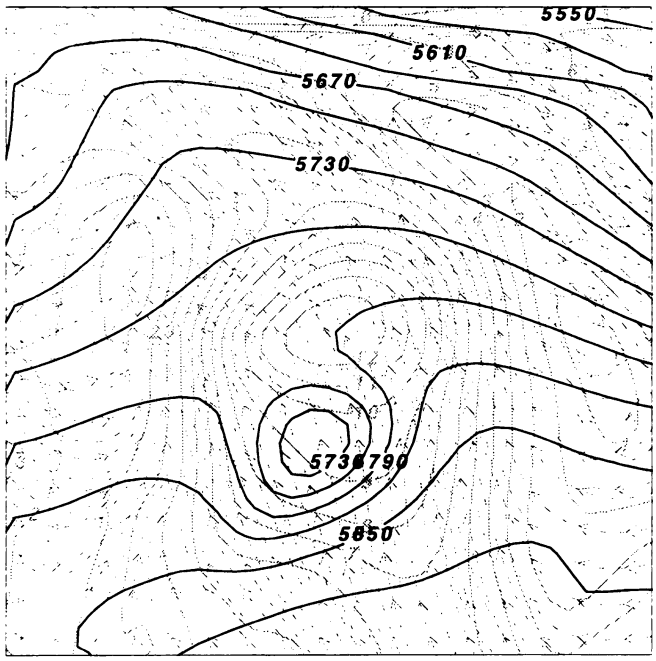

Figure 5.82. Composite 500-mb Geopotential Height plotted on Level 1 Composite Airflow Configuration – *LCC* Jets. As in Figure 5.5.

embedded in the southern branch. The distinct pattern at the mid-troposphere is also evident in the upper-tropospheric kinematic pattern (Figure 5.83). Compared with other types, the upper-level jet streak north and east of the low-level wind maximum is considerably weaker, and appears to be embedded in the northern branch of the upper-level split flow. Nevertheless, the right rear quadrant appears to be located over and to the east of the low-level wind maximum. Also, the largest mean values of 200-mb divergence are located directly above the low-level wind maximum core (Figure 5.84).

13. Summary

Variations in the large-scale setting are evident among the low-level wind maximum types. While the low-level jet core is generally located along the western edge of a pressure gradient between a high pressure system over the east and a low in the west, differences are, nevertheless, evident in the spatial configuration of the surface

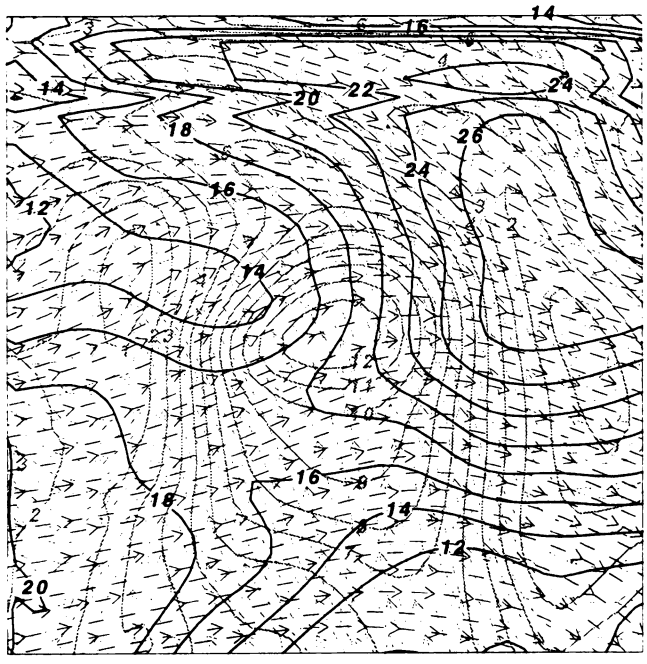

Figure 5.83. Composite 200-mb Isotachs and Streamlines plotted on Level 1 Composite Airflow Configuration – *LCC* Jets. As in Figure 5.6.

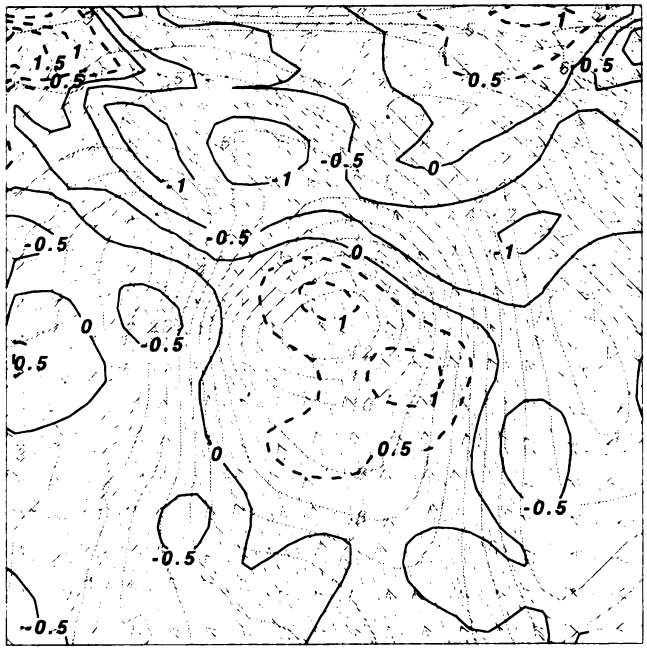

Figure 5.84. Composite 200-mb Divergence plotted on Level 1 Composite Airflow Configuration -- *LCC* Jets. As in Figure 5.7.

pressure centers. The exact location of the jet core is determined by the interplay of pressure gradient forcing and ageostrophic forcing. In a number of jet types, the jet core is not located where the strongest geostrophic forcing is observed. Frequently, the strongest geostrophic wind is observed to the northeast of the jet core. On the other hand, strong ageostrophic forcing is rather common to the northwest of the jet core. In terms of the relative contributions of geostrophic and ageostrophic forcing to the formation of the low-level wind maximum, considerable variation is evident. For types with weak pressure gradients (e.g. *AC_EW* jets), the ageostrophic component is the overriding mechanism whereas for types with a strong pressure gradient (e.g. *AC_SWNE* jets), the geostrophic component is the dominant mechanism.

The contribution of the ageostrophic component of the wind can likely be attributed to different causes. In the region northwest of the jet core, part of the ageostrophic vector seems to be due to a cross-frontal circulation. The ageostrophic vector oriented toward the confluence/frontal zone is particularly strong when surface pressure to the west of the confluence zone has risen substantially over the past 12 hours. Another possible explanation for the direction of the ageostrophic vector is an isallobaric contribution associated with pressure falls downstream of the surface cyclone or trough. These pressure falls are most likely the result of upper-level forcing. The rotation with latitude of the ageostrophic wind vector through the jet core is likely a reflection of the inertial component. This rotation is especially pronounced for jet types that have a preference for the morning hours (1200 UTC). A transverse circulation in the entrance and exit regions of the low-level wind maximum is another possible explanation for the rotation of the ageostrophic wind vector through the jet core. If transverse circulations are important, then upstream of the jet core an ageostrophic component directed toward lower pressure along the left flank of the wind maximum is expected. Downstream of the jet core an ageostrophic component directed toward the higher pressure along the right flank of the low-level wind maximum would be expected.

Another important finding is a secondary area of strong ageostrophic winds in the southwestern corner of the composite area. This phenomenon is likely caused by friction or a thermal low. Due to the topography of the southwestern US, the southwestern corner of the composite area is very close to the ground, particularly for jet types that are shallow. This region also coincides with a ridge of high temperatures.

In concert with the different supporting mechanisms for the development of low-level wind maxima, some variation is evident in the mid-tropospheric and upper-tropospheric environment. The most frequently observed mid-tropospheric height pattern is that of a longwave trough-ridge pattern. However, some jet types (*AC_EW*, *AC_SWNE*) are located under a 500-mb ridge. Similarly, almost all jet types seem to be in a likely location for a linkage between an upper-level jet streak and the lower-tropospheric wind maximum. A common location for low-level wind maxima is underneath the right entrance region of an upper-level jet streak. That region is also characterized by upper-level divergence.

In the next chapter, the findings of this study are related to previous studies. Wind maxima are put in the context of the climatology of convection in the Great Plains. The question of whether the low-level wind maxima are boundary-layer forced or synoptically-driven is investigated, and the lower-, mid-, and upper-tropospheric environment of the wind maxima is discussed.

Chapter 6

DISCUSSION AND CONCLUSIONS

In this chapter, low-level wind maxima are first related to convection in the Great Plains. Next, the question is investigated whether the wind maxima are boundary-layer forced or synoptically-driven phenomena. In the final section, the airflow configurations of the low-level wind maxima and their lower-, mid-, and upper-tropospheric environments are discussed.

1. The Climatology of Low-Level Wind Maxima and Convection in the Great Plains

Low-level wind maxima have long been identified as important components in the nocturnal convective environment of the Central Plains (Pitchford and London 1962; Bonner 1968). Their role in the initiation and enhancement of thunderstorm activity lies in destabilizing the preconvective environment through the advection of warm, moist air and in providing a means of lift through low-level convergence. The nighttime strengthening of the low-level flow was earlier shown to result in moisture inflow into the Great Plains that can be over 1.6 times the daytime value (Helfand and Schubert 1995).

As shown in Chapter 3, the monthly frequency distribution of jet cases[1] at eight rawinsonde stations across the Great Plains region of the United States closely mirrors the monthly variation of precipitation. During midsummer, the Central Plains and the Upper Midwest experience a depression in the warm-season precipitation profile

[1]The following discussion will adhere to the same terminology used in Chapters 3 and 4 where the term *jet case* is reserved for speed maxima in the vertical profiles at individual rawinsonde stations, whereas *jet event* is used to designate wind maxima in the horizontal that may include more that one rawinsonde station.

(Trewartha 1981a, 1981b; Harrington and Brown 1985; Keables 1989). The primary peak in precipitation totals in the Upper Midwest occurs during the month of June while a secondary maximum is evident in September (occasionally August). In the southern Great Plains, the primary peak occurs one month earlier, in May (Trewartha 1981b). This spatial pattern is also observed for the jet cases. At the three northern rawinsonde stations (HON, BIS, STC), the frequency of low-level wind maxima peaks in June and September, whereas the three southern stations (OUN, DDC, LBF, TOP, OVN) have maxima in May and August.

The depression in the precipitation totals during midsummer has been attributed to seasonal changes in the tropospheric circulation pattern (Harrington and Brown 1985; Keables 1989). The amplification of a ridge over or to the west of the Central Plains has been hypothesized to cause a decrease in rainfall amounts and frequency during midsummer (Harrington and Brown 1989). Mid- and lower-tropospheric northwesterly flow on the lee side of the ridge axis advects cooler, continental air into the region, thus leading to a reduction in available moisture compared with the moist tropical air that is often advected northward ahead of migratory low pressure systems when the Central Plains are influenced by predominantly southwesterly upper-level flow (i.e., when a trough axis is located upstream of the Central Plains). Furthermore, an upper-level ridge is typically associated with a dome of high pressure over the mid-continent and light and variable surface and lower-tropospheric winds. Alternatively, dry conditions during July/August in the Central Plains have been linked to zonal (i.e., westerly), rather than northwesterly, midtropospheric flow (Borchert 1950). Westerly airflow would also primarily transport drier air into the Central Plains.

The role of a surface high pressure system, and accompanying upper-level ridge, in the formation of low-level wind maxima is disputed. In case studies, Gerhardt (1962) and Hoecker (1965) describe low-level wind maxima that are located within extensive areas of surface high pressure. They note that sunny days and clear nights are

particularly conducive to the formation of strong, diurnally-oscillating wind maxima. Wexler (1961), similarly, attributes the formation of a strong southerly current to the westward extension of the subtropical high. Mitchell et al. (1995), on the other hand, found that, among five different synoptic patterns, a subtropical ridge was one of the two least conducive patterns for the occurrence of low-level wind maxima. However, Mitchell et al. limited the analysis of the synoptic pattern to the year 1992, a year with abnormally low 500-mb heights.

The findings of Chapters 4 and 5 support both lines of thought. That is, surface high pressure systems can both support and suppress the formation of low-level wind maxima. Only two of the low-level wind maximum types (among twelve) typically occur under a 500 mb ridge. Consequently, in terms of the large-scale setting, the location under a large-scale ridge does not appear very conducive to jet formation. On the other hand, the two types, *AC_SWNE* and *AC_EW* jets, have very distinct spatial patterns. One pattern, the *AC_SWNE* type, is embedded in a strong anticyclonically-curved airstream within the return flow or on the "backside" of a subtropical high pressure system (i.e., Bermuda High). The jet core is located along the western edge of a strong pressure gradient between the Bermuda high and a trough of low pressure to the west. This jet pattern has repeatedly been reported in other studies, as well (e.g. Wexler 1961; Bonner 1968). For *AC_EW* jets, on the other hand, the dominant surface pressure pattern, as described in Chapter 5, is a 'col'. *AC_EW* jets are embedded in a weak pressure gradient between a weak high pressure cell over the southeastern U.S. and a weak low to the southwest. A strong northeastern low pressure system and a strong northwestern high pressure system help explain the marked east-west confluence zone.

While the decrease in the number of jet cases toward midsummer is likely a result of changes in the large-scale atmospheric circulation (i.e., the more frequent occurrence of large-scale midtropospheric ridging), the frequency maxima in May and September are likely due to the interaction of synoptic and boundary layer influences. Mitchell et al.

(1995) attribute the frequency maximum in September, in particular, to a combination of decrease in surface moisture availability and the greater likelihood of favorable synoptic environments. Over dry soils, much of the incipient solar radiation is available for heating the atmospheric boundary layer. As a result, the wind is strongly retarded during the afternoon due to turbulence. In turn, where the wind is most strongly retarded during the afternoon, it becomes most strongly supergradient during the night (Blackadar 1957). Consequently, stronger low-level wind maxima are able to form (Paegle and McLawhorn 1983).

Synoptic environments that appear to be favorable to the occurrence of Central Plains low-level wind maxima are migratory cyclones that form to the west of the Central Plains (i.e., the Colorado cyclogenesis region) and then propagate eastward. Low-level wind maxima typically are embedded in the warm sector of all but the weakest low pressure systems migrating across the Central Plains (Newton 1967; Browning and Pardoe 1973; Uccellini and Johnson 1979; Djuric and Damiani 1980; Chen and Kpaeyeh 1993). The frequency of migratory cyclones agrees well with the May and September peaks in low-level wind maximum frequency. In general, during the warm season (i.e., April - September), cyclones are most frequently observed during May (Whittaker and Horn 1981). Cyclone frequency decreases in June and August, but increases again in August and September.

As shown above, the frequency distribution of jet cases at rawinsonde stations across the Great Plains is bimodal with a depression during mid-summer. In the analysis of the spatial configuration of the jet events (Chapters 4 and 5), however, low-level wind maxima were excluded if their streamlines did not originate over the Gulf of Mexico. A number of jet cases that are evident in the speed profile at rawinsonde stations in the northern Plains, particularly at the two northwestern stations (LBF and BIS), have streamlines originating over continental areas. Therefore, the jet events that are included in the spatial analysis are biased toward jet cores that were identified at

the southeastern stations. This bias is reflected in the monthly preference of the jet events. Unlike the bimodal distribution of *jet cases* with maxima in May and September, the *jet events* have a frequency maximum in July and a secondary maximum in September. The frequency maximum in July is primarily due to the strong monthly preference of *AC_SWNE* jets. Thirty-nine percent of *AC_SWNE* jets occurred during the month of July. If one discounts the strong preference of *AC_SWNE* jets for July, the other jet types are fairly evenly distributed across the six warm season months.

The importance of the contribution of low-level wind maxima to the nocturnal convective climatology of the Great Plains has long been known. The degree to which jet events are associated with cloud-to-ground lightning activity is astounding, however, especially considering the fact that the jet criteria that were applied in this study are relaxed compared with previous studies (e.g. Bonner 1968). The twelve distinct spatial patterns of jet events that were identified in this study are each associated with lightning activity between 84 and 100 percent of the time. *AC_SWNE* jets are least frequently associated with lightning activity. Considering the relatively unfavorable large-scale environment (i.e. a mid-tropospheric ridge), it is surprising that even for this jet type, cloud-to-ground lightning is observed in the vicinity of the jet cores during 84 percent of all *AC_SWNE* jets.

Although nocturnal low-level wind maxima have long been known to be important factors in the initiation and enhancement of nocturnal convection, this study indicates that low-level wind maxima are also fairly frequently present during periods of daytime convection. Considering that the percentage of jet events during the evening hours can reach 64 percent for individual types, the occurrence of low-level wind maxima during periods of daytime convection can thus not be ignored.

2. Boundary-Layer Forced Versus Synoptically-Driven Wind Maxima

While this study and others (Pitchford and London 1962; Bonner 1968) firmly established that low-level wind maxima are important contributors to convection in different synoptic environments, discussions are still ongoing regarding the relative contribution of various forcing mechanisms that lead to the formation of low-level wind maxima in the different large-scale settings. The literature abounds with case studies of low-level wind maxima, most of which are referred to as 'low-level jets', in a variety of different settings. In recent years, a number of researchers, recognizing that the wind maxima are found in different large-scale environments and are caused by varying contributions of different forcing mechanisms, have called for a differentiation of the wind maxima. The most frequently called for distinction is between wind maxima that are primarily boundary-layer forced and between wind maxima that are primarily synoptically driven (Chen et al. 1994, Uccellini 1990). While different nomenclature has been proposed to distinguish between the two primary types of low-level wind maxima, for example 'boundary-layer jet' (BLJ) versus 'low-level jet' (LLJ) (Chen et al. 1994), no climatological analysis isolating the characteristics of either type has been presented.

The findings in Chapter 3 of this study suggest that, while no clear-cut distinction is possible between BLJs and LLJs, some distinguishing features can be identified based on the speed profile of the low-level wind maxima. In the following discussion, please keep in mind that the analysis of the jet characteristics is strongly influenced by the vertical resolution of the rawinsonde observations (304 m) and the smoothing that was applied to the rawinsonde observations prior to archiving. While the grouping of the jet cases into three vertical layers (below 900 mb, 900-800 mb, 800-700 mb, or categories A, B, C) in this study follows natural break points in the data distribution, it nevertheless assigns individual jet cases to static height categories. Keeping in mind these limitations, the analysis of all jet cases combined, without regard for the synoptic situation, reveals that the wind maxima in the layer below 900 mb show the strongest response to

boundary-layer conditions, as evident in their seasonal variation, diurnal variation and latitude-dependence. Wind maxima above that layer (900-800 mb, category B) also seem to be modified by diurnally-changing boundary-layer conditions. However, their response is considerably less pronounced.

The diurnal variation in the number of low-level wind maxima is mainly confined to the layer below 900 mb. Jet cases in this lowest layer are very frequent at the 1200 UTC observation time and considerably less frequent at the 0000 UTC observation time. On the other hand, wind maxima above 900 mb, lack a pronounced diurnal oscillation. Therefore, jet cases occurring below 900 mb are likely to be strongly linked to diurnally varying boundary-layer conditions. The diurnally-oscillating wind field at low levels is believed to be part of a complex, three-layer tropospheric oscillation (Hering and Borden 1962; Darkow and Thompson 1968). The oscillation at the lowest level is bounded by a level of non-oscillation that previously had been reported to occur at 2 km, with maximum speeds within the boundary-layer occurring between 0.5 and 1.5 km above ground. The results presented here for the jet cases are in general agreement, except that they indicate that the upper boundaries provided earlier may be too high. Category A jets (i.e., those occurring at pressure levels of 900 mb or less) are usually at approximately 600 m mean sea level, and little diurnal oscillation is shown above.

The formation of diurnally-oscillating low-level wind maxima within the boundary-layer in the Great Plains that result in supergeostrophic nocturnal wind speeds has been attributed primarily to the inertial oscillation of the ageostrophic wind component (Blackadar 1957; Hoecker 1963; Hoxit 1975; Parish et al. 1988) and to the periodic behavior of thermally-induced pressure-gradient forcing over sloping terrain (Holton 1967; McNider and Pielke 1981). The inertial oscillation of the ageostrophic wind component, initiated by a sudden release of the frictional constraint near sunset, leads to supergeostrophic low-level wind maxima in the early morning hours. The resulting nocturnal wind speed is related to the strength of the ageostrophic wind component near

sunset. Where the wind is most strongly retarded during the afternoon due to the downward turbulent energy transfer, it becomes most strongly supergradient during the night (Blackadar 1957). Conditions that are favorable for strong turbulent energy transfer during the afternoon, in turn, are sunny days that result in strong atmospheric boundary layer heating (Hoecker 1963). The amplitude of the diurnal oscillation has been found to be largest at a level which is low enough for strong retardation of the wind during the day yet high enough for nearly frictionless flow at night (Hering and Borden 1962). The height of the nocturnal wind maximum has frequently been related to the height of the nocturnal inversion (Izumi and Barad 1963; Izumi 1964; Kaimal and Izumi 1965; Hoecker 1965; Parish et al. 1988). Hoecker (1965) found the jet nose to be sharper and located at lower elevations on nights with a surface inversion. While an analysis of the temperature profile at the time of the jet cases was not conducted in this study, the results of this study suggest that for all the rawinsonde stations, with the possible exception of LBF and HON, the height of the surface inversion rarely extends upward beyond 900 mb.

Other indications of the shallowness of the BLJ can be found in the vertical profiles of the geostrophic and ageostrophic wind components. In the vicinity of the jet core, the geostrophic wind component shows relatively small diurnal variations compared with the diurnal oscillation of the ageostrophic component (Zhong et al. 1996). In response to the diurnal temperature cycle, the strongest geostrophic winds during the afternoon are observed near the surface, while during the night, geostrophic winds increase with height in the atmospheric boundary layer. On the other hand, ageostrophic winds, which are at a maximum during the night, are largest at the lower levels and decrease sharply with height (Blackadar 1957). Although this study did not specifically investigate the diurnal variations in the ageostrophic component, strong ageostrophic winds were identified for jet types that primarily occurred at night and had average altitudes close to the earth's surface. These types included the *AC_EW*, and the *KC_SWNE* jets. On the other hand,

the geostrophic wind component was dominant for the types that were either equally frequent during the night and day or had higher average elevations.

Additional support for the notion that boundary-layer conditions are particularly important for wind maxima in the layer below 900 mb can be found in the monthly preference for jets in that layer. Unlike all jet cases combined, which have frequency maxima in May and September, wind maxima in the lowest layer are most frequently observed during the month of August. A secondary maximum for Category A jets occurs in May. Boundary-layer conditions would be expected to dominate over synoptic influences in August, when the Central Plains is dominated by a dome of high pressure and when soil moisture is small. In September, however, synoptic influences become equally important as indicated by the percentage of the different jet categories. The frequency maximum of jet cases in September is due to both a fairly large number of jet cases below 900 mb during the early morning hours (1200 UTC) and a large number of wind maxima above 900 mb that occur in the evening hours (0000 UTC).

The geographical distribution of jet cases below 900 mb, furthermore, supports the supposition that boundary-layer conditions are particularly influential for low-level wind maxima at that elevation. The frequency of jet cases in the early morning hours (1200 UTC), the time when the inertial oscillation of the ageostrophic wind vector is expected to result in strong wind maxima, shows a strong latitudinal dependence. Along the two south-north transects of rawinsonde stations across the Great Plains, a systematic decrease in the number of jet cases is evident. This decrease is particularly pronounced for jets with altitudes below 900 mb. In a modeling study, Paegle and Rasch (1973) predicted that the strongest response of the wind field to the diurnal oscillation of eddy viscosity occurs at a latitude of 30°. They calculated nocturnal wind speeds that were 50 percent supergeostrophic at 30° N and decreased to speeds that were only 30 percent supergeostrophic at 40° N. The modeling results, however, are not in perfect agreement with other observational studies. Winkler et al. (1996), for

instance, noted a dramatic decrease in diurnal wind differences at the 850-mb level northward from approximately 38°. The findings of this study indicate that the number of nocturnal jets decreases northward. This decrease is particularly for jet cases below 900 mb. In contrast, a latitudinal decrease in the frequency of jet cases is not evident for jets above 900 mb, or during the evening hours (0000 UTC).

Evidence of diurnal oscillations in other characteristics of low-level wind maxima, such as speed and direction, is similarly pronounced in the layer below 900 mb. The largest differences in average speed and average wind direction between the evening (0000 UTC) and morning hours (1200 UTC) is observed for jet cases with altitudes below 900 mb. Above that layer, a systematic decrease in the diurnal variation in speed and direction is evident. While the layer between 900 mb and 800 mb still shows some variation in the mean wind speed and wind direction between the two observation times, the layer between 800 mb and 700 mb is devoid of differences in the average values of both parameters.

In summary, the diurnal oscillation of the different characteristics of low-level wind maxima is particularly evident for jet cases with altitudes below 900 mb. Thus, it appears that boundary-layer forced wind maxima (BLJ) are dominant in that layer. For jet cases with altitudes above 800 mb, on the other hand, the frequency, average wind speed, and average direction completely lack a diurnal variation. Thus, synoptically-driven low-level jets (i.e., LLJs) are likely to predominate. The layer between 900 and 800 mb appears to represent a transition. There is some evidence among the jet cases for this layer of a diurnal oscillation in the wind speed and direction. Also, there is some evidence of an upward shift in the average height of jet cases in this layer between 1200 UTC and 0000 UTC. However, there was little or no difference in the frequency of early morning and evening cases for jets between 900 and 800 mb.

Thus, some distinction in the characteristics of low-level wind maxima can be drawn based on the speed profile of jet cases. However, these distinction should only

be viewed as tentative guidelines in the definition of different types of low-level wind maxima. An increasing body of evidence suggests that a comprehensive view of low-level wind maxima is necessary. While the mechanisms leading to the formation of low-level wind maxima can be broadly categorized into boundary-layer processes and synoptic-scale processes, they should not be viewed as competing or mutually exclusive. It is rather recommended to interpret low-level wind maxima, particularly stronger ones, as the result of contributions from both types of forcing (Mitchell et al. 1995).

3. Airflow Configurations of Low-Level Wind Maxima and the Relationship to Convection

The spatial pattern of low-level wind maxima in the Great Plains is much more varied than previously thought. The manual typing and subsequent compositing successfully collapsed the variation inherent in the individual jet events into twelve distinct types of low-level wind maxima. In Chapter 4, it was shown that each type of airflow configuration is strongly related to the composite low-level convergence field and to the location of convection. Furthermore, there are distinct temporal, geographical and height preferences for the different types. This climatological analysis greatly expands upon previous case studies that had reported variations in the spatial pattern of low-level wind maxima. For instance, Djuric and Damiani (1980) and Trier and Parsons (1993) showed that the orientation of low-level wind maxima associated with cyclogenesis varies over the course of the cyclone evolution. Case studies had also suggested that the orientation of low-level wind maxima can vary in the vertical (Bonner 1966). However, there had been no previous climatological study to identify the range of variations in the spatial configuration of Great Plains low-level wind maxima.

An important finding of this study is the frequent occurrence of multiple airstreams in the vertical during jet events. Again, the existence of multicored jets has been suggested in individual case studies (e.g. Hoecker 1963; Hoecker 1963; Ardanuy 1979; Dickison and Neumann 1982; Kotroni and Lagouvardos 1993), but had not been

validated in a climatological study. Also, previous studies had reported different trajectories for the multiple levels (Kottmeier 1978; Roth et al. 1979). However, the superposition of multiple convergence fields associated with multiple airstreams and their implications for the location of convection had not been investigated previously and is a contribution of this study.

The location of convection associated with low-level wind maxima is closely linked to the low-level convergence field. Earlier case studies had observed different locations of convective activity in connection with low-level wind maxima, such as downstream of the jet core (Pitchford and London 1962; Bonner 1966, 1968; Astling et al. 1985) or along the left flank (Bonner 1966, 1968). However, this study clearly shows that the convergence fields of the multiple airstreams of each jet type need to be considered in order to explain the location of cloud-to-ground lightning strikes. In general, strong convergence is typically found 1) in the vicinity of a strong confluence zone along the left flank of the jet core, 2) downstream of the jet core in an area of speed convergence, and, 3) where applicable, downstream of the jet core in areas of confluence on either side of a deformation zone. The convergence along the confluence and deformation zones is typically strongest for the jet level closest to the earth's surface, in general agreement with the decrease with height of the ageostrophic wind component observed in previous studies. At the second, and if applicable, the third jet levels, the convergence due to confluence is generally weaker than the speed convergence downstream of the jet core. Therefore, taking into consideration the strong low-level confluence zones, the veering of the wind direction with height for the multiple levels, and accounting for the stronger convergence downstream of the wind maximum at the higher levels than at the first level, a three-dimensional picture of convergence emerges.

This three dimensional picture of convergence can explain most of the spatial variation in cloud-to-ground lightning. A major finding of this study is that for some jet types (e.g. *AC_EW, KC_SWNE*) convective activity is very localized along convergence

zones resulting from either confluence or speed convergence at the multiple levels. These findings support earlier studies that have indicated the importance of boundary-layer convergence and resulting vertical velocity pattern to the initiation and prolonging of convective activity (Means 1954; Pitchford and London 1962; Bonner 1966). For other jet types, only some of the spatial pattern of the observed lightning activity can be related to the low-level convergence field (e.g. the *CC* types). Thus, for these jets, other factors besides the low-level convergence, such as isentropic lift, are important in determining the location of convection.

The veering of the multiple levels with height often leads to an eastward extension of convergence with height, particularly when viewed with respect to the first level convergence field. In other words, if only the first-level convergence field is considered, the spatial extent of the convergence associated with the low-level wind maximum would be underestimated. This eastward extension of the "overall" convergence field is often reflected in the location of lightning activity. Lightning activity is most frequent where convergence is strongest. That is, along the confluence zone to the left of the core, downstream of the wind maximum in an area of speed convergence, and where applicable, along the confluence zone to either side of a difluent airstream. In cases with difluent flow, the lightning activity is particularly frequent on the upstream side of the difluence zone. It is interesting to note that these locations are not mutually exclusive. The results presented here regarding the location of convection expand on earlier studies that had observed convective activity only in the terminus of a low-level wind maximum (Pitchford and London 1962; Bonner 1966, 1968; Astling et al. 1985) or along the left flank (Bonner 1966, 1968). No previous climatological study had considered multiple levels nor had the frequency of lightning activity associated with different flow been investigated before this study.

4. The Large-Scale Environment in which Central Plains Low-Level Wind Maxima Occur

Considerable differences were evident in the large-scale environments, particularly the surface pressure patterns, for the different airflow configuration types. While the jet core for all types was located along the western edge of a pressure gradient between a high pressure cell over the eastern/southeastern U.S. and a trough of low pressure or surface cyclone over the central and western U.S., the location and strength of these pressure systems differ. These variations are partly responsible for the differences in the horizontal extent, orientation, and confluence and difluence patterns of the low-level wind maxima. As indicated earlier, it is possible that some of the individual jet types represent stages in the evolution of low-level wind maxima. However, due to the coarse temporal resolution of the rawinsonde observations this possibility could not be investigated further. The discussion below is divided according to the mid-tropospheric large-scale setting. First, the wind maxima that form near a large-scale ridge axis are discussed. Next, the characteristics of the wind maxima that occur downstream of a midtropospheric trough are described.

a. Low-Level Wind Maxima Under Weak Midtropospheric Circulation

As previously mentioned, two of the identified twelve jet types, *AC_SWNE* and *AC_EW* jets, are located under a mid-tropospheric ridge. Uccellini (1980), in a review of 15 low-level wind maxima, contrasted wind maxima that are located under an upper-level ridge and weak upper tropospheric flow with those that occur with an upper-level pattern that includes troughing over the southwestern United States and the propagation of an upper-level jet streak toward the Great Plains. He noted that the boundary-layer jets that are characterized by a diurnal oscillation are associated with the first type of upper tropospheric pattern and a relatively weak surface pressure pattern. *AC_EW* jets are in agreement with his observations since they are located in a very weak pressure gradient across the southern Great Plains and they show a

pronounced preference for the early morning hours. Furthermore, they are limited to a very shallow layer of the atmosphere. Consequently, they seem to represent ideal examples of boundary-layer jets. This supposition is supported by the considerably larger contribution of the ageostrophic wind component to the actual wind compared to the geostrophic contributions for *AC_EW* jets. Based on the weak surface pressure pattern, where no area of pronounced pressure fall is evident, and the clustering of the jet cores about a median latitude of 36° N, the ageostrophic wind component is believed to be primarily due to an inertial oscillation rather than to isallobaric forcing. It is interesting to note that the ageostrophic wind vectors rotate anticyclonically with latitude through the jet core. The orientation of the ageostrophic vector to the left of the geostrophic vector can be attributed to the production of kinetic energy through work done by pressure forces (Bonner et al. 1968). While this mechanism helps explain the orientation of the ageostrophic wind vector upstream of the jet core, no comparable explanation for the area downstream of the jet core has been offered. The upper-tropospheric wind field does not appear to play an important role in the formation of *AC_EW* jets, since the northern boundary of the low-level wind maxima is located quite a distance south of the upper-tropospheric jet streak.

The other type of low-level wind maximum that occurs under a midtropospheric ridge, *AC_SWNE* jets, does not correspond with Uccellini's classification. Although, as previously discussed, *AC_SWNE* jets are most frequent in August when boundary-layer forcing is expected to dominate over synoptic scale forcing, the *AC_SWNE* jets were equally frequent at 0000 and 1200 UTC, and the jet cores were more dispersed across the Great Plains, particularly in comparison to the clustering evident for the *AC_EW* jets. The average height of *AC_SWNE* jets is greater than that for the *AC_EW* jets (874 mb). Also, contrary to the *AC_EW* jets, *AC_SWNE* jets are embedded within a strong pressure gradient that forms between a pronounced high pressure cell over the southeastern U.S. and a trough of low pressure to the west. The pressure gradient force

appears to be the driving mechanism behind this type of wind maximum, as suggested by the considerably stronger geostrophic wind component compared to the ageostrophic component. While *AC_SWNE* jets do not fit Uccellini's classification, they, nevertheless, resemble strongly-anticyclonically-curved wind maxima that have been reported in a number of previous studies (Wexler 1961; Bonner 1968; Cotton et al. 1989). As expected, given that a mid-tropospheric ridge is present, the upper-tropospheric wind field does not appear to play a role the formation of *AC_SWNE* jets. The region downstream of the low-level wind maximum is located underneath the right front quadrant of an anticyclonically-curved upper-level jet streak, a region that is characterized by upper-tropospheric convergence and thus sinking motion (Beebe and Bates 1955).

b. Low-Level Wind Maxima Under Strong Midtropospheric Circulation

The remaining 10 types of low-level wind maxima are located under a midtropospheric pattern that is characterized by troughing over the southwestern United States and ridging east of the low-level wind maximum. Four of these types do not extend north beyond the latitudes of the Great Lakes region (i.e., 'short' types) while the other six types are characterized by a longer horizontal extent (i.e., 'long' types). While the general location of the jet cores is upstream of a 500-mb ridge, the strength of the 500-mb height gradient and the longwave amplitude varies for the individual jet types.

The mid-tropospheric height field appears to have an influence on the horizontal extent of the individual jet types. Specifically, "long" types only occur with large-scale trough-ridge patterns. This contrast is most evident between the *LAC_SWNE* jet type and its "short" counterpart, *AC_SWNE* jets, which, as noted earlier, occur under a midtropospheric ridge. In general, synoptic-scale influences appear to be relatively more important for "long" jet types whereas for "short types" boundary-layer influences

appear equally or more important. Some evidence for this contention is that the jet cores of the long jet types are less clustered compared to those of short jet types, suggesting that the inertial component which is centered between 30-35° latitude is not as important for long types.

However, synoptic-scale forcing is important for "short" types, as well. For instance, a midtropospheric trough-ridge pattern is present for *KC_SWNE* jets. The northern portion of the composite suggests that a short-wave trough supports a surface low pressure system. This low may be the reason for the pronounced closed cyclonic circulation evident at the lowest jet level. The very fast wind speeds for *KC_SWNE* jets (among the fastest of all jet types) also suggest that synoptic-scale forcing is at least enhancing boundary-layer forcing. However, the typical location, temporal preference and height of the *KC_SWNE* jets supports the notion that boundary-layer influences, superimposed on the large-scale synoptic environment, are also important in creating this supergeostrophic wind maximum.

The orientation of low-level wind maxima depends on the location and strength of the surface pressure features. While an area of low pressure is always found southwest of the jet core, the nature of the pressure features in the other three quadrants relative to the jet core varies among the jet types. The location of the high pressure cell over the eastern United States relative to the jet core is key in determining the orientation of the wind maximum. For anticyclonically-curved flow, the high pressure cell is located south of the latitude of the jet core, compared with a more northern location of the high pressure cell for cyclonically-curved jets. When additional pressure cells are located downstream of the wind maximum, difluent flow frequently results. The jet types support earlier examples in the literature of anticyclonically-curved low-level wind maxima (Wexler 1961; Bonner 1968; Djuric and Damiani 1980; Djuric and Ladwig 1983; Achtor and Horn 1985), cyclonically-curved low-level flow (Trier and Parsons 1993), and difluent flow (Sangster 1979).

The possible role of cyclogenesis on low-level jet occurrence can be partly inferred from the characteristics of the *CC* and *LCC* jets. For both jet types, the relative contribution of the ageostrophic component of the wind equals that of the geostrophic component. This characteristic, along with the strong surface low and the large 12-h pressure falls associated with these jet types, suggests that the isallobaric component of the ageostrophic wind is an essential contributor to the strong low-level wind speeds. However, an investigation of the relative contributions inertial and isallobaric components, was outside the scope of this study. Therefore, the relative importance of either component can only be speculated upon. In previous studies, though, the isallobaric wind component has been shown to be an important factor in the formation of low-level jets. However, some researchers have shown that the temporal changes in the pressure gradient are less important than the frictional decoupling and inertial turning of the ageostrophic component (Parish et al. 1988; Frisch et al. 1992; Zhong et al. 1996). On the other hand, researchers have linked low-level jets to cyclone development (Djuric 1981; Djuric and Ladwig 1983; Glass 1993; Chen and Kpaeyeh 1993). These authors showed that the low-level jets were caused by the pressure fall associated with cyclone development. While low-level jets are commonly present in the warm sector of Colorado-cyclones (Newton 1967; Browning and Pardoe 1973; Uccellini and Johnson 1979; Djuric and Damiani 1980; Chen and Kpaeyeh 1993), the orientation of the cyclonically-curved low-level jets observed in this study differs from the low-level jets embedded within the warm conveyor belt as described by Carlson (1980). According to Carlson, the warm conveyor belt is an anticyclonically-curved airstream that ascends as it moves northward. Alternatively, the CC and LCC jets may be part of the cyclonically-turning moist airstream (referred to as CMA) that Bierly (1996) identified as important features of cold season (i.e. March through November) Colorado cyclones.

The connection of *CC* and *LCC* jets to cyclogenesis, both over the southern Great Plains and over the northern Plains, is further supported by the monthly preference for

the two types of jets. *CC* jets are most frequently observed during May/June and *LCC* jets during September. The location of *CC* jets extends north beyond the region generally associated with Colorado cyclogenesis (Reitan 1975; Achtor and Horn 1986), while *LCC* jets are located even farther north, across the northern Plains. During May, the time of maximum warm-season cyclone frequency (Whittaker and Horn 1981), the southern Plains as the region of preferred cyclogenesis is decreasing in importance from its spring maximum, while an increase in cyclone activity is evident over the northern United States and southern Canada (Harman 1991). During June, cyclogenesis continues to decrease over the southern US, and a relative maximum in frequency is observed for the Alberta cyclogenesis region. In September, the average location of the upper-level jet stream supporting surface low pressure systems restricts the most frequent support for cyclonic activity to the northern most United States and southern Canada (Harman 1991).

The other jet types that have fairly strong contributions by both geostrophic and ageostrophic forcing are the *KC_SWNE* jets and their 'long' counterparts, *LSKC_SWNE* jets. Similar to *CC* and *LCC* jets, these two jet types appear to be influenced by pressure gradient changes associated with a low pressure system. Also, like the *CC* and *LCC* jets, the *LSKC_SWNE* jets are located due east of a low pressure system and oriented toward a region that experienced large 12 h pressure falls. *KC_SWNE* jets, on the other hand, are located south of the low pressure center. However, for both *LSKC_SWNE* and *KC_SWNE* jets, the ageostrophic component does not appear to be influenced by the pressure falls east of the low pressure system. Instead, the ageostrophic wind vectors are oriented to the left of the geostrophic wind vectors and are indicative of the conversion of pressure gradient forcing to kinetic energy. Additionally, the orientation of the ageostrophic component toward the confluence/frontal zone suggests a cross-frontal circulation. In contrast, the ageostrophic vectors for the *CC* and *LCC* jets are oriented directly toward the region of pressure falls, and thus isallobaric forcing is suggested.

For the remaining six types of low-level wind maxima the pressure gradient forcing predominates. The strongest geostrophic wind is observed to the northeast of the actual jet core indicating that the contribution of the ageostrophic wind, although smaller than the geostrophic forcing, results in a displacement of the actual wind maximum to the west/southwest of the strongest pressure gradient. All jet types display an anticyclonic rotation in the orientation of the ageostrophic wind vector upstream of the jet core, whereas downwind of the jet core a rotation is only evident for a few types. As indicated previously, this rotation is likely a reflection of the speed increase upstream of the jet core and the decrease of the speed downstream of the jet core.

c. The Role of Upper-Level Jet Streaks

Upper-level jet streaks appear to contribute to the occurrence of almost all low-level wind maxima that form under a midtropospheric trough-ridge pattern. The right rear quadrant of an anticyclonically-curved 200-mb jet streak, an area of upper-level divergence (Beebe and Bates 1955), is generally superimposed upon an area of low-level speed convergence downstream of the low-level wind maxima. The two exceptions to this configuration are *LAC_SWNE* jets which are located under the right-front quadrant and *LCC* jets which may be influenced by a second jet streak located upstream. Another interesting observation is that the jet types with difluent flow, the upper-tropospheric divergence is generally located over the left branch of the split flow.

The right-rear quadrant of an upper-level jet stream, although previously shown to be conducive to the formation of convection (McNulty 1978; Beebe and Bates 1955), is not commonly associated with strong synoptically-forced disturbances. Whittaker and Horn (1981) and Hovanec and Horn (1975), for instance, found that spring season cyclogenesis commonly occurs under the left-front quadrant of jet streaks which propagate across the southern Rockies. The left-front quadrant of an upper-level jet has

also been shown to be instrumental in creating the upper-level divergence for a severe outbreak over Indiana and Ohio (Uccellini and Johnson 1979).

The location of the low-level wind maximum below the right rear quadrant does not present the most favorable configuration for the contribution of upper-level dynamics. Uccellini and Johnson (1979) showed that low-level jets under the left front quadrant of an upper tropospheric jet streak are embedded within an indirect transverse circulation in the exit region that is perpendicular to the upper-level jet. The lower branch of this ageostrophic transverse circulation is oriented from south to north, and thus would support, or even create, a low-level wind maximum. On the other hand, the entrance region of an upper-level jet streak is characterized by a direct circulation, again oriented perpendicular to the upper-level jet, but with a north-south oriented lower branch. This orientation of the lower branch is against the southerly flow of a low-level wind maximum. Thus, while it appears that there may be dynamic support from the superposition of the low-level convergence and upper-level divergence fields, the role of the ageostrophic component resulting from the transverse circulations associated with jet streaks is uncertain.

d. Temperature and Moisture Patterns

The average temperature and moisture patterns of the low-level wind maxima reflect the topography of the Great Plains. Relative to the jet cores, a ridge of warm temperatures is found to the southwest of the jet core and a moisture ridge to the southeast. For the different types of jets, the temperature and moisture values in the vicinity of the jet core depend upon both the strength of the lower tropospheric circulation as well as the geographical location of the individual jet cores.

The composites of the temperature and moisture fields presented here for the different configuration types clearly reflect the advective influences of the multiple airstreams of low-level wind maxima. Furthermore, veering of the streamlines with

height suggests the occurrence of differential moisture and temperature advection, particularly for those jet types that have a third level airstream originating over the hot and dry regions of the southwestern United States. Differential advection has been shown to promote the destabilization of the pre-convective environment (Beebe and Bates 1955; Pitchford and London 1962; Uccellini 1990) and to create potential instability (Carlson 1983).

The findings of Chapter 4 of this study are in agreement with previous studies that noted a preferred location for the development of southerly jets on the east side of the warm air maximum over the southwestern United States during the summer (Means 1954). Means (1952) noted the development of supergeostrophic winds where isotherms are approximately parallel to the streamlines with warmer air toward lower pressure. The resulting temperature pattern shows a gradient across the jet with highest temperature values in the southwest quadrant and the lowest in the northeastern quadrant (Bonner 1968). The vicinity of narrow and elongated warm tongues has been shown to be a favored location for the occurrence of severe thunderstorms (Means 1952). This location is particularly favored if the axis of warmest temperatures is displaced west of the axis of highest moisture values (Maddox and Doswell 1982).

5. Addressing the Research Questions

The following section provides a synopsis of the research findings by answering the specific research questions that were posed at the end of Chapter 1.

1) What impact does the definition of low-level wind maxima have on our interpretation of the climatology of this phenomenon, specifically in the Central Plains?

The results of this study indicate that, in order to fully understand the impact of low-level wind maxima on convection, the commonly-used definition devised by Bonner (1968) needs to be relaxed. Even with the more relaxed speed and height jet criteria

used in this study, cloud-to-ground lightning activity occurs for 84 to 100 percent of the jet events of individual jet types.

2) Is it possible to distinguish between boundary-layer forced (i.e., BLJs) and synoptically-driven (i.e., LLJs) lower tropospheric wind maxima based on their height and time of occurrence?

Based on the speed profile of low-level wind maxima, differences in the height and temporal characteristics of boundary-layer forced and synoptically-driven wind maxima were evident. Wind maxima below 900 mb show temporal, speed and directional characteristics that are reflective of diurnally-varying boundary-layer conditions, whereas wind maxima above 800 mb lack any diurnal variation. The layer between 900 and 800 mb seems to form a transition layer where wind maxima show evidence of some diurnal variation. However, the variation in that layer is not very pronounced.

3) Are there distinct airflow configurations (and related convergence) associated with low-level wind maxima in the Great Plains and can these be related to BLJs and LLJs?

Twelve distinct airflow configuration types were identified for warm-season wind maxima with trajectories off the Gulf of Mexico. The individual types differed from one another in their extent, orientation, and location of convergence. Only one of the jet configuration types, *AC_EW* jets, showed all the typical characteristics of a boundary-layer jet (i.e. location under midtropospheric ridge, strong diurnal oscillation, shallow height, short extent, weak pressure gradient, predominance of ageostrophic forcing) while the remaining eleven types had indications of some type of synoptic forcing. The synoptic forcing was particularly evident for 'long' jets which extended north into Canada. All of the 'long' jets were located under a midtropospheric trough-ridge pattern. For all 'long' types, the pressure gradient force was important in the formation of the jet. Additionally, synoptic forcing seemed strong for low-level jets associated with cyclogenesis or migratory low pressure systems.

4) How do moisture and temperature patterns differ among low-level wind maxima?

The composite analysis revealed little difference in the moisture and temperature pattern between the different low-level wind maxima. The jet core is always located at the intersection of a ridge of warm temperatures extending northeastward from the southwestern United States and a moisture ridge extending northward/northwestward from the Gulf of Mexico. An interesting finding of this study is the advective influence of the cyclonic branch of jet types with difluent flow.

5) How does the airflow configuration of low-level wind maxima influence the pattern of convection?

The pattern of convection closely reflects the low-level convergence field of low-level wind maxima. The composite map of cloud-to-ground lightning mirrors the convergence field not only at the lowest analysis level for a jet type but also at multiple levels for jet events with multiple airstreams.

6) What are the typical synoptic-scale environments for low-level wind maxima with different spatial configurations, and can the typical environments provide some insight into the relative importance of synoptic-scale forcing and boundary-layer forcing?

Low-level wind maxima are located under both a midtropospheric ridge and a trough-ridge pattern. The midtropospheric ridge pattern is less common than the trough-ridge pattern. However, the two types of jet configurations that were identified with large-scale ridges are very distinct. One pattern is the only jet type that is primarily boundary-layer forced while the other is primarily influenced by pressure gradient forcing. All the types of wind maxima with great horizontal extent are located under a trough-ridge pattern.

Chapter 7

FUTURE RESEARCH

This climatological analysis of low-level wind maxima was able to respond the specific research questions with a number of important findings. First, the spatial configuration of low-level wind maxima is much more varied than previously portrayed. Secondly, the existence of multiple airstreams for jet events is a rather common occurrence. Thirdly, most of the spatial variation of cloud-to-ground lightning activity can be related to the convergence fields of multiple airstreams during jet events. Furthermore, strong wind maxima are most often located under a midtropospheric trough-ridge pattern. However, even under fairly similar midtropospheric patterns, considerable variation in the relative contribution of the pressure gradient force and ageostrophic forcing is evident. Finally, for most of the jet types, the low-level wind maximum is located under the right-rear quadrant of an upper-level jet streak. The resulting upper-level divergence is superimposed upon low-level convergence associated with the low-level wind maximum. The findings of this study leave a number of unanswered questions, however. These are:

1. What are the relative contributions of the different ageostrophic wind components? In particular, what are the contributions of the inertial and isallobaric components of the ageostrophic wind? Previous research has suggested that the isallobaric wind is important in the formation of low-level jets associated with cyclogenesis (Djuric 1981; Djuric and Ladwig 1983; Chen and Kpaeyeh 1993; Glass 1993). In studies of the relative importance of the isallobaric versus the inertial component, however, the inertial component was seen to predominate (Parish et al.

1988; Frisch et al. 1992; Zhong et al. 1996). Comparable studies have not been conducted for types of jet configurations that are not as strongly related to cyclone development.

2. How does the height of the different airstreams relate to the temperature profile of low-level wind maxima? Boundary-layer jets have previously been shown to be closely related to the development of a nocturnal inversion (Gerhardt 1962; Izumi and Barad 1963; Izumi 1964; Kaimal and Izumi 1965). Furthermore, Beyrich (1994) has suggested that the time evolution of the stable boundary layer determines whether or not a low-level wind maximum will be present during the night. I am not aware of previous studies that have investigated the relationship between the temperature profile and the height of low-level wind maxima in a spatial study.

3. Do the jet configuration types identified in this study represent stages in the evolution of wind maxima? This study has shown that the orientation of low-level wind maxima is closely related to the position of surface pressure features. Given the migratory nature of low-pressure systems, a change in the orientation of low-level wind maxima embedded in the pressure gradient between a low-pressure system and downstream high pressure center with time is likely. Thus, some types of spatial configurations likely represent stages in the evolution of wind maxima. The developmental stages of low-level wind maxima should therefore be investigated with the use of data sets with finer temporal resolution than the rawinsonde observations used in this study, e.g. profiler data.

4. How does the chosen interpolation scheme affect the resulting spatial pattern of low-level wind maxima? Specifically, would an interpolation scheme that differentiates between the along-axis and cross-axis direction result in a different interpretation of the

low-level wind field? Endlich and Mancuso (1968) have suggested that the use of an interpolation scheme that gives upwind-downwind observations greater weight than crosswind observations has the advantages of aligning the isolines of the analyzed scalar with the flow direction. The isotach pattern resulting from the isotropic Barnes interpolation scheme applied in this study resulted in a rather circular appearance to the isotachs, while observational studies of low-level wind maxima have portrayed spatial patterns of the low-level wind maximum as an elongated feature (Bonner 1968). According to Endlich and Mancuso, an anisotropic scheme agrees with space correlation functions that fall off more rapidly crosswind than along the wind.

5. What influence does the airflow configuration have on the intensity of convection? This study has shown that the preferred locations of convective activity are closely related to the low-level convergence field that results from the different airflow configurations of multiple airstreams during jet events. While low-level wind maxima have been identified as important contributors to the development of large convective systems (Maddox 1983; Augustine and Caracena 1994) , and a number of different spatial patterns of convective storms have been identified in the literature (e.g. Houze et al. 1990), no study has attempted to relate the airflow pattern to the resulting intensity and organization of convection in a climatological analysis.

APPENDICES

APPENDIX A

APPENDIX A

GEMPAK INTERPOLATION SCHEME

GEMPAK (General Meteorological data assimilation, analysis, and display software PACKage) is an interactive computer software system developed at the Severe Storms Branch of NASA's Goddard Laboratory for Atmospheric Sciences (Koch et al. 1981, 1983). It was developed for use with various conventional and satellite meteorological data types. GEMPAK was designed to (1) convert the various types of data to a standard file structure, (2) vertically and horizontally interpolate the data to uniformly spaced grid points, (3) perform data assimilations to initialize numerical models, (4) compute diagnostic quantities, and (5) display the products onto various maps. For the purpose of performing interpolations, GEMPAK uses an adapted Barnes (1973) objective map analysis scheme (Koch et al. 1981).

To display parameters on a given constant pressure surface, the irregularly-spaced upper air observations are first interpolated vertically at the location of the rawinsonde station to the new pressure level and then interpolated horizontally to a regular grid. The vertical interpolation scheme is performed with respect to the logarithm of pressure and can be written as:

$$nlev = lowlev + (uplev-lowlev)*rmult$$

where

nlev	parameter value at interpolated pressure level
lowlev	value at lower pressure level
uplev	value at upper pressure level
rmult	multiplication factor

A modified Barnes Objective Analysis Scheme is used to then interpolate the parameters to a regularly spaced array of grid points. This grid provides the basis for isopleth mapping or for quantitative diagnostic and/or predictive calculations. As part of the objective analysis, smoothing is applied to reduce both "noise" in the data and gross errors. The reduction of error amplitudes is particularly important for the calculation of derived quantities such as divergence and vorticity from grid point values. The degree of smoothing is influenced by the weights applied to the data.

The Barnes (1964; 1973) interpolation uses a convergent weighted-averaging interpolation scheme. The weighting factor is based on the premise that the two-dimensional distribution of an atmospheric variable can be represented by the summation of an infinite number of independent harmonic waves. The weights are is explicitly related to the density of observations. The Barnes scheme assigns a non-zero weight to each observation according to its distance from a mesh point relative to the number and distance of all other observations within some cutoff radius. With increasing distance the weights asymptotically approach zero. Beyond a cutoff radius, all weights are assigned a value of exactly zero (Koch et al. 1981, 1983). Since the Barnes objective analysis is dependent on the data density, applications of the scheme are restricted to regions with reasonably uniform data distributions.

The Barnes objective analysis scheme employs successive corrections to restore the amplitude of large wavenumber components that were suppressed in the first interpolation-filtering pass. In its 1973 version (adapted for use within GEMPAK by Koch et al. 1981), the Barnes technique only requires two passes through the data to achieve the desired pattern recognition.

APPENDIX B

APPENDIX B

SOUTHERLY LOW-LEVEL WIND MAXIMA

This appendix provides a list of the 1522 southerly low-level wind maxima that were included in the first part of this study. As described in Chapter 2, the wind maxima were identified based on the vertical speed profiles at eight rawinsonde stations in the Great Plains. The temporal, spatial, height, speed, and directional characteristics of these wind maxima are discussed in Chapter 3.

Date	Time	Id	Type	Speed (ms^{-1})	Presure (mb)	Dir (°)	Hght (m MSL)
910401	12	oun	a4	11	953	230	610
910401	12	lbf	b4	9	881	235	1219
910401	12	lbf	b4	9	819	235	1829
910401	12	bis	a4	10	914	155	914
910401	12	ddc	b4	9	881	235	1219
910401	12	ddc	b4	9	819	235	1829
910401	12	top	a2	15	951	255	610
910402	0	ddc	b4	14	850	185	1508
910402	0	ddc	b4	14	818	190	1829
910402	12	lbf	b1	17	871	170	1219
910402	12	bis	a4	12	940	140	610
910402	12	ddc	a3	22	906	165	914
910402	12	ddc	a3	22	850	175	1446
910402	12	top	a3	13	947	195	610
910402	12	hon	a2	20	908	195	914
910402	12	stc	a2	14	950	150	610
910403	0	oun	b3	19	874	190	1219
910403	0	ovn	c	13	758	170	2438
910403	0	stc	c	15	789	210	2134
910403	0	stc	c	15	759	210	2438
910403	12	top	b3	13	850	170	1480
910403	12	top	b3	13	845	175	1524
910403	12	hon	a2	18	945	205	610
910403	12	stc	a3	15	948	210	610
910404	0	stc	c	13	788	190	2134
910405	12	lbf	b3	19	879	255	1219
910405	12	ddc	b4	10	850	225	1544
910405	12	top	a1	13	948	240	610
910405	12	ovn	a2	20	947	240	610
910405	12	stc	a2	17	941	235	610
910406	0	ovn	b3	18	850	225	1501
910406	0	ovn	b3	18	848	225	1524
910406	12	oun	a5	10	913	200	914
910406	12	oun	a5	10	880	195	1219
910406	12	ddc	b2	13	817	230	1829
910406	12	top	a2	23	944	230	610
910406	12	ovn	a2	22	939	230	610
910406	12	ovn	a2	22	906	245	914

910407	0	top	a5	14	941	195	610
910407	0	top	a5	14	908	200	914
910407	0	ovn	a2	16	905	210	610
910407	12	lbf	b3	14	865	220	1219
910407	12	ddc	a2	22	902	205	914
910407	12	top	b3	17	906	220	914
910407	12	top	b3	17	873	230	1219
910407	12	ovn	a2	21	935	215	610
910408	0	top	b4	14	811	205	1829
910408	0	ovn	b4	15	839	215	1524
910408	0	ovn	b4	15	809	215	1829
910408	12	oun	a3	19	933	180	610
910408	12	top	b1	15	870	225	1219
910408	12	ovn	b3	16	850	240	1401
910408	12	ovn	b3	16	808	230	1829
910410	12	lbf	b3	19	876	160	1219
910410	12	bis	a3	14	908	165	914
910411	0	ovn	b3	14	877	125	1219
910411	0	hon	a5	16	942	145	610
910411	12	oun	b3	23	841	190	1524
910411	12	lbf	b3	23	862	120	1219
910411	12	bis	c	23	723	110	2743
910411	12	ddc	b3	26	850	195	1375
910411	12	ddc	b3	26	805	225	1829
910411	12	top	b3	29	810	210	1829
910411	12	hon	b1	27	850	130	1451
910411	12	hon	b1	27	842	130	1524
910412	0	bis	b1	28	816	115	1829
910412	0	bis	b1	28	726	115	2743
910412	0	ovn	a1	25	942	115	610
910412	0	ovn	a1	25	907	120	914
910412	0	hon	b1	27	877	115	1219
910412	0	stc	c	23	760	115	2438
910413	0	top	b2	14	850	160	1465
910413	0	top	b2	14	785	195	2134
910413	0	ovn	a3	17	939	120	610
910413	0	hon	a3	18	908	110	914
910413	0	stc	b1	23	850	115	1508
910413	0	stc	b1	23	848	120	1524
910413	12	top	c	34	756	240	2438
910413	12	top	c	34	728	245	2743
910413	12	stc	a3	14	947	100	610
910413	12	stc	a3	14	912	110	914
910414	0	stc	b1	18	877	145	1219
910416	12	ddc	b3	24	872	220	1219
910416	12	top	b1	27	875	225	1219
910417	0	oun	a5	12	941	165	610
910417	0	oun	a5	12	846	185	1524
910417	12	oun	a2	15	909	205	914
910418	0	ovn	b1	14	815	185	1829
910421	0	ddc	c	14	759	240	2438
910421	12	lbf	b4	10	850	175	1461
910421	12	lbf	b4	10	843	175	1524
910421	12	bis	a5	9	909	195	914
910422	12	stc	b3	13	850	230	1389
910422	12	stc	b3	13	836	235	1524
910423	12	ddc	b4	12	872	260	1219
910423	12	ddc	b4	12	850	260	1430
910424	12	oun	b4	8	850	145	1490
910424	12	lbf	b4	10	850	220	1458
910424	12	lbf	b4	10	843	225	1524
910424	12	bis	a5	13	901	235	914
910424	12	hon	a5	11	906	215	914
910425	0	lbf	b4	13	872	160	1219
910425	0	lbf	b4	13	810	200	1829
910425	0	ddc	b4	13	850	145	1458
910425	0	ddc	b4	13	812	160	1829
910425	0	ovn	a5	9	943	170	610
910425	0	ovn	a5	9	784	205	2134
910425	0	hon	b4	11	850	185	1438
910425	0	hon	b4	11	811	195	1829
910425	0	stc	a3	13	941	185	610

910425	0	stc	a3	13	844	200	1524
910425	12	lbf	b4	11	870	245	1219
910425	12	lbf	b4	11	850	245	1416
910425	12	bis	b1	13	898	210	914
910425	12	top	a5	8	942	140	610
910425	12	top	a5	8	908	180	914
910425	12	ovn	a2	13	943	180	610
910425	12	ovn	a2	13	908	195	914
910425	12	hon	b1	14	808	205	1829
910425	12	stc	a3	14	941	215	610
910425	12	stc	a3	14	908	225	914
910426	0	ovn	a5	14	905	165	914
910426	0	hon	a2	18	931	175	610
910426	0	stc	a5	12	940	165	610
910426	0	stc	a5	12	812	180	1829
910426	12	ddc	b3	23	895	195	914
910426	12	top	b1	28	809	215	1829
910426	12	ovn	c	29	750	205	2438
910426	12	ovn	c	29	722	210	2743
910426	12	stc	a2	15	939	165	610
910426	12	stc	a2	15	850	170	1434
910427	12	stc	b3	29	850	150	1313
910427	12	stc	b3	29	799	160	1829
910428	0	stc	c	19	746	235	2438
910428	12	bis	b3	25	887	235	914
910428	12	top	a2	13	935	110	610
910428	12	ovn	a5	10	937	170	610
910428	12	ovn	a5	10	904	165	914
910429	0	top	b3	19	850	165	1386
910429	0	ovn	b3	18	850	125	1400
910502	12	oun	a2	18	945	150	610
910502	12	lbf	b3	21	813	185	1829
910502	12	ddc	b1	14	850	190	1485
910503	0	oun	c	30	729	185	2743
910503	0	ovn	c	16	703	220	3048
910503	0	ovn	c	16	700	220	3078
910503	12	oun	b3	19	812	240	1829
910503	12	top	b1	19	872	195	1219
910503	12	top	b1	19	841	195	1524
910503	12	ovn	a3	18	938	115	610
910503	12	hon	b3	22	839	155	1524
910503	12	stc	a1	15	947	95	610
910504	0	stc	c	25	724	175	2743
910504	12	oun	b3	12	874	220	1219
910504	12	oun	b3	12	843	215	1524
910507	12	ddc	b4	16	816	220	1829
910507	12	top	a2	22	946	210	610
910508	0	top	c	17	791	210	2134
910508	0	top	c	17	734	195	2743
910508	12	oun	a5	11	944	145	610
910508	12	bis	a2	15	912	165	914
910508	12	top	a5	11	948	185	610
910508	12	hon	a5	9	948	120	610
910508	12	hon	a5	9	914	150	914
910508	12	stc	a5	8	951	125	610
910508	12	stc	a5	8	883	135	1219
910509	0	stc	b4	9	882	165	1219
910509	0	stc	b4	9	850	170	1521
910509	12	lbf	b1	16	812	190	1829
910509	12	lbf	b1	16	783	205	2134
910509	12	bis	b1	25	868	205	1219
910509	12	bis	b1	25	850	205	1395
910509	12	ddc	b2	15	846	175	1524
910509	12	ovn	b3	13	880	200	1219
910509	12	ovn	b3	13	850	200	1509
910509	12	hon	a2	20	941	190	610
910509	12	stc	a2	14	946	180	610
910509	12	stc	a2	14	880	220	1219
910510	0	oun	c	10	759	145	2438
910510	0	ovn	b1	14	879	160	1219
910510	0	ovn	b1	14	789	180	2134
910510	0	hon	b1	21	874	170	1219

910510	0	hon	b1	21	850	170	1461
910510	0	stc	b1	13	850	190	1829
910510	0	stc	b1	13	790	220	2134
910510	12	lbf	c	23	784	200	2134
910510	12	lbf	c	23	756	200	2438
910510	12	bis	a5	19	902	170	914
910510	12	ddc	b2	16	878	175	1219
910510	12	ddc	b2	16	850	185	1490
910510	12	top	a5	9	947	170	610
910510	12	top	a5	9	850	175	1524
910510	12	ovn	a2	13	947	175	610
910510	12	ovn	a2	13	913	185	914
910510	12	hon	a3	23	908	185	914
910510	12	stc	a3	17	948	190	610
910511	0	lbf	c	20	787	175	2134
910511	0	lbf	c	20	760	180	2438
910511	0	ddc	a5	17	910	160	914
910511	0	ddc	a5	17	879	160	1219
910511	0	ovn	b4	11	851	155	1524
910511	0	hon	b1	18	850	175	1501
910511	0	stc	b2	12	822	185	1829
910511	12	oun	a5	11	946	160	610
910511	12	oun	a5	11	882	195	1219
910511	12	lbf	c	20	733	205	2743
910511	12	ddc	b1	20	879	190	1219
910511	12	stc	a3	12	950	215	610
910512	0	oun	b2	12	851	190	1524
910512	0	oun	b2	12	850	190	1537
910512	0	lbf	c	16	789	180	2134
910512	0	bis	c	13	707	182	3048
910512	0	ovn	b4	8	850	185	1535
910512	12	ddc	a3	23	908	190	914
910512	12	top	a3	13	912	220	914
910512	12	top	a3	13	880	220	1219
910513	0	hon	c	19	756	210	2438
910513	12	oun	a2	16	942	205	610
910513	12	top	a2	15	910	265	914
910513	12	top	a2	15	879	265	1219
910514	0	oun	a5	9	940	160	610
910514	0	oun	a5	9	908	165	914
910514	12	oun	a3	15	940	180	610
910514	12	oun	a3	15	907	185	914
910514	12	lbf	c	12	784	205	2134
910514	12	lbf	c	12	756	205	2438
910514	12	top	a2	21	941	230	610
910514	12	ovn	a2	13	941	210	610
910514	12	hon	a5	10	905	200	914
910514	12	hon	a5	10	874	200	1219
910515	0	oun	b2	12	874	170	1219
910515	0	oun	b2	12	850	170	1459
910515	0	ovn	b4	8	875	180	1219
910515	0	hon	b1	15	813	190	1829
910515	0	stc	a5	8	908	150	914
910515	0	stc	a5	8	877	150	1219
910515	12	oun	a5	12	937	170	610
910515	12	lbf	b1	15	810	180	1829
910515	12	ddc	b1	20	810	210	1829
910515	12	ovn	a3	13	940	155	610
910515	12	hon	b1	15	874	210	1219
910515	12	hon	b1	15	844	210	1524
910516	0	ddc	b4	17	850	155	1423
910516	0	top	b1	16	815	200	1829
910516	12	ovn	b1	18	815	225	1829
910517	12	oun	b3	15	850	230	1475
910518	0	ovn	c	10	756	240	2438
910518	12	oun	a4	8	946	185	610
910518	12	bis	b1	14	850	110	1551
910519	0	bis	a5	12	950	130	610
910519	0	bis	a5	12	917	130	914
910519	0	stc	b4	9	856	90	1524
910519	0	stc	b4	9	824	100	1829
910519	12	lbf	b1	20	822	200	1829

910519	12	bis	c	15	791	195	2134
910519	12	bis	c	15	763	200	2438
910519	12	ddc	b4	11	853	175	1524
910519	12	ddc	b4	11	823	170	1829
910519	12	stc	a5	10	922	125	914
910520	0	lbf	c	15	765	155	2438
910520	0	bis	c	19	761	200	2438
910520	12	lbf	b2	12	881	175	1219
910520	12	lbf	b2	12	850	190	1525
910520	12	stc	a5	8	952	185	610
910520	12	stc	a5	8	886	190	1219
910521	0	lbf	c	15	788	190	2134
910521	0	bis	c	21	732	180	2743
910521	0	ovn	b3	11	850	180	1533
910521	0	stc	c	13	711	120	3048
910521	0	stc	c	13	700	115	3172
910521	12	lbf	c	19	759	220	2438
910521	12	bis	a2	13	904	220	914
910521	12	ddc	a2	17	911	200	914
910521	12	top	a3	13	945	190	610
910521	12	ovn	a3	13	946	180	610
910521	12	hon	a2	19	941	185	610
910521	12	hon	a2	19	909	195	914
910521	12	stc	a2	15	947	195	610
910521	12	stc	a2	15	914	205	914
910522	0	bis	c	11	785	195	2134
910522	0	top	b3	12	880	170	1219
910522	0	top	b3	12	850	165	1519
910522	0	hon	a5	13	907	155	914
910522	0	hon	a5	13	816	190	1829
910522	0	stc	a5	10	945	160	610
910522	0	stc	a5	10	763	200	2438
910522	12	oun	a5	10	944	160	610
910522	12	oun	a5	10	911	165	914
910522	12	bis	a5	11	903	240	914
910522	12	bis	a5	11	841	260	1219
910522	12	ovn	a3	16	912	200	914
910522	12	hon	a3	18	907	210	914
910522	12	stc	a3	12	944	195	610
910522	12	stc	a3	12	880	220	1219
910523	0	oun	a5	12	943	155	610
910523	0	ddc	b4	16	847	180	1491
910523	0	ddc	b4	16	817	180	1524
910523	0	top	a2	13	945	180	610
910523	0	top	a2	13	912	185	914
910523	0	ovn	b3	18	879	180	1219
910523	0	ovn	b3	18	850	180	1504
910523	0	stc	b4	13	819	200	1829
910523	12	oun	a2	16	943	185	610
910523	12	oun	a2	16	911	190	914
910523	12	ddc	b1	17	878	200	1219
910523	12	top	b1	14	879	210	1219
910523	12	top	b1	14	848	215	1524
910523	12	ovn	b3	18	878	225	1219
910523	12	ovn	b3	18	850	230	1496
910523	12	stc	a3	16	941	195	610
910525	12	bis	a3	12	911	150	914
910525	12	hon	b4	9	850	105	1498
910526	0	stc	b2	12	850	95	1479
910526	12	oun	a3	13	908	205	914
910526	12	ddc	b3	17	844	210	1524
910527	0	oun	b2	16	817	215	1829
910527	12	ddc	b3	17	843	225	1524
910528	0	oun	c	15	792	175	2134
910528	12	oun	c	20	700	145	3183
910528	12	bis	a5	11	910	95	914
910528	12	ddc	b1	26	819	190	1829
910528	12	top	a2	22	912	220	914
910528	12	top	a2	22	881	220	1219
910528	12	ovn	b3	23	879	235	1219
910529	0	oun	b3	14	821	175	1829
910529	0	ddc	b2	22	876	165	1219

910529	0	ddc	b2	22	816	170	1829
910529	12	oun	a3	12	944	200	610
910529	12	oun	a3	12	880	210	1219
910529	12	lbf	b4	8	875	105	1219
910529	12	top	a5	11	943	220	610
910530	12	ddc	b1	27	839	190	1524
910530	12	top	c	23	756	245	2438
910531	0	top	c	20	728	215	2743
910531	0	ovn	c	19	753	215	2438
910531	12	lbf	b3	14	863	190	1219
910531	12	lbf	b3	14	850	195	1347
910531	12	ddc	b1	24	866	185	1219
910531	12	top	b3	20	871	215	1219
910531	12	top	b3	20	841	225	1524
910531	12	ovn	b3	22	869	220	1219
910601	0	oun	b1	16	874	180	1219
910601	0	ddc	b4	18	870	175	1219
910601	0	ddc	b4	18	850	175	1425
910601	0	ovn	a5	11	904	175	914
910601	0	ovn	a5	11	813	215	1829
910601	12	oun	a3	17	939	180	610
910601	12	oun	a3	17	907	190	914
910601	12	top	a2	14	907	215	914
910602	0	oun	b3	14	875	175	1219
910602	0	oun	b3	14	850	180	1474
910602	0	ovn	b3	20	847	250	1524
910602	0	ovn	b3	20	817	250	1829
910602	12	ddc	b1	23	875	190	1219
910602	12	top	b1	16	850	250	1483
910602	12	top	b1	16	816	255	1829
910603	0	ddc	c	16	759	165	2438
910603	0	ddc	c	16	732	170	2743
910603	0	top	c	8	700	230	2743
910603	12	oun	b1	13	876	245	1219
910603	12	lbf	c	12	785	165	2134
910603	12	bis	a5	9	909	145	914
910603	12	ovn	c	8	700	200	3125
910604	0	oun	b3	17	815	210	1829
910604	0	bis	b4	11	850	120	1478
910604	0	bis	b4	11	815	120	1829
910604	0	ovn	c	10	787	180	2134
910604	12	oun	a5	10	940	220	610
910604	12	oun	a5	10	877	250	1219
910604	12	bis	b1	15	850	125	1460
910604	12	top	a5	8	940	235	610
910604	12	top	a5	8	908	225	914
910604	12	stc	b3	16	881	125	1219
910605	0	ovn	a5	11	910	120	914
910605	0	ovn	a5	11	850	165	1498
910605	0	hon	b3	19	850	140	1488
910605	0	hon	b3	19	816	150	1829
910605	12	oun	a2	16	942	210	610
910605	12	lbf	b4	8	879	155	1219
910605	12	ovn	a2	12	947	135	610
910605	12	hon	a1	14	946	135	610
910605	12	stc	a3	12	918	135	914
910605	12	stc	a3	12	886	135	1219
910606	0	bis	c	12	791	165	2134
910606	0	ovn	a5	11	949	100	610
910606	0	ovn	a5	11	916	115	914
910606	0	hon	b2	12	883	140	1219
910606	12	bis	a3	12	916	175	914
910606	12	top	a1	13	951	115	610
910606	12	ovn	a1	12	953	135	610
910606	12	hon	a2	16	952	165	610
910606	12	stc	a4	10	956	180	610
910607	12	oun	a2	14	915	160	914
910607	12	lbf	b1	15	883	160	1219
910607	12	lbf	b1	15	850	170	1537
910607	12	bis	a3	15	913	175	914
910607	12	ddc	b3	14	883	155	1219
910607	12	top	a2	13	951	150	610

910607	12	ovn	a5	11	954	150	610
910607	12	hon	a2	16	951	180	610
910607	12	stc	a5	9	954	205	610
910607	12	stc	a5	9	921	215	914
910608	0	ovn	b4	9	823	160	1829
910608	0	ovn	b4	9	794	175	2134
910608	12	ddc	a5	13	913	215	914
910608	12	ovn	a2	14	916	165	914
910608	12	hon	a3	15	946	175	610
910609	0	oun	a5	12	946	160	610
910609	0	oun	a5	12	912	165	914
910609	0	lbf	b4	10	878	175	1219
910609	0	oun	a5	12	850	175	1504
910609	0	top	c	13	792	175	2134
910609	0	top	c	13	764	175	2438
910609	0	ovn	a5	11	915	185	914
910609	0	ovn	a5	11	821	220	1829
910609	0	stc	c	15	700	205	3156
910609	12	oun	a2	12	948	165	610
910609	12	lbf	b1	13	850	230	1500
910609	12	lbf	b1	13	848	230	1524
910609	12	top	b1	17	884	200	1219
910609	12	top	b1	17	850	195	1553
910609	12	ovn	b1	15	883	200	1219
910609	12	hon	a2	17	953	205	610
910609	12	hon	a2	17	888	245	1219
910609	12	stc	a3	15	946	210	610
910610	0	lbf	c	11	762	200	2438
910610	0	ovn	a5	12	915	195	914
910610	0	stc	b3	17	880	215	1219
910610	0	stc	b3	17	850	220	1517
910610	12	oun	a4	10	948	200	610
910610	12	oun	a4	10	915	200	914
910610	12	ddc	b1	12	821	260	1829
910610	12	ddc	b1	12	792	255	2134
910610	12	top	a2	13	915	225	914
910612	12	oun	a5	9	944	205	610
910612	12	lbf	b4	11	874	205	1219
910612	12	lbf	b4	11	844	200	1524
910612	12	bis	c	17	781	230	2134
910612	12	bis	c	17	754	225	2438
910612	12	ddc	b4	11	877	215	1219
910612	12	top	a5	11	944	220	610
910612	12	hon	a3	15	937	190	610
910612	12	hon	a3	15	906	200	914
910613	0	top	a5	9	911	175	914
910613	0	ovn	b4	8	819	190	1829
910613	0	ovn	b4	8	762	205	2438
910613	0	hon	a5	11	906	195	914
910613	0	hon	a5	11	876	190	1219
910613	0	stc	a5	11	942	170	610
910613	12	lbf	b3	13	872	180	1219
910613	12	hon	a3	19	904	210	914
910614	0	oun	c	16	735	225	2743
910614	0	oun	c	16	700	225	3155
910614	0	ddc	c	17	786	215	2134
910614	0	ddc	c	17	758	220	2438
910614	0	hon	a5	15	933	190	610
910614	0	hon	a5	15	902	190	914
910614	0	stc	c	15	759	225	2438
910614	12	stc	c	10	700	140	3079
910615	0	oun	b3	17	818	195	1829
910615	0	top	b3	20	816	210	1829
910615	0	top	b3	20	700	210	3134
910615	12	oun	b1	15	877	250	1219
910615	12	top	b3	20	875	260	1219
910615	12	stc	a1	12	935	255	610
910615	12	stc	a1	12	902	255	914
910616	12	lbf	b4	10	881	160	1219
910617	12	lbf	b1	16	877	225	1219
910617	12	ddc	b3	13	880	205	1219
910617	12	hon	b3	18	877	230	1219

910617	12	hon	b3	18	850	240	1486
910617	12	stc	a3	13	944	190	610
910618	0	lbf	b4	9	850	165	1487
910618	0	lbf	b4	9	817	170	1829
910618	0	ddc	b2	14	878	170	1219
910618	0	ddc	b2	14	850	170	1503
910618	0	hon	c	13	761	230	2438
910618	0	hon	c	13	734	235	2743
910618	12	lbf	b1	12	880	170	1219
910618	12	top	a4	9	946	175	610
910618	12	ovn	a4	10	945	180	610
910619	12	lbf	b1	16	820	190	1829
910620	0	lbf	b3	16	820	165	1829
910620	0	lbf	b3	16	792	175	2134
910620	12	lbf	b3	22	816	205	1829
910620	12	ddc	c	12	763	210	2438
910620	12	ddc	c	12	736	205	2743
910620	12	top	a2	13	947	175	610
910620	12	ovn	a3	18	946	185	610
910620	12	hon	a3	23	907	195	914
910620	12	hon	a3	23	876	215	1219
910621	0	ovn	a5	12	910	165	914
910621	0	ovn	a5	12	819	195	1829
910621	0	stc	c	18	790	220	2134
910621	12	top	a2	14	943	195	610
910622	0	oun	a5	12	909	200	914
910622	0	oun	a5	12	878	210	1219
910622	12	oun	b1	13	879	225	1219
910622	12	bis	a2	15	915	115	914
910622	12	bis	a2	15	882	115	1219
910623	12	bis	b1	16	879	185	1219
910623	12	bis	b1	16	847	190	1524
910624	12	oun	b4	10	882	215	1219
910624	12	lbf	b2	14	880	175	1219
910624	12	ddc	c	14	792	250	2134
910624	12	hon	a3	13	946	185	914
910625	0	lbf	c	19	788	180	2134
910625	0	lbf	c	19	760	190	2438
910625	0	ddc	c	17	764	200	2438
910625	0	ddc	c	17	737	215	2743
910625	0	ovn	b4	10	882	155	1219
910625	0	ovn	b4	10	850	155	1538
910625	0	hon	a5	14	943	160	610
910625	0	stc	b4	10	852	180	1524
910625	0	stc	b4	10	821	195	1829
910625	12	oun	a5	11	945	205	610
910625	12	lbf	b3	22	873	175	1219
910625	12	bis	a3	16	903	165	914
910625	12	ddc	b1	23	878	220	1219
910625	12	top	a5	10	946	180	610
910625	12	top	a5	10	882	210	1219
910625	12	ovn	a3	15	913	195	914
910625	12	hon	a2	23	939	170	610
910625	12	hon	a2	23	907	180	914
910625	12	stc	a3	13	914	200	914
910626	0	oun	a5	10	914	170	914
910626	0	lbf	c	22	700	215	3141
910626	0	top	b4	13	881	185	1219
910626	0	top	b4	13	793	210	2134
910626	0	ovn	b1	21	850	185	1509
910626	0	ovn	b1	21	849	190	1524
910626	0	hon	b4	16	850	190	1459
910626	0	hon	b4	16	844	190	1524
910626	12	ddc	b1	25	878	220	1219
910626	12	ddc	b1	25	850	220	1505
910626	12	top	a2	23	944	210	610
910626	12	ovn	a3	29	940	205	610
910626	12	stc	b3	25	874	215	1219
910627	0	top	b2	13	911	185	914
910627	0	top	b2	13	821	200	1829
910627	0	ovn	b1	25	818	220	1495
910627	0	ovn	b1	25	763	215	2438

910627	12	oun	a2	17	941	180	610
910627	12	lbf	b1	15	873	210	1219
910627	12	bis	b3	15	813	265	1829
910627	12	bis	b3	15	784	265	2134
910627	12	ddc	a2	24	909	200	914
910627	12	ddc	a2	24	878	205	1219
910627	12	top	a3	20	912	215	914
910627	12	ovn	a3	23	943	205	610
910627	12	ovn	a3	23	910	215	914
910628	0	lbf	c	15	789	175	2134
910628	0	ddc	b2	17	819	180	1829
910628	0	top	b4	10	881	175	1219
910628	0	top	b4	10	822	195	1829
910628	0	ovn	b4	13	880	175	1219
910628	0	ovn	b4	13	850	190	1524
910628	12	oun	a2	14	945	180	610
910628	12	lbf	b3	24	850	200	1455
910628	12	bis	a2	16	910	120	914
910628	12	ddc	a2	23	910	195	914
910628	12	top	a2	17	945	205	610
910628	12	top	a2	17	913	220	914
910628	12	ovn	a2	17	944	215	610
910628	12	ovn	a2	17	912	225	914
910629	0	oun	b4	10	882	170	1219
910629	0	top	a5	11	912	185	914
910629	0	top	a5	11	881	185	1219
910629	0	ovn	a5	12	942	190	610
910629	0	ovn	a5	12	792	210	2134
910629	12	oun	b1	12	881	205	1219
910629	12	oun	b1	12	850	195	1533
910629	12	lbf	b3	15	874	205	1219
910629	12	ddc	a2	23	909	200	914
910629	12	ddc	a2	23	878	215	1219
910629	12	top	a2	19	945	215	610
910629	12	ovn	a1	18	943	225	610
910629	12	ovn	a1	18	911	240	914
910630	0	oun	b2	14	851	200	1524
910630	0	lbf	c	15	761	180	2438
910630	0	top	a5	11	912	195	914
910630	0	ovn	c	11	792	195	2134
910630	0	hon	b1	14	850	130	1505
910630	0	hon	b1	14	848	125	1524
910630	12	oun	a3	19	913	215	914
910630	12	oun	a3	19	882	215	1219
910630	12	bis	a3	13	900	160	914
910630	12	ddc	b1	23	850	220	1497
910630	12	top	a1	18	943	220	610
910630	12	ovn	a2	19	942	210	610
910630	12	stc	a5	12	943	110	610
910701	0	oun	c	16	737	225	2743
910701	0	top	c	16	789	225	2134
910701	0	ovn	b1	16	816	210	1829
910701	0	ovn	b1	16	788	225	2134
910701	12	oun	a3	18	944	225	610
910701	12	oun	a3	18	912	230	914
910701	12	ovn	a3	13	940	225	610
910702	0	oun	c	13	793	230	2134
910702	0	top	c	9	764	235	2438
910702	12	oun	a4	11	945	220	610
910702	12	ddc	a2	14	911	180	914
910705	12	oun	a2	13	944	210	610
910705	12	lbf	b1	14	874	185	1219
910705	12	bis	a3	15	900	220	914
910705	12	ddc	a5	13	908	240	914
910705	12	top	a3	16	941	240	610
910705	12	hon	a3	14	936	190	610
910706	0	ovn	b3	15	817	235	1829
910706	12	ddc	b1	25	877	235	1219
910706	12	top	b1	26	877	245	1219
910706	12	ovn	a3	14	905	240	914
910707	0	top	a5	16	939	205	610
910707	12	oun	b4	8	881	220	1219

910707	12	lbf	b1	20	875	220	1219
910707	12	ddc	a2	17	910	230	914
910707	12	ddc	a2	17	879	235	1219
910707	12	top	a2	22	942	225	610
910708	12	oun	a5	13	950	200	610
910708	12	lbf	b4	10	884	110	1219
910709	0	top	b3	11	822	220	1829
910709	12	oun	a2	15	944	220	610
910709	12	oun	a2	15	912	230	914
910709	12	ddc	b1	17	850	240	1500
910709	12	ddc	b1	17	819	240	1829
910709	12	hon	a2	14	909	185	914
910709	12	hon	a2	14	877	185	1219
910709	12	stc	a4	8	946	155	610
910709	12	stc	a4	8	913	165	914
910710	0	oun	a5	11	942	175	610
910710	0	oun	a5	11	736	235	3048
910710	12	oun	a2	23	942	215	610
910710	12	bis	a5	8	909	140	914
910710	12	bis	a5	8	878	135	1219
910710	12	top	b3	15	847	260	1524
910711	0	oun	b2	12	850	190	1509
910711	0	oun	b2	12	763	235	2438
910711	12	oun	b3	16	879	240	1219
910711	12	lbf	c	9	789	266	2134
910711	12	lbf	c	9	761	255	2438
910711	12	stc	a5	9	945	145	610
910711	12	stc	a5	9	912	145	914
910712	0	oun	b2	13	850	205	1524
910712	12	oun	b1	13	883	245	1219
910714	12	hon	a1	12	949	185	610
910715	0	lbf	b4	11	850	175	1541
910715	0	lbf	b4	11	822	175	1829
910715	0	hon	a5	13	945	170	610
910715	0	hon	a5	13	850	195	1540
910715	12	lbf	b1	18	881	200	1219
910715	12	ddc	b1	15	884	215	1219
910715	12	ddc	b1	15	824	200	1829
910715	12	top	a5	9	950	190	610
910715	12	hon	a3	19	944	190	610
910715	12	stc	a2	17	949	205	610
910716	0	lbf	c	15	737	200	2743
910716	0	ovn	b1	14	824	210	1829
910716	0	hon	b1	17	850	195	1520
910716	0	stc	b3	15	853	215	1524
910716	0	stc	b3	15	823	220	1829
910716	12	oun	a1	12	950	180	610
910716	12	lbf	b1	20	881	200	1219
910716	12	ddc	b1	19	884	185	1219
910716	12	top	a1	13	950	200	610
910716	12	ovn	a2	18	949	210	610
910716	12	hon	a2	20	942	220	610
910716	12	stc	a1	22	945	210	610
910717	0	lbf	b2	14	880	170	1219
910717	0	ovn	b4	11	826	205	1829
910717	0	ovn	b4	11	769	230	2438
910717	12	oun	a4	10	948	190	610
910717	12	lbf	b1	15	879	190	1219
910717	12	ddc	b1	17	913	190	914
910717	12	top	a1	15	948	205	610
910717	12	ovn	a2	16	947	215	610
910717	12	ovn	a2	16	915	225	914
910717	12	hon	a3	13	942	230	610
910718	0	lbf	b4	9	818	180	1829
910718	0	lbf	b4	9	737	185	2743
910718	0	ovn	b4	11	852	200	1524
910718	0	ovn	b4	11	850	200	1542
910718	0	stc	a1	13	945	135	610
910718	0	stc	a1	13	913	140	914
910718	12	oun	a5	9	913	205	914
910718	12	oun	a5	9	881	215	1219
910718	12	lbf	b3	14	874	200	1219

910718	12	ddc	a3	22	909	195	914
910718	12	top	a1	14	912	205	914
910718	12	ovn	a2	14	911	205	914
910718	12	ovn	a2	14	880	200	1219
910718	12	hon	a3	21	936	205	610
910718	12	hon	a3	21	904	225	914
910718	12	stc	b1	22	877	240	1219
910719	0	ovn	b1	15	876	185	1219
910719	0	ovn	b1	15	735	250	2743
910719	0	stc	b3	23	815	225	1829
910719	12	oun	b1	16	879	220	1219
910719	12	top	a2	20	941	200	610
910720	0	oun	b4	9	820	200	1829
910720	0	oun	b4	9	792	210	2134
910720	0	ddc	b2	12	876	210	1219
910720	0	ddc	b2	12	700	240	3168
910720	0	top	c	11	792	190	2134
910720	0	top	c	11	764	195	2438
910720	0	ovn	c	11	737	205	2743
910720	12	bis	b3	13	844	250	1524
910720	12	ddc	c	15	764	225	2438
910720	12	top	a2	16	942	215	610
910720	12	ovn	b1	26	878	220	1219
910720	12	stc	a3	14	940	180	610
910721	0	top	b1	16	851	215	1524
910721	0	top	b1	16	850	215	1537
910721	12	bis	b1	12	819	185	1829
910721	12	bis	b1	12	791	190	2134
910721	12	ovn	a2	20	945	180	610
910721	12	ovn	a2	20	913	185	914
910721	12	hon	b4	8	880	130	1219
910721	12	hon	b4	8	792	110	2134
910722	0	bis	c	17	734	245	2743
910722	0	bis	c	17	700	245	3144
910722	0	top	a5	10	914	190	914
910722	0	top	a5	10	884	195	1219
910722	0	ovn	c	19	739	240	2743
910722	12	oun	a2	16	917	240	914
910722	12	ddc	b1	16	852	230	1524
910722	12	ddc	b1	16	823	235	1829
910722	12	top	a2	19	946	220	610
910722	12	top	a2	19	914	240	914
910723	0	top	c	11	795	230	2134
910723	0	top	c	11	741	235	2743
910723	12	oun	a1	12	949	215	610
910726	12	lbf	b1	15	882	195	1219
910726	12	lbf	b1	15	850	195	1543
910726	12	bis	a2	14	914	150	914
910726	12	ovn	a4	8	952	150	610
910726	12	hon	a4	10	950	165	610
910727	0	lbf	b2	14	881	170	1219
910727	0	lbf	b2	14	764	185	2438
910727	0	hon	a2	16	947	140	610
910727	12	lbf	b1	13	881	200	1219
910727	12	lbf	b1	13	851	210	1524
910727	12	bis	a4	11	913	130	914
910727	12	ddc	b2	12	883	195	1219
910727	12	ddc	b2	12	850	185	1547
910727	12	top	a2	15	950	145	610
910727	12	ovn	a2	14	951	175	610
910727	12	hon	a3	15	947	195	610
910727	12	hon	a3	15	914	210	914
910727	12	stc	a5	9	952	195	610
910727	12	stc	a5	9	850	175	1573
910728	0	bis	a5	8	914	95	914
910728	12	stc	a4	8	948	165	610
910729	12	bis	b3	15	881	195	1219
910729	12	bis	b3	15	821	250	1829
910730	12	bis	a3	17	907	215	914
910730	12	bis	a3	17	876	230	1219
910730	12	ddc	b1	15	883	245	1219
910731	0	ovn	b2	12	882	195	1219

910731	12	oun	a5	8	948	210	610
910731	12	ddc	a2	31	913	225	914
910731	12	top	b1	20	853	265	1524
910731	12	ovn	a5	10	912	155	914
910801	12	oun	b4	8	884	205	1219
910801	12	oun	b4	8	854	200	1524
910801	12	ddc	a2	18	913	230	914
910801	12	ovn	b4	9	850	185	1550
910801	12	ovn	b4	9	823	195	1829
910802	0	lbf	c	12	763	200	2438
910802	0	ovn	b2	12	880	195	1219
910802	12	oun	a5	9	882	195	1219
910802	12	bis	a1	12	909	110	914
910802	12	ddc	b1	23	879	220	1219
910802	12	top	a2	20	910	245	914
910802	12	ovn	a3	19	939	245	610
910803	0	oun	a5	9	912	175	914
910803	0	top	b2	13	820	220	1829
910803	0	top	b2	13	792	235	2134
910803	12	oun	a5	10	946	190	610
910803	12	top	c	15	738	260	2743
910804	12	oun	a4	10	947	205	610
910804	12	oun	a4	10	915	215	914
910804	12	lbf	b4	10	885	120	1219
910805	12	oun	a2	14	945	210	610
910805	12	bis	a2	15	911	155	914
910805	12	bis	a2	15	879	160	1219
910805	12	top	c	16	765	235	2438
910805	12	ovn	a5	9	948	145	610
910805	12	hon	a5	11	947	150	610
910806	0	hon	a5	14	943	145	610
910806	0	hon	a5	14	850	160	1507
910806	0	stc	a5	8	940	140	610
910806	0	stc	a5	8	823	145	1829
910806	12	oun	a2	13	946	220	610
910806	12	lbf	b4	9	848	240	1524
910806	12	ddc	b1	17	880	215	1219
910806	12	top	a4	11	946	200	610
910806	12	stc	a5	11	950	150	610
910806	12	stc	a5	11	885	150	1219
910807	0	ovn	b3	13	823	240	1829
910807	0	stc	a5	11	952	110	610
910807	0	stc	a5	11	886	130	1219
910807	12	oun	a2	13	950	200	610
910807	12	bis	a5	11	914	150	914
910807	12	ddc	a3	18	914	205	914
910807	12	ddc	a3	18	883	215	1219
910807	12	top	a2	16	949	230	610
910807	12	ovn	a3	14	948	230	610
910807	12	ovn	a3	14	850	235	1565
910808	12	ddc	a2	16	913	255	914
910808	12	top	c	21	765	255	2438
910809	12	bis	a5	9	917	185	914
910810	12	lbf	b1	12	884	155	1219
910810	12	bis	b4	10	883	175	1219
910810	12	hon	c	8	793	140	2134
910810	12	hon	c	8	765	145	2438
910811	12	lbf	b1	13	884	140	1219
910811	12	lbf	b1	13	823	180	1829
910811	12	bis	a2	15	916	155	914
910811	12	bis	a2	15	884	155	1219
910811	12	ddc	a5	12	916	165	914
910811	12	ddc	a5	12	884	175	1219
910811	12	top	a4	8	951	150	610
910812	12	bis	a2	15	919	160	914
910812	12	ddc	b1	14	854	180	1524
910812	12	ddc	b1	14	850	180	1569
910812	12	ovn	a5	8	954	155	610
910812	12	ovn	a5	8	889	150	1219
910812	12	hon	a5	10	954	150	610
910813	0	lbf	b2	13	825	135	1829
910814	12	lbf	b4	10	821	205	1829

910814	12	bis	a2	14	911	190	914
910815	0	hon	b4	10	878	180	1219
910815	0	hon	b4	10	818	185	1829
910815	12	lbf	b1	14	878	215	1219
910815	12	ddc	a5	13	913	200	914
910815	12	ovn	a2	12	945	205	610
910815	12	hon	a2	13	939	210	610
910816	0	ovn	c	11	791	230	2134
910816	12	oun	a5	9	913	205	914
910816	12	oun	a5	9	881	205	1219
910816	12	ddc	a2	20	909	210	914
910816	12	top	b1	21	880	230	1219
910816	12	ovn	a2	19	942	215	610
910817	12	oun	a5	11	912	265	914
910819	12	bis	a5	11	912	190	914
910819	12	bis	a5	11	881	200	1219
910820	12	lbf	b4	10	879	225	1219
910820	12	top	a4	9	947	155	610
910820	12	hon	a5	13	940	145	610
910820	12	stc	a2	15	945	195	610
910821	0	ovn	a3	14	912	220	914
910821	0	ovn	a3	14	880	230	1219
910821	0	stc	b4	10	850	175	1504
910821	0	stc	b4	10	848	175	1524
910821	12	oun	a4	13	945	210	610
910821	12	ovn	a1	20	944	245	610
910822	12	lbf	b4	8	885	245	1219
910822	12	bis	b1	13	879	130	1219
910823	0	ovn	a5	9	914	180	914
910823	0	ovn	a5	9	883	210	1219
910823	12	bis	a1	14	914	100	914
910823	12	ovn	b4	10	885	230	1219
910824	0	bis	a2	15	945	115	610
910824	12	lbf	b4	12	881	195	1219
910824	12	bis	b1	20	850	195	1495
910824	12	bis	b1	20	818	200	1829
910824	12	ddc	a2	16	916	205	914
910824	12	top	a5	8	950	185	610
910824	12	ovn	a5	11	950	180	610
910824	12	ovn	a5	11	918	205	914
910824	12	hon	a3	12	914	180	914
910824	12	hon	a3	12	883	185	1219
910825	0	lbf	c	9	794	195	2134
910825	0	lbf	c	9	740	200	2743
910825	0	ovn	c	12	797	220	2134
910825	0	hon	b1	18	850	190	1531
910825	0	hon	b1	18	821	195	1829
910825	0	stc	b1	17	885	195	1219
910825	12	lbf	b1	19	881	235	1219
910825	12	ddc	a2	20	917	210	914
910825	12	top	b1	12	887	225	1219
910825	12	ovn	a2	19	949	215	610
910825	12	hon	a3	14	941	220	610
910825	12	stc	b1	19	854	195	1524
910825	12	stc	b1	19	850	185	1567
910827	0	lbf	c	13	791	190	2134
910827	0	ovn	b4	10	850	200	1554
910827	0	ovn	b4	10	766	215	2438
910827	0	hon	a5	15	938	190	610
910827	0	hon	a5	15	850	205	1502
910827	0	stc	b1	17	881	215	1219
910827	12	oun	a1	12	947	225	610
910827	12	lbf	b1	15	878	205	1219
910827	12	bis	a5	8	906	95	914
910827	12	bis	a5	8	875	95	1219
910827	12	ddc	b1	17	882	200	1219
910827	12	top	a1	12	947	210	610
910827	12	ovn	a2	14	947	215	610
910827	12	hon	a1	19	940	205	610
910827	12	stc	a2	20	944	230	610
910827	12	stc	a2	20	912	240	914
910828	0	oun	b4	10	882	170	1219

910828	0	lbf	c	12	790	170	2134
910828	0	ovn	b4	10	822	200	1829
910828	0	ovn	b4	10	794	205	2134
910828	0	hon	a2	19	939	160	610
910828	0	stc	a2	13	945	195	610
910828	12	lbf	b1	16	877	180	1219
910828	12	bis	a3	20	903	185	914
910828	12	ddc	b2	19	850	210	1524
910828	12	top	a1	12	947	200	610
910828	12	top	a1	12	914	215	914
910828	12	ovn	a5	11	947	195	610
910828	12	ovn	a5	11	850	185	1548
910828	12	hon	a2	21	941	180	610
910828	12	stc	a2	16	947	205	610
910829	0	ovn	b4	10	850	185	1553
910829	0	ovn	b4	10	766	220	2438
910829	0	hon	a5	14	909	180	914
910829	0	hon	a5	14	791	210	2134
910829	0	stc	b3	14	850	185	1557
910829	0	stc	b3	14	823	200	1829
910829	12	top	a1	12	948	200	610
910829	12	top	a1	12	915	215	914
910829	12	ovn	a2	14	948	205	610
910829	12	hon	a3	14	911	260	914
910829	12	stc	b1	12	883	235	1219
910830	0	top	a4	10	948	110	610
910831	12	bis	a1	12	920	140	914
910901	12	oun	c	10	790	120	2134
910901	12	oun	c	10	762	120	2438
910901	12	bis	a2	15	913	185	914
910901	12	bis	a2	15	881	200	1219
910901	12	top	a4	8	948	115	610
910901	12	ovn	a1	12	951	145	610
910901	12	hon	a1	14	950	175	610
910901	12	stc	a1	12	954	155	610
910902	0	lbf	b4	11	821	175	1829
910902	0	bis	a5	17	908	175	914
910902	0	ovn	b4	10	885	135	1219
910902	0	ovn	b4	10	854	140	1524
910902	0	hon	b1	14	822	190	1829
910902	12	lbf	b1	13	880	200	1219
910902	12	lbf	b1	13	850	210	1524
910902	12	bis	a2	13	904	215	914
910902	12	hon	a3	20	943	190	610
910902	12	stc	a3	17	948	195	610
910902	12	stc	a3	17	915	205	914
910903	0	ovn	b4	9	822	220	1829
910903	0	ovn	b4	9	765	225	2438
910903	12	oun	a5	8	915	230	914
910903	12	ddc	b4	9	883	230	1219
910903	12	top	a5	10	947	230	610
910903	12	ovn	a2	13	948	265	610
910904	12	lbf	b4	9	888	150	1219
910905	12	lbf	b1	13	850	210	1524
910905	12	lbf	b1	13	791	230	2134
910905	12	top	a4	8	948	145	610
910905	12	ovn	c	14	763	265	2438
910905	12	stc	a3	22	944	240	610
910907	0	lbf	b3	16	880	175	1219
910907	0	lbf	b3	16	850	170	1525
910907	0	bis	c	12	761	240	2438
910907	0	ovn	b2	12	850	185	1574
910907	0	ovn	b2	12	825	195	1829
910907	0	hon	b1	16	850	200	1525
910907	0	stc	c	17	766	255	2438
910907	0	stc	c	17	700	265	3184
910907	12	lbf	b3	20	818	200	1829
910907	12	lbf	b3	20	789	200	2134
910907	12	bis	a4	11	907	195	914
910907	12	ddc	b3	18	883	200	1219
910907	12	ddc	b3	18	850	195	1546
910907	12	ovn	a3	15	949	195	610

910907	12	ovn	a3	15	885	205	1219
910907	12	hon	a3	19	943	200	610
910907	12	hon	a3	19	880	225	1219
910907	12	stc	b3	18	884	240	1219
910907	12	stc	b3	18	853	240	1524
910908	0	oun	b3	12	882	215	1219
910908	0	lbf	c	14	760	180	2438
910908	0	lbf	c	14	733	190	2743
910908	0	top	b3	18	882	180	1219
910908	0	top	b3	18	852	180	1524
910908	0	ovn	b3	19	882	175	1219
910908	0	hon	b3	13	850	185	1492
910908	0	hon	b3	13	789	210	2134
910908	0	stc	b1	15	882	165	1219
910908	12	oun	a2	20	913	210	914
910908	12	bis	a2	22	902	95	914
910908	12	ddc	a3	21	907	230	914
910908	12	ovn	a3	16	909	205	914
910908	12	ovn	a3	16	877	205	1219
910908	12	hon	a2	20	903	190	914
910908	12	stc	b3	20	850	200	1497
910908	12	stc	b3	20	847	200	1524
910909	0	ovn	b3	17	816	225	1829
910909	0	ovn	b3	17	760	240	2438
910909	0	hon	b4	12	871	185	1219
910909	0	hon	b4	12	850	190	1430
910909	0	stc	a3	16	907	195	914
910909	12	oun	b1	14	883	230	1219
910909	12	ddc	b4	13	878	245	1219
910909	12	top	b1	20	880	240	1219
910909	12	ovn	a1	14	942	230	610
910909	12	ovn	a1	14	909	235	914
910910	12	oun	a1	13	950	210	610
910910	12	ddc	a1	12	915	230	914
910911	0	oun	a5	8	948	170	610
910911	0	oun	a5	8	740	180	2743
910911	0	bis	b2	14	820	195	1829
910911	0	bis	b2	14	791	190	2134
910911	12	oun	b1	12	885	220	1219
910911	12	bis	a2	13	911	180	914
910911	12	bis	a2	13	879	180	1219
910911	12	ddc	b3	22	882	220	1219
910911	12	ddc	b3	22	850	215	1538
910911	12	top	a3	16	948	230	610
910911	12	hon	b3	12	818	165	1829
910911	12	hon	b3	12	789	180	2134
910912	0	oun	c	10	766	185	2438
910912	0	stc	a5	10	911	150	914
910912	12	ddc	a2	21	912	210	914
910912	12	ddc	a2	21	881	220	1219
910912	12	ovn	a3	12	944	255	610
910912	12	ovn	a3	12	880	270	1219
910913	12	ddc	a3	13	910	210	914
910913	12	ddc	a3	13	850	215	1507
910913	12	top	b1	19	881	230	1219
910913	12	ovn	b3	12	880	215	1219
910913	12	ovn	b3	12	849	210	1524
910913	12	hon	b4	8	817	105	1829
910914	0	bis	b2	13	850	155	1453
910914	0	bis	b2	13	843	155	1524
910914	0	ddc	b4	15	876	190	1219
910914	0	ovn	a3	14	938	190	610
910914	0	ovn	a3	14	907	195	914
910914	0	stc	a4	10	943	115	610
910914	12	lbf	b4	8	871	255	1219
910914	12	lbf	b4	8	850	260	1433
910914	12	ddc	b1	18	850	215	1465
910915	0	ovn	b3	15	814	225	1829
910915	12	top	b1	18	878	230	1219
910916	0	top	c	19	735	245	2743
910917	12	ddc	b3	14	850	215	1536
910917	12	ddc	b3	14	764	230	2438

910917	12	top	a4	11	948	215	610
910917	12	top	a4	11	915	205	914
910920	0	lbf	c	11	765	220	2438
910920	12	lbf	b1	17	885	205	1219
910920	12	lbf	b1	17	792	200	2134
910920	12	bis	a2	14	911	195	914
910920	12	ddc	b3	13	889	180	1219
910920	12	ddc	b3	13	825	170	1829
910920	12	ovn	a4	11	957	185	610
910920	12	hon	a2	14	917	215	914
910920	12	stc	a5	10	955	190	610
910921	0	ovn	b4	10	853	185	1524
910921	0	ovn	b4	10	822	195	1829
910921	0	hon	a2	18	944	190	610
910921	0	stc	b1	13	883	190	1219
910921	0	stc	b1	13	820	235	1829
910921	12	oun	c	13	792	235	2134
910921	12	oun	c	13	764	230	2438
910921	12	lbf	b1	13	874	190	1219
910921	12	bis	a4	10	932	195	610
910921	12	ddc	a3	19	910	200	914
910921	12	ovn	c	16	760	230	2438
910921	12	hon	a1	22	939	185	610
910921	12	stc	a3	20	945	205	610
910922	0	oun	b3	20	849	220	1524
910922	0	oun	b3	20	790	225	2134
910922	0	ddc	b2	17	845	200	1524
910922	0	top	b3	22	845	235	1524
910922	0	ovn	b3	17	850	190	1461
910922	0	ovn	b3	17	813	210	1829
910922	0	hon	a5	18	931	175	610
910922	0	hon	a5	18	899	180	914
910922	0	stc	b3	20	842	185	1524
910922	12	oun	a2	20	946	200	610
910922	12	oun	a2	20	913	210	914
910922	12	top	a2	17	911	240	914
910922	12	top	a2	17	879	270	1219
910923	12	lbf	b3	17	884	185	1219
910924	0	oun	b3	13	850	215	1524
910924	0	hon	a3	18	947	90	610
910925	12	ovn	a3	24	942	255	610
910927	12	ddc	a2	25	912	210	914
910927	12	ddc	a2	25	880	215	1219
910927	12	top	a1	19	947	230	610
910927	12	hon	a4	11	945	125	610
910928	0	oun	b4	10	882	200	1219
910928	0	oun	b4	10	850	215	1536
910928	0	top	c	13	791	260	2134
910928	0	top	c	13	762	285	2438
910928	12	oun	a2	14	949	200	610
910928	12	lbf	b4	9	880	145	1219
910928	12	hon	a1	14	949	170	610
910929	0	oun	b4	11	823	170	1829
910929	0	lbf	c	13	790	215	2134
910929	0	lbf	c	13	735	220	2743
910929	0	top	c	16	738	240	2743
910929	12	oun	a4	12	952	185	610
910929	12	top	a2	21	951	220	610
910929	12	ovn	a3	16	915	250	914
910929	12	hon	a2	15	943	150	610
910929	12	stc	a4	9	917	140	914
910930	0	lbf	b4	11	879	185	1219
910930	0	lbf	b4	11	820	195	1829
910930	0	ovn	a2	20	948	205	610
910930	0	stc	a3	19	948	125	610
910930	12	oun	a5	8	953	195	610
910930	12	oun	a5	8	919	205	914
910930	12	ddc	a2	20	917	205	914
910930	12	top	a2	14	919	230	914
920403	12	ddc	a5	12	908	255	914
920403	12	top	a2	16	940	260	610
920404	12	lbf	b4	10	870	145	1219

920404	12	bis	a2	15	901	150	914
920405	0	hon	a5	12	904	160	914
920405	0	hon	a5	12	872	180	1219
920405	12	oun	c	13	786	150	2134
920405	12	oun	c	13	757	155	2438
920405	12	lbf	b1	18	850	215	1421
920405	12	lbf	b1	18	781	220	2134
920405	12	ddc	b1	16	814	180	1829
920405	12	top	a2	12	910	170	914
920405	12	ovn	a2	18	943	165	610
920405	12	hon	b1	26	870	215	1219
920405	12	stc	a3	19	944	175	610
920406	0	oun	c	19	702	135	3048
920406	0	oun	c	19	700	135	3071
920406	0	lbf	c	19	753	195	2438
920406	0	ddc	b2	17	875	170	1219
920406	0	ovn	b4	17	876	180	1219
920406	0	ovn	b4	17	850	200	1475
920406	0	hon	c	25	724	215	2743
920406	0	stc	b3	21	850	190	1444
920406	12	oun	b4	10	850	120	1473
920406	12	oun	b4	10	784	115	2134
920406	12	lbf	b4	10	842	265	1524
920406	12	ddc	a2	15	909	205	914
920406	12	top	a2	14	944	205	610
920406	12	ovn	a3	19	943	230	610
920407	0	top	a5	8	942	165	610
920407	0	top	a5	8	909	175	914
920407	12	oun	a4	8	944	220	610
920407	12	ddc	b4	9	850	235	1467
920408	12	oun	a5	10	945	140	610
920408	12	lbf	b3	24	812	235	1829
920408	12	ovn	b3	12	850	200	1488
920408	12	ovn	b3	12	785	205	2134
920409	0	oun	c	16	787	235	2134
920409	12	oun	a2	17	941	215	610
920409	12	oun	a2	17	908	225	914
920409	12	ddc	a4	10	907	100	914
920409	12	stc	a3	14	944	265	610
920410	0	oun	a5	13	940	170	610
920410	0	oun	a5	13	850	195	1478
920410	0	ovn	a5	9	910	95	914
920410	0	ovn	a5	9	877	95	1219
920410	12	oun	a2	15	939	195	610
920410	12	oun	a2	15	907	205	914
920410	12	lbf	b3	19	837	245	1524
920410	12	bis	b3	14	867	160	1219
920410	12	ddc	b1	19	872	245	1219
920410	12	ovn	a3	16	903	220	914
920410	12	stc	a3	16	944	95	610
920411	0	top	a5	17	903	210	914
920411	0	stc	a5	11	938	105	610
920411	0	stc	a5	11	902	115	914
920411	12	oun	a2	17	937	195	610
920412	12	lbf	c	16	706	250	3048
920413	0	lbf	c	18	788	215	2134
920413	0	bis	b1	17	850	175	1509
920413	0	bis	b1	17	848	180	1524
920413	0	hon	a3	14	921	145	914
920413	0	hon	a3	14	885	150	1219
920413	12	oun	a2	12	918	175	914
920413	12	lbf	b3	14	850	185	1219
920413	12	lbf	b3	14	880	200	1495
920413	12	bis	a3	12	911	180	914
920413	12	ddc	c	12	791	190	2134
920413	12	ddc	c	12	762	190	2438
920413	12	top	a3	15	953	135	610
920413	12	top	a3	15	885	205	1219
920413	12	ovn	b3	18	884	200	1219
920414	0	oun	b2	13	852	220	1524
920414	0	oun	b2	13	850	215	1543
920414	0	top	b1	20	820	230	1829

920414	0	ovn	b3	15	817	230	1829
820414	12	oun	a2	17	947	205	610
820414	12	lbf	b4	11	815	190	1829
820414	12	ddc	a3	17	911	175	914
820414	12	top	a2	20	913	255	914
820414	12	hon	a4	11	946	140	610
820414	12	stc	a4	8	950	140	610
920415	0	oun	b4	14	819	175	1829
920415	0	top	a5	14	944	190	610
920415	0	ovn	c	20	788	225	2134
920415	0	ovn	c	20	761	225	2438
920415	12	oun	a3	19	944	195	610
920415	12	oun	a3	19	911	205	914
920415	12	ddc	b1	17	875	225	1219
920415	12	ddc	b1	17	850	220	1468
920415	12	ovn	a3	20	909	235	914
920415	12	ovn	a3	20	877	240	1219
920415	12	stc	c	10	758	205	2438
920416	0	top	b3	20	875	205	1219
920416	0	top	b3	20	844	215	1524
920416	0	ovn	c	19	754	230	2438
920416	0	ovn	c	19	727	225	2743
920417	12	bis	a2	17	906	165	914
920417	12	hon	a4	8	944	175	610
920417	12	hon	a4	8	910	170	610
920418	0	bis	b4	17	863	155	1219
920418	0	bis	b4	17	801	175	1829
920418	0	hon	a5	16	900	160	913
920418	0	hon	a5	16	850	185	1385
920418	12	oun	a2	17	932	180	610
920418	12	oun	a2	17	900	180	914
920418	12	bis	b4	12	886	175	914
920418	12	ddc	b1	28	864	190	1219
920418	12	top	b3	19	807	215	1829
920418	12	ovn	b3	18	850	220	1375
920418	12	stc	a3	14	900	165	914
920418	12	stc	a3	14	867	180	1219
920419	0	oun	b4	12	865	190	1219
920419	0	oun	b4	12	850	190	1371
920419	12	stc	c	23	716	175	2743
920419	12	stc	c	23	700	175	2927
920422	12	oun	a2	14	941	200	610
920423	0	top	c	26	728	235	2743
920423	12	oun	b1	25	876	235	1219
920423	12	oun	b1	25	845	250	1524
920427	12	lbf	b1	13	884	180	1219
920427	12	lbf	b1	13	820	220	1829
920427	12	bis	a1	20	914	180	914
920427	12	hon	a4	10	954	170	610
920427	12	hon	a4	10	919	155	914
920428	0	lbf	b3	13	818	185	1829
920428	0	lbf	b3	13	789	190	2134
920428	0	bis	a5	14	908	185	914
920428	0	bis	a5	14	844	205	1524
920428	0	hon	b4	13	880	185	1524
920428	12	oun	a3	17	947	150	610
920428	12	oun	a3	17	881	200	1219
920428	12	ovn	a2	18	947	185	610
920428	12	hon	a1	20	939	200	610
920428	12	stc	a2	20	944	200	610
920430	12	oun	a4	9	944	205	610
920430	12	lbf	b1	20	872	175	1219
920430	12	bis	b1	25	896	170	914
920430	12	ddc	a2	24	908	220	914
920430	12	top	a1	15	942	245	610
920430	12	hon	a3	18	903	180	914
920430	12	hon	a3	18	850	200	1434
920430	12	stc	a1	15	940	115	610
920501	0	ddc	b3	22	850	200	1442
920501	0	ddc	b3	22	813	200	1829
920501	0	top	b4	19	850	215	1465
920501	0	top	b4	19	815	230	1829

920501	0	ovn	b1	22	871	200	1219
920501	0	ovn	b1	22	850	195	1428
920501	12	oun	a2	20	940	205	610
920501	12	oun	a2	20	907	215	914
920501	12	ddc	a2	23	901	225	914
920501	12	top	b1	30	873	225	1219
920501	12	top	b1	30	850	230	1448
920501	12	ovn	a2	20	933	210	610
920501	12	ovn	a2	20	900	230	914
920502	0	oun	b1	19	816	230	1829
920502	0	top	b3	17	850	215	1447
920502	0	top	b3	17	813	240	1829
920502	12	oun	b1	22	876	250	1219
920503	12	lbf	b3	14	885	260	1219
920505	12	bis	a1	13	915	185	914
920506	12	lbf	b1	14	886	195	1219
920506	12	bis	a2	20	913	210	914
920506	12	hon	a1	19	953	205	610
920506	12	stc	a1	15	954	225	610
920507	0	bis	b2	12	850	230	1493
920507	0	stc	b4	12	822	225	1829
920507	12	lbf	b1	16	881	185	1219
920507	12	ddc	a2	19	917	195	914
920507	12	ddc	a2	19	850	220	1559
920507	12	hon	a2	20	944	210	610
920508	0	ddc	b2	13	880	200	1219
920508	0	ddc	b2	13	850	200	1524
920508	0	ovn	a5	12	915	180	914
920508	0	ovn	a5	12	883	185	1219
920508	0	hon	a5	12	910	195	914
920508	0	stc	b1	14	850	220	1531
920508	12	oun	a1	16	946	205	610
920508	12	ddc	b1	17	877	235	1219
920508	12	top	a5	12	914	200	914
920508	12	ovn	a2	18	946	180	610
920508	12	hon	a1	14	941	195	610
920508	12	stc	a2	16	945	220	610
920509	0	top	a5	11	942	145	610
920509	0	top	a5	11	909	170	914
920509	0	ovn	a5	14	941	170	610
920509	12	oun	a1	19	941	210	610
920509	12	lbf	b1	15	868	190	1219
920509	12	bis	b1	14	850	175	1387
920509	12	top	a2	14	941	210	610
920509	12	ovn	b3	13	850	240	1466
920509	12	hon	a3	19	934	165	610
920509	12	stc	a3	14	941	180	610
920509	12	stc	a3	14	908	175	914
920510	0	ddc	c	21	783	175	2134
920510	0	ddc	c	21	755	180	2438
920510	0	ovn	c	17	730	180	2743
920510	0	ovn	c	17	700	175	3085
920510	0	hon	a3	20	931	180	610
920510	0	hon	a3	20	753	190	2438
920510	0	stc	a3	15	939	150	610
920510	0	stc	a3	15	876	162	1219
920510	12	oun	b1	23	876	210	1219
920510	12	lbf	b3	16	807	230	1829
920510	12	ddc	b1	25	811	210	1829
920510	12	hon	a3	23	933	175	610
920510	12	hon	a3	23	850	215	1400
920510	12	stc	b3	21	876	195	1219
920510	12	stc	b3	21	845	190	1524
920511	0	ddc	c	26	726	230	2743
920511	12	top	b3	17	874	200	1219
920511	12	top	b3	17	850	200	1458
920512	0	ovn	b4	9	872	205	1219
920512	0	ovn	b4	9	850	205	1434
920512	0	stc	a5	12	902	235	914
920512	0	stc	a5	12	780	245	2134
920512	12	oun	a5	14	939	210	610
920514	12	bis	a3	14	905	205	914

920514	12	ddc	b1	19	846	215	1524
920514	12	ovn	a1	12	909	170	914
920514	12	hon	a1	15	942	160	610
920514	12	stc	a5	11	945	170	610
920515	12	oun	a4	11	942	200	610
920515	12	lbf	b4	13	873	185	1219
920515	12	ovn	a3	12	909	235	914
920515	12	stc	b3	16	874	255	1219
920516	0	oun	a5	9	941	175	610
920516	0	bis	a5	9	903	150	914
920516	0	ovn	a3	15	900	148	1001
920516	0	ovn	a3	15	877	155	1219
920516	0	hon	b1	22	873	125	1219
920516	0	stc	a4	8	943	160	610
920516	12	oun	b3	13	819	185	1829
920516	12	oun	b3	13	790	180	2134
920516	12	ddc	a3	20	907	200	914
920516	12	ddc	a3	20	876	205	1219
920516	12	top	a3	20	943	210	610
920516	12	top	a3	20	911	220	914
920516	12	hon	b3	25	869	220	1219
920516	12	hon	b3	25	780	225	2134
920516	12	stc	b1	23	813	225	1829
920516	12	stc	b1	23	755	215	2438
920517	0	oun	b1	16	850	150	1506
920517	0	oun	b1	16	818	150	1829
920517	0	top	c	14	762	215	2438
920517	0	top	c	14	735	215	2743
920517	12	top	a4	9	948	120	610
920518	12	lbf	b1	14	884	180	1219
920518	12	bis	a5	12	912	210	914
920518	12	hon	a1	14	951	170	610
920518	12	stc	a5	8	955	155	610
920519	0	hon	a5	16	913	170	914
920519	0	hon	a5	16	881	185	1219
920519	12	oun	a5	8	948	135	610
920519	12	lbf	b1	19	881	205	1219
920519	12	top	a5	10	917	165	914
920519	12	ovn	a1	14	951	205	610
920519	12	hon	a1	23	943	195	610
920519	12	stc	a2	20	947	195	610
920520	0	top	b4	9	823	185	1829
920520	0	ovn	c	9	794	165	2134
920520	0	hon	a2	19	910	185	914
920520	0	hon	a2	19	879	190	1219
920520	0	stc	a2	14	948	185	610
920520	12	oun	a5	11	947	175	610
920520	12	oun	a5	11	914	190	914
920520	12	bis	a3	20	905	195	914
920520	12	bis	a3	20	874	200	1219
920520	12	ovn	a3	13	949	200	610
920520	12	hon	a3	21	945	195	610
920520	12	stc	a3	16	949	205	610
920521	0	lbf	b2	16	876	145	1219
920521	0	bis	a3	20	904	170	914
920521	0	ddc	b1	18	879	165	1219
920521	0	ddc	b1	18	850	175	1510
920521	0	ovn	a2	20	915	175	914
920521	0	hon	b1	18	850	180	1518
920521	0	stc	b1	14	823	185	1829
920521	12	oun	b3	19	851	185	1524
920521	12	oun	b3	19	820	180	1829
920521	12	lbf	b3	19	846	200	1524
920521	12	lbf	b3	19	816	200	1829
920521	12	bis	b1	18	873	215	1219
920521	12	top	b3	15	850	205	1555
920521	12	ovn	a3	14	916	190	914
920521	12	hon	a3	19	944	180	610
920521	12	stc	b3	17	850	190	1556
920522	0	lbf	b3	17	850	170	1475
920522	0	ddc	b4	16	850	180	1508
920522	0	ddc	b4	16	789	185	2134

920522	0	ovn	b3	15	883	165	1219
920522	0	ovn	b3	15	850	175	1539
920522	0	hon	b2	14	878	180	1219
920522	0	hon	b2	14	850	175	1502
920522	12	oun	a5	11	948	200	610
920522	12	oun	a5	11	915	210	914
920522	12	ddc	a3	16	913	205	914
920522	12	ddc	a3	16	820	225	1829
920522	12	top	a3	14	949	190	610
920522	12	top	a3	14	916	200	914
920522	12	ovn	a3	17	915	215	914
920522	12	ovn	a3	17	852	220	1524
920522	12	stc	b3	22	881	240	1219
920522	12	stc	b3	22	850	245	1524
920524	12	lbf	b4	8	884	155	1219
920524	12	hon	a4	8	953	140	610
920524	12	stc	a4	9	956	100	610
920525	12	ddc	a5	12	910	215	914
920525	12	ovn	a2	16	944	195	610
920527	12	lbf	b4	11	850	135	1479
920527	12	bis	c	8	785	150	2134
920527	12	bis	c	8	755	155	2438
920527	12	ddc	b4	15	876	135	1219
920528	12	bis	b1	19	876	195	1219
920528	12	bis	b1	19	850	190	1467
920528	12	top	b4	11	815	105	1829
920528	12	ovn	c	9	787	145	2134
920528	12	hon	c	11	786	165	2134
920529	12	lbf	b4	11	847	185	1524
920529	12	hon	a2	12	945	225	610
920530	0	hon	a5	10	943	185	610
920530	12	lbf	b2	13	877	190	1219
920530	12	ovn	a4	8	947	205	610
920530	12	hon	a5	11	943	220	610
920530	12	hon	a5	11	910	230	914
920531	0	ddc	b4	10	850	165	1518
920531	0	ddc	b4	10	819	170	1829
920531	0	hon	a5	9	944	165	610
920531	0	hon	a5	9	912	170	914
920531	12	lbf	b1	12	879	190	1219
920531	12	lbf	b1	12	817	190	1829
920531	12	bis	b3	12	850	175	1478
920531	12	bis	b3	12	786	175	2134
920531	12	hon	a3	14	946	195	610
920531	12	hon	a3	14	913	195	914
920531	12	stc	a4	8	949	195	610
920601	0	ovn	c	12	790	160	2134
920601	0	ovn	c	12	761	165	2438
920601	0	stc	c	8	736	165	2743
920601	0	stc	c	8	700	165	3143
920601	12	oun	b4	9	878	215	1219
920601	12	oun	b4	9	846	230	1524
920601	12	top	a5	12	946	160	610
920601	12	ovn	b1	18	850	150	1502
920601	12	hon	a5	8	915	195	914
920601	12	hon	a5	8	882	185	1219
920602	0	ovn	b4	11	850	155	1511
920602	0	hon	b2	12	850	125	1518
920602	12	bis	a5	8	909	210	914
920602	12	top	a3	12	909	145	914
920602	12	top	a3	12	786	125	2134
920602	12	ovn	b4	10	817	135	1829
920602	12	ovn	b4	10	788	135	2134
920602	12	hon	b4	10	879	185	1219
920602	12	hon	b4	10	759	200	2438
920603	0	ovn	c	10	758	100	2438
920603	0	ovn	c	10	730	120	2743
920603	12	lbf	b4	9	875	185	1219
920603	12	lbf	b4	9	850	205	1463
920603	12	bis	a5	12	902	205	914
920603	12	ovn	c	15	785	130	2134
920603	12	hon	b1	19	814	185	1829

920604	0	hon	b2	13	871	200	1219
920604	0	hon	b2	13	811	225	1829
920605	12	lbf	b4	10	870	185	1219
920605	12	lbf	b4	10	850	175	1416
920605	12	ddc	b1	13	873	185	1219
920605	12	ddc	b1	13	850	185	1451
920606	0	oun	b3	15	811	220	1829
920606	0	ddc	b4	17	838	200	1524
920607	12	lbf	b3	14	878	190	1219
920607	12	lbf	b3	14	847	185	1524
920607	12	ddc	b4	11	880	165	1219
920608	12	oun	b3	12	818	200	1505
920608	12	ovn	c	16	789	195	2134
920609	0	top	a4	8	943	115	610
920609	0	top	a4	8	910	125	914
920609	12	oun	a5	8	942	185	610
920609	12	ovn	a1	13	944	130	610
920609	12	stc	a4	8	948	125	610
920610	0	ovn	b4	9	850	175	1501
920610	12	ovn	a5	8	944	160	610
920610	12	ovn	a5	8	848	160	1524
920611	0	ovn	c	15	788	100	2134
920611	12	lbf	b4	8	850	125	1518
920611	12	bis	a2	14	911	190	914
920611	12	top	a3	13	944	90	610
920611	12	ovn	b1	14	821	105	1829
920611	12	ovn	b1	14	762	95	2438
920611	12	hon	b4	11	822	170	1829
920611	12	hon	b4	11	792	165	2134
920612	0	ovn	c	13	709	110	3048
920612	12	lbf	b4	8	849	165	1524
920612	12	bis	a2	16	912	190	914
920612	12	top	b4	11	820	100	1829
920612	12	ovn	c	13	735	105	2743
920612	12	ovn	c	13	708	105	3048
920612	12	hon	c	12	764	175	2438
920613	0	ovn	c	9	708	100	3048
920613	0	hon	c	12	707	145	3048
920613	12	lbf	b1	15	875	170	1219
920613	12	lbf	b1	15	845	185	1524
920613	12	bis	a5	11	907	175	914
920613	12	ovn	c	10	760	125	2438
920613	12	hon	c	14	759	175	2438
920613	12	hon	c	14	732	175	2743
920614	0	bis	b4	11	850	135	1450
920614	0	bis	b4	11	813	135	1829
920614	12	oun	a2	18	906	190	914
920614	12	bis	b4	11	842	140	1524
920614	12	ddc	c	22	784	230	2134
920614	12	top	a5	9	938	175	610
920614	12	top	a5	9	906	180	914
920614	12	hon	c	15	729	160	2743
920615	0	ovn	b2	12	850	160	1463
920615	0	stc	a5	12	941	90	610
920615	12	oun	a2	20	938	180	610
920615	12	ddc	b1	22	871	185	1219
920615	12	ddc	b1	22	840	220	1524
920615	12	top	b3	11	850	220	1466
920615	12	ovn	b1	15	876	155	1219
920615	12	stc	a2	16	943	120	610
920616	0	top	b3	16	815	185	1829
920616	0	top	b3	16	787	195	2134
920616	0	stc	b4	14	877	135	1219
920616	0	stc	b4	14	850	150	1490
920616	12	oun	a2	20	939	195	610
920616	12	top	b1	21	850	215	1466
920616	12	top	b1	21	844	225	1524
920616	12	stc	a1	17	940	135	610
920617	0	top	c	26	700	225	3123
920617	0	ovn	c	25	754	215	2438
920617	12	stc	b1	25	859	195	1219
920617	12	stc	b1	25	850	190	1313

920619	12	ddc	b1	17	819	245	1829
920620	12	bis	a5	8	950	115	610
920620	12	bis	a5	8	850	105	1525
920621	12	lbf	b4	10	820	200	1829
920621	12	bis	a2	14	912	185	914
920621	12	hon	a4	11	916	170	914
920622	12	ddc	b4	9	881	230	1219
920622	12	top	a1	14	946	215	610
920622	12	ovn	a3	18	910	255	914
920622	12	ovn	a3	18	878	265	1219
920622	12	stc	a2	15	942	165	610
920624	12	ddc	a5	12	906	225	914
920626	12	lbf	b4	11	818	185	1829
920626	12	bis	a4	11	911	150	914
920627	0	lbf	b2	14	818	175	1829
920627	0	lbf	b2	14	788	190	2134
920627	12	bis	a4	9	907	190	914
920627	12	ddc	b3	15	879	160	1219
920627	12	ddc	b3	15	850	190	1512
920627	12	ovn	a4	9	946	150	610
920627	12	hon	a2	17	944	170	610
920628	0	ddc	b4	16	816	155	1829
920628	0	stc	c	15	787	240	2134
920628	12	top	a4	11	941	155	610
920628	12	top	a4	11	909	165	914
920628	12	ovn	a4	11	942	185	610
920628	12	ovn	a4	11	909	195	914
920628	12	stc	a2	18	939	235	610
920628	12	stc	a2	18	906	250	914
920630	12	lbf	b1	20	872	175	1219
920630	12	ddc	b4	11	875	165	1219
920630	12	hon	a2	18	938	115	610
920701	0	lbf	b4	16	808	185	1829
920701	0	ovn	b1	13	813	180	1829
920701	12	oun	a3	17	934	180	610
920701	12	top	b4	10	872	195	1219
920701	12	ovn	a2	14	937	190	610
920701	12	ovn	a2	14	904	190	914
920701	12	stc	b3	22	850	225	1431
920702	0	oun	a5	13	935	185	610
920702	12	oun	b3	25	873	245	1219
920704	12	oun	c	11	767	230	2438
920704	12	oun	c	11	740	230	2743
920704	12	lbf	b1	15	878	215	1219
920704	12	ddc	b1	19	850	215	1536
920705	0	oun	b1	17	850	220	1521
920705	0	ddc	b1	25	876	195	1219
920705	12	oun	a2	22	912	235	914
920705	12	bis	a5	8	911	145	914
920705	12	ddc	b1	15	816	255	1829
920705	12	top	a1	13	941	200	610
920706	12	oun	a1	18	941	225	610
920706	12	ddc	b4	9	847	220	1524
920706	12	ddc	b4	9	800	210	2134
920706	12	top	a4	11	943	110	610
920706	12	hon	a3	15	942	160	610
920706	12	hon	a3	15	908	165	914
920707	0	oun	b2	13	879	200	1219
920707	0	top	b4	11	880	170	1219
920707	0	ovn	a3	15	908	185	914
920707	12	oun	a2	26	942	215	610
920707	12	ddc	a2	20	904	225	914
920707	12	stc	a5	8	908	265	914
920708	0	oun	b1	18	850	210	1529
920708	0	top	c	20	762	250	2438
920708	12	oun	a2	23	947	230	610
920708	12	top	b3	24	848	270	1524
920709	0	oun	b2	13	850	210	1550
920709	0	oun	b2	13	823	220	1829
920709	12	oun	a1	21	947	210	610
920709	12	lbf	b1	14	887	205	1219
920709	12	lbf	b1	14	817	235	1829

920709	12	bis	b4	10	844	265	1524
920709	12	ddc	b1	19	820	235	1829
920710	0	oun	c	15	792	210	2134
920710	0	bis	a4	9	906	230	914
920710	0	ovn	b1	16	850	225	1485
920710	0	ovn	b1	16	846	225	1524
920710	12	oun	a2	20	945	200	610
920710	12	oun	a2	20	913	210	914
920710	12	top	b1	16	850	260	1518
920710	12	top	b1	16	820	270	1829
920711	0	oun	a5	12	944	190	610
920711	12	oun	b1	22	880	220	1219
920711	12	lbf	b3	13	876	125	1219
920711	12	ddc	b4	11	817	240	1829
920711	12	top	a2	17	912	215	914
920712	0	oun	b1	18	850	190	1505
920712	0	top	b3	20	817	235	1829
920712	0	top	b3	20	788	235	2134
920712	12	oun	a2	23	910	205	914
920712	12	ddc	b1	25	850	235	1440
920712	12	ddc	b1	25	842	245	1524
920712	12	top	b3	32	850	230	1467
920712	12	top	b3	32	815	240	1829
920712	12	ovn	b1	14	871	220	1219
920712	12	ovn	b1	14	850	210	1524
920713	0	oun	b1	18	847	210	1524
920713	12	oun	a3	22	910	210	914
920713	12	top	b3	26	875	235	1219
920713	12	stc	b4	8	815	125	1829
920713	12	stc	b4	8	785	140	2134
920714	0	oun	c	19	761	220	2438
920714	0	top	c	19	787	200	2134
920714	0	top	c	19	760	200	2438
920714	12	bis	a2	15	904	205	914
920715	12	oun	b4	11	878	235	1219
920715	12	ddc	a2	15	908	225	914
920715	12	ddc	a2	15	877	225	1219
920715	12	ovn	a2	14	939	180	610
920716	0	top	c	15	788	265	2134
920718	12	lbf	b4	9	852	210	1524
920718	12	bis	b4	11	880	245	1219
920719	12	lbf	b4	11	880	185	1219
920719	12	ovn	a1	12	945	265	610
920721	12	lbf	b1	12	882	160	1219
920721	12	lbf	b1	12	851	170	1524
920722	0	lbf	c	17	786	205	2134
920722	0	bis	b4	11	818	130	1829
920722	0	bis	b4	11	788	125	2134
920722	0	hon	b1	14	881	135	1219
920722	0	hon	b1	14	818	115	1829
920722	12	oun	a2	17	946	215	610
920722	12	oun	a2	17	913	220	914
920722	12	bis	b1	13	818	110	1829
920722	12	bis	b1	13	759	105	2438
920722	12	ddc	a2	15	909	205	914
920722	12	ddc	a2	15	878	215	1219
920723	0	ddc	c	9	737	200	2743
920724	0	lbf	b4	11	819	185	1829
920724	0	lbf	b4	11	735	200	2743
920724	0	stc	a4	10	950	145	610
920724	12	oun	a2	14	916	215	914
920724	12	top	b3	14	884	230	1219
920724	12	hon	a5	14	946	175	610
920724	12	stc	a2	12	915	170	914
920724	12	stc	a2	12	883	170	1219
920725	0	oun	c	12	700	230	3216
920725	0	ddc	c	14	794	195	2743
920725	0	stc	b3	12	851	225	1524
920725	12	oun	a2	17	917	220	914
920725	12	ddc	b1	23	881	225	1219
920725	12	top	b3	19	884	235	1219
920725	12	ovn	a2	19	913	200	914

920726	0	top	b1	18	850	220	1524
920726	0	top	b1	18	851	225	1539
920726	12	oun	a2	19	946	225	610
920727	0	bis	b4	9	850	225	1521
920727	0	bis	b4	9	820	230	1829
920727	12	lbf	b4	8	851	250	1524
920727	12	lbf	b4	8	821	255	1829
920727	12	hon	b4	11	881	210	1219
920728	0	stc	b3	17	850	250	1496
920728	12	lbf	b1	19	880	240	1219
920728	12	ddc	a5	10	914	210	914
920729	12	top	a5	11	944	245	610
920729	12	top	a5	11	912	245	914
920729	12	hon	a4	9	945	100	610
920730	0	oun	c	9	791	230	2134
920730	0	oun	c	9	763	225	2438
920730	12	oun	a2	18	910	240	914
920801	0	stc	b3	14	882	250	1219
920801	12	lbf	b4	10	882	265	1219
920801	12	lbf	b4	10	850	265	1539
920801	12	hon	a4	9	946	240	610
920802	0	ovn	b4	9	852	215	1524
920802	12	oun	a2	17	947	220	610
920802	12	ddc	a5	10	912	270	914
920802	12	top	a1	15	945	225	610
920803	12	oun	a1	15	945	245	610
920804	12	lbf	b1	16	880	140	1219
920804	12	bis	a2	13	913	145	914
920804	12	top	a1	12	948	100	610
920804	12	ovn	a4	8	950	120	610
920804	12	hon	a5	11	948	140	610
920805	0	hon	a1	15	947	130	610
920805	0	hon	a1	15	913	135	914
920805	12	oun	c	17	791	265	2134
920805	12	oun	c	17	764	270	2438
920805	12	bis	b4	8	850	155	1513
920805	12	top	a5	9	945	160	610
920805	12	top	a5	9	912	175	914
920805	12	ovn	a1	14	947	120	610
920805	12	hon	a5	11	914	155	914
920805	12	hon	a5	11	881	165	1219
920806	0	bis	b4	8	850	165	1505
920806	12	oun	b4	10	883	235	1219
920806	12	lbf	b1	17	850	190	1510
920806	12	bis	a4	9	909	160	914
920806	12	ovn	a5	9	915	185	914
920806	12	hon	b4	11	880	195	1219
920806	12	stc	a5	11	949	180	610
920807	0	lbf	b3	15	816	190	1829
920807	0	lbf	b3	15	788	200	2134
920807	0	ddc	c	15	792	205	2134
920807	0	ddc	c	15	764	205	2438
920807	0	top	b4	10	882	185	1219
920807	0	top	b4	10	850	195	1541
920807	0	ovn	b1	13	881	190	1219
920807	0	hon	b3	15	877	185	1219
920807	0	hon	b3	15	850	200	1489
920807	0	stc	b3	13	881	185	1219
920807	0	stc	b3	13	850	195	1526
920807	12	oun	a2	22	944	205	610
920807	12	ddc	a2	20	907	250	914
920807	12	ddc	a2	20	850	250	1492
920807	12	top	b3	21	850	235	1500
920807	12	hon	a5	9	938	165	610
920808	0	oun	a5	14	944	195	610
920808	0	oun	a5	14	912	200	914
920808	12	oun	a2	20	946	215	610
920808	12	lbf	b1	13	878	215	1219
920808	12	lbf	b1	13	848	215	1524
920808	12	bis	a4	10	905	205	914
920808	12	top	a5	10	943	235	610
920809	0	oun	b4	11	850	200	1524

920809	0	oun	b4	11	853	195	1554
920809	0	top	b1	13	852	205	1524
920809	0	top	b1	13	823	210	1829
920809	0	ovn	b4	8	881	195	1219
920809	0	ovn	b4	8	850	195	1537
920809	0	hon	b4	14	877	220	1219
920809	0	hon	b4	14	819	245	1829
920809	12	oun	a1	20	947	215	610
920809	12	lbf	b4	9	878	270	1219
920809	12	lbf	b4	9	850	255	1504
920809	12	ddc	b3	16	821	240	1829
920809	12	ddc	b3	16	793	245	2134
920809	12	hon	a3	13	940	210	610
920809	12	hon	a3	13	878	220	1219
920809	12	stc	b3	14	879	255	1219
920810	0	oun	a5	10	915	180	914
920810	0	oun	a5	10	850	195	1555
920810	0	ddc	c	10	794	205	2134
920810	0	ddc	c	10	767	205	2438
920810	0	top	b3	16	823	260	1829
920810	0	top	b3	16	794	255	2134
920810	12	oun	a1	15	946	220	610
920811	12	oun	c	14	792	95	2134
920811	12	oun	c	14	764	105	2438
920811	12	lbf	b4	11	885	125	1219
920813	12	lbf	b1	12	885	200	1219
920813	12	bis	a2	11	916	205	914
920814	12	lbf	b1	12	887	150	1219
920814	12	bis	a1	15	918	210	914
920814	12	ddc	a4	8	919	130	914
920816	0	ddc	b4	11	854	180	1524
920816	0	ddc	b4	11	850	180	1566
920816	12	bis	a3	11	942	235	610
920816	12	ddc	a2	17	916	200	914
920816	12	top	a4	8	951	185	610
920816	12	ovn	a4	9	917	200	914
920816	12	hon	a1	16	946	190	610
920816	12	stc	a5	11	950	205	610
920817	0	ovn	b4	11	884	185	1219
920817	12	ddc	b4	12	882	195	1219
920817	12	top	a4	11	950	185	610
920817	12	ovn	a2	15	949	195	610
920818	12	ddc	b4	10	885	150	1219
920819	12	lbf	b4	11	850	205	1552
920819	12	bis	a1	15	912	165	914
920819	12	ddc	b4	9	824	145	1828
920819	12	ddc	b4	9	794	150	2134
920819	12	hon	a4	8	949	180	610
920820	12	lbf	b4	10	879	205	1219
920820	12	bis	a3	15	906	220	914
920820	12	ddc	c	10	793	205	2134
920820	12	ovn	a4	11	949	185	610
920820	12	stc	a2	16	947	205	610
920821	0	ovn	b4	8	882	180	1219
920821	0	ovn	b4	8	852	190	1524
920821	0	stc	b1	14	850	230	1527
920821	12	lbf	b4	11	880	205	1219
920821	12	ddc	a2	15	914	195	914
920821	12	ovn	a2	13	949	205	610
920822	0	lbf	b4	11	820	175	1829
920822	0	lbf	b4	11	791	180	2134
920822	0	ovn	a5	8	949	155	610
920822	0	ovn	a5	8	823	215	1829
920822	12	oun	a4	7	948	155	610
920822	12	lbf	b1	21	876	175	1219
920822	12	lbf	b1	21	850	195	1482
920822	12	bis	b3	15	870	205	1219
920822	12	ddc	a2	21	913	190	914
920822	12	top	a1	11	949	180	610
920822	12	ovn	a2	15	948	195	610
920822	12	hon	a3	27	940	190	610
920822	12	stc	a3	19	947	200	610

920823	0	ddc	b2	19	819	185	1829
920823	0	ddc	b2	19	763	210	2438
920823	0	top	a5	8	947	175	610
920823	0	top	a5	8	914	175	914
920823	0	ovn	b1	15	881	175	1219
920823	0	ovn	b1	15	850	190	1525
920823	0	hon	a3	20	946	170	610
920823	0	hon	a3	20	850	200	1551
920823	12	oun	a2	15	946	175	610
920823	12	oun	a2	15	913	190	914
920823	12	lbf	b3	19	871	205	1219
920823	12	ddc	a2	24	908	195	914
920823	12	ddc	a2	24	850	215	1489
920823	12	top	a2	13	914	190	914
920823	12	ovn	a2	22	944	185	610
920823	12	hon	a1	17	937	185	610
920823	12	stc	a3	21	910	215	914
920823	12	stc	a3	21	878	225	1219
920824	0	oun	c	10	792	175	2134
920824	0	oun	c	10	764	180	2438
920824	0	top	a5	11	945	180	610
920824	0	top	a5	11	792	215	2134
920824	0	ovn	b1	18	850	190	1515
920824	0	hon	b3	18	815	215	1829
920824	0	stc	c	24	789	220	2134
920824	12	ovn	b1	18	850	220	1529
920825	0	oun	c	14	737	205	2743
920825	0	oun	c	14	711	205	3048
920825	0	ddc	c	15	736	200	2743
920825	0	ddc	c	15	700	205	3164
920825	12	oun	a3	17	948	195	610
920825	12	oun	a3	17	916	205	914
920825	12	top	a3	22	914	210	914
920825	12	ovn	b3	21	850	210	1524
920826	0	oun	b4	9	850	195	1555
920826	0	oun	b4	9	766	215	2438
920827	12	bis	a5	11	912	210	914
920828	12	ddc	a2	16	913	265	914
920828	12	hon	a3	13	910	230	914
920829	12	oun	a1	22	945	215	610
920829	12	ddc	a2	17	909	230	914
920829	12	ddc	a2	17	878	235	1219
920829	12	top	a2	16	910	235	914
920829	12	ovn	a3	16	940	200	610
920830	0	oun	b4	11	881	190	1219
920830	0	oun	b4	11	821	195	1829
920830	12	oun	a1	22	947	205	610
920831	0	ddc	c	13	792	185	2134
920901	0	oun	b4	10	820	190	1829
920901	0	oun	b4	10	791	190	2134
920901	0	lbf	b2	12	818	170	1829
920901	0	lbf	b2	12	789	180	2134
920901	0	ddc	b2	11	880	155	1219
920901	0	ovn	c	8	764	210	2438
920901	0	ovn	c	8	736	230	2743
920901	12	oun	b1	15	851	190	1524
920901	12	bis	a2	12	906	195	914
920901	12	top	c	11	736	215	2743
920901	12	ovn	a2	15	947	170	610
920901	12	ovn	a2	15	914	185	914
920901	12	hon	a3	16	944	170	610
920901	12	hon	a3	16	911	185	914
920901	12	stc	a5	9	949	145	610
920902	0	top	a3	20	941	180	610
920902	12	oun	b3	23	850	240	1493
920902	12	top	b3	20	814	270	1829
920902	12	top	b3	20	785	270	2134
920902	12	ovn	a3	14	904	240	914
920902	12	ovn	a3	14	872	255	1219
920904	0	oun	b4	8	850	90	1551
920904	0	oun	b4	8	823	90	1829
920904	12	lbf	b1	26	850	205	1494

920904	12	ddc	b1	17	882	180	1219
920904	12	ddc	b1	17	850	180	1542
920904	12	top	a2	12	949	170	610
920904	12	ovn	a2	22	947	190	610
920904	12	ovn	a2	22	915	200	914
920905	0	oun	a5	9	913	155	914
920905	0	oun	a5	9	850	160	1532
920905	0	ddc	b3	21	850	170	1496
920905	0	top	c	11	765	190	2438
920905	0	hon	b3	31	784	200	2134
920905	0	hon	b3	31	758	205	2438
920905	12	oun	a2	20	944	185	610
920905	12	oun	a2	20	912	195	914
920905	12	ddc	b3	27	815	240	1829
920905	12	top	a2	25	942	195	610
920905	12	top	a2	25	879	205	1219
920905	12	ovn	b3	29	850	215	1475
920905	12	ovn	b3	29	816	215	1829
920905	12	stc	b3	33	843	210	1524
920906	12	lbf	b4	11	880	165	1219
920906	12	ddc	a2	13	913	125	914
920906	12	top	a5	9	946	225	610
920906	12	hon	a2	13	945	125	610
920907	0	stc	b4	9	882	95	1219
920908	0	top	c	16	764	245	2438
920908	12	bis	a2	17	908	210	914
920909	0	oun	c	15	765	225	2438
920909	0	oun	c	15	738	240	2743
920909	0	ddc	b3	25	817	220	1829
920909	0	ddc	b3	25	789	230	2134
920909	0	hon	b3	20	850	205	1428
920909	0	stc	b3	13	876	190	1219
920909	0	stc	b3	13	850	205	1467
920909	12	oun	a2	23	943	205	610
920909	12	oun	a2	23	911	215	914
920909	12	top	b1	31	874	230	1219
920909	12	top	b1	31	850	230	1460
920910	0	oun	b4	11	850	210	1500
920910	0	oun	b4	11	790	240	2134
920911	0	oun	b4	11	823	95	1829
920911	12	oun	a4	10	953	115	610
920911	12	lbf	b1	20	883	200	1219
920911	12	lbf	b1	20	850	205	1542
920911	12	bis	b3	15	875	230	1219
920911	12	ddc	b1	16	850	170	1576
920911	12	ddc	b1	16	825	175	1829
920911	12	top	a4	8	954	140	610
920911	12	hon	b1	22	881	230	1219
920912	0	lbf	b4	13	819	185	1829
920912	0	ddc	c	15	793	195	2134
920912	0	top	b4	11	855	165	1524
920912	0	top	b4	11	850	160	1577
920912	0	ovn	b1	17	853	200	1524
920912	0	ovn	b1	17	850	200	1555
920912	0	hon	b1	17	878	195	1219
920912	0	stc	b1	19	850	230	1524
920912	0	stc	b1	19	820	235	1829
920912	12	oun	a3	12	950	175	610
920912	12	lbf	c	14	788	205	2134
920912	12	lbf	c	14	734	200	2743
920912	12	bis	a5	11	937	105	610
920912	12	ddc	a2	25	912	205	914
920912	12	ddc	a2	25	850	220	1522
920912	12	top	a3	16	950	190	610
920912	12	ovn	a2	20	948	190	610
920912	12	hon	a5	15	941	195	610
920912	12	stc	a3	23	945	210	610
920912	12	stc	a3	23	912	225	914
920913	0	oun	b1	15	822	220	1829
920913	0	top	b1	19	850	200	1525
920913	0	ovn	b1	23	817	215	1829
920913	0	hon	a3	20	903	190	914

920913	0	hon	a3	20	850	200	1428
920913	0	stc	b3	19	877	185	1219
920913	0	stc	b3	19	850	200	1488
920913	12	oun	a2	20	946	185	610
920913	12	ddc	b1	27	850	225	1487
920913	12	top	a3	27	912	225	914
920913	12	ovn	b3	26	876	235	1219
920913	12	stc	b3	23	872	225	1219
920913	12	stc	b3	23	841	240	1524
920914	0	oun	c	14	763	210	2438
920914	0	oun	c	14	736	210	2743
920914	0	ddc	b4	18	850	190	1482
920914	0	top	b1	19	819	215	1829
920914	0	top	b1	19	791	220	2134
920915	0	oun	b2	12	821	195	1829
920915	0	oun	b2	12	792	200	2134
920915	0	ddc	b4	11	850	200	1505
920915	0	ddc	b4	11	819	205	1829
920915	0	top	b4	13	881	195	1219
920915	0	top	b4	13	821	210	1829
920915	0	ovn	b1	17	819	215	1829
920915	0	ovn	b1	17	791	220	2134
920915	12	ovn	b1	17	947	200	610
920915	12	ovn	b1	17	915	205	914
920915	12	bis	b3	19	872	155	1219
920915	12	bis	b3	19	850	165	1436
920915	12	ddc	b2	22	879	205	1219
920915	12	top	a2	23	946	220	610
920915	12	ovn	b1	18	850	245	1518
920916	0	stc	b3	20	879	200	1219
920916	12	oun	a2	16	948	190	610
920916	12	ddc	b3	23	850	220	1519
920916	12	ddc	b3	23	820	230	1829
920916	12	top	a2	22	914	220	914
920916	12	top	a2	22	883	230	1219
920916	12	ovn	a3	20	943	210	610
920916	12	ovn	a3	20	910	230	914
920917	12	oun	a1	14	945	195	610
920917	12	lbf	b3	12	850	210	1468
920917	12	lbf	b3	12	759	250	2438
920917	12	bis	a3	20	901	195	914
920917	12	bis	a3	20	869	195	1219
920917	12	ddc	a2	18	908	225	914
920917	12	top	a2	21	911	235	914
920917	12	ovn	b4	9	877	235	1219
920918	0	oun	b4	10	817	205	1829
920918	0	ddc	b4	13	873	210	1219
920918	0	ddc	b4	13	815	215	1829
920918	0	top	a3	17	907	195	914
920918	12	oun	a2	16	940	215	610
920919	12	oun	c	19	790	245	2134
920919	12	oun	c	19	762	255	2438
920919	12	lbf	b1	18	877	185	1219
920919	12	bis	a2	16	902	205	914
920919	12	top	a4	9	948	105	610
920919	12	hon	a2	21	942	200	610
920920	0	ddc	b3	15	813	220	1829
920920	0	top	b4	11	850	195	1476
920920	0	top	b4	11	786	200	2134
920920	0	ovn	b3	14	844	230	1524
920920	0	hon	a5	12	934	190	610
920920	0	hon	a5	12	902	195	914
920923	0	lbf	c	12	764	225	2438
920923	12	lbf	b1	25	881	210	1219
920923	12	ddc	a2	15	919	190	914
920923	12	ddc	a2	15	887	190	1219
920923	12	ovn	a2	13	952	180	610
920923	12	ovn	a2	13	918	200	914
920924	0	lbf	b2	20	878	175	1219
920924	0	top	c	8	794	120	2134
920924	0	top	c	8	765	125	2438
920924	0	ovn	b1	15	823	190	1829

920924	0	ovn	b1	15	793	195	2134
920924	0	hon	b1	21	877	185	1219
920924	0	stc	b1	21	850	230	1525
920924	12	oun	a4	8	949	155	610
920924	12	oun	a4	8	915	155	914
920924	12	lbf	b1	24	877	190	1219
920924	12	bis	b4	11	896	195	914
920924	12	bis	b4	11	865	210	1219
920924	12	ddc	a2	16	913	185	914
920924	12	top	a1	14	950	160	610
920924	12	ovn	a2	17	949	175	610
920925	0	lbf	b4	17	812	175	1829
920925	0	ddc	b2	14	850	170	1491
920925	0	ddc	b2	14	817	175	1829
920925	0	ovn	b3	15	850	185	1495
920925	0	stc	b1	23	816	215	1219
920925	12	oun	a1	12	942	170	610
920925	12	lbf	b3	20	874	185	1219
920925	12	lbf	b3	20	784	230	2134
920925	12	ddc	a2	24	904	190	914
920925	12	top	a3	16	909	190	914
920925	12	ovn	a3	20	941	190	610
920925	12	stc	a3	23	907	195	914
920926	0	oun	a3	15	939	155	610
920926	0	oun	a3	15	850	185	1463
920926	12	oun	b3	21	876	215	1219
920927	12	lbf	b3	20	850	225	1506
920927	12	lbf	b3	20	848	230	1524
920927	12	bis	a3	23	903	205	914
920927	12	ddc	b1	13	884	205	1219
920927	12	hon	a3	14	943	180	610
920927	12	hon	a3	14	877	210	1219
920929	12	lbf	b4	15	887	200	1219
920929	12	ddc	b1	15	857	230	1524
920929	12	ddc	b1	15	850	230	1597
920930	0	ddc	b2	13	850	200	1576
920930	0	ddc	b2	13	796	220	2134
920930	12	ovn	a4	10	952	235	610

APPENDIX C

APPENDIX C

AIRFLOW CONFIGURATION TYPES

In this appendix, the individual events that were assigned to a particular airflow configuration type are listed by type. The types are given in the order in which they are discussed in the body of this dissertation. The date and time are provided for each case, as well as the latitude and longitude locations of the jet core on the pressure surface closest to the ground. In addition, to provide an indication of the three-dimensional nature of some of the jet events, the pressure of the individual analysis levels is given, together with the rawinsonde station that was closest to the jet core at that analysis level and the speed profile category at the rawinsonde station.

1. AC_EW Jets

Date	Time UTC	Center °lat/°lon	Level 1[1] mb, cat[2]., id	Level 2 mb, type, id
910702	12	37/-103	911, a2, oun	
910803	12	34/-102	946, a5, oun	
910817	12	33/ -98	912, a5, oun	
910930	12	37/-101	917, a2, ddc	
920407	12	36/-102	944, a4, oun	
920409	12	36/-102	941, a2, oun	908, a2, oun
920411	12	36/-104	937, a2, oun	
920619	12	36/-101	819, b1, ddc	
920707	12	35/-103	942, a2, oun	904, a2, ddc
920710	12	36/-100	945, a2, oun	850, b1, top
920726	12	36/-102	946, a2, oun	
920802	12	38/-104	947, a2, oun	
920830	12	36/-104	947, a1, oun	
920918	12	36/-102	940, a2, oun	

[1] Level 1 and Level 2 refer to the height of the pressure surfaces that were used in the compositing.
[2] Cat. refers to the vertical speed category described in Chapters 2 and 3.

2. AC_SWNE Jets

Date	Time UTC	Center °lat/°lon	Level 1 mb, type, id	Level 2 mb, type, id	Level 3 mb, type, id
910406	00	42/ -95	850, b3, ovn		
910528	12	36/-100	819, b1, ddc		
910610	00	45/ -92	880, b3, stc		
910610	12	30/ -92	915, a4, oun		
910615	12	38/ -94	877, b1, oun		
910705	12	38/ -97	941, a3, top		
910706	12	38/ -97	877, b1, ddc/top		
910707	12	38/ -96	942, a2, top		
910719	12	37/-101	941, a2, top		
910720	00	36/-100	820, b2, ddc	737, b2, ddc	
910720	12	39/ -99	942, a2, top	878, b1, ovn	
910723	00	38/-101	795, c, top		
910815	12	40/-103	878, b1, lbf		
910816	12	38/ -96	880, b1, top		
910903	12	33/-100	883, b4, ddc		
910907	00	42/-100	850, b3, lbf		
910913	12	38/ -96	880, b1, top		
910915	12	39/ -92	878, b1, top		
910917	12	36/-103	948, a4, top		
910922	00	43/ -99	931, a5, hon	845, b3, top	813, b3, ovn
910929	00	39/ -90	790, c, lbf		
920414	00	40/ -95	820, b1, top		
920423	12	36/ -95	876, b1, oun		
920709	12	36/-104	947,a1, oun	887, b1, lbf	820, b1, ddc
920710	00	38/ -94	792, c, oun		
920714	00	40/ -90	787, c, top		
920725	12	38/ -99	884, b3, top		
920726	00	40/ -95	850, b1, top		
920809	00	44/ -99	881, b4, ovn		
920810	00	38/ -96	794, c, ddc		
920829	12	38/-104	945, a1, oun		

3. KC_SWNE Jets

Date	Time UTC	Center °lat/°lon	Level 1 mb, type, id	Level 2 mb, type, id	Level 3 mb, type, id
910601	12	35/-103	939, a3, oun		
910626	12	40/ -98	940, a3, ovn	850, b1, ddc	
910627	00	39/-103	911, b2, top	821, b2, top	
910829	12	40/-100	948, a2, ovn	915, a1, top	
910909	12	38/ -96	909, a1, ovn		
910922	12	36/-102	946, a2, oun		
920415	12	36/-102	944, a3, oun,	877, a3, ovn	758, c, stc
920501	12	38/-100	933, a2, oun		
920708	12	36/-103	947, a2, oun	848, b3, top	
920902	12	34/ -96	872, a3, ovn		
920909	12	36/-101	943, a2, oun	850, b1, top	

920916	12	39/ -98	943, a3, ovn	883, a2, top

4. SD_SWNE Jets

Date	Time UTC	Center °lat/°lon	Level 1 mb, type, id	Level 2 mb, type, id
910408	12	35/-100	933, a3, oun	870, b1, top
910416	12	38/-103	872, b3, ddc	
910511	00	38/-104	850, b1, hon	
910516	12	34/ -98	815, b1, ovn	
910527	12	35/-103	843, b3, ddc	
910602	00	41/ -97	850, b3, oun	817, b3, ovn
910609	12	42/-100	948, a2, hon/oun	888, a2, hon
910721	00	37/ -97	850, b1, top	
910905	12	45/ -94	944, a3, stc	850, b1, lbf
920415	00	38/-100	819, b4, oun	761, c, ovn
920508	12	36/-104	946, a1, oun	877, b1, ddc
920605	12	40/-104	873, b1, ddc	
920823	12	40/-103	910, a3, stc	850, a2, ddc
920824	12	36/-102	850, b1, ovn	
920825	12	36/-102	948, a3, oun	850, b3, ovn
920906	12	34/ -98	913, a2, ddc	
920914	00	38/ -98	850, b4, ddc	819, b1, top

5. SD_NWSE Jets

Date	Time UTC	Center °lat/°lon	Level 1 mb, type, id	Level 2 mb, type, id
910528	00	36/-100	792, c, oun	
910603	12	36/-102	876, b1, oun	700, c, ovn
910604	00	35/ -99	815, b3, oun	
910604	12	33/-101	940, a5, oun	
910630	12	40/ -98	942, a1, top	
910701	00	39/ -97	816, b1, ovn	
910701	12	35/-103	944, a3, oun	
910710	12	34/-100	878, a5, bis	847, b3, top
910721	12	40/ -92	945, a2, ovn	819, b4, hon
910801	12	36/-102	884, b4, oun	
910802	12	40/ -94	910, a2, top	879, b1, ddc
910910	12	36/-101	915, a1, ddc	
910912	12	40/ -91	944, a3, ovn	912, a2, ddc
910914	00	38/ -96	876, b4, ddc	
910929	12	38/ -98	952, a2, top	
920414	12	38/ -96	913, a2, top	
920705	00	38/-102	876, b1, ddc	
920705	12	34/-102	941, a1, top	
920706	12	34/-101	943, a4, top	
920713	12	38/ -94	875, b3, top	785, b4, stc
920729	12	33/-102	944, a5, top	

6. CC Jets

Date	Time UTC	Center °lat/°lon	Level 1 mb, type, id	Level 2 mb, type, id	Level 3
910411	12	40/ -98	862, b3, lbf	723, c, bis	
910412	00	42/-101	942, a1, ovn	816, b1, bis	
910413	00	42/-101	939, a3, ovn	850, b1, stc	
910417	00	35/-104	941, a5, oun	846, a5, oun	
910502	12	36/-103	945, a2, oun	850, b1, ddc	
910503	12	42/-100	938, a3, ovn	839, b3, hon	812, b3, oun
910509	12	44/ -98	941, a2, hon	868, b1, bis	
910512	00	37/-102	850, b2, oun	789, c, lbf	
910515	00	39/-105	908, a5, stc		
910529	00	37/-102	876, b2, ddc	821, b2, ddc/ b3, oun	
910601	00	34/-102	904, a5, ovn		
910612	12	32/-105	944, a5, oun	844, b4, lbf	
910620	12	41/-100	946, a3, ovn	816, b3, lbf	
910621	12	38/ -99	943, a2, top		
910625	00	38/-105	882, b4, ovn	788, c, lbf	764, c, ddc
910630	00	39/-104	912, a5, top	761, c, lbf	
910830	00	36/-101	948, a4, top		
910924	00	42/-102	947, a3, hon		
920410	00	36/-104	940, a5, oun	877, a5, oun/ovn	
920410	12	36/-102	939, a2, oun	837, b3, lbf	
920509	00	40/-100	942, a5, ovn	909, a5, top	
920509	12	36/-104	941, a1, oun	908, a3, stc	
920510	00	44/-106	939, a3, stc	783, c, ddc	
920516	00	42/-100	943, a4, stc	903, a5, bis	
920521	00	45/-101	915, a2, ovn		
920613	12	40/-104	875, b1, lbf		
920615	12	36/-104	938, a2, oun	871, b1, ddc	
920616	00	42/ -98	850, b4, stc	787, b3, top	
920616	12	36/-102	939, a2, oun	850, b1, top	
920630	12	43/-105	938, a2, hon	872, b1, lbf	
920702	00	37/-103	935, a5, oun		
920711	00	34/-102	944, a5, oun		
920722	00	39/-103	881, b1, hon	788, b4, bis	
920807	12	36/-103	944, a2, oun	907, a2, ddc	850, a2, ddc
920822	12	43/ -99	940, a3, hon	876, b1, lbf	
920902	00	39/ -98	941, a3, top		
920904	12	42/ -96	947, a2, ovn	850, b1, lbf	
920907	00	35/-103	882, b4, stc		

7. LAC_SWNE Jets

Date	Time UTC	Center °lat/°lon	Level 1 mb, type, id	Level 2 mb, type, id	Level 3
910515	12	37/-102	940, a3, ovn	844, b1, hon	810, b1, ddc
910522	00	44/ -98	907, a5, hon	763, a5, stc	
910522	12	45/ -97	907, a3, hon		
910523	12	37/-101	943, a2, oun		

910530	12	37/-102	839, b1, ddc	756, c, top
910608	12	43/ -98	946, a3, hon	
910613	12	44/ -96	904, a3, hon	
910614	00	38/-105	933, a5, hon	700, c, oun
910627	12	38/-101	878, a2, ddc	
910716	12	46/ -94	942, a2, hon	884, b1, ddc
910718	12	38/-101	909, a3, ddc	
910719	00	46/ -92	815, b3, stc	
910824	12	48/-100	850, b1, bis	
910902	00	45/-101	854, b4, ovn	
910902	12	50/-102	943, a3, stc	
920406	12	41/ -96	944, a2, top	
920512	00	33/ -94	850, b4, ovn	780, a5, stc
920517	00	46/ -87	818, b1, oun	735, c, top
920522	12	36/-104	881, a3, ddc	
920601	12	40/ -97	946, a5, top	882, a5, hon
920622	12	40/-100	942, a2, stc	
920708	00	37/ -94	850, b1, oun	
920824	00	38/-100	850, b1, ovn	
920825	00	37/ -99	737, c, ddc	
920905	00	44/ -98	913, a5, oun	784, b3, hon
920915	00	40/ -95	821, b4, top	
920925	12	38/-102	904, a2, ddc	

8. L2A Jets

Date	Time UTC	Center °lat/°lon	Level 1 mb, type, id	Level 2 mb, type, id	Level 3 mb, type, id
910402	00	37/-103	850, b4,ddc	818, b4, ddc	
910403	00	38/ -98	874, b3, oun	758, c, ovn	
910403	12	38/ -95	948, a3, stc	850, b3, top	
910428	12	37/ -91	904, a5, ovn	937, a5, ovn	
910603	00	38/-100	759, c, ddc	700, c, top	
910605	12	39/ -98	879, b4, lbf		
910624	12	38/-100	946, a3, hon	880, b2, lbf	792, c, ddc
910709	12	39/ -95	912, a2, oun	877, a2, hon	850, b1, ddc
910711	12	40/ -97	945, a5, stc	879, b3, oun	
910715	00	45/-102	945, a5, hon	850, b4, lbf	
910715	12	37/-102	944, a3, hon	884, b1, ddc	
910805	12	38/-103	945, a2, oun	911, a2, bis	765, c, top
910806	12	44/ -96	885, a5, stc		
910807	00	45/ -97	823, b3, ovn		
910821	12	43/ -93	944, a1, ovn		
910908	00	36/ -96	882, a3, ovn		
910911	12	42/ -99	911, a2, bis	789, b3, hon	
920527	12	31/-101	876, b4, ddc	850, b4, lbf	
920707	00	36/ -96	908, a3, ovn		
920724	00	40/-100	819, b4, lbf	735, b4, lbf	
920724	12	39/-100	946, a5, hon		
920806	12	42/ -98	850, b1, lbf		
920807	00	43/ -99	850, b4, top	816, b3, lbf	
920819	12	35/-101	850, b4, lbf		

9. LSKC_SWNE Jets

Date	Time UTC	Center °lat/°lon	Level 1 mb, type, id	Level 2 mb, type, id
910406	12	40/ -97	939, a2, ovn	913, a5, oun
910417	12	34/ -98	909, a2, oun	
910426	12	40/ -96	809, b1, top	750, c, ovn
910531	12	38/ -98	869, b3, top	
910621	00	46/ -94	819, a5, ovn	
910629	12	40/ -98	943, a1, ovn	878, a2, ddc
910722	12	39/ -97	946, a2, top	852, b1, ddc
910915	00	47/ -86	814, b3, ovn	
920406	00	45/ -96	850, b4, ovn	724, c, hon
920418	12	38/-100	867, a3, stc	850, b3, ovn
920419	00	36/ -92	865, b4, oun	
920516	12	42/ -99	911, a3, top	819, b3, hon
920519	00	45/-100	913, a5, hon	881, a5, hon
920522	00	40/-101	850, b4, ddc	
920702	12	34/ -98	873, b3, oun	
920712	12	38/ -96	871, b1, ovn	815, b3, top
920715	12	32/ -98	939, a2, ovn	
920730	12	34/ -96	910, a2, oun	
920809	12	37/-103	947, a1, oun	821, b3, ddc
920823	00	48/ -94	850, b1, ovn	763, b2, ddc
920905	12	36/-102	942, a2, oun	850, b3, ovn
920913	00	44/ -96	877, b3, stc	822, b1, oun
920913	12	40/ -99	912, a3, top	
920918	00	40/ -95	907, a3, top	

10. LSPLIT Jets

Date	Time UTC	Center °lat/°lon	Level 1 mb, type, id	Level 2 mb, type, id	Level 3 mb, type, id
910511	12	38/-102	879, b1, ddc	733, c, lbf	
910512	12	38/-102	908, a3, ddc		
910513	12	35/-101	942, a2, oun		
910521	12	43/ -99	941, a2, hon		
910526	12	31/-101	908, a3, oun	844, b3, ddc	
910615	00	41/ -93	818, b3, oun	700, b3, top	
910625	12	44/-100	914, a2, hon	878, b1, ddc	
910628	00	37/-102	850, b4, top		
910628	12	38/-103	850, b3, lbf		
910629	00	45/ -94	882, a5, ovn	792, a5, ovn	
910717	12	39/-100	948, a1, top		
910722	00	40/ -96	884, a5, top	739, c, ovn	
910731	12	38/-101	912, a2, ddc	853, b1, top	
910827	12	44/ -97	940, a1, hon	882, b1, ddc	
910828	00	44/ -98	882, b4, oun	822, b4, ovn	
910828	12	46/-100	903, a3, bis	877, b1, lbf	850, b2, ddc
910907	12	42/-101	943, a3, hon	818, b3, lbf	
910914	12	38/ -96	871, b4, lbf		

920519	12	49/ -92	947, a2, stc	881, b1, lbf
920520	12	48/ -93	945, a3, hon	874, a3, bis
920521	12	39/-104	944, a3, hon	851, b4, top/oun
920530	12	41/-103	877, b2, lbf	
920607	12	40/-102	880, b4, ddc	847, b3, lbf
920711	12	33/ -98	880, b1, oun	
920712	00	36/-101	850, b1, oun	788, b3, top
920808	12	36/-102	946, a2, oun	848, a4, bis
920821	12	38/-104	914, a2, ddc	880, b4, lbf
920909	00	43/ -97	876, b3, stc	817, b3, ddc
920912	12	42/ -97	941, a5, hon	850, a2, ddc
920915	12	38/ -99	947, a2, top	879, b2, ddc
920917	12	38/ -98	908, a2, ddc	877, b4, hon

11. LKC_SWNE Jets

Date	Time UTC	Center °lat/°lon	Level 1 mb, type, id	Level 2 mb, type, id	Level 3
910407	00	44/ -86	905, a2, ovn		
910510	12	46/-100	902, a5, bis	784, c, lbf	
910829	00	47/ -95	850, b3, stc	766, b4, ovn	
910909	00	48/ -92	907, a3, stc	816, b3, ovn	
920411	00	43/ -88	902, a5, stc		
920416	00	40/ -91	844, b3, top	754, c, ovn	
920510	12	51/ -91	850, a3, hon		
920520	00	45/ -96	910, a2, hon	823, b4, top	
920617	12	43/ -91	859, b1, stc		
920701	12	47/ -94	872, b4, top		
920920	00	49/ -94	902, a5, hon	850, b4, top	786, b4, top

12. LCC Jets

Date	Time UTC	Center °lat/°lon	Level 1 mb, type, id	Level 2 mb, type, id	Level 3
910402	12	38/-102	906, a3, ddc	850, a3, ddc	
910510	00	44/ -98	879, b1, ovn	790, b1, ovn	
910607	12	44/-100	915, a2, oun	883, b3, ddc	
910726	12	47/-103	914, a2, bis	882, b1, lbf	
910727	12	38/-102	950, a2, top	914, a3, hon	883, b2, ddc
910908	12	48/ -99	902, a2, bis		
910928	12	41/-103	949, a1, hon	880, b4, lbf	
920805	12	40/-100	947, a2, ovn	881, a5, hon	791, c, oun
920901	00	38/-103	880, b2, ddc	791, b4, oun	
920901	12	42/-100	947, a2, ovn	914, a3, hon	850, b1, oun

CITED LITERATURE

CITED LITERATURE

Achtor, T.H. and L.H. Horn, 1986: Spring season Colorado cyclones. Part I: Use of composites to relate upper and lower tropospheric wind fields. *J. Clim. and Appl. Meteor.*, **25**, 732-743.

Anderson, D.L.T., 1984: An advective mixed-layer model with applications to the diurnal cycle of the low-level East African jet. *Tellus*, **36A**, 278-291.

Ardanuy, P., 1979: On the observed diurnal oscillation of the Somali jet. *Mon. Wea. Rev.*, **107**, 1694-1700.

Astling, E.G., J. Paegle, E. Miller and C.J. O'Brien, 1985: Boundary layer control of nocturnal convection associated with a synoptic scale systen. *Mon. Wea. Rev.*, **113**, 540-552.

Augustine, J.A. and F. Caracena, 1994: Lower-tropospheric precursors to nocturnal MCS development over the central United States. *Wea. Forecasting*, **9**, 116-135.

Balling, R.C., Jr., 1985: Warm season nocturnal precipitation in the Great Plains of the United States. *J. Climate Appl. Meteor.* **24**, 1383-1387.

Bardossy, A, L. Duckstein, and I. Bogardi, 1995: Fuzzy rule-based classification of atmospheric circulation patterns. *Int. J. Climatol.*, **15**, 1087-1097.

Barnes, S.L., 1973: *Mesoscale objective map analysis using weighted time-series observations.* NOAA Tech. Memo ERL NSSL-62, NSSL, Norman, OK.

------, 1964: A technique for maximizing details in numerical weather map analysis. *J. Appl. Meteor.* **3**, 396-400.

Baur, F., P. Hess and H. Nagel., 1944: *Kalender der Großwetterlagen Europas 1881-1939*, Bad Homburg.

Beebe, R.G. and F.C. Bates, 1955: A mechanism for assisting in the release of convective instability. *Mon. Wea. Rev.*, **83**, 1-10.

Beyrich, F., 1994: Sodar observations of the stable boundary layer height in relation to the nocturnal low-level jet. *Meteorol. Zeitschrift*, **N.F. 3**, 29-34.

Bierly, G.D., 1996: The configuration and evolution of airstreams in cold season Colorado cyclones. Ph.D. Dissertation. Department of Geography. Michigan State University.

Blackadar, A.K., 1957: Boundary layer wind maxima and their significance for the growth of nocturnal inversions. *Bull. Amer. Meteor. Soc.* **38**, 283-290.

Blanchard, D.O., 1990: Mesoscale convective patterns of the southern High Plains. *Bull. Amer. Meteor. Soc.* **71**, 994-1005.

Bluestein, H.B., 1993: *Synoptic-Dynamic Meteorology in Midlatitudes. Vol II: Observations and Theory of Weather Systems.* New York: Oxford University Press, 594pp.

——, 1992: *Synoptic-Dynamic Meteorology in Midlatitudes. Vol I: Principles of Kinematics and Dynamics.* New York: Oxford University Press, 431pp.

Bonner, W.D. and J. Paegle, 1970: Diurnal variations in boundary layer winds over the south-central United States in summer. *Mon. Wea. Rev.* **98**, 735-744.

——, 1968: Climatology of the low level jet. *Mon. Wea. Rev.*, **96**, 833-850.

——, S. Esbensen and R. Greenberg, 1968: Kinematics of the low-level jet. *J. Appl. Meteor.*, **7**, 339-347.

——, 1966: Case study of thunderstorm activity in relation to the low-level jet. *Mon. Wea. Rev.*, **94**, 167-178.

Borchert, J.R., 1950: The climate of the Central North American grassland. *Annals Assoc. Amer. Geograph.*, **11**, 469-471.

Bradley, A.A. and J.A. Smith, 1994: The hydrometeorological environment of extreme rainstorms in the southern Plains of the United States. *J. Appl. Meteor.*, **33**, 1418-1431.

Brezowsky, H., 1964: Morbidity and weather. *Medical Climatology*, Ed. E. Licht, Waverly Press, 753 pp.

Brook, R.R., 1985: The Koorin nocturnal low-level jet. *Bound.-Layer Meteor.*, **32**, 133-154.

Browning, K.A., 1990: Organization of clouds and precipitation in extratropical cyclones. In: *Extratropical Cyclones*. Ed. C. Newton and E.O. Holopainen, American Meteorological Society: Boston, pp. 129-153.

------ and G.A. Monk, 1982: A simple model for the synoptic analysis of cold fronts. *Quart. J. Roy. Meteor. Soc.*, **108**, 435-452.

------ and C.W. Pardoe, 1973: Structure of low-level jet streams ahead of mid-latitude cold fronts. *Quart. J. Roy. Meteor. Soc.*, **99**, 619-638.

------ and T.W. Harrold, 1970: Air motion and precipitation growth at a cold front. *Quart. J. Roy. Meteor. Soc.*, **96**, 369-389.

Buajitti, K. and A.K. Blackadar, 1957: Theoretical studies of diurnal wind-structure variations in the planetary boundary layer. *Quart. J. Roy. Meteor. Soc.*, **48**, 486-500.

Burk, S.D. and W.T. Thompson, 1996: The summertime low-level jet and marine boundary layer structure along the California coast. *Mon. Wea. Rev.*, **124**, 668-686.

Cahir, J.J., G.S. Forbes, W.D. Lottes and T. Staskiewicz, 1985: Structural aspects of the warm conveyor belt. Unpublished manuscript, Department of Meteorology, Pennsylvania State University. Cited in Browning (1990).

Carlson, T.N., 1991: *Mid-Latitude Weather Systems*. New York: Harper Collins Academic, 507 pp.

------, S.G. Benjamin, G.S. Forbes, and Y.-F. Li, 1983: Elevated mixed layers in the regional severe storm environment: conceptual model and case studies. *Mon. Wea. Rev.*, **111**, 1453-1473.

------, 1980: Airflow through midlatitude cyclones and the comma cloud pattern. *Mon. Wea. Rev.*, **108**, 1498-1509.

Carr, F.H. and J.P. Millard, 1985: A composite study of comma clouds and their association with severe weather over the Great Plains. *Mon. Wea. Rev.*, **113**, 370-387.

Chen, G.T.-J. and C.-C. Yu, 1988: Study of low-level jet and extremely heavy rainfall over northern Taiwan in the Mei-Yu season. *Mon. Wea. Rev.*, **116**, 884-891.

Chen, T.-C. and J.A. Kpaeyeh, 1993: The synoptic-scale environment associated with the low-level jet of the Grat Plains. *Mon. Wea. Rev.*, **121**, 416-420.

Chen, Y.-L., X.A. Chen and Y.-X. Zhang, 1994: A diagnostic study of the low-level jet during TAMEX IOP 5. *Mon. Wea. Rev.*, **122**, 2257-2284.

Chen, X.A. and Y.-L. Chen, 1995: Development of low-level jets during TAMEX. *Mon. Wea. Rev.*, **123**, 1695-1719.

Chiba, O., and S. Kobayashi, 1986: A study of the structure of low-level katabatic winds at Mizuho Station, East Antarctica. *Bound.-Layer Meteor.*, **37**, 343-355.

Chou, L.C., C.-P. Chang and R.T. Williams, 1990: A numerical simulation of the Mei-Yu front and the associated low level jet. *Mon. Wea. Rev.*, **118**, 1408-1428.

Cotton, W.R., M.-S. Lin, R.L. McAnelly and C.J. Tremback, 1989: A composite model of mesoscale convective complexes. *Mon. Wea. Rev.*, **117**, 765-783.

Cummins, K.L., W.L. Hiscox, A.E. Pifer, and M.W. Maier, 1992: Performance analysis of the U.S. National Lightning Detection Network. *Expanded Paper 9th Intl. Conf. on Atmospheric Electricity*, St. Petersburg, Russia, June 15-19.

Curtis, R.C. and H.A. Panofsky, 1958: The relation between large-scale vertical motion and weather in summer. *Bull. Amer. Meteor. Soc.*, **39**, 521-531.

Darkow, G.L. and O.E. Thompson, 1968: Diurnal oscillations of the tropospheric wind field above a low-level jet. *J. Atmos. Sci.*, **25**, 39-46.

Dickison, R.B.B. and H.H. Neumann, 1982: The occurrence of nocturnal low-level jets in New England and the Canadian Maritimes. *Atmosphere-Ocean*, **20**, 287-300.

Djuric, D. and D.S. Ladwig, 1983: Southerly low-level jet in the winter cyclones of the southwestern Great Plains. *Mon. Wea. Rev.*, **111**, 2275-2281.

------, 1981: A numerical model of the formation and evolution of a low-level jet. *Mon. Wea. Rev.*, **109**, 384-390.

----- and M.S. Damiani, Jr., 1980: On the formation of the low-level jet over Texas. *Mon. Wea. Rev.*, **108**, 1854-1865.

Douglas, M.W. and D.J. Stensrud, 1996: Upgrading the North American upper-air observing network: What are the possibilities? *Bull. Amer. Meteor. Soc.*, **77**, 907-924.

------, 1995: The summertime low-level jet over the Gulf of California. *Mon. Wea. Rev.*, **123**, 2334-2347.

Doyle, J.D. and T.T. Warner, 1991: A Caroline coastal low-level jet during GALE IOP 2. *Mon. Wea. Rev.*, **119**, 2414-2428.

Easterling, D.R., 1990: Persistent patterns of thunderstorm activity in the central United States. *J. Climate*, **3**, 1380-1389.

Endlich, R.M. and R.L. Mancuso, 1968: Objective analysis of environmental conditions associated with severe thunderstorms and tornadoes. *Mon. Wea. Rev.*, **96**, 342-350.

Fast, J.D. and M.D. McCorcle, 1990: A two-dimensional numerical sensitivity study of the Great Plains low-level jet. *Mon. Wea. Rev.*, **118**, 151-163.

Fawbush, E.J. and R.C. Miller, 1954: The types of air masses in which North American tornadoes form. *Bull. Amer. Meteor. Soc.*, **35**, 154-165.

Findlater, J., 1969: A major low-level air current near the Indian Ocean during the northern summer. *Quart. J. Roy. Meteor. Soc.*, **95**, 362-380.

Fritsch, J.M., R.J. Kane and C.R. Chelius, 1986: The contribution of mesoscale convective weather systems to the warm-season precipitation in the United States. *J. Clim. Appl. Meteor.*, **25**, 1333-1345.

Fuelberg, H.E. and D.E. Buechler, 1989: Energy analysis of convectively induced wind perturbations. *Mon. Wea. Rev.*, **117**, 745-764.

Gerhardt, J.R., 1962: An example of a nocturnal low-level jet stream. *J. Atmos. Sci.*, **19**, 116-118.

Glass, F.H., 1993: The role of ageostrophic motions associated with an upper tropospheric jet streak on the pre-storm environment. *Prepr. 17th Conf. Severe Loc. Storms / Conf. Atm. Electr.*, AMS, St. Louis, 112-117.

Haltiner, G.J., 1961: A note on the diurnal wind variation. *Tellus*, **13**, 438-439.

------, 1959: The diurnal variation of the wind. *Tellus*, **11**, 452-458.

Harman, J.R., 1991: *Synoptic Climatology of the Westerlies: Process and Patterns.* Washington, D.C.: Association of American Geographers.

Harrington, J.A., Jr. and B.J. Brown, 1985: A synoptic climatology of depressions in warm season precipitation profiles from the upper middle west. *Physical Geography*, **5**, 186-197.

Helfand, H.M. and S.D. Schubert, 1995: Climatology of the simulated Great Plains low-level jet and its contribution to the continental moisture budget of the United States. *J. Climate*, **8**, 784-806.

Hemler, M.G., 1987: Dopper wind profiler examination of cloud edges. M.S. thesis, Department of Meteorology, Pennsylvania State University. Cited in Browning (1990).

Hering, W.S. and T.R. Borden, Jr., 1962: Diurnal variations in the summer wind field over the central United States. *J. Atmos. Sci.*, **19**, 81-86.

Hess, P. and H. Brezowsky, 1969: Katalog der Großwetterlagen Europas. *Berichte des Deutschen Wetterdienstes* Nr. 113, Bd. 15, 2. neubearbeitete und ergänzte Auflage, Offenbach a. Main, Selbstverlag des Deutschen Wetterdienstes.

Hobbs, P.V., T.J. Matejka, P.H. Herzegh, J.D. Locatelli and R.A. Houze, Jr., 1980: The mesoscale and microscale structure and organization of clouds and precipitation in midlatitude cyclones. I: A case study of a cold front. *J. Atmos. Sci.*, **37**, 568-596.

Hoecker, W.H., 1965: Comparative physical behavior of southerly boundary-layer wind jets. *Mon. Wea. Rev.*, **93**, 133-144.

———, 1963: Three southerly low-level jet systems delineated by the Weather Bureau special PIBAL network of 1961. *Mon. Wea. Rev.*, **91**, 573-582.

Holton, J.R., 1967: The diurnal boundary layer wind oscillation above sloping terrain. *Tellus*, **19**, 199-205.

Houze, R.A., Jr, B.F. Smull and P. Dodge, 1990: Mesoscale organization of springtime rainstorms in Oklahoma. *Mon. Wea. Rev.* **118**, 613-654.

Hovanec, R.D. and L.H. Horn, 1975: Static stability and the 300 mb isotach field in the Colorado cyclogenetic area. *Mon. Wea. Rev.*, **103**, 628-638.

Hoxit, L.R., 1975: Diurnal variations in planetary boundary-layer winds over land. *Bound.-Layer Meteor*, **8**, 21-38.

Huschke, R.E. (Ed.), 1989: *Glossary of Meteorology*. Boston: American Meteorological Society, 638 pp.

Izumi, Y., 1964: The evolution of temperature and velocity profiles during breakdown of a nocturnal inversion and a low-level jet. *J. Appl. Meteor.*, **3**, 70-82.

——— and M.L. Barad, 1963: Wind and temperature variations during development of a low-level jet. *J. Appl. Meteor.*, **2**, 668-673.

Johns, R.H., 1993: Meteorological conditions associated with bow echo development in convective storms. *Wea. Forecasting*, **8**, 294-299.

Jury, M.R., and G.R. Tosen, 1989: Characteristics of winter boundary layer over the African Plateau: 26 degrees S. *Bound.-Layer Meteor.*, **49**, 53-76.

------, and G. Spencer-Smith, 1988: Doppler sounder observations of trade winds and sea breeze along the African west coast near 34 degrees S, 19 degrees E. *Bound.-Layer Meteor.*, **44**, 373-405.

Kaimal, J.C. and Y. Izumi, 1965. Vertical velocity fluctuations in a nocturnal low-level jet. *J. Appl. Meteor.*, **4**, 576-584.

Kastendeuch, P.P. and P. Kaufmann, 1997: Classification of summer wind fields over complex terrain. *Int. J. Climatol.*, **17**, 521-534.

Keables, M.J., 1989: A synoptic climatology of the bimodal precipitation distribution in the Upper Midwest. *J. Climate*, **2**, 1289-1294.

Keenan, T.D., J. McBride, G. Holland, N. Davidson, and B. Gunn, 1989: Diurnal variations during the Australian monsoon experiment (AMEX) phase II. *Mon. Wea. Rev.*, **117**, 2535-2552.

Kelbe, B., 1988: Features of westerly waves propagating over southern Africa during summer. *Mon. Wea. Rev.*, **116**, 60-70.

Key, J. and R.G. Crane, 1986: A comparison of synoptic classification schemes based on 'objective' procedures. *J. Climatol.*, **6**, 375-388.

Klink, K., 1986: Space-time analysis of the surface wind field using vector-based principal components analysis. *Publications in Climatology* **34 (2)**, C.W. Thornthwaite Associates, Laboratory of Climatology, Elmer, NJ, 42 pp.

Koch, S.E., M. des Jardins and P.J. Kocin, 1983: An interactive Barnes objective map analysis scheme for use with satellite and conventional data. *J. Clim. Appl. Meteor.*, **22**, 1487-1503.

------, M. des Jardins and P.J. Kocin, 1981: *The GEMPAK Barnes objective analysis scheme. NASA Tech. Memo 83851.* NASA, Goddard Space Flight Center, MD.

Kottmeier, C., 1978: Trajektorien unter Einfluß eines nächtlichen Grenzschichtstrahlstromes. *Meteorol. Rundsch.*, **31**, 129-133.

Kotroni, V., Y. Lemaitre and M. Petitdidier, 1994. Dynamics of a low-level jet observed during the Fronts 87 experiment. *Quart. J. Roy. Meteorol. Soc.*, **120**, 277-303.

------ and K. Lagouvardos, 1993: Low-level jet streams associated with atmospheric cold fronts: seven case studies from the FRONTS 87 experiment. *Geophys. Res. Lett.*, **20**, 1371-1374.

Kreitzberg, C.W., 1968: The mesoscale wind field in an occlusion. *J. Appl. Meteor.*, **7**, 53-67.

Kuettner, J., 1971: Cloud bands in the earth's atmosphere. *Tellus*, **23**, 404-426.

Maddox, R.A., K.W. Howard, D.L. Bartels and D.M. Rodgers, 1986. Mesoscale convective complexes in the middle latitudes. In: *Mesoscale Meteorology and Forecasting*. Ed. P.S. Ray, Boston: American Meteorological Society, pp. 390-413.

------, 1983: Large-scale meteorological conditions associated with midlatitude, mesoscale convective complexes. *Mon. Wea. Rev.*, **111**, 1475-1493.

----- and C.A. Doswell III, 1982: An examination of jet stream configuration, 500 mb vorticity advection and low-level thermal advection patterns during extended periods of intense convection. *Mon. Wea. Rev.*, **110**, 184-197.

Mahrt, L., 1977: Influence of low-level environment on severity of High-Plains moist convection. *Mon. Wea. Rev.*, **105**, 1315-1329.

McCorcle, M.D., 1988: Simulation of surface-moisture effects on the Great Plains low-level jet. *Mon. Wea. Rev.*, **116**, 1705-1720.

McNider, R.T. and R.A. Pielke, 1981: Diurnal boundary-layer development over sloping terrain. *J. Atm. Sci.*, **38**, 2198-2212.

McNulty, R.P., 1978: On upper tropospheric kinematics and severe weather occurrence. *Mon. Wea. Rev.*, **106**, 662-672.

Means, L.L., 1954: A study of the mean southerly wind-maximum in low levels associated with a period of summer precipitation in the middle west. *Bull. Amer. Meteor. Soc.*, **35**, 166-170.

------, 1952: On thunderstorm forecasting in the central United States. *Mon. Wea. Rev.*, **80**, 165-189.

Mitchell, M.J., R.W. Arritt, and K. Labas, 1995: A climatology of the warm season Great Plains low-level jet using wind profiler observations. *Wea. Forecasting*, **10**, 576-591.

Modahl, A.C., 1979: Low-level wind and moisture variations preceding and following hailstorms in Northeast Colorado. *Mon. Wea. Rev.*, **107**, 442-450.

Moran, J.M. and M.D. Morgan, 1986: *The Atmosphere and the Science of Weather*. Edina, MN: Burgess, 502 pp.

Muller, R.A., 1977: A synoptic climatology for environmental baseline analysis. *J. Appl. Meteorol.*, **16**, 20-33.

Nagata, M. and Y. Ogura, 1991: A modeling case study of interaction between heavy precipitation and a low-level jet over Japan in the Baiu season. *Mon. Wea. Rev.*, **119**, 1309-1336.

Newton, C.W., 1967: Severe convective storms. *Adv. Geophys.*, **12**, 257-308.

Nicolini, M., K.M. Waldron and J. Paegle, 1993: Diurnal oscillations of low-level jets, vertical motion, and precipitation: a model case study. *Mon. Wea. Rev.*, **121**, 2588-2610.

Orville, R.E., R.W. Henderson, and R.B. Pyle, 1990: The national lightning detection network--Severe storms observations. *Prepr. 16th Conf. Sev. Loc. Storms, Conf. on Atm. Electricity*, Amer. Meteor. Soc., Boston, MA: 327-330.

Paegle, J. and D.W. McLawhorn, 1983: Numerical modeling of diurnal convergence oscillations above sloping terrain. *Mon. Wea. Rev.*, **111**, 67-85.

----- and D.W. McLawhorn, 1973: Correlation of nocturnal thunderstorms and boundary-layer convergence. *Mon. Wea. Rev.*, **101**, 877-883.

------ and G.E. Rasch, 1973: Three-dimensional characteristics of diurnally varying boundary-layer flows. *Mon. Wea. Rev.*, **101**, 746-756.

Parish, T.R., A.R. Rodi and R.D. Clark, 1988: A case study of the summertime Great Plains low level jet. *Mon. Wea. Rev.*, **116**, 94-105.

Pierce, E.T., 1970: Latitudinal variation of lightning parameters. *J. Appl. Meteor.*, **9**, 194-195.

Pielke, R.A., R.A. Stocker, R.W. Arritt, and R.T. McNider, 1991: A procedure to estimate worst-case air quality in complex terrain. *Environ. Int.*, **17**, 559-594.

Pitchford, K.L. and J. London, 1962: The low-level jet as related to nocturnal thunderstorms over midwest United States. *J. Appl. Meteor.*, **1**, 43-47

Porter, J., L. Means, J. Houde and W. Chappell, 1955: A synoptic study on the formation of squall lines in the north central United States. *Bull. Amer. Meteor. Soc.*, **36**, 390-396.

Raymond, D.J., 1978: Instability of the low-level jet and severe storm formation. *J. Atmos. Sci.*, **35**, 2274-2280.

Reitan, C.H., 1975: Frequencies of cyclones and cyclogenesis for North America, 1951-1970. *Mon. Wea. Rev.*, **102**, 861-868.

Reiter, E.R., 1963: *Jet-Stream Meteorology*. Chicago, U of Chicago Press, 515 pp.

Roth, R., C. Kottmeier, and D. Lege, 1979: Die lokale Feinstruktur eines Grenzschicht-strahlstromes. *Meteorol. Rundsch.*, **32**, 65-72.

Sangster, W.E., 1979: Warm season nocturnal quantitative precipitation forecasting for eastern Kansas using the surface geostrophic wind chart. NOAA Tech. Memo. NWS CR-64. 44pp.

Schroeder, M.J., 1950: The Hudson Bay high and the spring fire season in the Lake states. *Bull. Amer. Meteor. Soc.*, **31**, 111-118.

Schwartz, B.E. and C.A. Doswell III, 1991: North American rawinsonde observations: Problems, concerns, and a call to action. *Bull. Amer. Meteor. Soc.*, **72**, 1885-1896.

Sechrist, F.S. and T.M. Whittaker, 1979: Evidence of jet streak vertical circulation. *Mon. Wea. Rev.*, **107**, 1014-1021.

Shen, T.-C., and D. Djuric, 1981: Formation of the low-level jet under an inversion. *Prepr. Fifth Conf. Numer. Weath. Pred.*, Amer. Meteor. Soc., Monterey, 301-302.

Sjostedt, D.W., J.T. Sigmon and S.J. Colucci, 1990: The Carolina nocturnal low-level jet: synoptic climatology and a case study. *Wea. Forecasting*, **5**, 404-415.

Sladkovic, R. and H.-J. Kanter, 1977: Low-level jet in the Bavarian pre-alpine region. *Arch. Met. Geoph. Biokl., Ser. A*, **25**, 343-355.

Smith, J.A., A.A. Bradley and M.L. Baeck, 1994: The space-time structure of extreme storm rainfall in the southern Plains. *J. Appl. Meteor.*, **33**, 1402-1417.

Sortais, J.-L., J.-P. Cammas, X.D. Yu, E. Richard, and R. Rosset, 1993: A case study of coupling between Low- and Upper-level Jet-front systems: Investigation of dynamical and diabatic processes. *Mon. Wea. Rev.*, **121**, 2239-2253.

Stensrud, D.J., M.H. Jain, K.W. Howard, and R.A. Maddox, 1990: Operational systems for observing the lower atmosphere: Importance of data sampling and archival procedures. *J. Atmos. Oceanic Technol.*, **7**, 930-937.

Tao, S., and L. Chen, 1987: A review of recent research on the East Asian summer monsoon in China. *Monsoon Meteorology*, C.P. Chang and T.N. Krishnamurti, Eds., Oxford University Press, 60-92.

Thorpe, A.J. and T.H. Guymer, 1977: The nocturnal jet. *Quart. J. R. Met. Soc.*, **103**, 633-653.

Tobler, W., 1988: Resolution, resampling and all that. In: H. Mounsey and R.F. Tomlinson (Eds.) *Building Databases for Global Science*, Philadelphia: Taylor and Francis, pp. 129-137.

Trewartha, G.T., 1981a: The bimodal warm season precipitation profile of the Upper Middle West. *Ann. Assoc. Amer. Geog.*, **71**, 566-71.

------, 1981b: *The earth's problem climates*. University of Wisconsin Press, 371 pp.

Trier, S.B., and D.B. Parsons, 1993: Evolution of environmental conditions preceding the development of a nocturnal mesoscale convective complex. *Mon. Wea. Rev.*, **121**, 1078-1098.

Uccellini, L.W., 1990: The relationship between jet streaks and severe convective storm systems. *Prepr. 16th Conf. on Severe Local Storms / Conf. on Atmosph. Electricity*, Kananaskis Park, Alta., Oct 22-26, pp. 121-130.

------, R.A. Petersen, K.F. Brill, P.J. Kocin, and J.J. Tuccillo, 1987: Synergistic interactions between an upper-level jet streak and diabatic processes that influence the development of a low-level jet and a secondary coastal cyclone. *Mon. Wea. Rev.*, **115**, 2227-2261.

------, R.A. Petersen, K.F. Brill, P.J. Kocin, and J.J. Tuccillo, 1986: Factors which influence the development of a low-level jet and coastal cyclogenesis. *Prepr. 11th Conf. Weather Forecasting and Analysis*, Kansas City, June 17-20, American Meteorological Society, pp. 253-258.

-------, 1980: On the role of upper tropospheric jet streaks and lee side cyclogenesis in the development of low-level jets in the Great Plains. *Mon. Wea. Rev.*, **108**, 1689-1696.

------ and D.R. Johnson, 1979: The coupling of upper and lower tropospheric jet streaks and implications for the development of severe convective storms. *Mon. Wea. Rev.*, **107**, 682-703.

VanBebber, W.J and W. Köppen, 1895. Die Isobarentypen des Nordatlantischen Ozeans und Westeuropas, ihre Beziehung zur Lage and Bewegung der Barometrischen Maxima und Minima. *Arch. Dtsch. Seewarte* (Hamburg), **18**, 27 pp.

Virji, H., 1982: An estimate of the summertime tropospheric vorticity budget over South America. *Mon. Wea. Rev.*, **110**, 217-224.

-------, 1981: A preliminary study of summer time tropospheric circulation patterns over South America from cloud winds. *Mon. Wea. Rev.*, **109**, 599-610.

Wallace, J.M., 1975: Diurnal variations in precipitation and thunderstorm frequency over the conterminous United States. *Mon. Wea. Rev.*, **103**, 406-419.

Wexler, H., 1961: A boundary layer interpretation of the low-level jet. *Tellus*, **13**, 368-378.

Whittaker, L.M. and L.H. Horn, 1981: Geographical and seasonal distribution of North American cyclogenesis, 1958-1977. *Mon. Wea. Rev.*, **109**, 2312-2322.

Wilczak, J.M., R.G. Strauch, F.M. Ralph, B.L. Wever, D.A. Merritt, J.R. Jordan, D.E. Wolfe, L.K. Lewis, D.B. Wuertz, J.e. Gaynor, S.a. McLaughlin, R.R. Rogers, A.C. Riddle, and T.S. Dye, 1995: Contamination of wind profiler data by migrating birds: Characteristics of corrupted data and potential solutions. *J. Atmos. Oceanic Technol.*, **12**, 449-467.

Wilson, J.W. and W.E. Schreiber, 1986: Initiation of convective storms at radar-observed boundary-layer convergence lines. *Mon. Wea. Rev.* **114**, 2516- 2536.

Wilson, M.A., 1975: Atmospheric tidal motions over Australia below 20 kilometers. *Mon. Wea. Rev.* **103**, 1110-1120.

Winkler, J.A., J.R. Harman, E.A. Waller, and J. T. Brown, 1996: Climatological characteristics of springtime lower tropospheric airflow over Central and Eastern North America. *Int. J. Clim.*, **16**, 739-755.

-------, B.R. Skeeter and P. D. Yamamoto, 1988: Seasonal variations in the diurnal characteristics of heavy hourly precipitation across the United States. *Mon. Wea. Rev.* **116**, 1641-1658.

Yarnal, B., 1993. *Synoptic Climatology in Environmental Analysis*, London: Belhaven Press, 195 pp.

-------, 1984. A procedure for the classification of synoptic weather maps from gridded atmospheric pressure surface data. *Comput. Geosci.*, **10**, 397-410.

Zeman, O., 1979: Parameterization of the dynamics of stable boundary layers and nocturnal jets. *J. Atmos. Sci.*, **36**, 792-804.

Zhong, S., J.D. Fast, and X. Bian, 1996: A case study of the Great Plains low-level jet using wind profiler network data and a high-resolution mesoscale model. *Mon. Wea. Rev.*, **124**, 785-806.

MICHIGAN STATE UNIV. LIBRARIES
31293013947431